U.S. Department of Transportation
Federal Railroad Administration
and
New York State Energy Research
and Development Administration

Magnetic Levitation
Transportation System
Technology Assessment
DOT/FRA/NMI - 92/07

FINAL REPORT

Influence of Guideway Flexibility on Maglev Vehicle/Guideway Dynamic Forces

DTF53-91-C-0045

by

Parsons Brinckerhoff Quade & Douglas, Inc.

Battelle

Intermagnetics General

Dr. G. Gregorek, Ohio State University

July 1992

Technical Report Documentation Page

1. Report No. DOT/FRA/NMI - 92/07	**2. Government Accession No.**	**3. Recipient's Catalog No.**
4. Title and Subtitle Influence of Guideway Flexibility on Maglev Vehicle/Guideway Dynamic Forces		**5. Report Date** July 1992 **6. Performing Organization Code**
7. Author(s) L. E. Daniels[1], D. R. Ahlbeck[2], Dr. Z.J. Stekly[3], Dr. G. M. Gregorek[4]		**8. Performing Organization Report No.**
9. Performing Organization Name and Address Parsons Brinckerhoff Quade & Douglas, Inc. 460 Spring Park Place, Suite 100 Herndon, VA 22070		**10. Work Unit No. (TRAIS)** **11. Contract or Grant No.** DTF 53-91-C-0045
12. Sponsoring Agency Name and Address U.S. Department of Transportation Federal Railroad Administration National Maglev Initiative Washington, DC 20590		**13. Type of Report and Period Covered** Final Report July 1991 - July 1992 **14. Sponsoring Agency Code** RDV-7

15. Supplementary Notes

[1]PBQ&D; [2]Battelle, [3]Intermagnetics General Corporation, [4]Aeronautical & Astronautical Research Laboratory, OSU,
COTR: Andrew Sluz, Volpe National Transportation Systems Center

16. Abstract

This report presents the results of a study investigating the dynamic interaction between aerial structures and maglev vehicles. The study includes three dimensional responses for attractive (EMS) maglev vehicle and repulsive (EDS) maglev vehicles and six different guideway structures. The analysis is conducted using original time domain computer models which incorporate up to 52 degrees of freedom for EMS systems and 44 degrees of freedom for the EDS systems, including multiple span guideways, multiple-vehicle trains, aerodynamic inputs with the special relations and structural properties associated with each major system component, and with appropriate maglev suspension characteristics interconnecting vehicle to guideway. The various guideway structure and vehicle combinations are analyzed separately for two representative guideway lengths of 21m and 39m.

Results are presented for vehicle accelerations in terms of ride comfort accelerations and for guideway accelerations and bending moments. Comparisons from the analysis include EMS vs. EDS system responses, effects of span length, effects of position in car, effects of multiple-vehicle trains, effects of multiple simple span guideways vs. continuous span guideways, effects of wind gusts, and effects of beam bearing pad stiffness. Costs of each guideway is estimated in 1992 dollars.

17. Key Words maglev, magnetic levitation, transit, ground transportation, aerial structure dynamics, vehicle dynamics, high speed guideways, aerodynamics, guideway costs, magnetic suspension characteristics, structural design codes.	**18. Distribution Statement** DOCUMENT IS AVAILABLE TO THE PUBLIC THROUGH THE NATIONAL TECHNICAL INFORMATION SERVICE, SPRINGFIELD, VIRGINIA 22161

19. Security Classif.(of this report)	**20. Security Classif.(of this page)**	**21. No. of Pages**	**22. Price**
Unclassified	Unclassified	222	

Form DOT F 1700.7 (8-72) Reproduction of completed page authorized

ACKNOWLEDGMENTS

This work is supported by the Federal Railroad Administration and the New York State Energy Research & Development Administration.

The work has benefited from the insights and patient assistance of the following people:

Andrew Sluz, COTR, Volpe National Transportation System Center (VNTSC)

Jon Pietrak, Volpe National Transportation System Center

Dr. David N. Wormley, Massachusetts Institute of Technology

James Smailes, National Maglev Initiative Office

It is a particular pleasure to acknowledge the collaborators in this study who have shown great skill in developing the analysis and reports for this study. The principal collaborators, their contributions, and their affiliations are:

Donald R. Ahlbeck, Dynamicist, Battelle

Dr. John Stekly, Magnetic Suspensions, Intermagnetics General, Inc.

Dr. Gerald Gregorek, Aerodynamics, Ohio State University
Dr. Gregorek is assisted by Robert Boyd

The Parsons Brinkerhoff staff who built the beam designs on paper are Wassim Dergham and John Michels with direction and assistance from David Charters, Alex Rosenbaum, and Frank Balsamo. The cost estimates for the structures are the work of Richard Roberts, Parsons Brinckerhoff.

These individuals and the support staffs of each participating organization are gratefully acknowledged. Any errors, incorrect judgments, and misstatement of fact are solely the responsibility of the Project Manager.

L. E. Daniels
Project Manager
PBQ&D

EXECUTIVE SUMMARY

INFLUENCE OF GUIDEWAY FLEXIBILITY ON MAGLEV/GUIDEWAY DYNAMIC FORCES

This study investigates the dynamic interactions between magnetically levitated (maglev) vehicles and elevated guideways.

Emphasis in this study is on guideway design issues and related pragmatic concerns for:

1. The applicability of existing U.S. structural design guidelines to high speed service,
2. The engineering representation of the physics required for maglev suspension systems (which has direct effect on guideway design methods),
3. The dynamic resonant conditions between vehicle and guideway,
4. The aerodynamic effects on dynamic response at very high speeds, and
5. The implications for guideway tolerances and guideway materials in maglev systems.

The study treats both the Electromagnetic System (EMS) of levitation, which achieves levitation by attraction between magnetically opposite poles and is referred to in the report as an "attractive" system, and the Electrodynamic System (EDS) of levitation, which achieves levitation by repelling magnetically equal poles that is referred to as a "repulsive" system.

The study develops

- Four alternative guideways designed to current U.S. guidelines [1].

- Dynamic models that include the following major representations in three dimensions for both the attractive (EMS) and repulsive (EDS) maglev suspensions:

  - Vehicle properties (mass, length, bending stiffness and secondary suspension)
  - Beam properties (mass, length, bending stiffness and end conditions)
  - Aerodynamic forces
  - Multi-vehicle trains
  - Multi-span guideways

The analysis is conducted over a range of speeds to 600 km/h, separately for each guideway and maglev suspension configuration, and separately for two representative span lengths, 21 m and 39 m, using simple span and two-span continuous designs for each span length.

Incorporating the vehicle, suspension and aerodynamic parameters with the beam parameters, the dynamic models developed by the study represent up to 52 degrees of freedom for the EMS system, and 44 degrees of freedom for the EDS system.

Important criteria selected for the study are:

Impact Factor = 30%
Span deflection/span length = 1/1000

Ride Comfort:

0.036g rms maximum vertical acceleration and
0.025g rms maximum lateral acceleration.

The selected guideway structures are illustrated in Table A which lists the estimated cost of each structure.

---

1 For comparison purposes, a fifth guideway is developed which is conceptually similar to the Japanese HSST system but compatible with the vehicle in this study, and a sixth guideway uses the published dimensions of the German Transrapid steel guideway.

TABLE A
STRUCTURE COSTS

Description		Beam Length (m)	Unit Cost ($/m)	Cost/km [One Gdwy] ($)	Cost/km [Dual Gdwy] ($)
1 Steel Girders w/ concrete deck	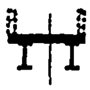	21.336	$5,090	$5,089,690	**$10,179,380**
		39.624	$4,809	$4,809,470	**$9,618,940**
2 Concrete Box		21.336	$4,401	$4,400,980	**$8,801,960**
		39.624	$4,943	$4,942,970	**$9,885,940**
3 Trapezoidal Box		21.336	$4,920	$4,920,220	**$9,840,440**
		39.624	$4,957	$4,957,430	**$9,914,860**
4 Twin Box (HSST)		21.336	$3,422	$3,422,230	**$6,844,460**
		39.624	$3,216	$3,216,330	**$6,432,660**
5 Steel "V" (Transrapid)		24		Costs not estimated	
6 AASHTO Concrete Girders		21.336	$4,622	$4,622,360	**$9,244,720**
		39.624	$4,372	$4,372,440	**$8,744,880**

Cost Estimates Include:

1. **7.6m pier height**
2. **Complete substructure from piles upward**
3. **10% mobilization cost and 15% contingency**
4. **Costs in 1992 dollars, based on 1992 R.S. Means Building Construction Costs Data**

Cost Estimates do not include:

a. **Magnetic Reaction coils/plates in guideway**
b. **Engineering costs, Construction Management costs**
c. **Right of Way acquisition or preparation**
d. **Non-structural system components (power, signal facilities)**

Summary of the Results

Vertical Dynamics

- The dynamic load did not exceed the maximum allowable vertical bending moment for any guideway designed to existing U.S. guidelines, although the dynamic acceleration exceeded the 30% design impact factor in many cases.

- Beams designed to existing U.S. guidelines experience lower dynamic accelerations than the comparison beam design. The lower dynamics in the beams designed to U.S. guidelines are attributed to their significantly larger mass even though the span deflection to span length ratio used in the U.S. designs is 1/1000 whereas the comparison beam reportedly uses a stiffer 1/4000 ratio. The beam used for comparison is all steel where the other designs are composite steel-concrete or all concrete designs.

- Mid-car accelerations are lower than the forward end of the car which, in turn, are generally lower than the rear end of the car for both EMS and EDS maglev systems.

- Mid-car peak accelerations exceed ride comfort criteria for the **EDS system** on all guideway configurations for speeds between 200 and 350 km/h on the short span, and between 100 and 250 km/h on the longer span.

- Mid-car peak accelerations exceed ride comfort criteria for the **EMS system** on all guideway configurations above approximately 500 km/h on the short span, and for all speeds on the long span.[2]

- **EMS systems** on short, light structures generate vertical car body accelerations well above the desired comfort limit over the entire speed range analyzed.

- Where ride comfort criteria is marginally exceeded, optimization of the vehicle's secondary suspension is expected to provide compliance.

---

2 The analysis of the long span with EMS systems only included a steel girder design and an AASHTO concrete girder span design.

Comparison of Continuous Span Structures to Simple Spans

- In **EMS systems**, continuous span structures generally offer significant reductions in vertical car body and beam accelerations compared to simple spans (exceptions are expected; a 500 to 550 km/h exception is documented in guideway accelerations for the single configuration analyzed).

- In **EDS systems**, continuous span structures reduced vertical beam accelerations compared to simple spans, while reducing ride quality (that is, adversely affecting ride comfort) in the beams analyzed.

Lateral and Torsional Dynamics

- All of the systems and configurations analyzed on tangent guideway produced acceptable lateral ride comfort and beam accelerations. In the worst case analyzed with vehicle speeds of 400 km/h and 115 km/h side wind gust, the vehicle is stable but the ride is rough. Curved geometries remain to be analyzed.

Guideway Support Stiffness - Bearing Pads

- At high speeds, the beam bearing pad stiffness is observed to be a larger influence on vehicle/guideway interaction than previously documented. For a 21 m AASHTO concrete girder and within the practical ranges of bearing pad stiffness,

    - **EMS system's** ride comfort becomes unacceptable when the softest bearing is used, while the **EDS system's** ride comfort is unaffected by bearing pad stiffness value;
    - **EMS system's** beam peak acceleration is unaffected by bearing stiffness, while **EDS system's** beam accelerations decrease as the bearing is made softer.

Design Criteria and Guidelines for High Speed Aerial Structures

- There are no U.S. design codes, guidelines or approved methods[3] for assessing dynamic loads and deflections on aerial structures for speeds over 200 km/h.

- The amplitude of peak guideway accelerations increases with the ratio of vehicle mass to guideway mass (mass ratio) for a given span length for both EMS and EDS maglev systems.

- The mass ratio and the crossing frequency ratio (the ratio of crossing frequency, V/l_s, to fundamental span frequency) appear to provide reasonable indications of dynamic thresholds.

- Under conditions studied, beam accelerations are expected to be less than the 30% impact factor when the crossing frequency ratio is less than 1.0 and, simultaneously, when the mass ratio is less than the following values:

Maximum Allowable Mass Ratio

	for 21m spans	for 39m spans
EMS Systems	0.6	0.3*
EDS Systems	0.3*	0.18

* approximate

(References of interest on these parameters are Richardson and Wormley [63], Maotoh [47] and Wilson [77].

Construction Issues Effecting Design

- Guideway steel such as rebar will interfere with magnetic fields only in EDS Systems and only when the steel is sufficiently close to track coils. Magnetic force loss of 1% is expected when guideway steel is within 0.37 m of the track coil center and a 5% loss for 0.24 m clearance using conservative estimates. However, the rebar may be placed to

3 See reference [69], Wormley, et al, as example of proposed analysis methodologies.

existing requirements (25mm to 50mm of concrete cover) if the rebar does not form an electrical current loop, i.e. is electrically discontinuous.

- Industry construction tolerances for aerial structures are large compared to the expected alignment irregularity allowances for maglev. Consideration is urged for guideway magnet mounting designs that permit construction and maintenance adjustment.

- The design of the beams is effected by requirements for transportation of beams to construction sites and handling requirements of the beams during construction.

- Design analysis for corrosion effects from magnetic fields and for stray current control is required for maglev systems as is required for new transit systems. There is no concern at this time that magnetic flux fields will have any more corrosive effect on conductive structural elements than is currently experienced in existing DC powered transit systems. Existing methods of treatments for stray current and corrosion control are expected to be fully adequate in maglev applications with minor adjustments for the physics analysis inherent in maglev technology.

Other Topics Reported

The report contains

- developments of primary suspension characteristics (spring rates and damping) derived from magnetic principles, separately for EDS and EMS levitation systems,

- developments of aerodynamic drag coefficients for maglev with numeric examples and discussion of aerodynamic issues related to high speed operation,

- presentation of dynamic modeling methods implemented in this study.

- complete details of the guideway cost estimates shown in Table A.

The report also discusses effects of vehicle length on dynamic performance, the benefits of covering (enclosing) the guideway, the requirements for validating the computer models developed for this study, and the expected variances in future systems from this study's results.

Additional topics for research are also offered.

In Summary

This study offers insights on the nature of increased dynamics that can be expected in high speed maglev systems. The study shows that future vehicle and guideway designs for high speed maglev systems requires detailed dynamic analysis to accomplish cost effective configurations with acceptable ride quality. The guidelines and methodology for executing these designs is unavailable in accepted U.S. standards and criteria. It is therefore important that suitable structural design guidelines for high speed applications are validated early in the development of maglev technology.

Influence of Guideway Flexibility on
Maglev Vehicle /Guideway Dynamic Forces

TABLE OF CONTENTS

Table of Tables

Table of Figures

Symbol Table

Symbol	Meaning	Units	Sections Referenced
q	Dynamic pressure		5.2.5
γ	Gust angle relative to track centerline	degrees	5.2.5, 5.2.4
ρ	Local atmospheric density		5.2.5
ϕ	Magnetic flux		5.1.1.2
μ	Local atmospheric viscosity		5.2.5
ℓ	Span length	m	1.2
β	Relative wind angle		5.2.3
μ_0	Permeability constant of air $= 4\pi x10^{-7}$		5.1.1.2
A_p	Total Pole Area	m^2	Table 5.1.1.2-A
A	Vehicle maximum cross-sectional area	m^2	5.2.5
B	Average field in gap	Tesla	5.1.1.2, Table 5.1.1.2-A
C	Damping Coefficient		Table 5.1.5-A
C_D	Drag Force Coefficient		Figure 5.2.1-1
C_{DW}	Drag Coefficient corrected for L/D		5.2.5.1.1
C_F	Drag Coefficient		5.2.5
C_l	Rolling moment coefficient		5.2.3
C_L	Lift force coefficient		5.2.3
C_m	Pitching moment coefficient		5.2.3
C_n	Yawing moment coefficient		5.2.3
C_0	Constant damping coefficient		5.1.5
C_{PHIP}	Bearing Pad Roll Damping	Newtons-secs/meters	Table 5.3.3-C
CR,CFR	Crossing Frequency Ratio		
C_Y	Side force coefficient		5.2.3
CYP	Bearing Pad Lateral Damping	Newtons-secs/meters	Table 5.3.3-C
CZP	Bearing Pad Vertical Damping	Newtons-secs/meters	Table 5.3.3-C
D	Effective diameter (hydrodynamic)	meters	5.2.5
E_c	Modulus of elasticity	psi	1.2
EI_{xx}	Beam Bending Rigidity	$N\text{-}m^2$	Table 5.3.3-C
EI_{yy}	Beam Bending Rigidity	$N\text{-}m^2$	Table 5.3.3-C
F	Applied Force	Newtons	Table 5.1.2.3-A, 5.1.1.2, 5.1.2.2
f_1	Fundamental natural frequency	Hz or 1/sec	1.2
F_D	Magnetic Drag Force	Newtons	5.1.4, 5.1.2
GK	Beam Torsion Rigidity	$N\text{-}m^2$	Table 5.3.3-C
H	height	meters	Figure 5.2.2-1
I	Current	Amperes	5.1.1.2, 5.1.4
I	Impact Factor		1.2
I_a	Moment of Inertia of uncracked section	m^4	1.2
I_o	Initial Current	Amperes	5.1.1.2
I_{xx}	Moment of Inertia (x-axis)	cm^4	Table 4.2-B
I_{yy}	Moment of Inertia (y-axis)	cm^4	Table 4.2-B
KYP	Bearing Pad Lateral Stiffness	Newton/meters	Table 5.3.3-C
KZP	Bearing Pad Vertical Stiffness	Newton/meters	Table 5.3.3-C
l	length	meters	Figure 5.2.2-1
l_s	Span length		
L	Inductance		5.1.1.2

LL	Live Load, Vertical Standard Vehicle Loads		1.2
L	Total vehicle length	meters	5.2.5
L_S	Span Length	meters	Table 5.3.3-C
M	Mass per unit length of guideway	kg/m	1.2
m	vertical position	meters	Table 5.1.4-B
MS	Mass/Unit Length	kg/m	Table 5.3.3-C
N	Ampere turns		5.1.1.2
NI	Ampere turns in vehicle coil	number	5.1.1.2
NI_0	Design or Nominal Operating, Ampere Turns		Table 5.1.1.1-A
PJS	Beam Mass Moment in Pitch	$kg\text{-}m^2$	Table 5.3.3-C
R	Circuit Resistance	Ohms	5.1.1.2, 5.1.4
RJS	Beam Mass Moment in Roll	$kg\text{-}m^2$	Table 5.3.3-C
S	Vehicle surface area exposed to moving airflow		5.2.5
S_v	Vehicle Motion		Table 5.1.5-A
t	Time	secs	5.1.1.2
v	Velocity	km/h, m/sec	5.1.2, 8.2, 5.1.4
V	Voltage	Volts	5.1.1.2
V_∞	Vehicle track speed	km/h	5.2.4
VCF	Vehicle Crossing Frequency	(no units)	1.2
V_G	Gust Strength		5.2.4
Vo	Initial Voltage, or Nominal operating voltage	Volts	5.1.1.2
V_{true}	Airspeed relative to vehicle	km/h	5.2.4
W	Vehicle Weight	kg	5.1.2.2, Table 5.1.4-B, Table 5.1.2.3-A, 3.3.3
X_{PHIP}	Bearing Pad Roll Stiffness	Newton/meters	Table 5.3.3-C
Z	Normalized Gap		Table 5.1.1.1-A
Z_0	Design Levitation Gap, Nominal Operating Gap	cm, mm	Table 5.1.1.1-A, 5.1.1

Influence of Guideway Flexibility on Maglev Vehicle Guideway Dynamic Forces

1.0 Introduction

1.1 Purpose

This report presents the results of an investigation of the dynamics of aerial guideway structures' interaction with high speed Magnetic Levitated (maglev) Vehicles.

1.2 Background

Maglev is a new technology offering substantially increased speeds with implications for dynamic effects and magnetic effects. Existing U.S. guidelines and practices for designing elevated guideway structures permit their application only to speeds less than 200 km/h and require dynamic analysis above 200 km/h. Guideway designs for maglev will necessarily require understandings of the implications of magnetic fields on design details such as steel and other conductors in the guideways. With elevated guideways expected to be a major feature of maglev systems at something on the order of 60% of the total cost (excluding right-of-way), these pragmatic design concerns become central to the implementation progress of the maglev technology. This study addresses these concerns by simulating maglev operations over several comparative guideways designed to U.S. guidelines. The exercise intends to provide insight into the dynamic interaction that may occur in high speed operation, as well as the consequences in extending existing design guidelines to high speed operation. The cost of Maglev guideways from existing systems and proposed systems are shown in Table 1.2-A along with comparative cost from recent aerial structures constructed for U.S. transit rail transportation. Costs in Table 1.2-A are intended to be comparable values of superstructures and substructures exclusive of other systems and hardware (magnets, signals, traction power, vehicles, etc.) and exclusive of right of way acquisition although the basis of figures could not be fully confirmed.

All accepted U.S. guidelines such as Standard Specifications for Highway Bridges by the American Association of State Transportation Officials (AASHTO) and "Analysis and Design of Reinforced Concrete Guideway Structures", ACI 358.1R-86 by the American Concrete Institute, (ACI) preclude application of their requirements at high speeds (generally above 160 to 200 km/h), without independent dynamic analysis of the designs. The only guideline directly addressing guideway/vehicle dynamic interaction is ACI

TABLE 1.2-A
COST OF CONSTRUCTION PER MILE
(EXCLUDING LAND ACQUISITION)

System	Cost per Mile (Million $)	Cost per km (Million $)	Comment/ (Reference)
Conventional Systems:			
Transit Track Aerial Structure	27	17	Actual (1)
Maglev Systems:			
Japan MLU 00X	36	22	Actual (2)
Japan MLU 001	36	22	Actual (2)
German Transrapid	24	15	Actual (2)
Transrapid Proposals for U.S.			
LA-Las Vegas	6.5-7.7	4-5	Estimated (3)
Chicago-Detroit	9.4	5.8	Estimated (4)
Chicago-St. Louis	9.4	5.8	Estimated (3)
Chicago-Milwaukee	6.0	3.7	Estimated (3)
Boston-NY-Washington, DC (Attractive)	27.2	17	Estimated (5)
Other Proposed Systems			
Boston-NY-Washington, DC (Repulsive)	10.5	6.5	Estimated (6)
*Cable Stayed	4-9	2.5-5.6	Estimated (7)
Magna plane	9	5.5	Estimated (2)
"V" Shape	10	6	Estimated (2)
Inverted "V"	10	6	Estimated (2)
Monorail	16.5	10	Estimated (2)
Box Beam	15-18	9-11	Estimated (2)
Grumman Proposal	8.5	5.3	Estimated (2nd Maglev Symposium)

*Estimate is for non-maglev but believed to be realistic for maglev also.

358.1R-86, para 5.3, which limits the criteria's application to moderate speed (160 km/h and less). The relevant section of the guideline is shown in the following box as information.

FROM ACI 358.IR:

5.3 Transient Loads

5.3.1 Vertical standard vehicle loads *LL*

The vertical live load should consist of the weight of one or more standard vehicles positioned to produce a maximum load effect in the element under consideration. The weight and configuration of the maintenance vehicle are to be considered in the design.

5.3.2 Impact factor *I*

The following dynamic load allowance [5.1] should be applied to the vertical vehicle loads, unless alternative values based on tests or dynamic analysis are approved:

	Rubber-tired vehicles and continuously welded rail	Jointed Rail
For simple-span structures		
$I = \frac{VCF}{f_1} - 0.1$	≥ 0.10	≥ 0.30
For continuous structures		
$I = 1/2 \frac{VCF}{f_1} - 0.1$	≥ 0.10	≥ 0.30

ACI 358.IR Para. 5.3 (Cont'd)

where

$$VCF = \frac{\text{vehicle speed, (m/sec)}}{\text{span length, (m)}}$$

and natural frequency 5.5

$$f_1 = \frac{\pi}{2\ell^2}\sqrt{\frac{E_c I_a}{M}}$$

where

ℓ = span length, (m)

M = mass per unit length of guideway, which includes all the sustained loads the beam carries including its own weight, (kg/m)

E_c = modulus of elasticity, (Pa)

I_a = moment of inertia of uncracked section, (m^4)

The dynamic load allowance should not be applied to footings and piles

From the foregoing excerpt, ACI 358.1R adopts a span crossing speed, VCF, in ratio to the beam natural frequency as an indicator of impact load. The impact factor is similar in formulation to a "crossing frequency ratio" conceived by M.I.T. collaborators [62, 67, 68, 69, 70]. However, M.I.T. uses the crossing frequency ratio as an indicator of speeds that may experience dynamic amplification of beam motion; the crossing frequency ratio contains no information concerning the amount of amplification that will occur. The M.I.T. work states that guideway motion amplifies when the crossing frequency ratio approaches a value of 1, with maximum dynamic deflections for simple spans occurring between values of 1.1 and 1.4, depending on the design. Two-span continuous structures have maximum deflections when the crossing frequency ratio equals approximately 2.0. If extended to speeds above 160 km/h, the impact factor formula stated in ACI 358.1R increases proportionately with speed and guideway length which may result in unnecessarily costly designs.

Criteria for impact factors in the rail transportation industry vary significantly. Values of impact factors currently published for transportation structures are summarized in Figure 1.2-1 [46]. Values from ACI 358.1R are not directly comparable and are therefore not shown in the figure. All values should be considered applicable to speeds less than 160 km/h. Acronyms used in Figure 1.2-1, with the respective references, are:

AASHTO -	"Standard Specifications for Highway Bridges", 11th Edition, American Association of State Highway and Transportation Officials.
ACI-443 -	"Analysis and Design of Reinforced Concrete Bridge Structures" reported by ACI Committee 443, American Concrete Institute.
AREA -	Manual of Recommended Practice, American Railway Engineering Association.
BART -	Bay Area Rapid Transit
BS-116 -	British Standards Institute
CSA-S1 -	Canadian Standards Association
CTA -	Chicago Transit Authority
MARTA -	Metropolitan Atlanta Rapid Transit Authority
TTC -	Toronto Transit Commission
WMATA -	Washington Metropolitan Area Transit Authority

From the comparison of impact factors for speeds less than 160 km/h (Figure 1.2-1), the wide range of values reflects the industry's uncertainty concerning dynamic interactions even at moderate speeds.

Based on concerns that higher speeds available through maglev technology is a more severe, less certain dynamic environment for aerial structures than existing systems, significant efforts have been undertaken to understand the structural dynamics and vehicle interactions of higher speed transit operations. Table 1.2-B summarizes previous dynamic studies, showing parameters contained in each study. The following is a brief review of developments and findings of previous investigators into vehicle/guideway dynamics.

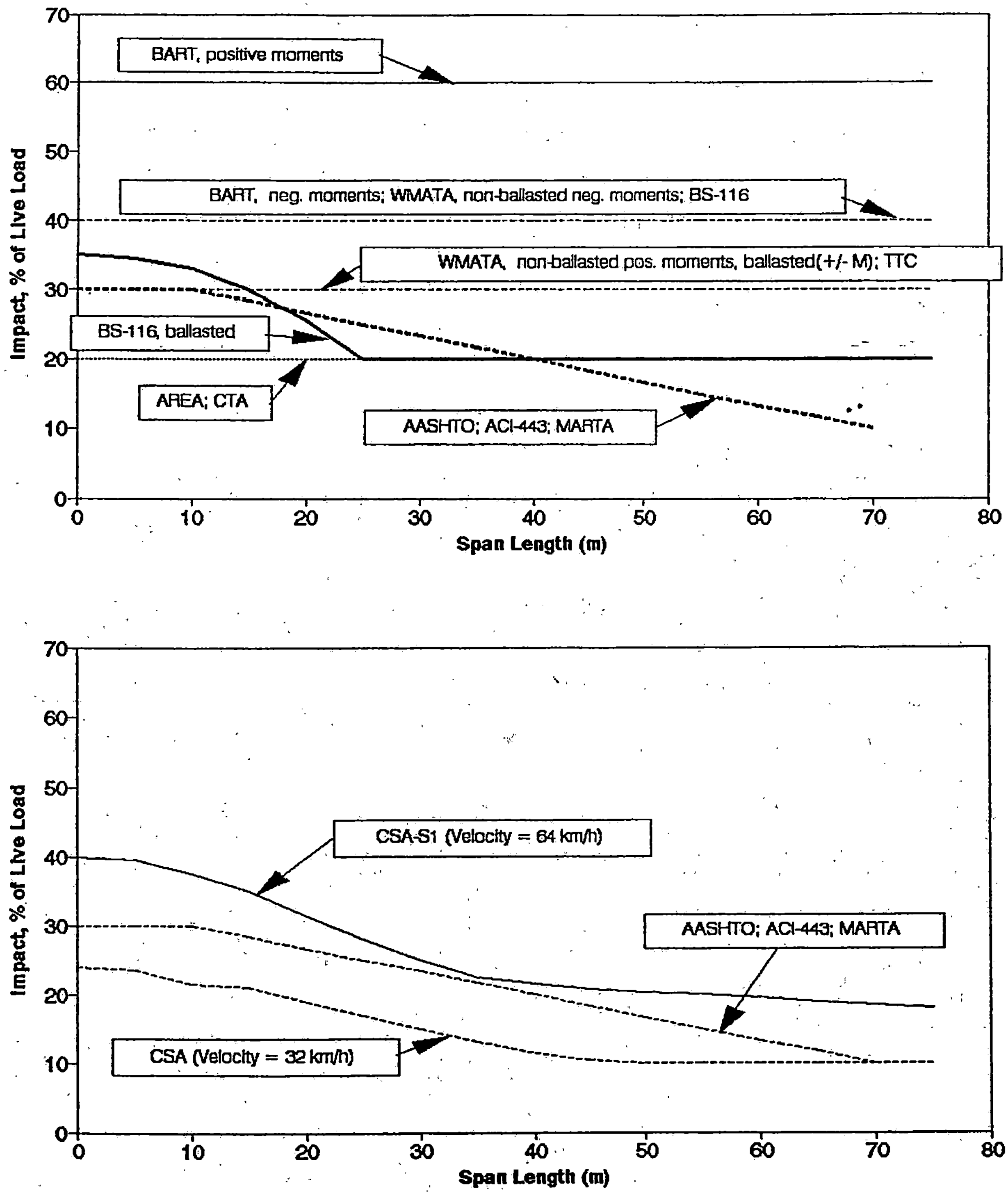

FIGURE 1.2-1 Comparison of Impact Factors

TABLE 1.2-B
Essential Parameter Representations

(Ref.)	Author	Non-Linear Maglev Suspensio	Flexible Guideway	Flexible Vehicle	Multi-Span Guideway/ Multi-Vehicle	Guidance Force & Lateral Response	Guideway Material	Beam End Condition	High Speed	Aero-dynamics
7.	Whitelaw, R.L.		X		X/	X	X	X		
9.	Coffey, et al	X						X		
12.	Kortum, W., Utzt, A.		X			X				
15.	Wilson, J.F.		X					X		
17.	Snyder, J.E., Wormley, D.N.		X		X/					
18.	Chung, Y.I., Genin, J.		X		X/				X	
19.	Cherchas, D.B.	X	X		X/	X			X	
20.	Wilson, J.F., et al		X		X/			X		
21.	Kortum, W., Wormley, D.N.	X	X		X/X					
62.	Smith, C.C., et al		X							
67.	Chin, W.S., Wormley, D.N., Smith, R.C., Richardson, H.H.		X						X	
68.	Wormley, D.N., Nagurka, M.L., Isaacs, G.		X	X	X/			X	X	
70.	Hedrick, J.K., Ravera, R.J., Anderes, J.R.		X	X			X		X	

Early maglev research in 1969, extending into the early 1970's, was part of a growing interest in high speed ground transportation that laid groundwork for advanced systems concepts such as air cushioned vehicles, rocket powered vehicles and linear induction motor propelled vehicles. The most widely quoted maglev work is that performed by Stanford Research Institute (SRI) and Ford Motor Company (Ford Scientific Research Laboratories) between 1971 and 1975. While focusing on the early question of the levitation technology feasibility, these studies advanced to the point that guideway interactions were addressed.

In small scale demonstrations at SRI with a deliberately rigid guideway, vehicle motion with attractive (EMS) maglev suspension was found to be stable when perturbations were as great as 25% of the levitated height.[9] Active damping coils significantly improved ride quality over passive damping. An analytic model provided good correlation with the experimental results with a linear, representation of suspension force vs. deflection. Extension of the model results to full scale was not investigated. Aerodynamic influences were not included.

In 1976, Duke University [9] also evaluated guideway and vehicle interaction dynamics, although their model used an air cushion suspension rather than maglev suspension. Using multiple span models (analytic and experimental), it was found that system resonances occur at the expected natural frequency of the vehicle/guideway system and also at a frequency about half the system's natural frequency. The natural frequency halving generally only occurs in non-linear systems.

More recent work on maglev guideway/vehicle dynamic interaction in other countries [11,12,13] suggests that for a Transrapid-type EMS system:

- Hovering (speed = 0) can create unstable vehicle/guideway interactions when the vehicle and the guideway are independently stable (control systems have since resolved this difficulty).

- Active car body steering improves undesirable vibrations and associated forces.

- Appropriate damping can improve vehicle/guideway dynamic interaction by as much as 50% over non-optimized systems.

- Vertical and lateral stability can be accomplished automatically (in theory) by inclining the guideway - and thereby the reaction magnets - from horizontal (or from vertical for side guidance).

Guideway-vehicle dynamic mathematics models were developed for advanced ground transportation systems parallel to the applied research at Ford, SRI, and Pueblo, Colorado Transportation Test Center. In 1970, Massachusetts Institute of Technology [67] published basic models for vehicle/guideway interaction at high speeds (160 to 180 km/h) for vertical plane motion only. This study found that the ride comfort criteria was the limiting criteria rather than structural strength requirements. Without considering vehicle length or flexure, the study found that maximum vehicle vertical accelerations occured when vehicle suspension frequency is matched to the span passing frequency (train speed/span length) and when, simultaneously, the vehicle-span transit time is equal to half of the span natural period. In other words, stiffer and more massive beams are required to move this combination of parameters above the operating speed range and attention is required to tune the suspension to the guideway. The study noted the resonance range can be quite large, covering a significant portion of the practical higher speed range, depending on various system parameters.

The mid-1970's work on elevated guideway dynamics focused on air-cushioned vehicle levitation. These concepts are formulated on general principles that are useful to maglev systems. Smith et al, [62] concluded that continuous guideways produce lower dynamic reactions than simple span guideways. The importance of span crossing frequency increased as the ratio of speed to span length and beam natural frequency increased above a value of 1.0, for simple spans with notable dynamics occurring in 2-span continuous beams at a ratio of 2.0., where guideway deflections are 5.0 times static deflections. As reported by Chiu [67], passenger comfort requirements governed the design rather than structural or vehicular strength requirements. This work is more realistic than previous efforts, by inclusion of vehicle length and bending properties confirming the importance of vehicle to guideway mass ratios and frequency properties to the system design for high speeds (the study reported results up to 480 km/h). The work in reference [62] is fully developed in reference [69], including the computer code for the analysis. In a confirmation of the foregoing work, Wormley et al [68] produced another computer model focusing on more conventional, lower speed transit systems. The report makes the subtle but important point that guideway damping is highly important but is known only within a range of values, where construction and final material selection affect the actual value. This work is based on point loads for rail vehicles rather than distributed loads in previous studies for air cushion vehicles.

A process for modeling the effects of guideway tolerances is developed by

Hedrick et al [70]. Guideway camber, construction tolerances, post construction deviations (pier settlement) and misalignments are considered for train speeds to 480 km/h. The work includes a full vehicle/guideway parameter set for vertical motion with the vehicle supported on two "cushions". The analysis relations are linear but report that attractive maglev suspensions require retention of nonlinear terms. The report concluded that desired ride quality performance can be achieved by balancing the least costly combinations of surface profile error, pier survey error and camber tolerance error. In 1977, Wormley, Hedrick, et al, and others [65] applied the foregoing methodology to an Automated Guideway Transit System. Also in 1977, the method is expanded by Snyder and Wormley [17].

Agreement was found among authors who evaluated higher-speeds that amplified guideway/vehicle dynamic interaction occur between speeds of approximately 250 and 400 km/h.

Maotoh [47] and Wilson [77] suggest live load dynamic amplification will be negligible if the following two conditions are satisfied:

1. The mass, m_V, of all moving vehicles on any one span length, l_S (the length between consecutive pier supports) must be less than 30 percent of that span's mass, m_S. that is,

$$\frac{m_V}{m_S} < 0.3\ \%$$

2. For a vehicle of constant speed, v, the ratio of the vehicle crossing frequency [CF] (v/l_S or $v/2l_S$, according to whether it is simple span or multispan) to the fundamental guideway frequency, f_S (Hz), in transverse vibration must be less than 0.2. that is,

$$\frac{CF}{f_S} < 0.2$$

[Ref 47, pg 31]

Richardson and Wormley [63] cite a value of 0.25 for the vehicle mass (one car's sprung mass) divided by the beam mass, below which vehicle and guideway motion is theoretically independent.

This background of current structural design guidelines and preceding work conducted on high speed systems is the starting point of the subject of this report. This starting point, in summary, is:

- Existing structural design guidelines do not address higher train speeds anticipated in maglev applications, either explicitly or implicitly.

- Extension of existing published guidelines, specifically, ACI 358.1R, to higher speed applications may lead to overly conservative designs with attendant costs.

- A substantial uncertainty exists for the dynamic load factors that should be applied in design, to existing, slower speed systems, raising concern that higher speed applications will provide even more uncertainty where dynamic interactions between vehicle and guideway are expected to be a more fine balance of system parameters.

- Previous work addressing high speed structures and vehicle interdynamics is reviewed noting proposed findings, models, methodologies and dynamic stability thresholds.

1.3 Order of the Report

This report provides a project description first, followed by the baseline criteria used to develop data for the remainder of the study. The vehicle and guideway structures for this study are then selected and described. The modeling relationships for each discipline are presented, followed by the analytical results from the models. Data on structural costs precedes a discussion of the results. A summary of the principal findings and recommendations for extension of the work complete the report.

2.0 Project Description

2.1 Objective

The primary objective of this study is to investigate the interactive dynamic forces between maglev vehicles and the guideway.

To accomplish this goal, subordinate objectives are:

a. Identify/develop mathematical dynamic model(s) capable of evaluating vehicle/structure interactions for various structure types and different methods of magnetic levitation.

b. Assess the relevance of current design codes and practices for very high speed transportation.

c. Evaluate the need for and relative effectiveness of treatments such as beam support flexibility, secondary vehicle suspensions and design controls for corrosion on materials from maglev physics.

2.2 Project Scope

The scope of this study is to provide a dynamic analysis of the interaction between selected guideway structures and various maglev vehicle systems.

The items of work for this study are:

a. Identify structures and vehicle system configurations for analysis.
b. Identify design criteria for use in evaluating the results of the analysis.
c. Identify/develop relationships and parameter values for the defined structures and systems.
d. Implement analytic computer model(s) for evaluating the interactive dynamics of the chosen systems.
e. Compare the analytic results against the foregoing design criteria.
f. Develop comparative cost estimates for the structures evaluated, incorporating findings from the analytic work.

An intent of the project is to develop simulations of practical systems, in a manner that allow as full an understanding of the maglev technology systems dynamics as possible within budget constraints. To meet this intent, the study includes three dimensional analysis of :

- Multiple vehicle trains operating up to speeds of 800 km/h.

- Simple span and continuous span guideway designs
- Multiple guideway spans
- 2 different guideway span lengths, (21 m and 39 m)
- 6 representative guideway designs
- 2 maglev suspension systems
- Aerodynamics including ranges of wind gusts to 115 km/h

A single vehicle configuration (length, width, weight and body flexure properties) is selected for all combinations of suspensions and guideways.

3.0 Criteria for the Study

3.1 Ride Comfort

Many of the previous investigators cited in section 1 of this report found that ride comfort criteria govern the design more than structural requirements.

Ride comfort criteria establish the upper boundary of acceptable vehicle dynamic response. These criteria also dictate route alignment limits, such as maximum curvature (horizontally and vertically), spiral geometrics and curve superelevation for steady-state operation.

The ride comfort criteria adopted for this study are listed in Table 3.1-A. These are intended to be compatible with Table 3.1-B and Figures 3.1-1 and 3.1-2, from a December, 1991 Ride Quality Workshop at Volpe National Transportation Systems Center. That work shop decided to set 1 hour comfort limits as the design goal.

TABLE 3.1-A
RIDE COMFORT 1 HOUR CRITERIA
(all values are rms)

Maximum Vertical Acceleration -	0.036g (4 to 8 Hz)
Maximum Lateral Acceleration -	0.025g (1 to 2 Hz)

TABLE 3.1-B
RIDE QUALITY CRITERIA
(From: "Ride Quality Workshop")

1. Curving Performance
   Average Value for Event (i.e., Spiral or Curve)

	Design	Min. Req.	Seat/Belt
Lateral Curves			
Bank Roles	24°	30°	45°
Roll Rate	5°/s		10°/s
Lateral	0.1 g	0.16g	0.2g
Roll Accel	15°/s²		
Vertical Curves			
Vertical (UP)	0.05g	0.1g	0.1g
Vertical (DN)	0.2g	0.3g	0.4g
Acceleration and Braking			
Normal	0.16g	0.2g	0.6g
Vector Combinations			
Lat/Long	0.2g	0.3g	0.6g
Lat/Vert	0.2g	0.3g	0.4g
Total	0.24g	0.36g	0.6g

2. JERK (g's /sec filtered at 0.3 Hz.) or JOLT (peak-to-peak g's in 1 sec.)

	Design	Min. Req.	Seat/Belt
Lateral	0.07g/sec	0.25g/sec	0.25g/sec
Vertical	0.1g/sec	0.3g/sec	0.3g/sec
Longitudinal	0.07g/sec	0.25g/sec	0.25g/sec

Other Factors

Temperature	18-23°C
Noise	70-75 dba

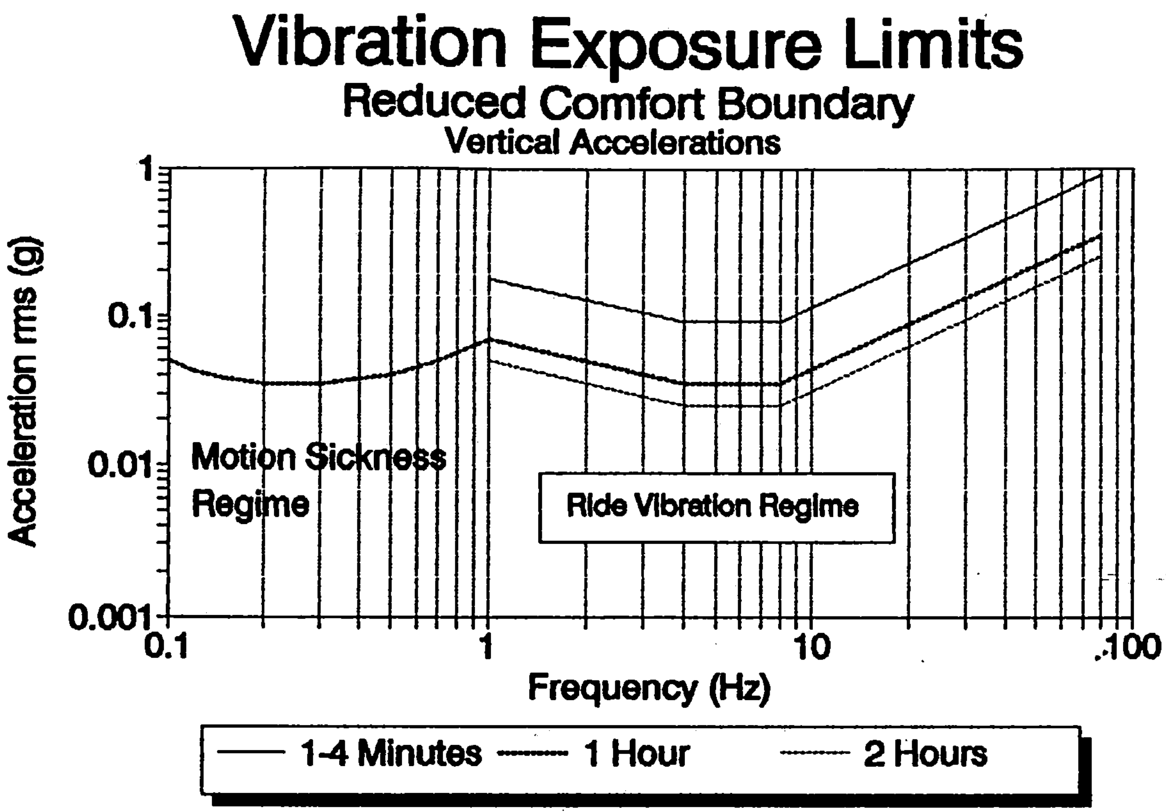

[Ref: ASCC ADV PUB 61/17A (18 AUGUST 1982)]

FIGURE 3.1-1

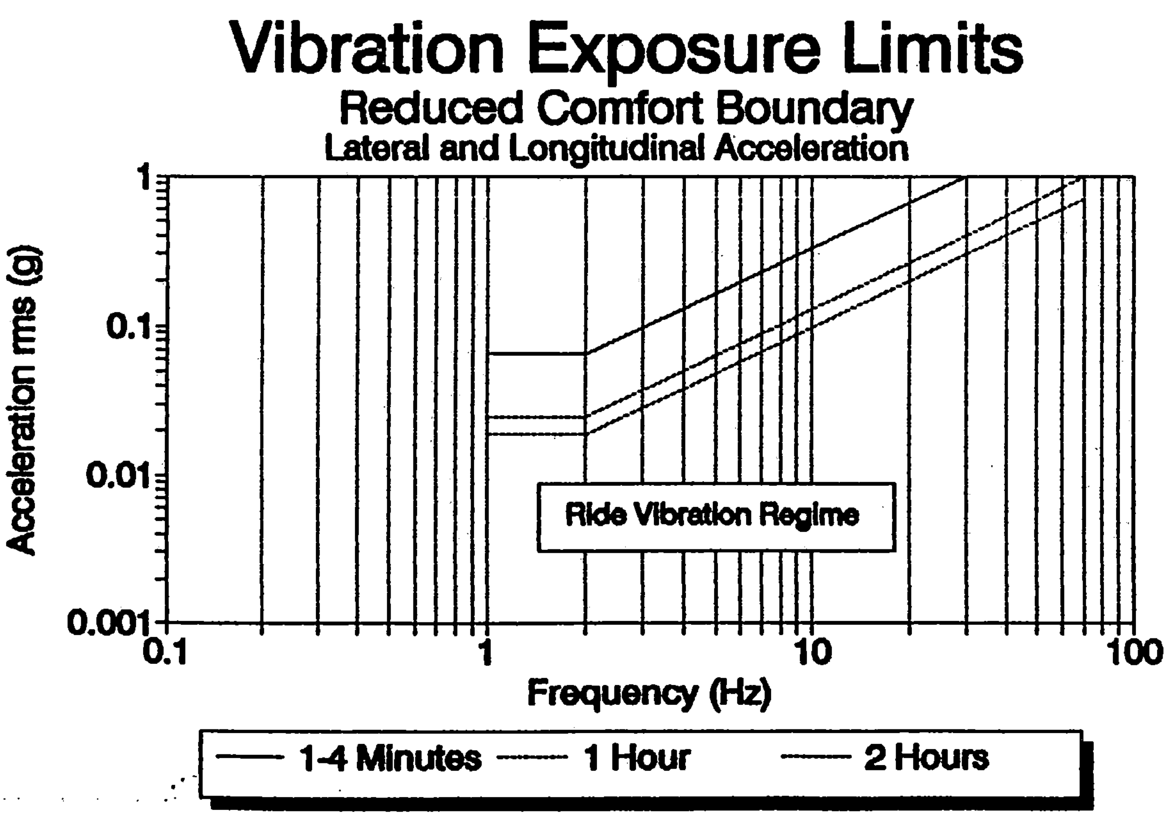

[Ref: ASCC ADV PUB 61/17A (18 AUGUST 1982)]

FIGURE 3.1-2

3.2 Assumed Gross Vehicle Weight.

The gross vehicle weight assumed for this study is 45,359 kg. This value is chosen to be consistent with proposed and prototype operating maglev systems that have the capacity required by BAA 90 Workshop statements. For the comparative purposes of this study, the selected value is similar to the Transrapid system.

3.3 Structural Criterion

The structural criteria for this study uses current industry codes and practices to develop guideway designs.

The relevant structural codes applied to this study and assumed criteria are listed below:

General Codes:

- Standard Specifications for Highway Bridges, 14th edition, 1989, with interim specifications through 1991, American Associations of State Highway and Transportation Officials (AASHTO)

- ACI Manual of Concrete Practice, through 1991, The American Concrete Institute.

3.3.1 Specific Criterion

- System Capacity: 2000 to 12000 seats per hour per train direction.

- Mid-Span Deflection: Maximum Deflection $< \frac{\text{Span}}{1000}$

- Span Lengths: 21m and 39m between piers, continuous spans have the same pier spacing. Span arrangements are illustrated in figure 3.3-1.

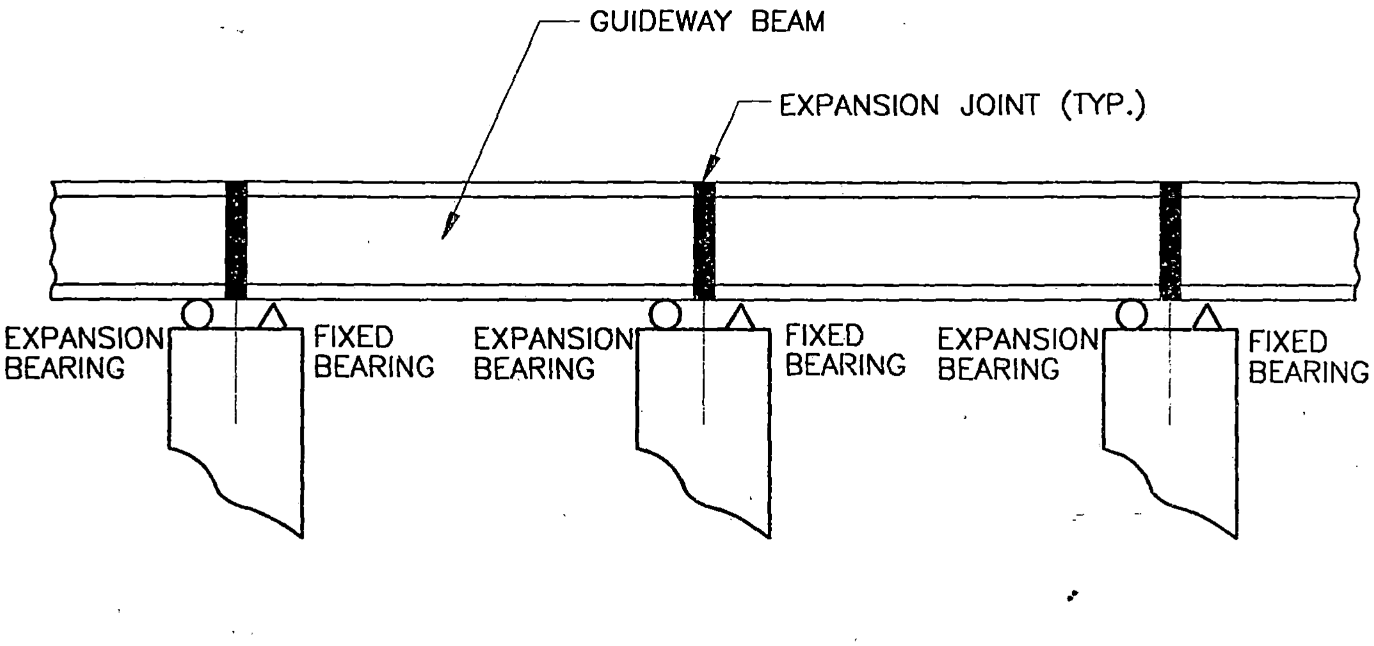

a. SIMPLE SPAN

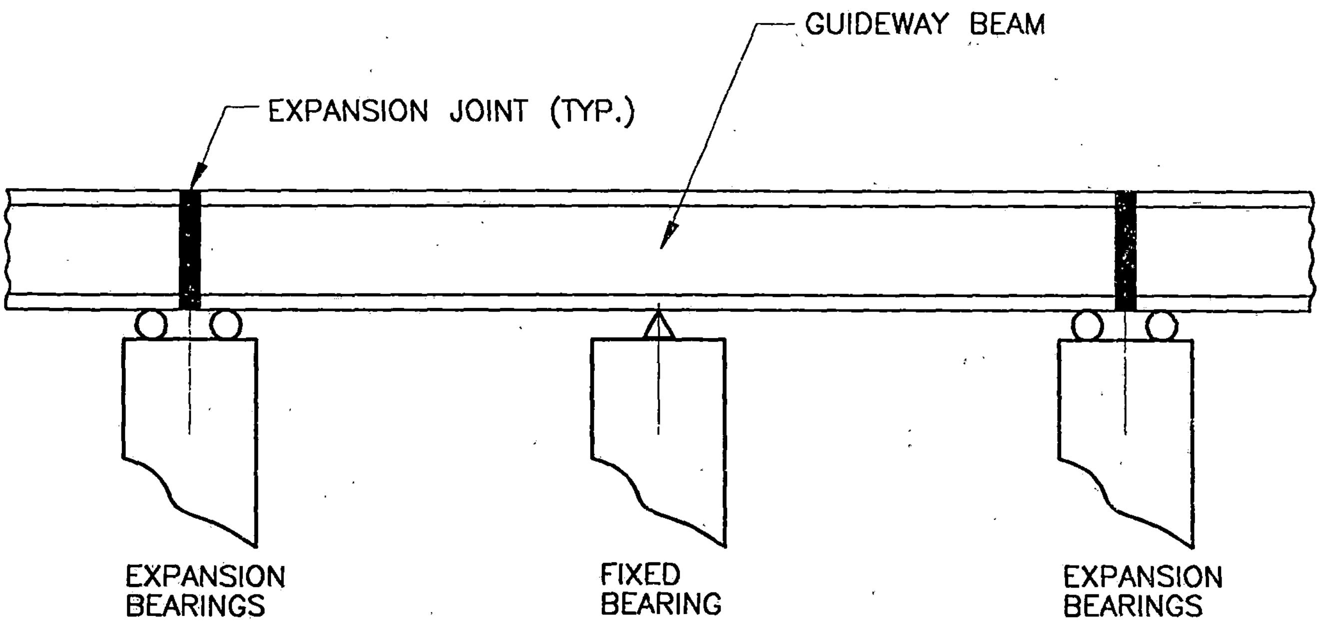

b. TWO SPAN CONTINUOUS

Figure 3.3-1

- Load Assumptions:
    - Multi-car consist
    - Beam design based on concentrated loads
    - Impact - 30% of live load (vehicle weight).
    - Dead loads - Guideway weight.
    - Lateral Loads: 45kN per car.

3.3.2 Explanation of criteria selection

Published Mid-span deflection criteria for bridge applications varies from /900 in Canadian Structural Association guidelines (where is span length) to /64 in American Railway Engineering Association's Manual for Recommended Practice. German Transrapid publications [80] state that the Transrapid structures are designed to /4000 mid-span deflection ratio. The mid-span deflection value of /1000 is chosen for this study to be reasonably consistent with North American practice, while limiting mid-span deflections that will appear as guideway deviations to the vehicle as speeds increase.

Span lengths of 21 and 39m are chosen as representative of a range of typical span lengths.

Simulation of multiple car train consists is required to meet capacity requirements of 12,000 passengers per hour per direction.

The beams are designed with concentrated loads or point loads similar to a rail vehicle. Maglev vehicles have broader load distribution patterns, frequently referred to as "pads". For EDS systems, loads are distributed to the guideway from discrete magnets over a 5m spread. For EMS systems, magnets are mounted along the full length of the vehicle, which is approximately a uniform weight distribution. Because only one set of beam configurations could be designed within project resources, the point load assumption was chosen as approximating the discrete EDS system, promising that the resulting designs would be conservative for the EMS systems' uniform load distribution. Section 8 quantifies the effects on beam design if actual load distributions could have been used in all cases.

While the beams are designed using point loads, the dynamic models use actual load distributions for the levitation supports as appropriate for each system.

Impact load criteria for structural design is chosen as 30% of live load, or 0.3g in acceleration equivalent terms, because it is a conventional value. The uncertainty surrounding choices of impact load criteria is documented in Section 1 of this report. Section 8 of the report contains further discussion of impact factors.

Lateral load criteria was chosen as a single value to represent curving forces and dynamic forces. Wind, earthquake and local conditions are additions to this lateral-force requirement. The value chosen is consistent with other criteria and offers a suitably conservative value for tangent guideway structural design. This lateral load is equivalent to a 0.1g lateral acceleration of the assumed vehicle.

For steady state curving, these criteria require that the guideway cant or bank angle is 5.5 degrees for equilibrium. The following are the allowable minimum curve radii to meet these criteria:

Speed (km/h)	Minimum Curve Radius (m)
160	2,015
320	8,060
480	18,140
640	32,250

An implication in these criteria is that the guideway must provide a path that is relatively free of irregularities. As speed increases, geometry irregularities will have greater effect on dynamic response. It is not reasonable to assume that aerial structure tolerances can be tightened to the degree required by this assumption without great cost. Pier settlement, beam camber changes with time, and beam seasonal changes are all realities that the design must accommodate. The assumption is, therefore, that the reactance coils in the guideway and the guidance elements of the maglev system that are in the guideway have significant adjustment features that are expected to be on the order of 50mm from ideal design. Coils must have a vertical and lateral adjustment capability relative to the guideway's main structure. Section 8.0 provides further discussion of tolerances based on study results.

4.0 Selected Systems

4.1 Vehicle Configuration

This section develops the vehicle parameters for use in the study.

4.1.1 General Guidelines

For this study, guidelines for the vehicle are:

a. Vehicle length, cross section and gross weight are assumed to be the same for all structures to obtain comparable dynamic results for various structures.

b. Interface with existing inner city transit cross sections is adopted as a constraint. The rationale for constraining the vehicle to existing transit cross sections is the inner city access is the most difficult and costly portion of system while it is also the most important to the success of the system in terms of ridership. Assuming maglev technologies are attractive as a full transportation mode of the future including commuter transportation, transforming existing inner city transit facilities to maglev is expected to be cost effective if the configurations can be made compatible.

4.1.2 Vehicle Width and Length

To achieve compatibility with existing corridors, the car must meet clearances of each existing system. Many proposed maglev vehicles are on the order of 33 m long and 5 seats across (~ 3.5 m wide) whereas most existing transit vehicles are generally less than 18 m long and 3 m wide. The length of 18 m is required for compatibility with existing inner city transit routes to maintain mid-chord offsets in curves.

The penalties of a shorter vehicle are a slight increase in per seat cost for construction and maintenance because of the number of equipment unit increases. Benefits include maintenance and operating flexibility because there are more cars for the same number of seats which aids vehicle replacement/redirection.

From a dynamics viewpoint, the 33 m length vehicle will have a car bending natural frequency in the range of 5 to 8 Hz which are the most sensitive frequencies for ride comfort. In comparison, an 18 m vehicle can have natural frequencies between 14 and 18 Hz, which is outside the most sensitive band for human comfort.

The vehicle width of 3.5m is chosen for increased capacity per car, permitting shorter station platforms. Aerodynamic drag will increase approximately proportionate to the added capacity of 20%, although the propulsion power increases non-linearly with increased drag. The 3.5 m width would require some modifications to existing transit routes, such as trimming platform widths by 0.25m. Full compatibility with existing routes can be achieved by using 3m wide, 4 seat across vehicles. The reader is referred to the following information on existing car dimensions and route clearances:

Transit car dimensions	-	Roster of North American Rapid Transit Cars [78]
Freight car dimensions	-	Association of American Railroads Manual of Standards and Recommended Practices, specifically plates B and C of Freight Car Design Data.
Clearances	-	Standard clearance diagrams are obtained from each transit property, or each railroad.

4.1.3 Vehicle Structure

The vehicle illustrated in Figures 4.1.3-1 and 4.1.3-2 is compatible with foregoing rationale and is proposed for this study. In this vehicle the main structural elements are two longitudinal under floor pairs of six inch aluminum I beams providing bending stiffness and longitudinal buckling resistance. The cabin shell has 100 mm aluminum square tubes longitudinally supporting an aluminum skin. Z shape aluminum sections ring the cabin perimeter between the longitudinal square tubes on thirty-eight inch (965 mm) centers to provide torsional restraint.

One version of the vehicle has an 8 Hz vertical bending natural frequency, and a second version has a 15 Hz natural frequency. The 8 Hz vehicle is chosen for this study as being similar dynamically to other proposed maglev vehicles.

Table 4.1.3-A lists the vehicle properties.

TABLE 4.1.3-A
VEHICLE PROPERTIES

	8 Hz Design	15 Hz Design
Width	3.5 m	3.5 m
Length	18.0 m	18.0 m
Moments of Inertia		
Vertical	4.4×10^6 cm^4	4.2×10^6 cm^4
Lateral	4.4×10^6 cm^4	4.4×10^6 cm^4
Polar	8.8×10^6 cm^4	8.6×10^6 cm^4
Natural Bending Freq.		
Vertical	8.3 Hz	14.74 Hz
Lateral	8.3 Hz	15.15 Hz
Weight of Structure	183 kN	55 kN

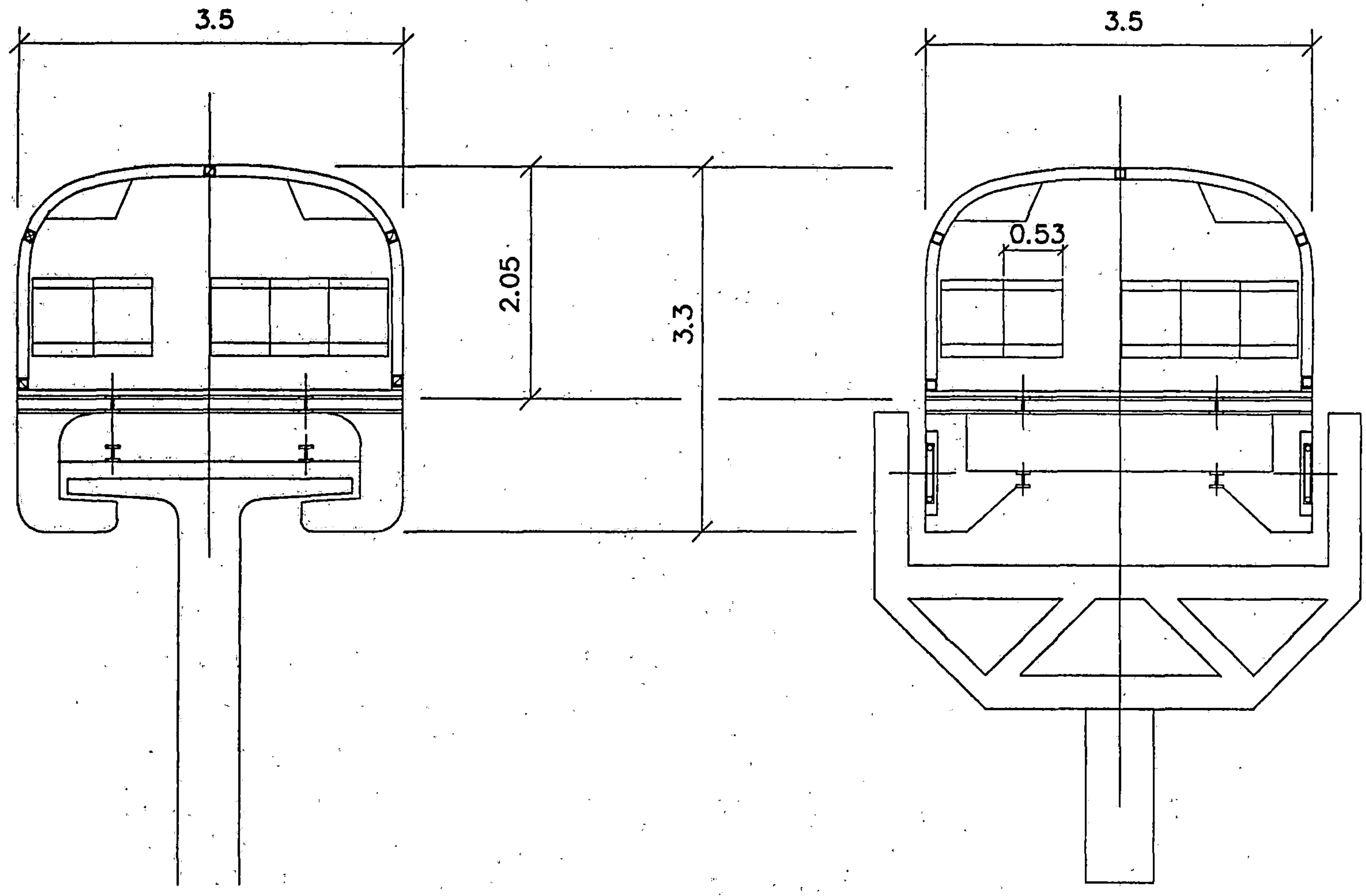

a. EMS (ATTRACTIVE) VEHICLE

b. EDS (REPULSIVE) VEHICLE

Figure 4.1.3-1 Vehicle Typical Cross Sections

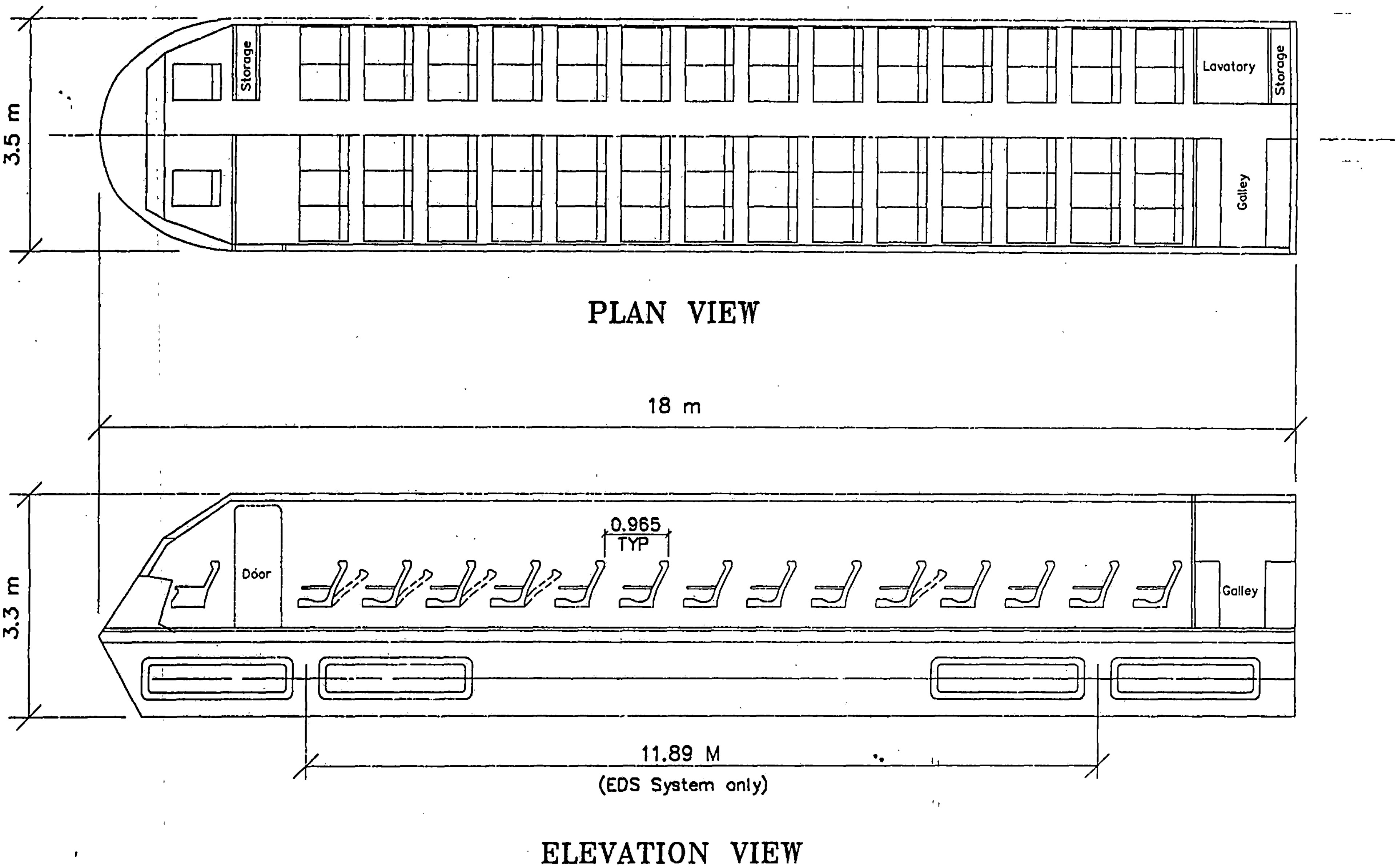

Figure 4.1.3-2 Vehicle Plan and Profile

4.2 Selected Structures

The selection process for structures adopted in this study reviewed possible systems and related structures, then narrowed the field of choices to those which potentially offered a range of performance alternatives.

The initial group of structures that were considered for the study included:

- Existing structures for maglev:
  - German Transrapid
  - Japanese HSST (twin concrete box)
  - Japanese MLU (concrete U-shape)

- Proposed systems:
  - Magnaplane (semi-circular shape)
  - T-Shapes
  - Single central box shapes
  - "Hat" shapes (T shape with box on top for vehicle to straddle)
  - "V" and inverted "V" shapes
  - Suspended vehicle systems
  - Cable stayed structures

Variations on these included incorporating principles from several concepts into one, such as "T" guideways with magnets canted toward guideway center line to provide guidance and levitation from one set of magnets.

Criteria for final selections are:

a. The guideway must have a safe walking surface for inspection, maintenance and patron debarkation in emergencies.

b. The guideway must be reasonably economical.

c. The structures must be inherently compatible with magnet constraints (primarily flux field interference).

d. The structures and the systems as a whole should have reasonable expectations for near term development to prototype or revenue service.

e. The structures selected can be designed and analyzed within the budget of this project. (Cable-stayed structures look promising by construction cost, but are very complex to design and model, which caused this alternative to be dismissed from the study).

f. Several existing systems should be included as reference structures.

h. For this study's purpose only, the structures cross section should have the capability to be adapted to either of the repulsive (EDS) or Attractive (EMS) maglev technologies, except for existing maglev systems, to allow comparison of dynamic performance between the two suspension systems.

The German Transrapid system was selected as the existing system which could be used as a basis of comparison. The German system uses an attractive magnetic levitation technology. The solid steel structures by Transrapid are selected because full dimensional information has been published [80]. The project uses a vehicle of about the same weight, but shorter in length, producing a higher load density, compared to the actual Transrapid prototypes, although the Transrapid has a span deflection/length ratio of $\ell/4000$ compared to $\ell/1000$ for other beams in the study.

The Japanese HSST (EMS) and the MLU Japanese U-shape (EDS) are adopted in concept but the structures are designed by the project team for the candidate vehicle because the Japanese vehicle is much lighter, precluding the comparisons needed by the study.

"V" shapes and inverted "V" shapes are avoided because the concepts require a single set of magnets to provide lift and guidance. These are two separate functions require different control response characteristics.

In the criteria above, a goal is to select structures that will have a range of cost and performance (for study purposes). Steel girders and AASHTO concrete girder beam designs were initially believed to offer lower cost alternatives, while concrete box beams and more aesthetically pleasing trapezoidal box beams would be more costly, as well as more massive.

The girder designs and box beams designs were expected to have weights and bending stiffness values that cover a broad class of structure types and possible permutations such that the broader dynamic experience with these structures is intended to provide insight into most anticipated future structures, regardless of specifics of the design.

The choices for beams in this study are therefore, in separate versions for 21m span and 39m span:

- 4 beams to be designed to U.S. guidelines, convertible to either EMS or EDS maglev configurations.

  - 2 girder designs:
    * Steel Girders
    * AASHTO Concrete Girders

  - 2 Box beam designs:
    * Rectangular Box Beam
    * Trapezoidal Box Beam

- 2 Comparison Beams
  - German Transrapid Steel "V", 24m length only, with EMS maglev
  - HSST Twin Box, modified to the vehicle in this study. HSST is an EMS system, but the study takes some liberties analyzing the beam with both maglev types.

All beam sections, except the Transrapid, are designed to the "preliminary engineering" level of completeness, which is development of concepts to functional dimensions but without refinements associated with site specific requirements. All beams except the Transrapid Beam were designed to the criteria and loadings described in Section 3.0, Criteria for the Study. The Transrapid beam uses published dimensions [80] from which weight and bending stiffness values are calculated by the study.

Structure dimensions are developed only for simple spans. Continuous spans will generally require lighter structures. (See Section 8, Discussion).

The girder and box beam structures are designed to be converted to either maglev system. Structures for EMS have a flat top. Structures for EDS have side walls. The weight of the side walls is included in the total structure weight for both EDS and EMS simulations. The side wall weight and contribution to the structural strength is relatively small compared to the overall structure parameter values without the side walls. The guideway cross sections used in this study are illustrated in Figures 4.2-1 through 4.2-3. Each illustration indicates the dimensions for both 21 m and 39 m span. These structures are described below.

1. Steel Plate Girders

    The structure is a composite steel/concrete structure having built-up steel plate girders and a composite cast-in-place reinforced concrete deck. This design is preferred over the cast-in-place concrete boxes described below for locations with difficult beam delivery circumstances.

2. Concrete Rectangular Single Box

    This option consists of a single box girder of rectangular shape with cantilevered extensions of its upper flange forming the deck slab. The curbs are cast at the edge of the cantilevered slab. The girder is too large to be precast from end to end. It has been conceived as cast-in-place box or as segmental girder where precast short units are joined together and post-tensioned with longitudinal cables.

3. Concrete Trapezoidal Single Box

    This option is similar to the rectangular box girder except it provides shorter cantilevered extensions of the flange forming the deck slab. This box might require internal bracing of its top flange as the top flange gets wider.

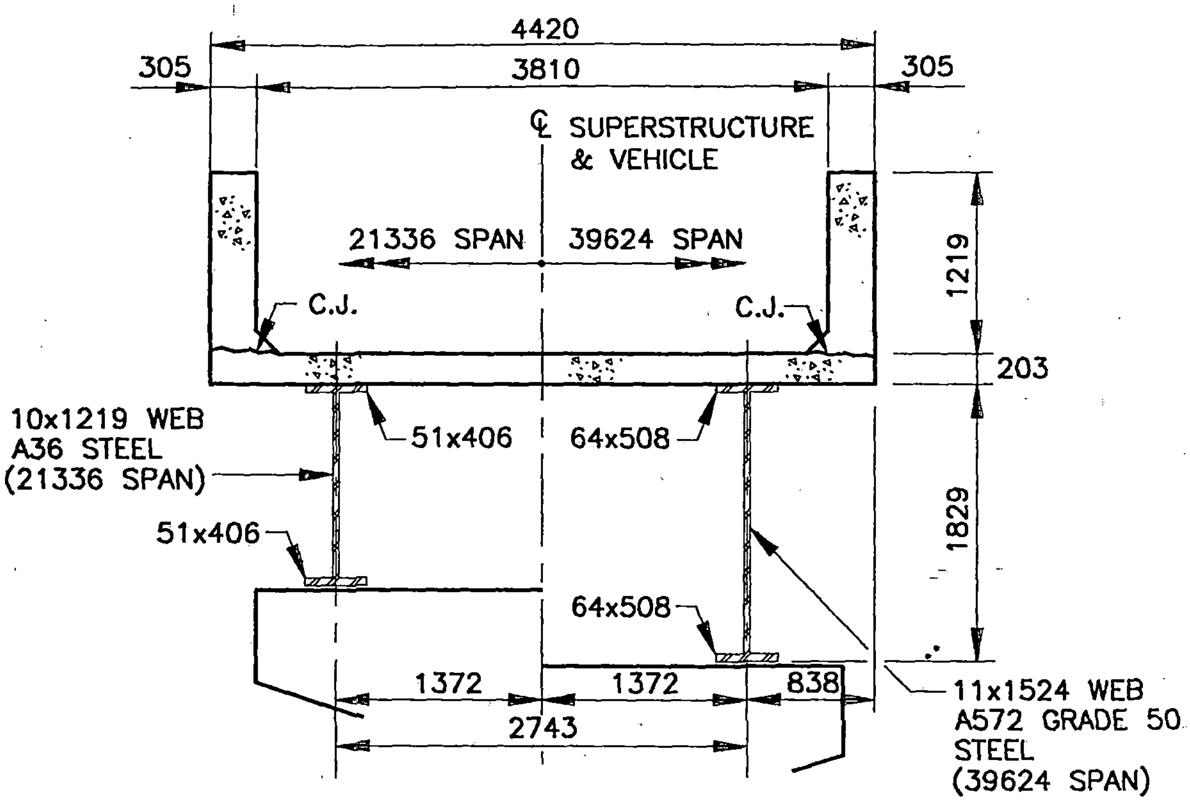

1. STEEL GIRDERS WITH CONCRETE DECK

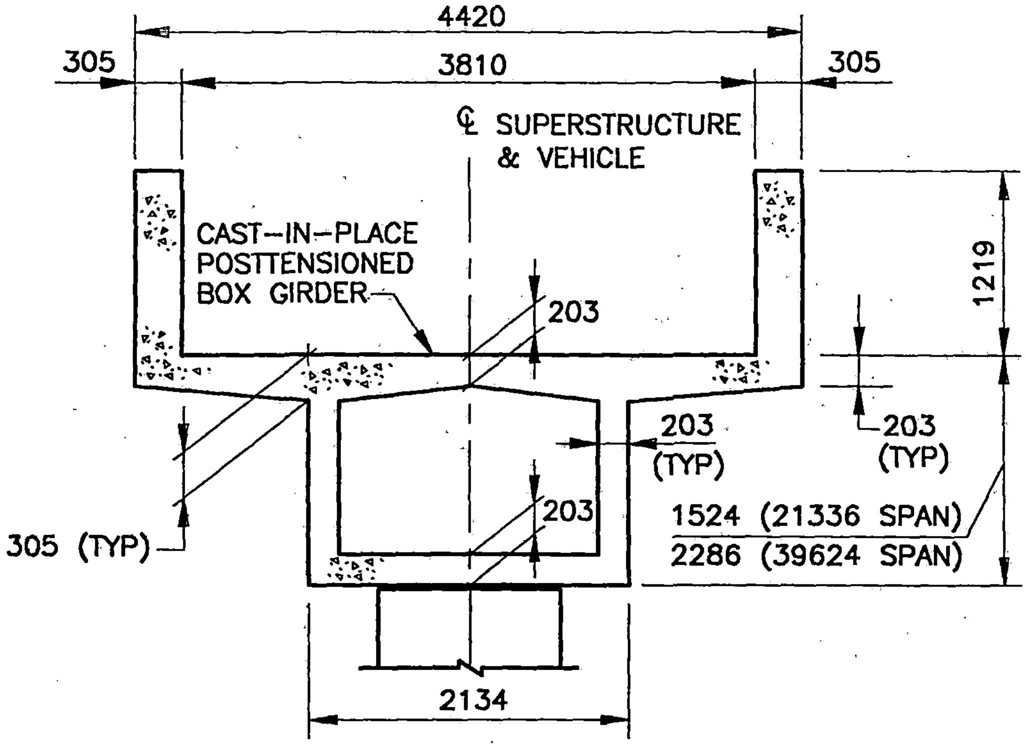

2. BOX BEAM

Figure 4.2-1

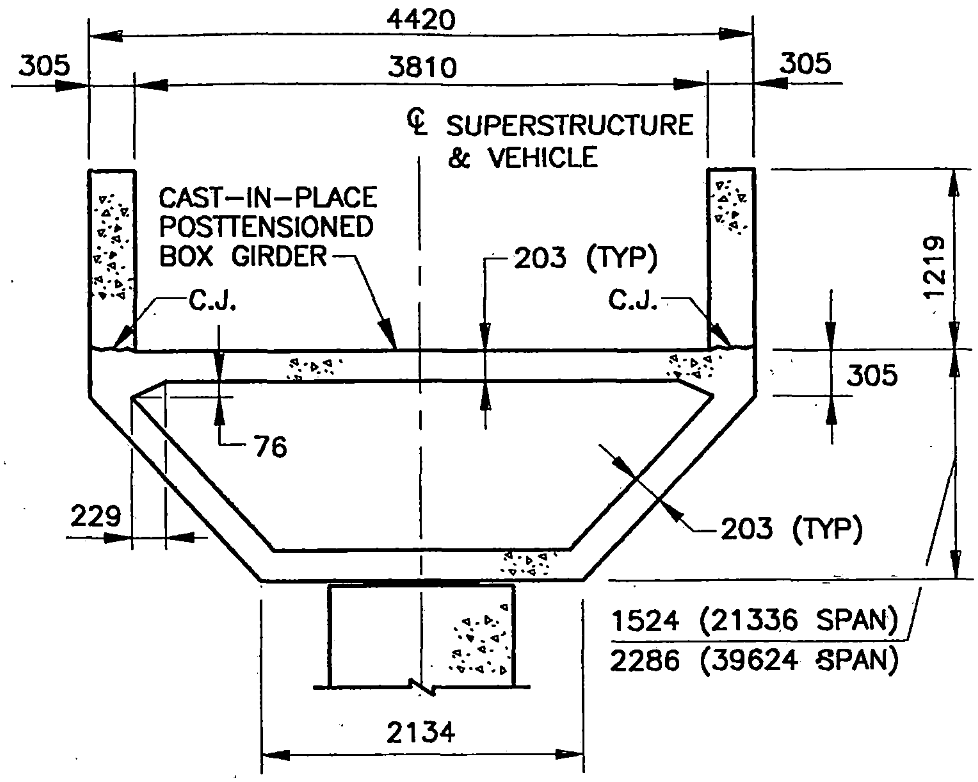

3. TRAPEZOIDAL BOX BEAM

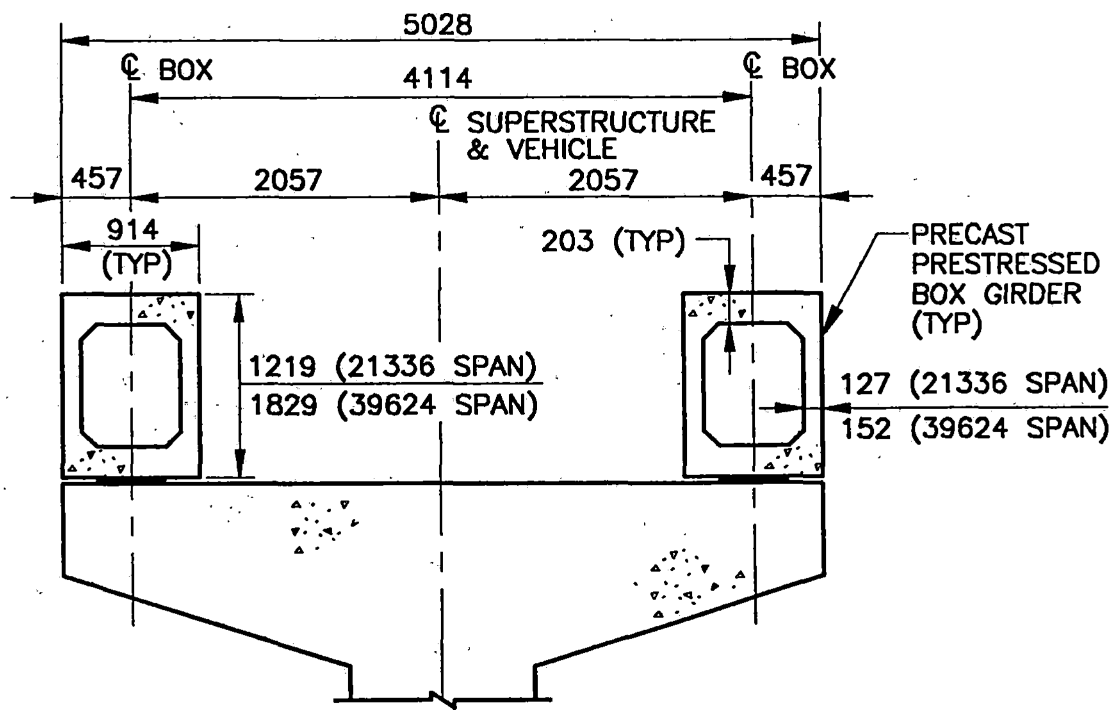

4. TWIN BOX BEAM

REFERENCE: HSST CONFIGURATION

Figure 4.2-2

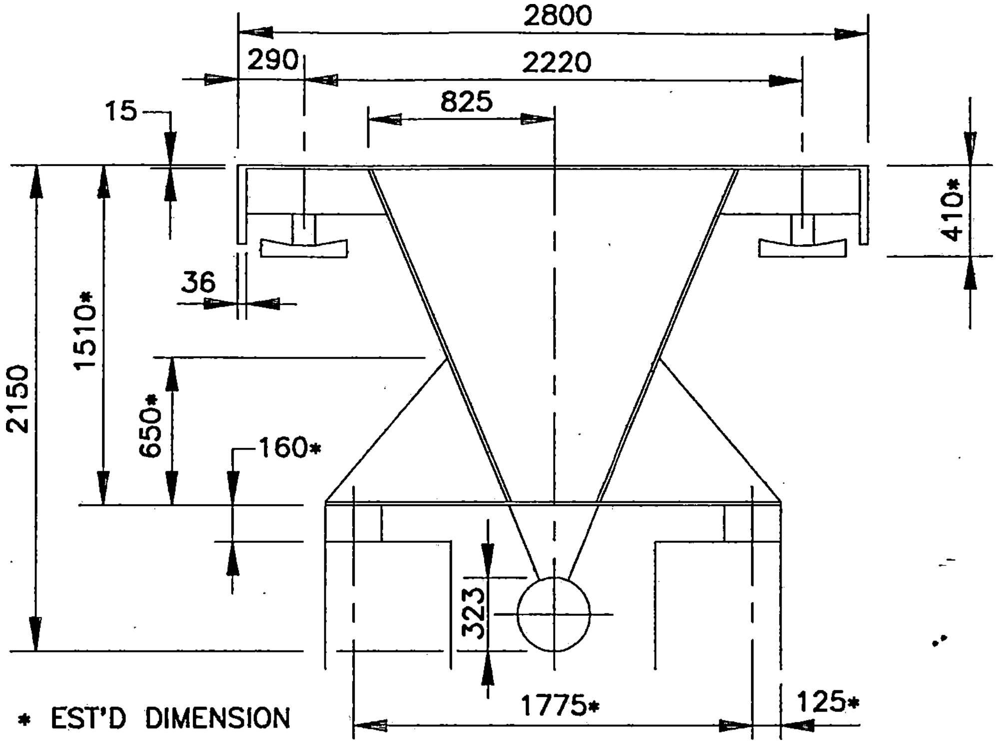

5. TRANSRAPID "V" STEEL BEAM

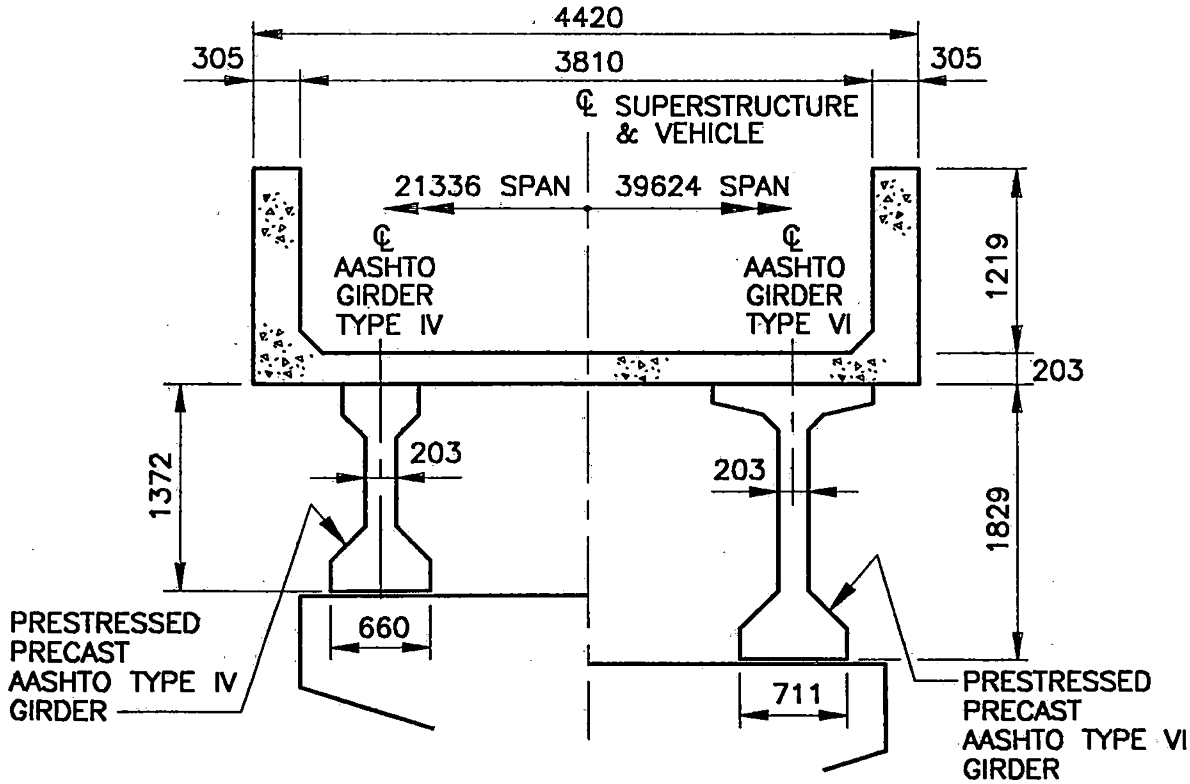

6. AASHTO GIRDER

Figure 4.2-3

4. Two Separate Rectangular Boxes

   (HSST Simulated Structure) The two boxes are placed directly under the vehicle point loads. The boxes have been used as precast prestressed concrete girders. One of the disadvantages to this type of superstructure is controlling the induced upward camber in the box. Since there is not a deck slab, this camber has to be overcome by other means than the opposite dead load deflections. The two boxes cannot be assumed to act together or be made to act together as one superstructure. For the latter reason, this structure arrangement is not recommended for high speed transportation.

5. Transrapid Steel V

   This structure is that illustrated in Figure 5, Transrapid Maglev System, page 28, printed by Hesta-Verlag Darmstadt [80].

6. Standard Concrete AASHTO Girders

   The structure consists of two AASHTO-type prestressed precast concrete girders supporting a cast-in-place composite reinforced concrete deck slab. The girders are placed nine feet apart and rest on hammerhead-type concrete pier. The 21 m spans and the 39 m spans require AASHTO Type IV and Type VI girders, respectively.

Design concerns have been raised that steel elements in the guideway (rebar, steel plates, etc.) will interfere with magnetic flux fields. Please see Section 8 of this report for a complete discussion. The rebar designs have not been analyzed for magnetic flux interference, but it is expected that rebar can be located without significant magnetic field interference or change in beam shapes and properties.

Magnetic field influence on guideway metal corrosion is suggested to be a problem. The beam designs in this study are expected to be fully compatible with any required corrosion control and stray current control requirements.

The final design will include design measures to control stray currents from appropriate design analysis.

The beam properties for the selected structures are listed in Table 4.2-A, Beam Properties. The table provides vertical and lateral moments of inertia, areas, unit weights and modules of elasticity for each beam and span length of 21 m and 39 m. The natural frequencies of each configuration are also calculated. The fundamental natural frequency for each beam is the first mode, mode 1 in the table; the dynamic models include the first four modes of vibration, also shown. Natural frequencies are for simple spans and for continuous beams of equal length. The maximum design moments for each structure for simple spans are listed in Table 4.2-B.

TABLE 4.2-A

BEAM PROPERTIES

Description		Moments of Inertia Ixx (cm^4)	Iyy (cm^4)	X-Sect. Area (cm^2)	Unit Weight (kgf/m)	Mod. of Elast (N/cm^2	Beam Length (m)	Vert. or Lateral	Natural Freq. (Hz.) Mode: 1.0	2.0	3.0	4.0
1 Steel Girders w/ concrete deck	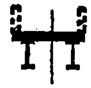	6.82E+06	3.8E+07	2180.6	2976.2	2.0E+07	21.336	Vertical	7.39	29.56	66.51	118.24
								Lateral	17.50	69.98	157.46	279.92
		1.46E+07	4.9E+07	2748.4	3437.5	2.0E+07	39.624	Vertical	2.91	11.65	26.22	46.62
								Lateral	5.35	21.40	48.16	85.61
2 Concrete Box	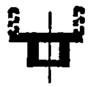	6.05E+07	2.3E+08	19896.7	4776.8	3.0E+06	21.336	Vertical	6.78	27.12	61.02	108.48
								Lateral	13.31	53.26	119.83	213.03
		1.65E+08	2.6E+08	22993.5	5520.9	3.0E+06	39.624	Vertical	3.02	12.06	27.14	48.25
								Lateral	3.81	15.23	34.27	60.92
3 Trapezoidal Box		5.90E+07	2.4E+08	17296.7	4151.8	3.0E+06	21.336	Vertical	7.18	28.72	64.63	114.89
								Lateral	14.53	58.13	130.79	232.52
		1.56E+08	3.1E+08	21019.3	5044.7	3.0E+06	39.624	Vertical	3.07	12.27	27.61	49.08
								Lateral	4.33	17.30	38.93	69.21
4 Twin Box (HSST)		2.17E+07	1.2E+07	11561.3	2767.9	3.0E+06	21.336	Vertical	5.33	21.33	48.00	85.34
								Lateral	3.90	15.62	35.14	62.47
		6.40E+07	1.8E+07	16103.2	3869.1	3.0E+06	39.624	Vertical	2.25	8.98	20.21	35.93
								Lateral	1.19	4.76	10.70	19.02
5 Steel "V" (Transrapid)		3.47E+06	1.1E+07	1450.3	1041.7	2.0E+07	24	Vertical	7.04	28.16	63.36	112.64
								Lateral	12.64	50.55	113.75	202.21
6 AASHTO Concrete Girders	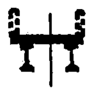	5.24E+07	1.2E+08	17516.1	4598.2	3.0E+06	21.336	Vertical	6.43	25.72	57.86	102.86
								Lateral	9.78	39.13	88.04	156.52
		1.10E+08	1.2E+08	21335.4	5520.9	3.0E+06	39.624	Vertical	2.47	9.86	22.19	39.44
								Lateral	2.62	10.49	23.59	41.94

TABLE 4.2 - B
Maximum Structural Design Forces & Moments

Structure Description	21 m Span			39 m Span		
	Moment Total (kN-m)	Shear-Dead Load (kN)	Shear-Live Load (kN)	Moment Total (kN-m)	Shear-Dead Load (kN)	Shear-Live Load (kN)
1 Steel Girders w/ concrete deck 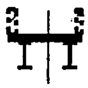	5,732	574	574	17,923	1,139	738
2 Concrete Box 	6,605	752	574	21,921	1,539	738
3 Trapezoidal Box 	6,180	703	574	20,965	1,446	738
4 Twin Box (HSST) 	4,311	320	574	14,675	810	738
5 Steel "V" (Transrapid) 	not avail.	not avail.	not avail.	not avail.	not avail.	not avail.
6 AASHTO Concrete Girders 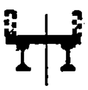	6,372	703	574	21,288	1,477	738

NOTES:

1. **Total Moment = Total Maximum Moment**
   = Sum of Moments from
   Dead Loads + Live Loads + Impact Loads.

2. **Maximum Moments are at Mid-span between piers.**

3. **Maximum Shear Forces are at Piers.**

5.0 Models

5.1 Magnetic Levitation Suspension Characteristics

5.1.1 Characteristics of Attractive Maglev Suspensions (EMS)

5.1.1.1 General

Attractive maglev makes use of the magnetic attractive force that exists between two essentially parallel iron surfaces when a magnetic field is present.

Figure 5.1.1.1 is a simplified block diagram of a one dimensional attractive suspension.

The magnet is suspended under an iron track. When current is supplied to the magnet, an attractive force is generated in a direction that will tend to close the gap between the magnet pole area and the track. The major design parameters relating force generated by coil current to magnetic field, magnet pole area, and ampere turns in the magnet are included in the following Section 5.1.1.2.

An attractive system of this sort is unstable. Controls are necessary for stable operation. Sensors measure the gap between the magnet and the vehicle positions and their rates of change. The feedback from the sensors controls the voltage applied to the coil terminals to appropriately control the coil current and keep the gap constant.

Attractive systems using resistive coils have small gaps typically on the order of 10 mm or slightly less. Super conducting systems are being considered with gaps of the order of 50 mm. These systems are limited by the capacity and reaction time of the power supply.

The attractive magnetic suspension system characteristic is that of a negative spring constant that must be overcome by active control of the coil currents.

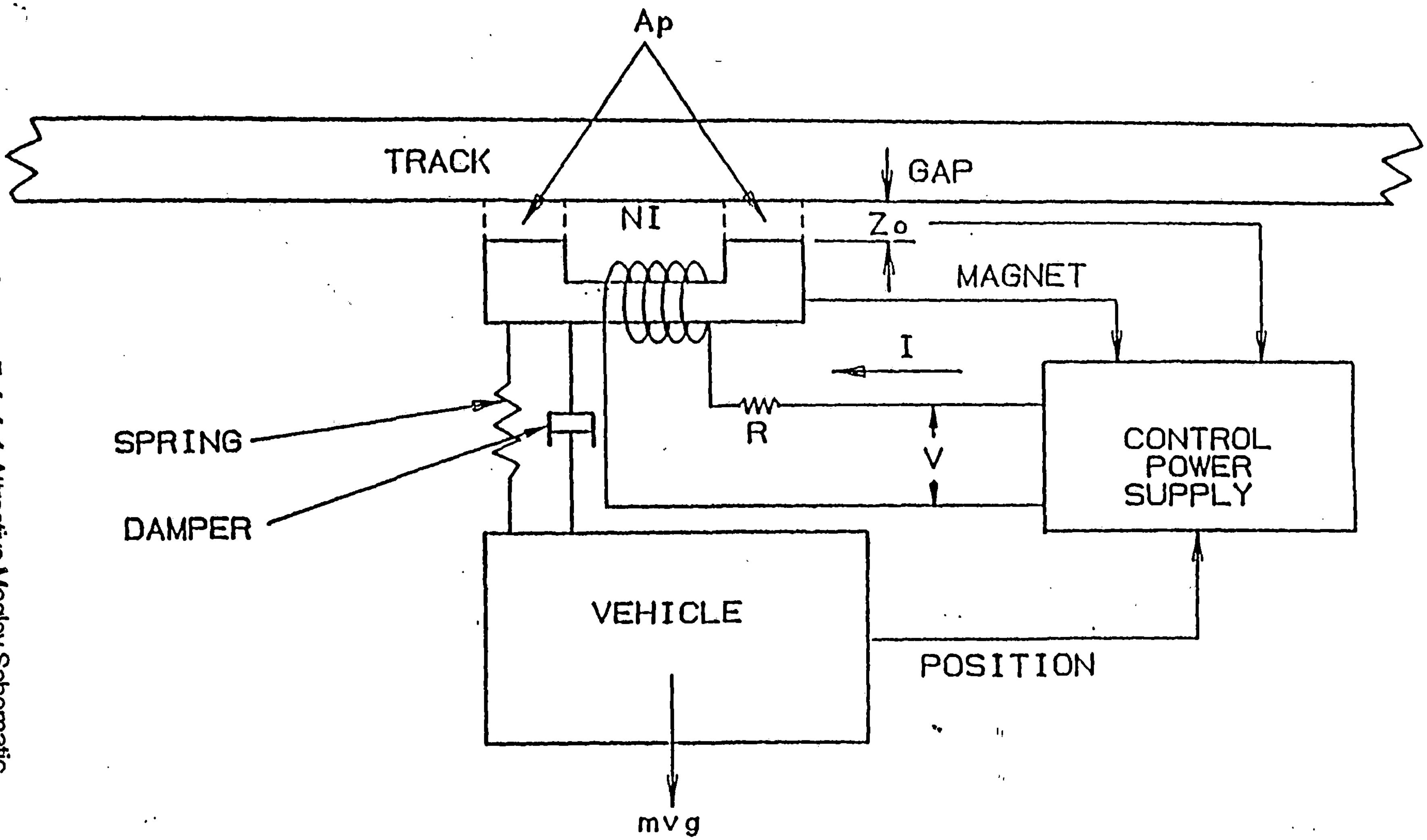

Figure 5.1.1.1 Attractive Maglev Schematic

The following tables represent steady state initial and end conditions. The transient between these depends on the characteristics of the controller and its ability to respond rapidly.

Table 5.1.1.1-A is of normalized force versus normalized gap and current. This table shows that at constant current a force increases rapidly with smaller gaps [a large negative spring constant]. Table 5.1.1.1-B shows force versus gap and control current settings for 36,287 kg and 45,360 kg vehicles with nominal 1 cm gap.

TABLE 5.1.1.1-A
NORMALIZED FORCE FOR ATTRACTIVE SYSTEM

LEVITATION FORCE/VEHICLE WEIGHT

Normalize Gap Z/Zo	Normalized Current (NI/NIo)						
	0.4	0.6	0.8	1	1.2	1.4	1.6
1.6	0.062	0.141	0.250	0.391	0.562	0.766	1.000
1.4	0.082	0.184	0.326	0.510	0.735	1.000	1.306
1.2	0.111	0.250	0.444	0.694	1.000	1.361	1.778
1.00	0.160	0.360	0.640	1.000	1.440	1.960	2.560
0.8	0.250	0.562	1.000	1.562	2.250	3.062	4.000
0.6	0.444	1.000	1.778	2.780	4.000	5.444	7.111
0.4	1.000	2.250	4.000	6.250	9.000	12.250	16.000

This table illustrates the relative forces required in an attractive maglev system. The levitation force is designed to equal the Vehicle Weight for a specified gap, Zo, with a required current, NIo. When the actual current and gap are at the design values, their normalized values are 1.0 (shaded values in the table). The levitation force at the design value also normalizes to 1, equal to the vehicle weight. As the gap changes as a result of dynamics or other external force, the table illustrates how the coil current, the gap, and the force levels change.

Example:
If the gap distance decreases to 40% of the design gap (0.4 in the first column), and the coil current is constant, then the attractive force in the gap is 6.25 times the design force (5th column, bottom row).

TABLE 5.1.1.1-B
LEVITATION FORCE (kN)
ATTRACTIVE (EMS) LEVITATION

GAP (cm)	for Vehicle Weight = 45,360 kgf			for Vehicle Weight = 36,287 kgf		
	Levitation Current (% of design value)			Levitation Current (% of design value)		
	80%	100%	120%	80%	100%	120%
1.2	20.1	31.5	45.4	16.1	25.2	36.3
1.0	29.0	45.4	65.3	23.2	36.3	52.2
0.8	45.4	70.8	102.1	36.3	56.7	81.6

This table is the same as the preceeding table (Table 5.1.1.1-A) using assumed values for the designed gap (= 1.0 cm) and for the vehicle weights. The design values are shaded. The table illustrates the instability of the attractive (EMS) levitation system where changes in gap dimensions generate levitation forces that accentuate the change if no other control is exerted on the magnetic levitation forces.

5.1.1.2 Attractive Maglev Characteristics

In attractive maglev systems, appropriate vehicle parameters are measured and compared with desired values and fed back with suitably adjusted control gains as control voltages to the levitation magnets.

A suitably general model of the system with controls follows.

Pole area is adjusted to provide required lift force:

$$F = B^2 / (2\mu_o) * (A_p) = 2o^2 / (\mu_o A_p) = (\mu_o (NI)^2 A_p) / (8Z_o^2)$$

Where

F = Levitation lift force (N)

B = Average field in gap (Tesla)

A_p = Total face area of poles. (m^2)

$B = \mu_o (NI) / 2Z_o$

$\mu_o = 4 \ \ x\ 10^{-7}$ H/m = permeability constant of air

NI = Ampere turns in vehicle coil

Z_o = Nominal operating gap

Magnetic Flux:

$$\varnothing = (B A_p) / 2 = (\mu_o NI A_p)/(4Z_o) = \sqrt{(\mu_o A_p F)/2}$$

Individual levitation elements, or magnets, will have separate controls. In general, vehicle is suspended by at least four levitation elements (two on each side of vehicle); The German Transrapid System has 7 magnets per side of the vehicle contained in 4 magnet support frames (unsprung masses) where the intermediate magnets share adjacent frames.

The individual control elements are characterized by:

$V \;= iR + L\, di/dt - L\, I_o / Z_o\, dz/dt$

$\quad = IR + (\mu_o N^2 A_p)/(4Z_o)\, di/dt - (\mu_o N^2 I_o A_p)/(4Z_o^2) dz/dt$

For steady state:

$V_o = I_o R$

where:

V	=	voltage
i	=	current (amperes)
R	=	resistance (ohms)
L	=	inductance (Henrys)
I_o	=	nominal or design current to lift vehicle to design elevation, Z_o, with the design voltage, V_o
N	=	number of conductors in coil
ϕ	=	Magnetic Flux (Webers or Tesla -m^2)

Normalizing:

$$V/V_o = i/I_o + (\mu_o N^2 A_p)/(4Z_o R I_o)\, di/dt - (\mu_o N^2 A_p)/(4Z_{o2} R)\, dz/dt$$

$$V/V_o = i/I_o + L/(R I_o)\, di/dt - L/(R Z_o)\, dz/dt$$

Inductance:

$$L = (\mu_o N^2 A_p)/4Z_o = N\phi/I_o = (N/I_o) \sqrt{(\mu_o A_p F)/2}$$

The relationship between individual conductor area, the number of conductors in a coil and the magnetic field is shown in Table 5.1.1.2-A for levitating a vehicle weighing 45,350 kg.

TABLE 5.1.1.2-A

POLE AREA AND AMPERE TURNS REQUIRED TO LEVITATE 45,350 kgf

ATTRACTIVE (EMS) LEVITATION SYSTEM

B (Flux Density)	Ap (Total Pole Area)	Ampere Turns [NI] Required	
		for 5cm GAP	for 10cm GAP
[Tesla]	[sq. m]		
0.1	111.800	7.95	15.90
0.2	28.000	15.90	31.80
0.5	4.470	39.80	79.50
1.0	1.118	79.50	159.00
1.5	0.497	120.00	239.00

The table illustrates the design trade-offs between magnet power and magnet dimensions that are required to achieve the flux densities to carry the design load in attractive (EMS) levitation systems.

5.1.2 Characteristics of Superconducting Repulsive (EDS) Maglev Suspension

5.1.2.1 General

Repulsive systems use superconducting coils on the vehicle. As the vehicle moves over appropriately configured conductors in the guideway, currents are induced providing levitation and guidance forces.

The simplest configuration is shown in Figure 5.1.2.1-1, which has the coils on the bottom of the vehicle. The guideway could be made up of individual coils, continuous conducting sheets, or ladder-like continuous strips under each vehicle conductor with periodic cross connections.

An exact 3D solution is possible once vehicle and guideway conductors are specified; however, a two-dimensional model was assumed to be representative for purposes of determining vehicle and guideway dynamics.

The resistance of the track coils or sheets is an important design parameter. Due to electrical resistance, the induced track currents decay with time. For higher vehicle speeds, this decay is small. Increasing the conductor area allows higher currents but decreases the electrical resistance while increasing the time for the currents to decay as well as increasing cost. Conductor cross-sectional area also influences the system damping coefficients which occurs from track coil resistance.

For super conducting coils on the vehicle and resistive conductors in the track, conductor cross section determines the magnetic drag force, an additional force in the direction of motion that must be overcome by the propulsion system.

5.1.2.2 Approach

In order to allow some generality in the results, the following approach was taken for each configuration:

a) A two-dimensional analysis of each configuration was carried out.

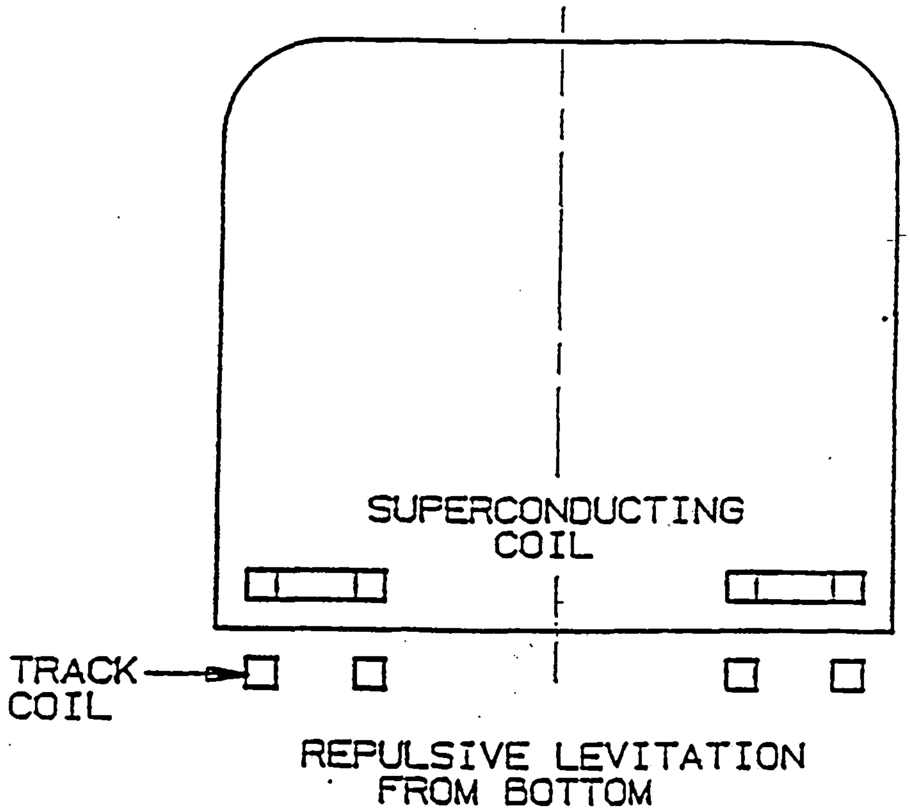

Figure 5.1.2.1-1 Repulsive Levitation from Bottom

b) Track currents and normalized forces versus position were computed assuming high speed or small decay of track currents.

c) Forces per unit length for the various configurations were then used to provide forces versus relative vehicle position (deflection) for actual vehicle weights.

d) Magnetic drag, damping were computed assuming negligible decay of track currents.

Table 5.1.2.2-A shows the levitation force as a function of distance from the center of the vehicle coil to the center of the track current for the configuration shown in Figure 5.1.2.1-1.

The table assumes a nominal center to center distance of 0.2m. For this center to center distance, a physical separation (gap) of 0.1m from the vehicle surface to the track coil surface results. The +/- .06m variation presented in the table represents a dynamic physical gap variation from .04m to .16m.

This table is a vehicle supported from below with vehicle and track coils in the horizontal plane. If the force is interpreted as force normal to the coil plane, the table is valid for coils with tilted guideways at any angle.

The table shows three sets of forces versus center to center distances. These were all computed using a conductor to conductor distance of 0.5m for both the vehicle and track coils. The first set is normalized with respect to the nominal force, F, = vehicle weight, W at a separation of 0.2m. This increases to F=2.03W at 0.14m and decreases to F=.548W at 0.26m.

The difference in load ($\triangle$F/W) divided by the difference in separation $\triangle$h(m) is also shown in the table.

Scaling to any nominal value is appropriate to deal with a single magnet or the whole vehicle.

Also shown are forces and effective spring constants for nominal loads of 45,360 kg and 36,287 kg.

TABLE 5.1.2.2-A

EQUIVALENT SPRING RATE (Force vs. Deflection)
SIMPLE REPULSION (EDS)

[Nominal Center to Center Distance = 0.2m]

	Magnet Center to Center Distance [Note 1] (cm)	Normalized Force [Note 2] F/W	For 45,360 kg Vehicle: Levitation Force [Note 3] (kN)	For 45,360 kg Vehicle: Equivalent Spring Rate [Note 4] (kN/cm)	For 36,287 kg Vehicle: Levitation Force [Note 3] (kN)	For 36,287 kg Vehicle: Equivalent Spring Rate [Note 4] (kN/cm)
	14.00	2.03	903.0		722.5	
				102.3		81.9
	16.00	1.57	698.4		558.8	
				71.2		56.9
	18.00	1.25	556.0		444.9	
				55.6		44.5
Design ->	20.00	1.00	444.8		355.9	
				42.0		33.6
	22.00	0.811	360.8		288.6	
				32.7		26.2
	24.00	0.664	295.4		236.3	
				25.8		20.6
	26.00	0.548	243.8		195.0	

NOTES:

1. **Center to Center Distance is the distance between the vehicle and track coil centers. The actual levitated distance or height is the center to center distance minus half the thickness of the track and vehicle coils, which may total 10 to 12 cm.**

2. **Normalized Force: Levitating Force, F, divided by the Vehicle Weight, W.**

3. **Levitation Force required to suspend the vehicle at the center to center distance shown, where the design center to center height is 20 cm.**

4. **Equivalent Spring Rate is the force/deflection characteristic of the magnetic suspension that is analogous to a mechanical spring.**

5.1.2.3 Null Flux Levitation

Levitation of the vehicle from underneath makes use of simple repulsion. In this case, vehicle coils and guidance coils are essentially lined up facing each other with forces normal to the plane of the coils. In contrast, null flux levitation on the vehicle sides (see Figure 5.1.2.3-1) makes use of the fact that when coils are offset, forces parallel to the coil plane are also generated. The null flux configuration in Figure 5.1.2.3-1 is being used by the Japanese, and makes use of figure-eight shaped coils in the guideway.

When the vehicle coil is centered vertically with respect to the figure-eight magnet shape, there is no current flow because the flux induced in the upper half is equal and opposite to the lower half. As the vehicle coil moves away from the center of the figure eight shape, current flows in the coil generating vertical levitation forces (guidance forces are also generated).

Table 5.1.2.3-A presents the force versus distance (effective spring rate) for a system with center to center distance of 0.2m, with vehicle and track conductor bundles spaced 0.5m apart. Three sets of numbers are presented: normalized with respect to a general normalized (non-dimensional) vehicle weight, W and for W = 445 kN and W = 356 kN.

The force is zero when centered vertically and reaches a peak value at 0.2m vertical displacement. This peak is set to 2W for the computations, meaning that at a maximum dynamic load of 2W the deflections are at the extreme of the magnet geometries.

If the maximum deflection is exceeded, the vehicle will drop out of the magnetic suspension field (and crash). This behavior is quite different from the simple repulsion where the force continues to grow with displacement.

Because no currents flow unless vertical lift is required, the resistive losses and magnetic drag is considerably lower for a configuration of this type.

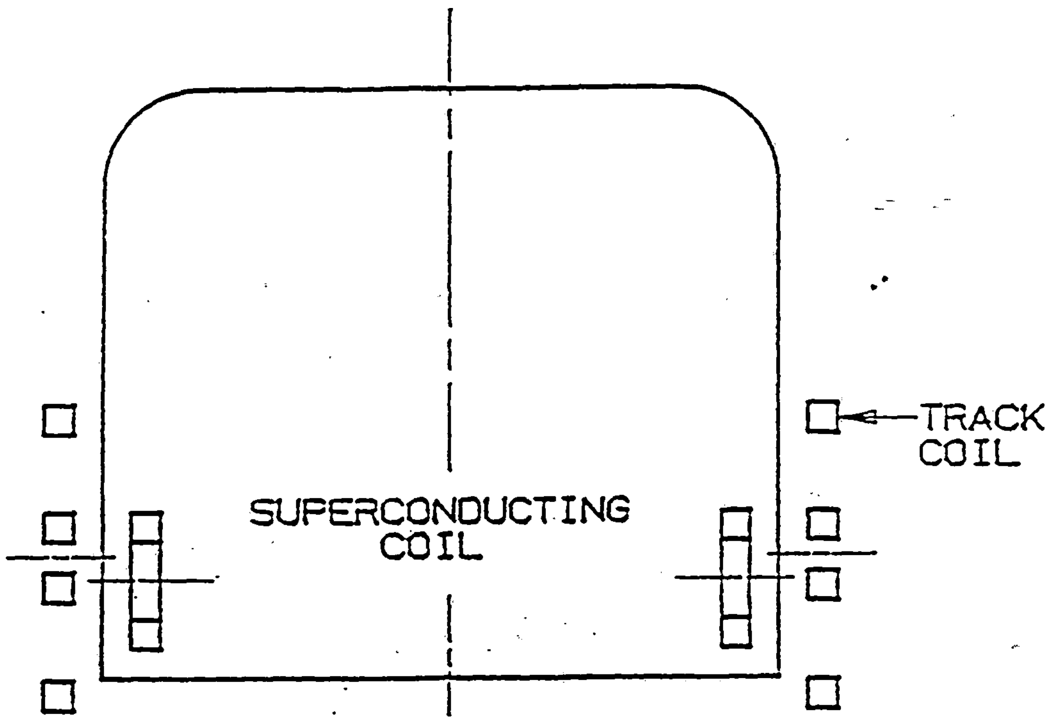

Figure 5.1.2.3-1 Null Flux Levitation Figure "8" Shaped Track Coils

TABLE 5.1.2.3-A

EQUIVALENT SPRING RATE (Force vs. Deflection)
NULL FLUX LEVITATION (EDS)

[Nominal Center to Center Distance = 0.2m]

		For 45,360 kg Vehicle		For 36,287 kg Vehicle	
Relative Vertical Position	Normalized Force	Levitation Force	Equivalent Spring Rate	Levitation Force	Equivalent Spring Rate
[Note 1] (cm)	[Note 2] F/W	[Note 3] (kN)	[Note 4] (kN/cm)	[Note 3] (kN)	[Note 4] (kN/cm)
0	0	0		0.0	
			72.9		58.4
5.00	0.82	365		292	
			72.9		58.4
10.00	1.64	729		584	
			32.0		25.6
15.00	2.00	890		712	
20.00	1.70	756		605	
25.00	0.72	320		256	

NOTES:

1. **Relative vertical position is the distance the vehicle is displaced vertically from the center, or null position, of the track's figure-eight coils. For this example, a load of twice the vehicle weight is arbitrarily assummed to cause a displacement of 15 cm from the null position.**

2. **Normalized Force: Levitating Force, F, divided by the Vehicle Weight, W.**

3. **Levitation Force required to suspend the vehicle at the displaced position shown in column 1.**

4. **Equivalent Spring Rate is the force/deflection characteristic of the magnetic suspension that is analogous to a mechanical spring. Note that the vehicle "falls out" of the magnetic field once the maximum displacement is exceeded, and there is no longer a levitation suspension and therefore no spring rate.**

5.1.3 Lateral Guidance

A lateral guidance system is shown in Figure 5.1.3-1.

In operation, track coils on each side of the guideway keep the vehicle positioned in the center. The basic operation is very similar to simple repulsive levitation (Figure 5.1.2.1-1). Table 5.1.2.2-A applies to this case, also.

When centered, equal repulsive forces exist on each side and there is no net force. If the vehicle moves laterally, the repulsive force on the side with the smaller gap increases and the force on the side with the larger gap decreases. The net effect is a lateral restoring force.

Table 5.1.3-A shows the guidance force per unit length for displacement from 0 to -0.06 m. For a practical system with 0.10 m physical gap, lateral motion of 0.04 m under non-emergency conditions is probably an upper limit and is so indicated on the table.

The computed values of normalized guidance force/per unit length are presented in the second column of the table.

The guidance design will generally select a total magnet length and ampere turns in order to achieve the proper guidance force for each vehicle.

For illustrative purposes, the table also shows the nominal restoring forces at 0.04 m lateral displacement of 5,000 to 50,000 lbs. While the force at 0.02 m is not exactly one half of the 0.04 m value, a constant spring is a good approximation.

One of the disadvantages of a simple guidance system is that the next guidance force is produced by opposing two large forces. In the central position, large currents produce large forces with no net force - a very inefficient condition.

A more efficient approach to guidance is shown in Figure 5.1.3-2. Track coils on each side of the guideway are connected in series opposition. If the vehicle is centered, no net current flows. With the vehicle offset laterally, the same magnitude of current now flows on both sides resulting in repulsion on one side and attraction of the other. In addition to the currents being lower, the forces are more equally distributed on both sides of the vehicle.

The null flux system does reduce the load per unit length so that larger coils or more ampere turns are required to achieve the same lateral restoring force as the simple repulsive lateral guidance.

The scaled characteristics of forces versus distance presented in Table 5.1.3-A are also valid for the null flux case.

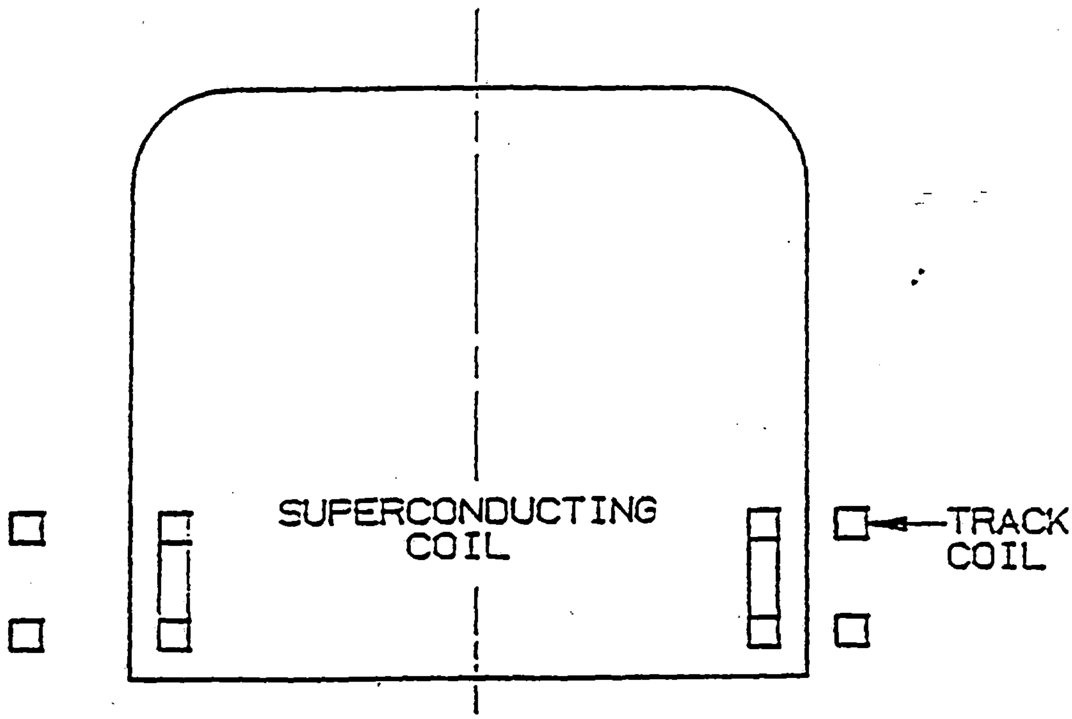

Figure 5.1.3-1 Lateral Repulsive Guidance

TABLE 5.1.3-A

LATERAL GUIDANCE FORCE

Lateral Displacement from Center Position [Note 1] (cm)	Normalized Force [Note 2]	Design Lateral Force @ 4 cm Lateral Displacement [Note 5]					
		22,241 N		44,482 N		88,964 N	
		Magnetic Force [Note 3] (kN)	Equivalent Spring Rate [Note 4] (kN/cm)	Magnetic Force [Note 3] (kN)	Equivalent Spring Rate [Note 4] (kN/cm)	Magnetic Force [Note 3] (kN)	Equivalent Spring Rate [Note 4] (kN/cm)
0	0	0.0		0.0		0.0	
			5.3		10.6		21.1
2.00	0.3955	10.6		21.2		42.3	
			5.8		11.6		23.4
4.00	0.8287	22.2		44.5		89.0	
			8.1		16.2		32.2
6.00	1.4351	38.5		77.0		153.5	

Notes:

1. **This table provides lateral spring equivalents for the guidance magnets assuming the lateral allowable displacement from a central position is about 4 cm. The table also assumes the maximum lateral force imposed by the vehicle at the 4 cm displacement (see Note 5).**

2. **Normalized force: Imposed force from the vehicle per unitlength of the magnet divided by the force produced by the coil. The force produced by the vehicle will comply with the relation**

   Magnetic guidance force = (4*pi*10^-7)*(Coil Current^2)

3. **Magnetic Force: Force produced by magnetic coils.**

4. **Equivalent Spring Rate: Lateral force/deflection characteristic of the magnetic field that is analogous to a mechanical spring.**

5. **The table assumes a maximum imposed force from the vehicle due to curving or dynamics. The coil design would in practice be designed to produce the force shown for the design displacement. From this, the proper lateral spring constant can be derived, as illustrated in this table**

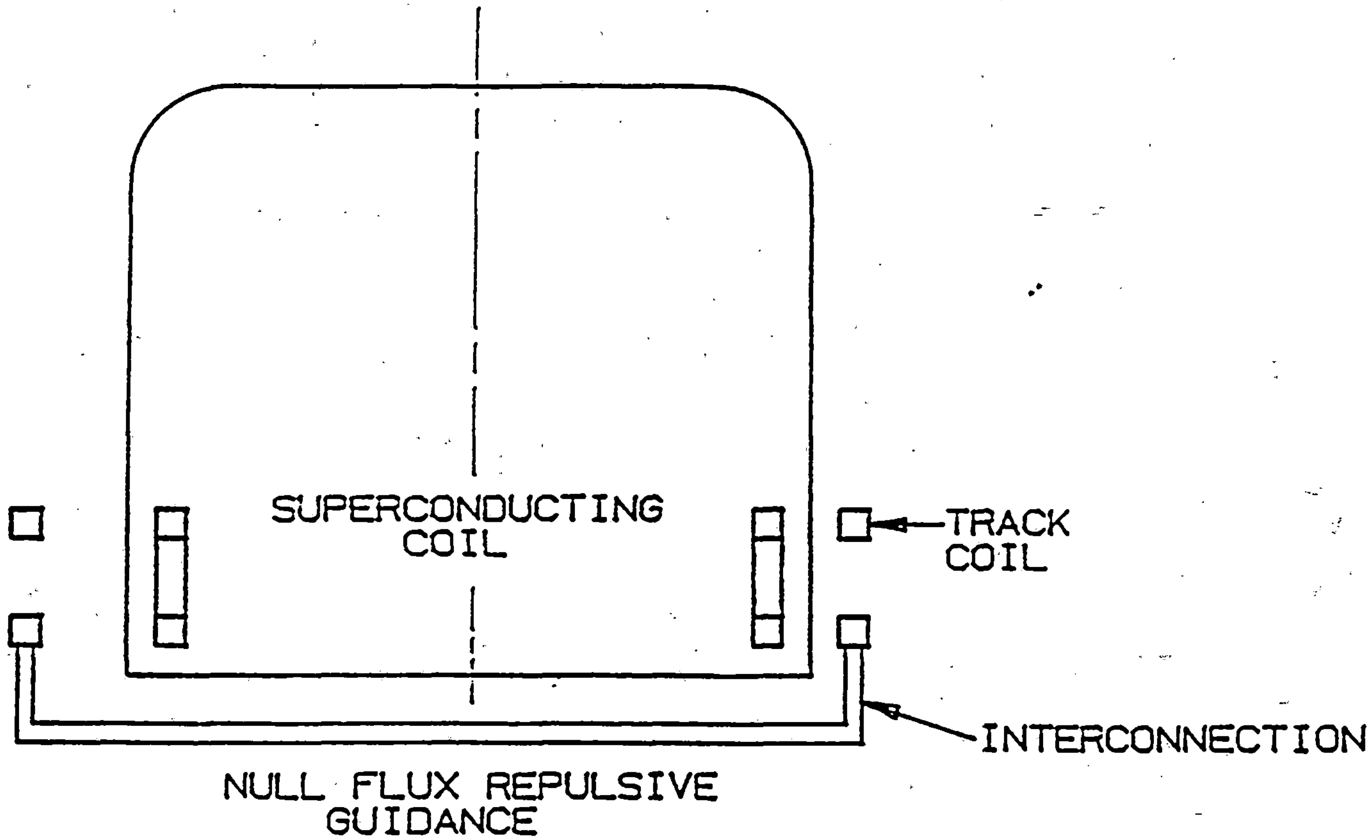

Figure 5.1.3-2 Null Flux Repulsive Guidance

5.1.4 Magnetic Drag

In a system consisting of super conducting coil and track conductors only, the only dissipation of energy is the resistive losses in track conductors. These lead to a magnetic drag force that must be supplied by the propulsion system. Magnetic damping of vehicle motion also is directly dependent on the resistive losses in the track conductors. If track conductors had zero resistance, there would be no magnetic drag and no magnetic damping of vehicle motion. The magnetic drag and damping are related effects.

In a two-dimensional model of the system, track currents can be computed assuming negligible current decay while the vehicle is passing by (high speed limit). For a given configuration of track conductors, the resistive power can be computed. Because at the high speed limit the track current is independent of speed, the resistive losses are also independent of speed and appear as a magnetic drag.

Because at high speed the resistive power is independent of speed, the magnetic drag force FD times the velocity v is also constant:

$F_D * v = I^2 R$; Magnetic Drag Power

$F_D = I^2 R/v$; Magnetic Drag Force

This leads to the conclusion that at high speeds, magnetic drag power is independent of speed and magnetic drag force varies as 1/v. These are valid at all speeds where current decay is small, and current fully penetrates track conductors.

The magnetic drag power and forces are presented in two tables (Table 5.1.4-A and -B) for 45,360 kg and 36,287 kg vehicles for the various configurations of maglev.

The simple suspension results in magnetic drag power of about 1.1 MW for a 45,360 kg vehicle. An 36,287 kg vehicle has proportionately lower magnetic drag power of 0.88 MW in the same track.

The magnetic drag force corresponding to speed of 161 to 483 km/h is also presented in the table. The null flux figure-eight side levitation system uses considerably lower power than the simple supported configuration for the same vehicle weight.

Two sided simple guidance has magnetic drag power of 0.521 MW (at 0.04m displacement), compared with 0.039 MW at the same force and displacement for a null flux guidance system. This clearly illustrates the higher effectiveness of the null flux approach.

TABLE 5.1.4-A

MAGNETIC DRAG CHARACTERISTICS

EDS, Simple Suspension
[Nominal Center to Center Coil Distance = 20 cm]

	Vertical Displacement from Null Position (cm)	Magnetic Drag Power (MW)		Magnetic Drag Force (kN)					
		Vehicle Weight							
		45,359 kgf	36,287 kgf	Vehicle Wt = 45,359 kgf			Vehicle Wt = 36,287 kgf		
				161 km/hr	322 km/hr	483 km/hr	161 km/hr	322 km/hr	483 km/hr
Simple Susp. .2m center to center		1.106	0.885	25	12	8	20	10	7
Two sided Guidance	2	0.408	0.326	9	5	3	7	4	2
	4	0.521	0.417	12	6	4	9	5	3
	6	0.571	0.457	13	6	4	10	5	3
Null Flux Two sided Guidance	2	0.0096	0.0077	0.21	0.11	0.07	0.17	0.08	0.06
	4	0.039	0.031	0.88	0.44	0.29	0.70	0.35	0.24
	6	0.092	0.074	2.06	1.03	0.69	1.65	0.82	0.55

* Guidance adjusted for 0.2g at .04m

TABLE 5.1.4-B

MAGNETIC DRAG CHARACTERISTICS
(NULL FLUX LEVITATION)

Vertical Displcmnt from Null Position [Note 1]	Drag Power (MW)		Magnetic Drag Force (kN)					
	Vehicle Weight		Vehicle Wt = 45,359 kgf			Vehicle Wt = 36,287 kgf		
(cm)	45,359 kgf	36,287 kgf	161 km/hr	322 km/hr	483 km/hr	161 km/hr	322 km/hr	483 km/hr
5.00	0.194	0.155	4.3	2.2	1.4	3.5	1.7	1.2
10.00	0.881	0.705	19.7	9.9	6.6	15.8	7.9	5.3
15.00	1.820	1.460	40.8	20.4	13.6	32.6	16.3	10.9

Notes:

1. **Vertical position is relative to the vertical center, or null, position of the track's figure-eight coils. There is no drag at the null position for the Null Flux levitation technique.**

2. **The table is constructed assuming the design of the magnetic levitation system will accomodate twice the vehicle weight and the coil geometry will produce the required levitation force at 15 cm displacement of the vehicle from the null position.**

5.1.5 Damping

As discussed in the previous sections, magnetic damping of vehicle motion is a result of resistive losses in track conductors and is related to magnetic drag power.

The estimated damping coefficients presented in Table 5.1.5-4 make use of the magnetic drag power and the decay time constant of the track currents. The basic character of the damping is a constant damping coefficient C_0 at low frequencies. At higher frequencies, the damping coefficient decreases as the square of the frequency. This high frequency characteristic results in constant damping power for a fixed amplitude of oscillation.

TABLE 5.1.5-A
ESTIMATED DAMPING COEFFICIENT

	Co [sec/m]
Levitation Simple Propulsion	179000
Null Flux Side Levitation	700000
Simple Guidance	15000
Null Flux Guidance	200000

NOTES:

1. **Damping is determined from power loss. Power loss is a result of track resistance. Vehicle motion, Sv, is assumed to be sinusoidal, where a damping constant can be determined from the average power.**

   Motion = Sv = [Delta Sv]*e^(j*Omega*t)
   Velocity = V = j*Omega*[Delta Sv]*e^(j*Omega*t)
   Force = C*V = C*j*Omega*[Delta Sv]*e^(j*Omega*t)
   Power = Force[F] * Velocity[V] = C * V^2
   Average Power = 1/2 (C*[Delta Sv]^2 *Omega^2)

   where [Delta Sv] = vehicle displacement from the nominal position (m)
   Omega = Frequency of oscillation of motion (Hz)
   e = exponential constant = 2.7182818
   j = square root of (-1)
   t = time (sec)

2. **Damping Coefficients, C, are calculated using the above table values for Co, a coefficient determined by track coil geometries, and the following relation:**

   C = Co/(1+0.0413*Omega^2)
   Co = a constant related to track coil configuration (N^2/Omega)
   0.0413 is a time constant for track coils, which is dependent on conductor size.

5.2 Aerodynamics

5.2.1 General

This section presents the aerodynamics characteristics of a candidate maglev vehicle. The vehicle modeled is a generic, two-car maglev configuration, with separate aerodynamic expressions developed for repulsive (EDS) and attractive (EMS) suspension systems, since the guideway clearance for each suspension system differs. Quasi-steady force and moment coefficient functions of vehicle speed and wind gust are developed. While these results are configuration specific, the representations are sufficiently general for tailoring to other maglev vehicles. The representations of the aerodynamic characteristics are formulated to facilitate use within the maglev vehicle/guideway dynamic models by Battelle.

Assuming vehicle velocities ranging to 800 km/h, definition of the aerodynamic forces on the vehicle is of paramount importance. As shown in Figure 5.2.1-1, vehicle power required for steady travel increases with the square of the velocity. Wind gusts up to 115 km/h are assumed at random incidence angles to the vehicle trajectory. Extremely strict tolerances on the distance between the train bottom and the guideway surface at these high speeds require a vehicle both low in aerodynamic drag and highly resistant to buffeting effects in crosswind. From these constraints and the additional size limitations provided by Battelle and Parsons Brinckerhoff Quade & Douglas, the following vehicle evolved.

5.2.2 Vehicle Description

The vehicle under study (please refer to Section 4.1) is a symmetric, two-car magnetically levitated train, with each car having a length (L) of 18 meters, width (w) of 3.5 meters, and height between 3.3 and 4 meters (Figure 5.2.2-1).

The vehicle is assumed to have an ellipsoidal nose cone of axis ratio 3:1 oblate parallel to the guideway surface. Two types of levitation are under study, attractive and repulsive suspension, which yield slightly different cross-sections (Figure 5.2.2-2).

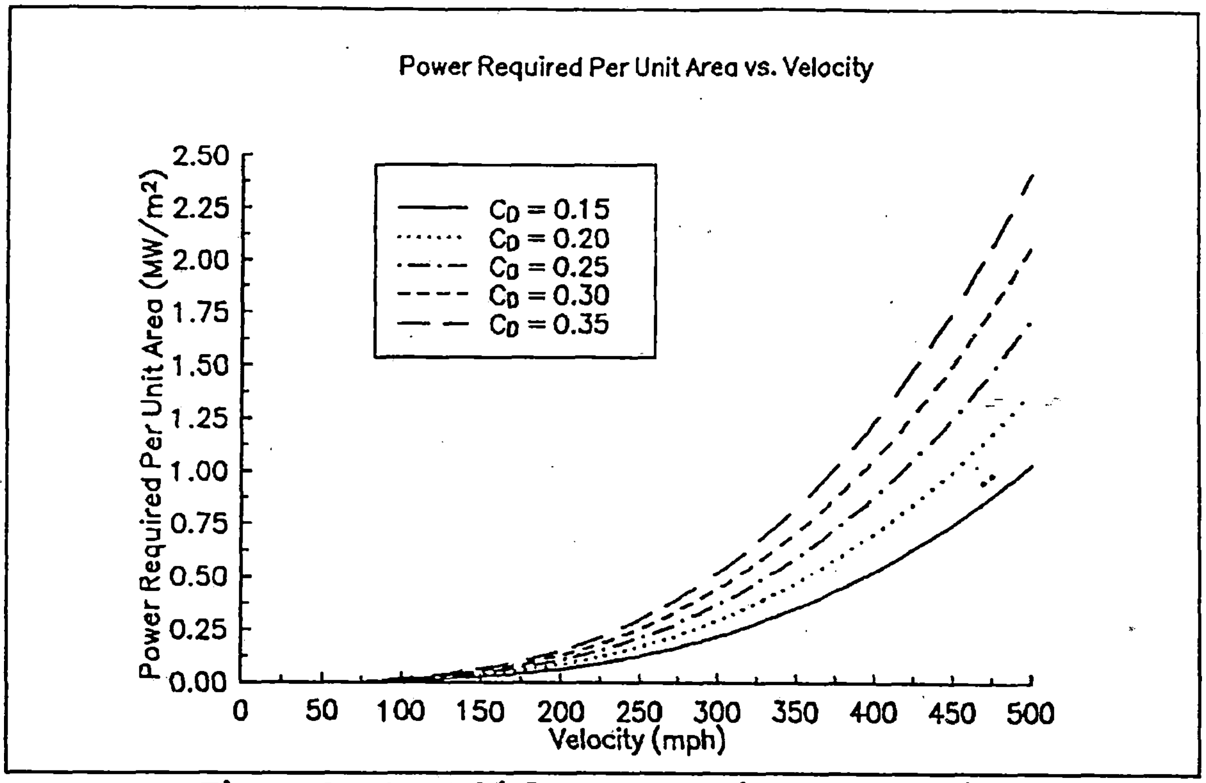

Figure 5.2.1-1 Vehicle Power Required vs. Velocity

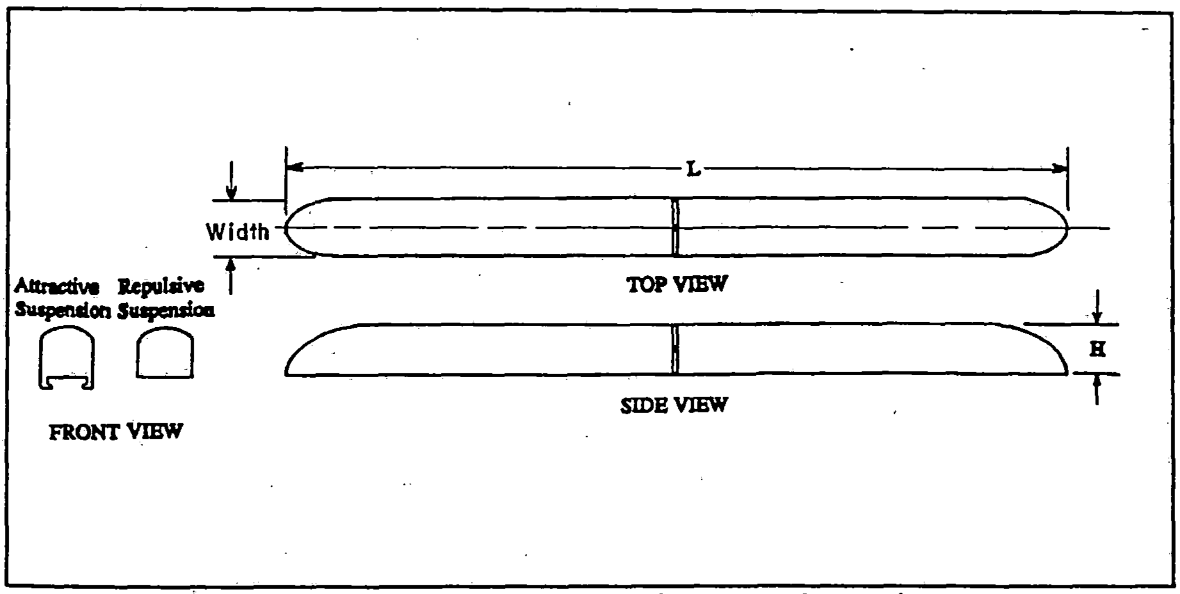

Figure 5.2.2-1 MAGLEV Vehicle Configuration

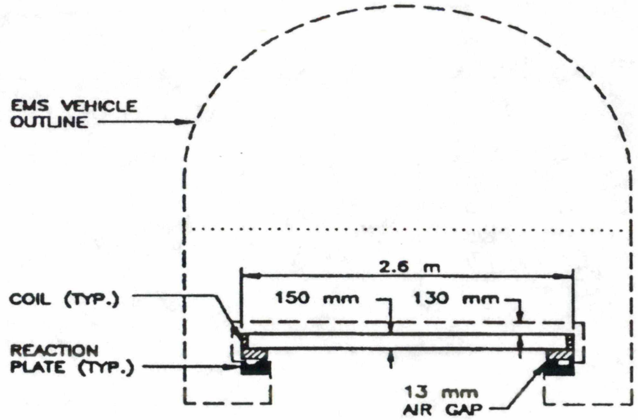

General Guideway Deck Arrangement
for Attractive Suspension

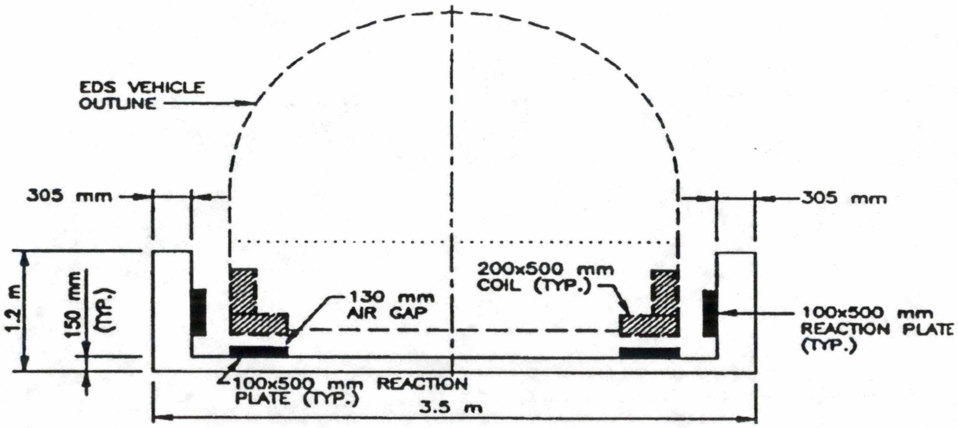

General Guideway Deck Arrangement
for Repulsive Suspension
"U" Shaped Guideway

Figure 5.2.2-2. MAGLEV Vehicle Suspension Types

For purposes of the aerodynamic analysis, the significant difference between these configurations lies in the air gap height between the train bottom surface and the guideway; a 13 mm* separation is expected for the attractive suspension while the repulsive system allows a 130 mm* air gap. Since parameterizing this effect in sidewind is difficult, the data is presented in two sets, one for each suspension system.

The vehicle is assumed to have zero pitch angle, a consequence of the extremely strict tolerances in gap height which allow little deviation in pitch angle from zero degrees. Also, all surfaces are assumed aerodynamically smooth, with some allowance for standard plate roughness. The gap between cars is assumed small and covered by some flexible membrane, therefore the vehicle surface is treated as continuous. Results from this analysis are extremely sensitive to vehicle cross-section in side wind, and significant alterations of the given shapes (Figure 5.2.2-1) can result in deviations from the results provided.

5.2.3 Definition of Forces and Moments

For the two-car configuration, the aerodynamic forces and moments are applied at two separate center-of-gravity locations (Figure 5.2.3-1). The location of these centers, which are near the geometric centroid, are determined by the dynamic analysis group at Battelle. Positive side force and moment directions are indicated by arrows; similarly, the positive relative wind angle, β, is shown. The following list summarizes the coefficients and their definitions, relative to standard aerodynamic forces and moments.

Lift force coefficient	C_L = Lift/(q A)
Drag force coefficient	C_D = Drag/(q A)
Side force coefficient	C_Y = Sideforce/(q A)

*Approximations used in this study. Actual design values for German Transrapid TR-07 is 8mm (attractive maglev systems) and for Japanese MLUX is about 100mm (repulsive maglev system). Proposed German Corp System has a 50mm gap in an attractive maglev concept.

Rolling moment coefficient	C_l = Rolling Moment /(q A D)
Pitching moment coefficient	C_m = Pitching Moment/(q A D)
Yawing moment coefficient	C_n = Yawing Moment/(q A D)

5.2.4 Wind Gust Characterization

For purposes of this analysis, a wind gust is defined as an air velocity perturbation in the vehicle frame of reference which has a known speed and direction. For ease of analysis the gust strength (V_G) and direction (γ) are measured relative to the vehicle guideway, and are assumed constant at any given time instant (Figure 5.2.4-1). This quasi-steady analysis allows for variable gusts to be input in a time-stepping fashion. Note that the direction of the gust may result in an increase (or decrease) in the airspeed relative to the vehicle (V_{true}) or a change in the wind angle (β). The following equations relate the vehicle track speed (V_∞), gust angle and strength to the derived vehicle speed and relative wind angle:

$$V_{true} = V_\infty + V_G \cos\gamma \qquad [5.2\ (1)]$$

$$\beta = \tan^{-1}\left(\frac{V_G \sin\gamma}{V_{true}}\right)$$

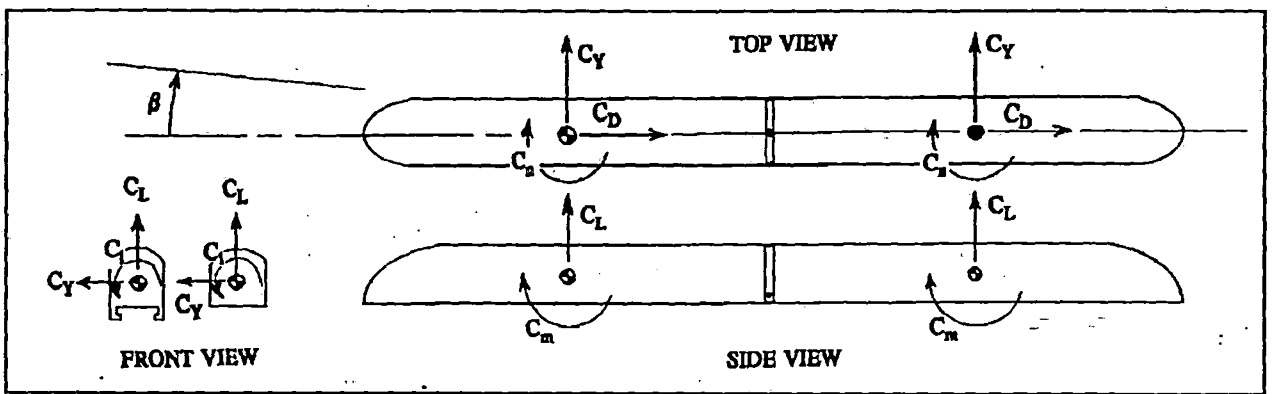

Figure 5.2.3-1 Force and Moment Coefficient Definition

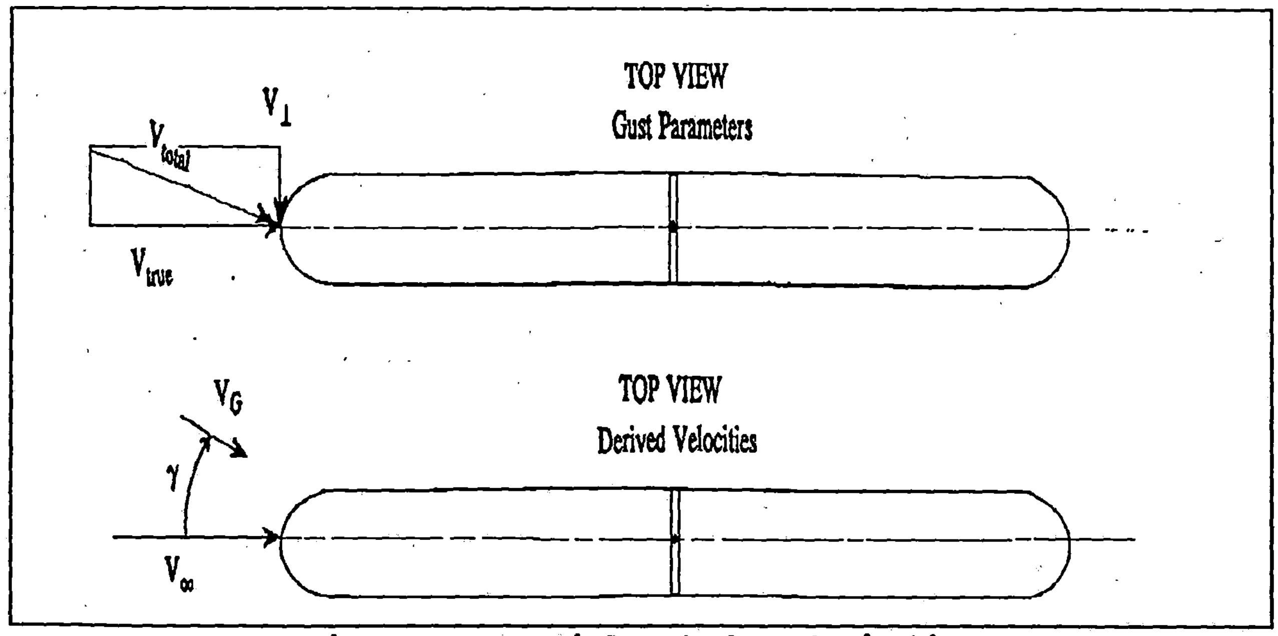

Figure 5.2.4-1 Wind Gust Characterization

5.2.5 Results

The results shown for the maglev vehicle configuration consider a variety of aerodynamic phenomenon and are correlated from numerous sources. Included are the effects of skin friction, vehicle pressure field (most notably base drag), length-to-diameter ratio, gap height, and side wind.

Given the complex three-dimensional nature of the flowfield, especially in side wind, theoretical results are difficult to obtain. Without the benefit of extensive computational fluid dynamic analysis and experiment, the best correlations for the current maglev vehicle are found from previous experimental results. All the aerodynamic effects are included in the given analysis with the exception of gap height, which is reflected by the separate data sets, for repulsive and attractive suspension systems.

The calculation of forces and moments consists of two parts. First, the drag coefficient at zero relative wind angle is computed for a given condition. Then, the relative wind angle, β, is found from the given velocities [Equation 5.2(1)], and the true force and moment coefficients are computed using the algebraic curve fits given at the end of this section. Once the coefficients are known, calculation of forces and moments proceeds from the definitions of the coefficients since the reference area, diameter, and dynamic pressure are known (see table below).

The Table 5.2.5-A gives the symbol definitions for the required inputs:

Table 5.2.5-A
AERODYNAMIC INPUT VARIABLES

L = Total vehicle length
V_∞ = Vehicle forward speed relative to the guideway
A = Vehicle maximum cross-sectional area
D = Effective diameter (hydrodynamic diameter); defined as the diameter of the vehicle if the given cross sectional area (A) were circular, given by eq. [5.2(2)]

$$D = \sqrt{\frac{4A}{\pi}} \qquad [5.2\ (2)]$$

S = Vehicle surface area exposed to moving airflow (including vehicle underbody)
ρ = Local atmospheric density
μ = Local atmospheric viscosity
V_G = Gust velocity
γ = Gust angle relative to track centerline
β = Relative wind angle
q = Dynamic pressure, $q = 0.5\rho V_{true}^2$

5.2.5.1 Drag Coefficient Computation

5.2.5.1.1 Zero Relative Wind Angle

The drag calculation at zero relative wind angle is based on turbulent boundary layer theory, with modification for length-to-diameter ratio and base drag. The basic equation is:

$$C_F = 0.074 \left[\frac{\rho V_{true} L}{\mu}\right]^{-0.2} \qquad [5.2\ (3)]$$

For standard sea level density and viscosity, this becomes:

$$C_F = .0099325\ (V_{true} L)^{-0.2} \qquad [5.2\ (4)]$$

For practical plate roughness, an absolute minimum value for CF is set at 0.003, any results below this are unrealistic.

The drag coefficient, corrected for variation in L/D is:

$$C_{Dw} = C_F\ [1 + 1.5\ \ (L/D)^{-3/2}]\quad S/A \qquad [5.2(5)]$$

Finally, correcting for base drag gives the result:

$$C_{D\beta=0} = 0.5\left[C_{Dw} + \frac{0.029}{\sqrt{C_{Dw}}}\right] \qquad [5.2(6)]$$

5.2.5.1.2 Including Relative Wind Angle Effects

The drag coefficient is increased when the relative wind deviates from the vehicle path; i.e.. contains a side component in velocity. For the slender vehicles under consideration this additional drag is accounted for as below.

$$C_D = C_{D\beta=0} + 0.00011\ \beta^2$$

5.2.5.2 Forward Car Force and Moment Calculation

Force and moment coefficients of the forward car are shown in graphic form (Figures 5.2.5.2-1 to -4) and in functional curve fits for computer modeling.

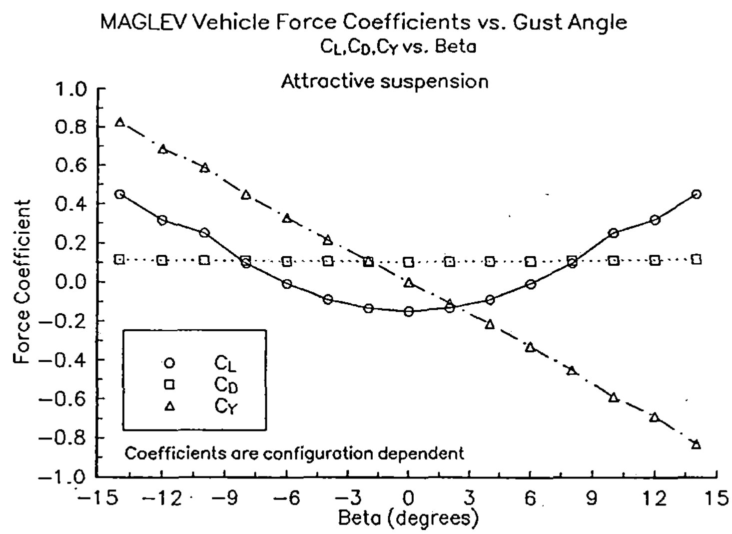

Figure 5.2.5.2-1 Attractive Suspension Forces

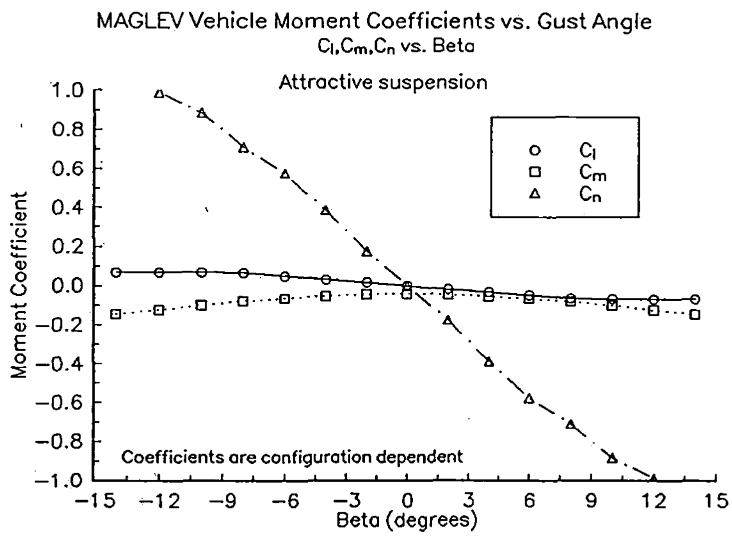

Figure 5.2.5.2-2 Attractive Suspension Moments

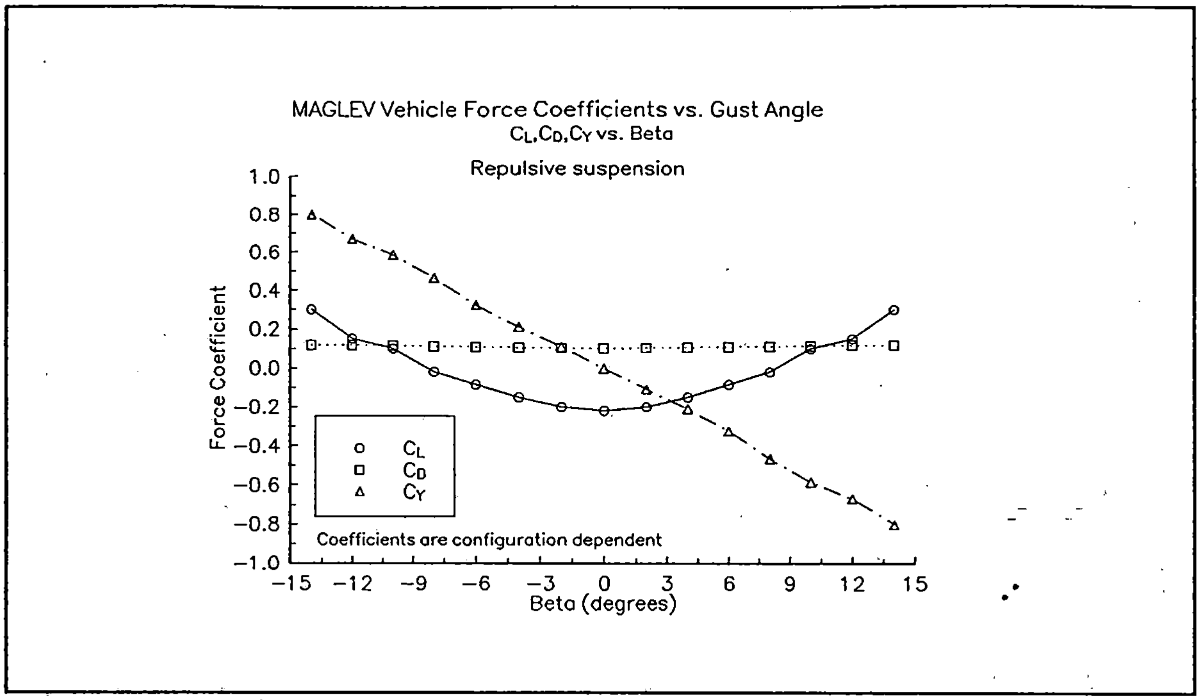

Figure 5.2.5.2-3 Repulsive Suspension Forces

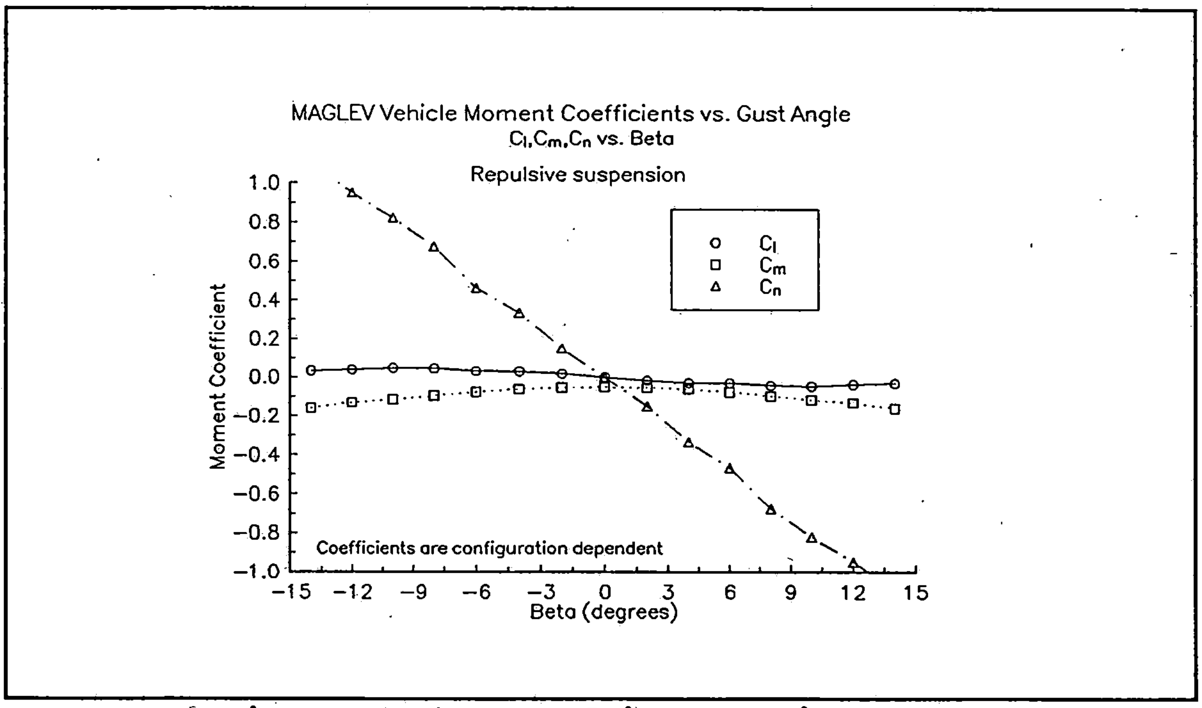

Figure 5.2.4.2-4 Repulsive Suspension Moments

There are two sets of curves, one for the attractive suspension and one for the repulsive suspension. Where a piecewise-smooth curve is required, a prescribed slope is given at the junction points. Also, note the coefficient modifications for the rear car, listed after the forward car relationships.

5.2.5.3 Curve Fits for all Data

Attractive Suspension

$C_L = -0.07658 + 0.001991\,\beta^2$ $\quad -10 < \beta < 10$

$= 0.351045 - 0.0574275\,|\beta| + 0.003459\,\beta^2$ $\quad |\beta| > 10$

[Note: slope at $\beta = 10$ is 0.0197]

$C_D = C_{D\beta=o} + 0.00011\,\beta^2$

$C_Y = -0.027542\,\beta - 0.000011\,\beta^3$

$C_l = -0.008767\,\beta + 0.000020\,\beta^3$

$C_m = -0.044723 - 0.000532\,\beta^2$

$C_n = -0.093979\,\beta + 0.00005\,\beta^3$

Repulsive Suspension

$C_L = -0.109192 + 0.002097\,\beta^2$ $\quad -4 < \beta < 4$

$= -0.096 + 0.0012725\,\beta^2$ $\quad |\beta| > 4$

[slope at $\beta = 4$ is 0.0185]

$C_D = C_{D\beta=o} + 0.000265\,\beta^2$ $\quad -6 < \beta < 6$

$= C_{D\beta=o} + 0.001991\,|\beta| - 0.00005\,\beta^2$ $\quad |\beta| > 6$

[slope at $\beta = 6$ is 0.00089]

$C_Y = -0.027004\,\beta - 0.000015\,\beta^3$

$C_l = -0.006904\,\beta + 0.000024\,\beta^3$ $\quad -10 < \beta < 10$

$= -0.11309 + 0.009175\,|\beta| - 0.000237\beta^2$ $\quad |\beta| > 10$

[slope at $\beta = 10$ is - 0.0007375]

$C_m = 0.056040 - 0.000545\,\beta^2$

$C_n = -0.083013\,\beta + 0.000022\,\beta^3$

A numerical example of the application methodology is provided in Section 5.2.5.5.

5.2.5.4 Rear Car Force and Moment Coefficients

Due to the nature of the dynamic model developed at Battelle, force and moment coefficients are specified at the center of gravity of each car. Previously, these coefficients were specified for the forward car, but due to the symmetry of the vehicle, these coefficients need only be modified slightly to represent the rear car. The modifications below reflect the pressure field alteration due to the vehicle wake and the sign reversal due to vehicle symmetry. All coefficients not shown are identical for both front and rear cars.

$C_{mrear} = -0.5\ C_{mfront}$

$C_{mrear} = -0.8\ C_{mfront}$

5.2.5.5 Numerical Example

For the following representative vehicle, both suspension types and three gust loading conditions are computed exemplifying the force variation in a variety of sidewinds. For simplicity, the comparison is made at a vehicle track speed of 400 km/h, with wind gusts of 0 km/h at 0° incidence, 50 km/h at 45° incidence and 115 km/h at 90° incidence. These gust conditions span the expected design range for this vehicle. The computation of the 50 km/h gust is shown as an example, with the results for all three cases summarized in Tables 5.2.5.5-A and -B.

Vehicle Parameters

Repulsive and Attractive Suspension

Length = 50 m Weight = 350,000 N

v = 400 km/h (track speed) ρ = 1.225 kg.m^3 (sea level)

μ = 1.789 x 10^{-5} kg/m/s S = 580 m^2

$A_{repulsive}$ = 10.4 m^2, thus D = 3.64 m

$A_{attractive}$ = 10.88 m^2, D = 3.72 m

V_{Gust} = 0, 50, 115 km/h γ = 0, 45, 90 degrees

Computation for 50 km/h Gust

V_{true} $= V_{\infty} + V_{Gust} \cos\gamma = 400 + 50 \cos 45 = 435$ km/h
$= 120.8$ m/s

$= \tan^{-1}[V_{Gust} \sin\gamma\ )/V_{true}] = \tan^{-1} [(50 \sin 45)/435] = 4.65$ degrees

C_F $= 0.0099325\ (V_{true}\ L)^{-0.2} = 0.0099325\ (120.8 \times 50)^{-0.2}$
$= 0.00135$
since this is below realistic estimates, $C_l = 0.003$

C_{Dw} $= C_F\ [1+1.5\ (L/D)^{-1.5}]S/A = 0.003\ [1+1.5\ (50/4.3)^{-1.5}]\ 580/14.54$
$= 0.1242$

$C_{D\beta=o} = 0.5\ (C_{Dw}+0.029/sqr(C_{Dw})) = 0.5\ (0.1242+0.029/sqr(0.1242))$
$= 0.10325$

From the functional forms for repulsive vehicle suspension, we get the coefficients:

C_L $= -.096 + 0.0012725\ \beta^2 = -0.096 + 0.00127725\ (4.65)^2$
$= - 0.0685$

C_D $= C_{D\beta=o} + 0.000265\ \beta^2 = 0.10325 + 0.000265\ (4.65)^2$
$= 0.10895$

C_Y $= - 0.027004\ \beta - 0.000030\ \beta^3 = -0.027004\ (4.65) - 0.00003\ (4.65)^3$
$= - 0.127$

C_l $= - 0.006904\ \beta + 0.000024\ \beta^3 = - 0.006904\ (4.65) + 0.000024\ (4.65)^3$
$= - 0.0297$

C_m $= - 0.05604 - 0.000545\ \beta^2 = - 0.05604 - 0.000545\ (4.65)^2$
$= - 0.0678$

C_n $= - 0.083013\ \beta + 0.000022\ \beta^3 = -0.083013\ (4.65) + 0.000022\ (4.65)^3$
$= - 0.384$

Actual forces and moments are calculated from the equations below:

Force = C_{*} q A

Moment = C_{*} q A D

Where C_{*} is the coefficient of the force to be calculated.

Results for all three cases are tabulated in Tables 5.2.5.5-A and B.

NUMERICAL EXAMPLE RESULTS

Table 5.2.5.5-A

Repulsive Suspension	V_G = 0 km/h	V_G = 50 km/h 45 degrees	V_G = 115 km/h 90 degrees
FORCES (N)			
Lift	-8580	-6370	18,060
Drag	8120	10,130	13,270
Sideforce	0	-11,800	-43,800
MOMENTS (N-m)			
Roll	0	-10,050	-3360
Front Pitch	-16,040	-22,950	-55,990
Rear Pitch	8020	11,470	27,990
Front Yaw	0	-130,050	-354,580
Rear Yaw	0	104,000	283,660

Table 5.2.5.5-B

Attractive Suspension	V_G = 0 km/h	V_G = 50 km/h 45 degrees	V_G = 115 km/h 90 degrees
FORCES (N)			
Lift	-6285	-3250	26,310
Drag	8490	10,270	10,820
Sideforce	0	-16,780	-40,080
MOMENTS (N-m)			
Roll	0	-14,010	-17,750
Front Pitch	-13,680	-20,340	-55,570
Rear Pitch	6840	10,180	27,770
Front Yaw	0	-156,270	-398,200
Rear Yaw	0	125,030	318,560

5.2.6 Discussion

Considering the overall design requirements for a maglev system from an aerodynamic standpoint, as represented in the preceding numerical example, several important trends can be observed. First, the most important driver in vehicle drag minimization at a given velocity is the vehicle cross-sectional area (given a fixed length). The smaller the area, the lower the drag. Comparing attractive and repulsive systems yields a similar result, larger intercept area means higher drag. For this reason it is likely that an attractive system would yield slightly higher drag for a fixed cabin size given the expected extra area due to the suspension system location under the track (Figure 5.2.2-2). Another observation is the effect of configuration in crosswind. The attractive systems are more susceptible to buffeting in crosswind than the repulsive systems, especially for repulsive systems with solid sidewalls partially covering the vehicle. All of these effects, however, are severely outweighed by the effect of velocity (Figure 5.2.1-1). Since all the forces, most notably drag, vary with the square of the forward velocity, a modest decrease in velocity can easily outweigh the difference between attractive and repulsive systems. Also, audible noise varies directly with at least the cubic power of forward velocity, thus noise increases drastically with velocity. For this reason, very serious consideration of the velocity requirement should be the primary aerodynamic design driver.

Modification of the vehicle guideway would certainly impact the aerodynamic forces on the vehicle. One suggestion is to cover the vehicle and guideway with a low-cost shell, with some allowance for venting along the sidewalls. This concept could significantly reduce the sizing of the control magnet, as natural crosswinds would be eliminated, thus greatly improving ride quality. Also, concerns about track debris, bird strikes, or other impediments would be significantly reduced. The shell would also act as a noise barrier, reducing the impact of the maglev operation on the surrounding community. The side vents would be necessary to relieve some of the high pressure created by the "bow wave" ahead of the vehicle. Without this relief, the drag of the vehicle would increase significantly. Also, some oversizing of the shell relative to the vehicle size is merited to reduce vehicle drag. Overall, the additional cost of a shell of this type may be saved in reduced control magnet size and operations cost. Certainly this concept is worth further study.

Within the assumed parameters, a model of the aerodynamic forces on a two-car maglev vehicle has been created. Since the aerodynamic flowfield around a vehicle of this type is highly shape dependent, significant deviations from the given configuration may give misleading results. For reasonable sidewind angles, less than 20 degrees, the model will provide estimates of force deviation from the quiescent case. As in the numerical example, a variety of wind gust strengths and directions can be computed for the candidate vehicle. Consideration of the maximum force and moment envelope provides the guidelines for guideway and suspension design.

5.2.7 Summary

The aerodynamic forces and moments for a generic, two-car maglev configuration have been modeled as a function of vehicle velocity and wind gust. The models presented here provide estimates for the assumed vehicle configuration at speeds up to 800 km/h in wind gusts ranging from 0-155 km/h, separately for attractive (EMS) and repulsive (EDS) suspensions systems. The work is formulated in a manner suitable for dynamic modeling of the vehicle's entire expected aerodynamic envelope. Without further experimental testing and/or more complex computational analyses, the precise nature of the three-dimensional flowfield of the candidate vehicle cannot be determined. Thus the models presented represent the best correlation of aerodynamic theory and historical data possible at this time.

5.3 Dynamic Models

Several modeling approaches have been taken to analyze the effects of moving loads over elastic beam type guideways. Generally the Bernoulli-Euler equations for a fixed uniform beam are used in conjunction with a moving-force vehicle model. Solution techniques include lumped-parameter approximations, modal analysis methods, finite difference models (FDM), or finite-element models (FEM).

The modal analysis method provides a relatively efficient means of addressing the dynamic interactions of a flexible guideway span with a moving vehicle load. The assumed space-related vibration modes of the span interact with the vehicle primary suspension (the magnets) through the time-dependent modal amplitudes. This technique was used by Battelle in a recent study of bridge span vibrations induced by impact loads under freight car wheel flats. The method has somewhat limited applicability, since it is restricted to a uniform beam.

For this study, a time-domain solution of the vehicle/guideway system differential equations was chosen. This is a straightforward (although perhaps a crude) method of analysis. It allows the inclusion of nonlinear elements when these are of importance.

The resulting mathematical models of different vehicle and guideway configurations have been programmed for solution on a 486 PC. Program inputs are vehicle and guideway physical characteristics, vehicle speed, guideway geometry errors, wind gust parameters, and specific run-related elements such as distance run and integration time step. Output formats include optional input parameter printouts, optional time-history printouts or plot files, and maximum/minimum value summary tables for key response variables per speed run.

5.3.1 Maglev Vehicle Model

To control the total number of degrees of motion freedom (DOF) in the vehicle/guideway model, the vertical (bounce/pitch) and lateral (roll/yaw/lateral) motions were separated into different models. This is a practical and legitimate approach if small angular motions are assumed and if there are no significant nonlinearities within the frequency range of interest (about 0.5 to 50 Hz).

The two radically different types of maglev vehicles were considered. First, the attractive electromagnetic system (EMS) such as the German Transrapid TR-07 and the Japanese HSST designs. These vehicles utilize a magnetic suspension that wraps around the active guideway elements, achieving levitation by attraction upward toward the guideway surface. The second electrodynamic system (EDS) such as the Japanese MLU-002 vehicle achieves levitation through repulsive eddy currents generated in guideway-mounted coils. Relatively high speed (150 km/h or more) is required for sufficient induction to levitate.

These two systems produce radically different models. For the EMS vehicle, four magnet support frames (unsprung masses) were assumed per car, and 15 magnet pairs (seven shared between frames) were assumed per two-car trainset. This approximates the TR-07 vehicle. Since each magnet must operate within a nominal 10 to 13 mm gap, the effective magnetic stiffness is high (in a closed-loop gap control system) and the dynamic coupling to the guideway structure is strong. Without a secondary suspension system, the car body bounce and pitch natural frequenices would be in the 10 to 13 Hz range, far too stiff for passenger comfort. A secondary suspension between frame and car body is therefore necessary.

The EDS-type vehicle was assumed to have two magnet frames (unsprung masses) per car body and two magnet pairs per frame. This makes the EDS more similar in configuration to a standard two-bogie rail vehicle. Variants on this arrangement were noted in the literature: Two frames at the front end of the power car and one shared frame between power and trailer car, for example. Typically, the EDS magnetic suspension operates at a nominal gap of 100 to 130 mm with an effective vertical stiffness nearly an order of magnitude less than the EMS magnetic stiffness. Without a secondary suspension, car body bounce and pitch natural frequencies are in the 1.5 to 2.5 Hz range. This is still too stiff for good ride quality, so a secondary suspension between frame and car body is included in the model.

In the bounce/pitch configuration, each frame is modeled in the vertical and pitch motions. Although the magnets are attached to the frames by complex suspension and linkage elements, these masses have been combined with the frame masses for simplicity. Each car body is modeled in vertical and pitch rigid-body and first vertical (free-free) bending modes, coupled to the adjacent car body through shear and torsional springs and damping. The EMS vehicle model (22 DOF) is sketched in Figure 5.3.1-1, while the EDS vehicle model (14 DOF) is shown in Figure 5.3.1-2.

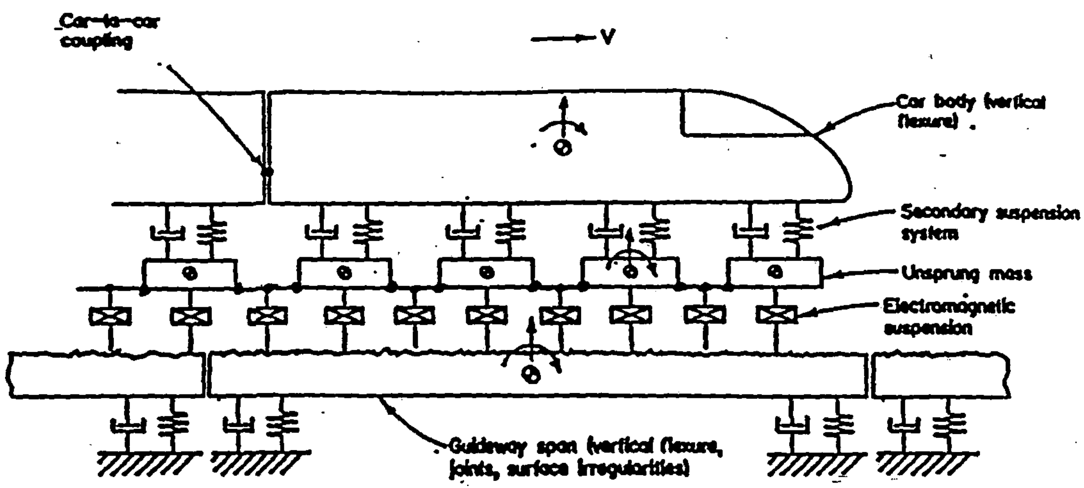

SKETCH OF MODEL OF TYPICAL MAGLEV VEHICLE ON MULTI-SPAN GUIDEWAY SYSTEM

Figure 5.3.1-1 Model of EMS-Type Maglev Vehicle on Guideway

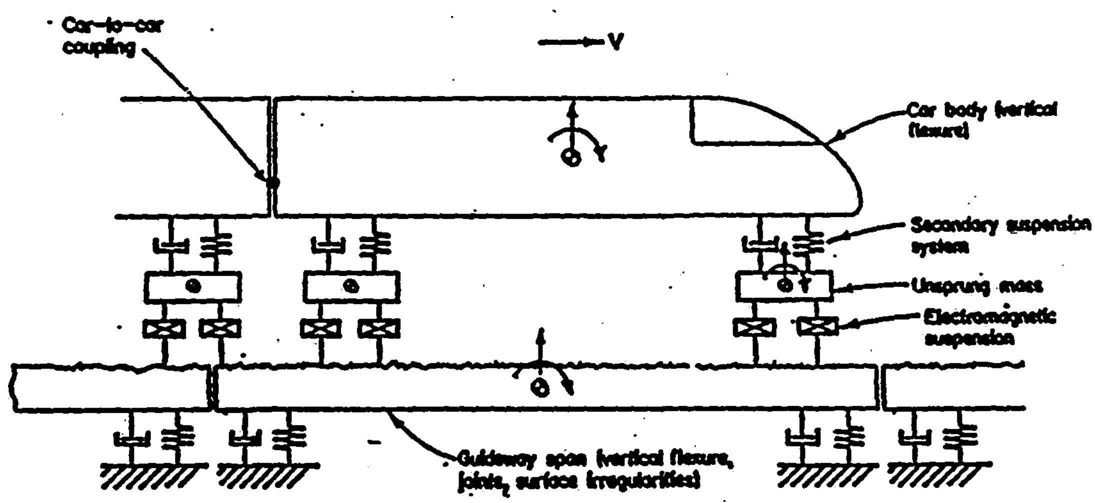

SKETCH OF MODEL OF TYPICAL MAGLEV VEHICLE ON MULTI-SPAN GUIDEWAY SYSTEM

Figure 5.3.1-2 Model of EDS-Type Maglev Vehicle on Guideway

A similar approach was applied to the lateral models. Magnet frames were modeled in lateral and roll motions. Each car body was modeled in lateral, yaw, and roll rigid-body motions, coupled through shear and torsion to the adjacent car body. Since the car body lateral and torsional bending natural frequencies are substantially higher than the vertical bending frequency, these modes were not included. This again results in a 22-DOF EMS-type vehicle model and a 14-DOF EDS-type vehicle model.

5.3.2 Guideway Structure Model

The guideway structure was modeled as a series of longitudinal beams, each beam represented by the Bernoulli-Euler equations [74]. A time-domain solution of these equations is implemented by the mode acceleration method in response to vehicle interactive loads.

In the vertical plane, each guideway span is represented in five degrees of motion freedom: rigid body bounce and pitch (on column stiffness and damping), and the first three modes of vertical bending. Two methods for representing the flexibility of the guideway beams are used. First, the traditional method of modeling was used, considering the span a pinned-pinned beam (at the end columns). In the second, the beams are considered "free-free", resting at the ends on resilient column stiffness and damping elements for vertical motion. In each method, the first three vertical bending modes are modeled by using the mode acceleration method. Mode influence coefficients are calculated for the resilient connection points. These include the moving locations of the individual electromagnetic pads. Pad forces are introduced onto (and off from) beam ends as a function of exposed area. Pad and guideway vertical motions, as well as geometry errors such as beam camber, influence coupling forces through changes in the effective electromagnetic gap size. Geometry errors are averaged over the length of the pad.

A check on these two methods for representing the vertical guideway beam is given in Figure 5.3.2-1 by a comparison of mid-span acceleration response to a passing EDS-type vehicle. The nominal span bearing stiffness is 2×10^8 N/m, which is a typical catalog value for commercially available elastomeric "sandwich" bearings. By increasing this value by an order of magnitude, the "free-free" beam response approaches that of the pinned-pinned configuration.

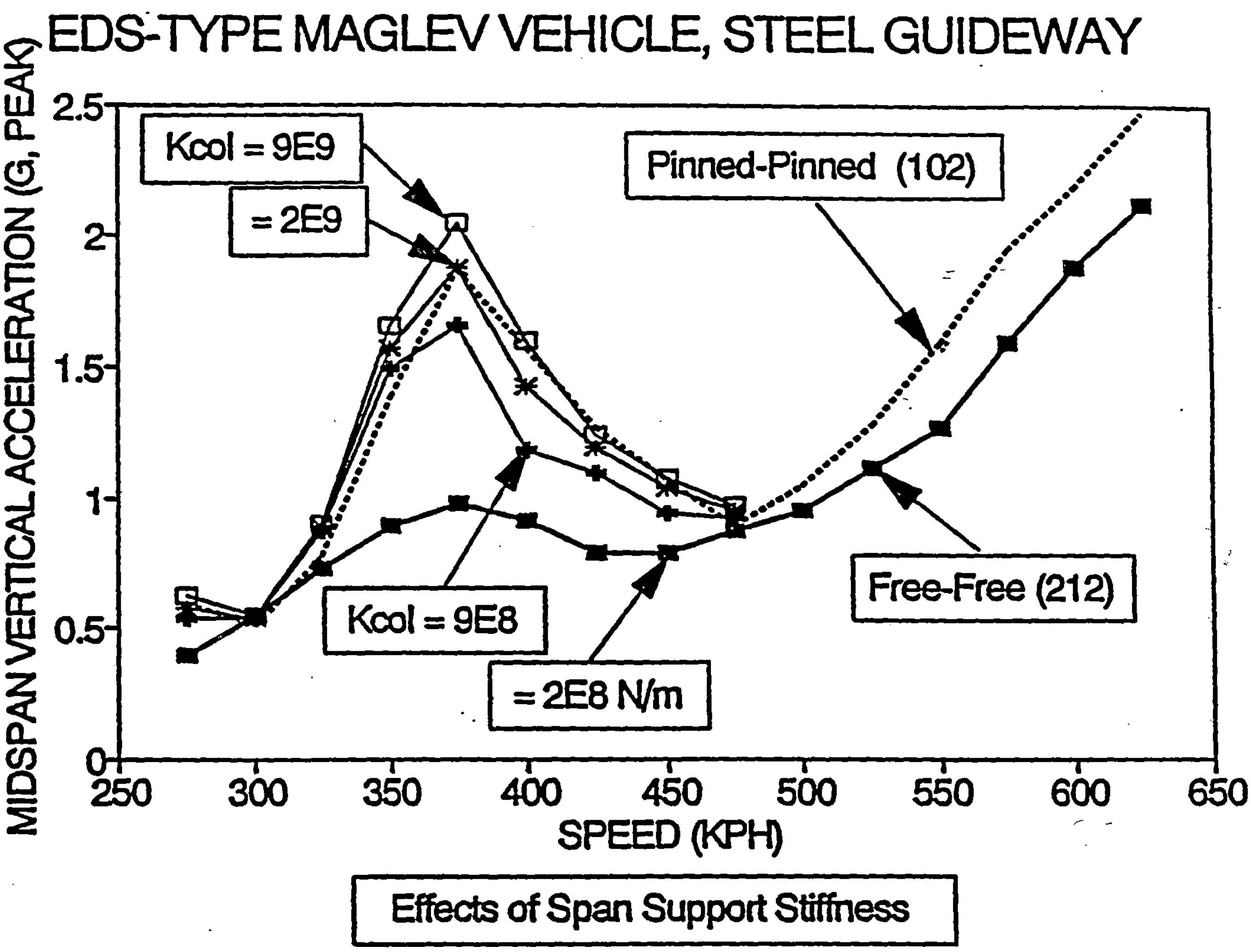

Figure 5.3.2-1 Comparison of Free-Free and Pinned-Pinned Response

A similar guideway structure model was developed to represent the lateral degrees of freedom. Each span included the lateral, yaw, and roll rigid-body motions, plus the first lateral and torsional free-free bending modes. Since the lateral bending mode natural frequency is substantially higher than the vertical and torsional frequencies, this mode was eliminated (after a few runs) in favor of the second (symmetrical) torsional bending mode.

Two consecutive guideway beams are represented in the "working" version of the model, which results in a total vehicle/guideway model of 32 DOF for the EMS-type vehicle, and 24 DOF for the EDS-type vehicle. These guideway beams may be simply supported or may be "continuous" (two spans) with a supporting column in the center.

An expanded version of the model was generated on the computer using the Advanced Computer Simulation Language (ACSL). This model includes six consecutive spans for a total of 52 DOF with an EMS-type vehicle. By using a "daisy-chain" solution routine, resetting Span #1 to zero and putting it in the Span #7 position, an effectively continuous guideway may be simulated. Because of increased computation time, this version was used only to "spot check" vehicle/guideway response at selected speeds to assure that a stable response was achieved. An example of guideway beam acceleration response at the first and sixth beams is shown in Figure 5.3.2-2, confirming that a two span representation is adequate for simply supporting beams. Four spans are used for two-span-continuous guideways.

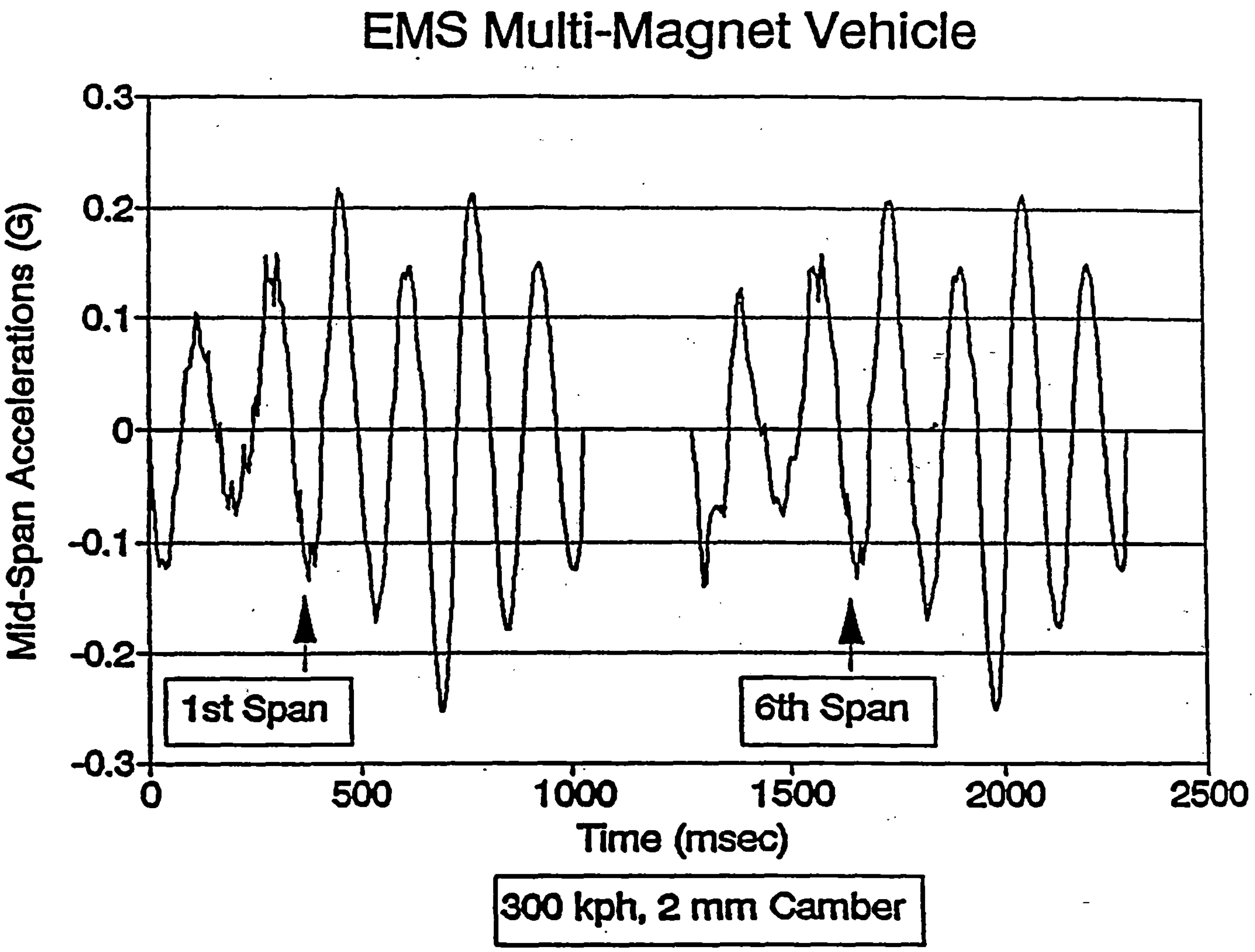

Beam Mid-Span Vertical Accelerations, PBQ&D Guideway #1

Figure 5.3.2-2 Guideway Response at 1st and 6th Beam Span.

5.3.3 Vehicle/Guideway Model Parameters

The design of maglev vehicles and guideways is at present in a state of flux, so to speak. A German trainset, the Transrapid TR-07, is currently under test. The Japanese MLU-002 test program is temporarily on hold as the vehicle is rebuilt. A range of vehicle and guideway systems are under review in the four DOT/FRA System Concept Definition Studies. As a result, few of the vehicle parameters are known currently with any degree of certainty. Therefore engineering estimates of values were used for the maglev vehicle models in this study.

A 45-tonne vehicle with an overall length of 18 meters, 36 m for the two-car train, was assumed (Section 4.1). The TR-07 is roughly this same weight, but has a car body length of 25 meters. A secondary suspension providing a 1.2 Hz bounce natural frequency with 20 percent of critical damping was modeled. This is not an optimal vehicle design, but gives conservative results for analysis. Finally, an 8-Hz vertical body bending frequency was chosen. Published reports on the TR-07 vehicle cite a calculated 6.5-Hz bending mode for this longer vehicle. [75]

Effective magnetic stiffnesses for levitation and guidance were based on the work of Dr. Stekly under this BAA study (Section 5.1). The attractive EMS configuration results in a "negative stiffness", which requires a closed-loop gap control system. An effective stiffness sufficient to maintain position within the 10-mm gap was calculated for the model.

The "baseline" sets of vehicle parameters are given in Tables 5.3.3-A (EMS vehicle) and 5.3.3-B (EDS vehicle). Guideway structural parameters for the model, given in Table 5.3.3-C, were based on the PBQ&D structural evaluation (Section 4.2).

5.3.4 Evaluation Criteria

The different vehicle/guideway structure combinations were evaluated by three basic criteria:

- Passenger ride comfort.
- Loads and bending moments on the beam.
- Peak acceleration response of the beam.

Ride comfort limits were based on the International Standards Organization (ISO 2681) one-hour reduced comfort limits in the most sensitive frequency range [76]. These are summarized from Section 3.1:

- Vertical -- 0.036 g rms (4 to 8 Hz)
- Lateral -- 0.025 g rms (1 to 2 Hz)

These values refer to one-third octave band rms values of random vibration. If the response is relatively discrete sinusoids, as it indeed appears to be, it is reasonable to increase these levels to peak values:

- Vertical -- 0.051 g peak (4 to 8 Hz)
- Lateral -- 0.036 g peak (1 to 2 Hz)

Beyond these frequency ranges, human sensitivity to vibration decreases rapidly (roughly an order of magnitude per decade increase in frequency).

Maximum bending moments for each guideway beam configuration were established by PBQ&D in their structural evaluation. These are given in Tables 4.2-B and repeated in Table 6.2-A. A maximum beam acceleration level of 0.3 g was established as a desirable limit on structural dynamic response. (Section 3.5).

TABLE 5.3.3-A
Input Parameters for EMs-Type Maglev Vehicle Model

CAR #1 BODY MASS, MCAR1	=	35700. KG
CAR #2 BODY MASS, MCAR1	=	35700. KG
UNSPRUNG MASS, PER FRAME, MUNS	=	2440. KG
CAR #1 MASS MOMENT IN PITCH, PJCAR1	=	0.1010E+07 KG-M^2
CAR #2 MASS MOMENT IN PITCH, PJCAR2	=	0.1010E+07 KG-M^2
UNSPRUNG MASS MOMENT IN PITCH, PER FRAME, PJUNS	=	0.2745E+04 KG-M^2
LEVITATION MAGNET PAIR STIFFNESS, KZE	=	0.2500E+08 N/M,
SECONDARY SUSPENSION STIFFNESS, PER FRAME, KZS	=	0.5070E+06 N/M
SECONDARY SUSP. PITCH STIFFNESS, PER FRAME, KTHES	=	0.1260E+07 N-M/RAD
COUPLING VERTICAL STIFFNESS, KZC	=	0.5000E+05 N/M
COUPLING TORSIONAL (PITCH) STIFFNESS, KTHEC	=	0.5000E+06 N-M/RAD
LEVITATION MAGNET (PAIR) DAMPING, CZE	=	0.4940E+05 N-SEC/M
SECONDARY SUSPENSION DAMPING, PER FRAME, CZS	=	0.2690E+05 N-S/M
SECONDARY SUSP.PITCH DAMPING, PER FRAME, CTHES	=	0.1350E+06 N-M-S
COUPLING VERTICAL DAMPING, CZC	=	0.5000E+04 N-S/M
COUPLING TORSIONAL (PITCH) DAMPING, CTHEC	=	0.5000E+05 N-M-S
CAR OVERALL LENGTH, LOV	=	18.00 M
FRONT END, CAR #1, TO C.G., LCG1	=	9.20 M
COUPLING, CAR #2, TO C.G., LCG2	=	8.80 M
MAGNET CENTER-TO-CENTER, LMAG	=	2.25 M
EFFECTIVE LENGTH OF MAGNET, PODL	=	2.00 M
DISTANCE FORWARD, CG1 TO FRAME 1	=	6.95 M
DISTANCE FORWARD, CG1 TO FRAME 2	=	2.45 M
DISTANCE FORWARD, CG1 TO FRAME 3	=	-2.05 M
DISTANCE FORWARD, CG1 TO FRAME 4	=	-6.55 M
DISTANCE FORWARD, CG2 TO FRAME 5	=	6.55 M
DISTANCE FORWARD, CG2 TO FRAME 6	=	2.05 M
DISTANCE FORWARD, CG2 TO FRAME 7	=	-2.45 M
DISTANCE FORWARD, CG2 TO FRAME 8	=	-6.95 M
CAR BODY FIRST BENDING MODE DAMPING RATIO, ZETC	=	0.0200
CAR BODY FIRST BENDING MODE NATURAL FREQ., FNC	=	8.0000 HZ
CALCULATED STEADY-STATE LOADS --		
NO. 1 MAGNET VERTICAL LOAD	=	70.61 kN
NO. 7 MAGNET VERTICAL LOAD	=	70.61 kN
NO. 8 MAGNET VERTICAL LOAD	=	70.61 kN
NO.15 MAGNET VERTICAL LOAD	=	70.61 kN
NO. 1 SUSPENSION VERTICAL LOAD	=	82.86 kN
NO. 4 SUSPENSION VERTICAL LOAD	=	92.20 kN
NO. 5 SUSPENSION VERTICAL LOAD	=	92.20 kN
NO. 8 SUSPENSION VERTICAL LOAD	=	82.86 kN

TABLE 5.3.3-B
Input Parameters for EDS-Type Maglev Vehicle Model

CAR #1 BODY MASS, MCAR1	=	35700. KG
CAR #2 BODY MASS, MCAR1	=	35700. KG
UNSPRUNG MASS, PER FRAME, MUNS	=	4000. KG
CAR #1 MASS MOMENT IN PITCH, PJCAR1	=	0.1010E+07 $KG\text{-}M^2$
CAR #2 MASS MOMENT IN PITCH, PJCAR2	=	0.1010E+07 $KG\text{-}M^2$
UNSPRUNG MASS MOMENT IN PITCH, PER FRAME, PJUNS	=	0.5600E+04 $KG\text{-}M^2$
LEVITATION STIFFNESS (PER MAGNET PAIR), KZE	=	0.1100E+07 N/M
SECONDARY SUSPENSION STIFFNESS, PER FRAME, KZS	=	0.1010E+07 N/M
SECONDARY SUSP. PITCH STIFFNESS, PER FRAME, KTHES	=	0.2500E+07 N-M/RAD
COUPLING VERTICAL STIFFNESS, KZC	=	0.5000E+05 N/M
COUPLING TORSIONAL (PITCH) STIFFNESS, KTHEC	=	0.5000E+06 N-M/RAD
LEVITATION DAMPING (PER MAGNET PAIR), CZE	=	0.3100E+05 N-SEC/M
SECONDARY SUSPENSION DAMPING, PER FRAME, CZS	=	0.5370E+05 N-S/M
SECONDARY SUSP.PITCH DAMPING, PER FRAME, CTHES	=	0.1330E+06 N-M-S
COUPLING VERTICAL DAMPING, CZC	=	0.5000E+04 N-S/M
COUPLING TORSIONAL (PITCH) DAMPING, CTHEC	=	0.5000E+05 N-M-S
CAR OVERALL LENGTH, LOV	=	18.00 M
FRONT END, CAR #1, TO C.G., LCG1	=	9.20 M
COUPLING, CAR #2, TO C.G., LCG2	=	8.80 M
MAGNET CENTER-TO-CENTER, LMAG	=	3.00 M
EFFECTIVE LENGTH OF MAGNET, PODL	=	2.50 M
DISTANCE FORWARD, CG1 TO FRAME 1	=	6.00 M
DISTANCE FORWARD, CG1 TO FRAME 2	=	-5.90 M
DISTANCE FORWARD, CG2 TO FRAME 3	=	5.90 M
DISTANCE FORWARD, CG2 TO FRAME 4	=	-6.00 M
CAR BODY FIRST BENDING MODE DAMPING RATIO, ZETC	=	0.0200
CAR BODY FIRST BENDING MODE NATURAL FREQ., FNC	=	8.0000 HZ
CALCULATED STEADY-STATE LOADS --		
NO. 1 MAGLEV VERTICAL LOAD, FZE1	=	106.41 kN
NO. 2 MAGLEV VERTICAL LOAD, FZE3	=	107.88 kN
NO. 3 MAGLEV VERTICAL LOAD, FZE5	=	107.88 kN
NO. 4 MAGLEV VERTICAL LOAD, FZE7	=	106.41 kN
NO. 1 SUSPENSION VERTICAL LOAD, FZS1	=	173.58 kN
NO. 2 SUSPENSION VERTICAL LOAD, FZS2	=	176.53 kN
NO. 3 SUSPENSION VERTICAL LOAD, FZS3	=	176.53 kN
NO. 4 SUSPENSION VERTICAL LOAD, FZS4	=	173.58 kN

TABLE 5.3.3-C
List of Guideway Model Parameters

Parameter	Description	Guideway Number					
		1	2	3	4	5	6
LS	Span Length, m	21.33	21.33	21.33	21.33	24.00	21.33
MS	Mass/Unit Length (kg/m)	2976	4777	4152	2768	1042	4598
EIxx	Beam Bending Rigidity (N-m^2)	1.364E+10	1.839E+10	1.794E+10	6.597E+09	6.940E+09	1.593E+10
EIyy	Beam Bending Rigidity (N-m^2)	7.640E+10	7.083E+10	7.357E+10	3.526E+09	2.240E+10	3.678E+10
GK	Beam Torsion Rigidity (N-m^2)	3.470E+08	8.420E+09	1.550E+10	1.150E+09	3.850E+10	4.380E+09
PJS	Beam Mass Moment in Pitch (kg-m^2)	2.41E+06	3.86E+06	3.36E+06	2.24E+06	1.20E+06	3.72E+06
RJS	Beam Mass Moment in Roll (kg-m^2)	1.70E+05	1.96E+05	2.00E+05	2.21E+05	3.27E+04	1.27E+05
KZP	Bearing Pad Vertical Stiffness (N/m)	1.75E+08	1.75E+08	1.75E+08	1.75E+08	1.75E+08	1.75E+08
CZP	Bearing Pad Vertical Damping (N-s/m)	2.00E+06	2.00E+06	2.00E+06	2.00E+06	2.00E+06	2.00E+06
KYP	Bearing Pad Lateral Stiffness (N/m)	9.63E+06	9.63E+06	9.63E+06	7.00E+06	9.63E+06	9.63E+06
CYP	Bearing Pad Lateral Damping (N-s/m)	1.10E+05	1.10E+05	1.10E+05	9.40E+04	1.10E+05	1.10E+05
KPHIP	Bearing Pad Roll Stiffness (N/m)	3.29E+08	2.50E+07	2.50E+07	7.41E+08	1.38E+08	3.29E+08
CPHIP	Bearing Pad Damping (N-s/m)	3.76E+06	7.60E+05	7.60E+05	8.47E+06	1.58E+06	3.76E+06

6.0 DYNAMIC ANALYSIS RESULTS

6.1 Vehicle/Guideway Analysis Matrix

The PBQ&D structural engineers evaluated a range of elevated guideway-supporting structures as candidates for a maglev system. Five guideway beam configurations were chosen for the dynamic analysis in both 21 and 39 meter span lengths. A sixth configuration approximating the Transrapid steel structure was also chosen in a 24 meter length. In addition, both single-span (simply supported) and two-span continuous beam configurations were to be considered for a total of 22 possible guideway structural combinations. Cross-sectional outlines of the six basic guideway structures are shown for reference in Figure 6.1-1.

Using the baseline parameters for the two different vehicles (EDS and EMS) and the two separate models (vertical/pitch and roll/yaw/lateral), a 22 by 4 matrix of 88 baseline runs was possible. This presented a formidable computation and analysis task. A pragmatic approach was taken to reduce this number by sampling the matrix. Certain runs were eliminated based on analysis of some of the earlier computer runs. A more complete survey was conducted with the EDS vehicle which (at 24 DOF) completed a run in less than 40 percent of a comparable EMS vehicle run. Three of the structures were found to respond in a dynamically similar way, reducing the number of combinations necessary with both the EMS vehicle and with two-span continuous beam configurations.

Because typical guideway structures are more rigid in lateral bending and twist, the primary dynamic action of a vehicle on an elevated structure is in the vertical bending response. For this reason, much more emphasis was given in this study on the vertical/pitch model. Representative runs were made with the roll/yaw/lateral model including a simulation of a "worst case" wind gust condition.

Computer runs were made over a 200 to 600 km/h speed range at increments of 25 km/h. Where lower-speed resonances were suspected, runs were made to as low as 50 km/h. The final matrix of runs completed versus possible combinations is shown in Table 6.1-A. Because of time and cost constraints, only a few additional runs were made to explore variations in vehicle and guideway support parameters.

Figure 6.1-1. Outline Sketches of Guideway Structures.

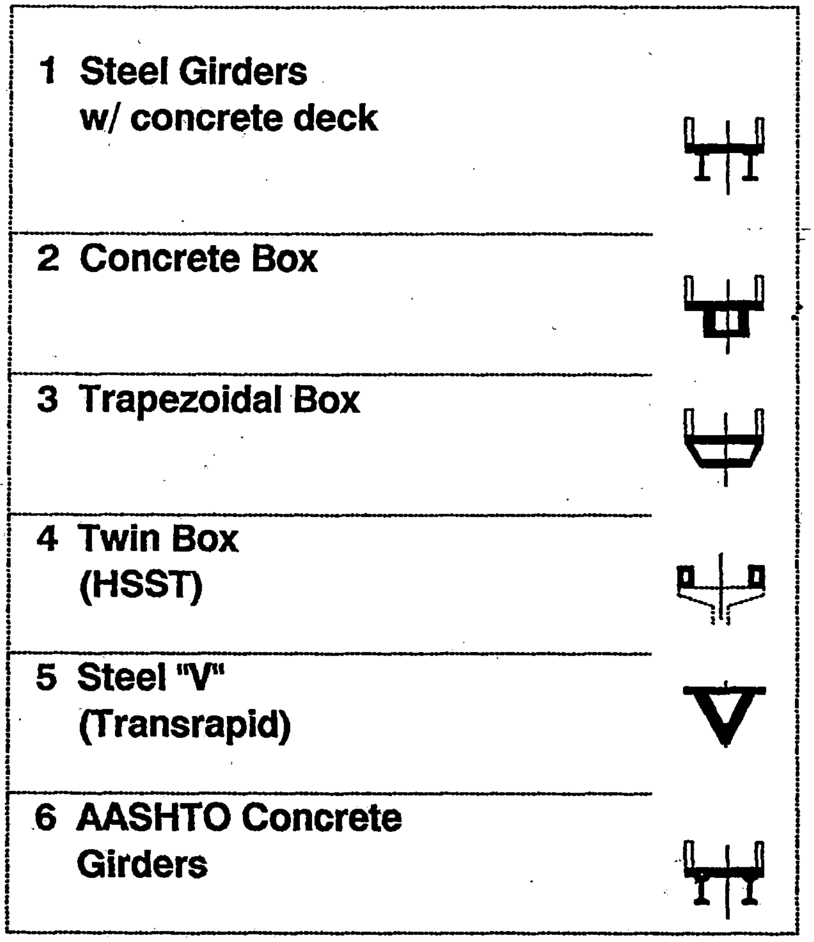

TABLE 6.1-A

Matrix of Computer Simulation Runs.

	EMS-Type Vehicle		EDS-Type Vehicle	
Guideway	Run No. (Vertical Model)	Run No. (Lateral Model)	Run No. (Vertical Model)	Run No. (Lateral Model)
1[a]	651	821	251	451
2	652		252	
3	653		253	
4	654	824	254	454
5	655	825	255	
6	660	826	260	460
1P[b]	656		256	
2P			257	
3P			258	
4P			259	
6P	661		261	
1D[c]			271	
2D			272	
3D			273	
4D	674		274	
5D	675		275	
6D	676		276	

Notes:

a -- One-span simply supported beam, 21.33 m length (Guideway 5 is 24 m length).

b -- One-span simply supported beam, 39.62 m length.

c -- Two-span "continuous" beam (center support), 42.67 m length.

6.2 Effects of Guideway Configurations

The matrix of computer runs (Table 6.1-A) were made simulating a two-car maglev vehicle passing over two elevated guideway spans (two beams, four spans in the case of the center-supported beams). Example time histories of car body vertical accelerations are given in Figures 6.2-1 and 6.2-2 for an EMS-type maglev vehicle at 300 km/h crossing Guideway #1, the steel beam with concrete deck guideway support structure. After an initial transient, the vehicle car body assumes steady state response with slight modulation from lower-frequency body modes. The primary frequency is at about 4 Hz plus the 8-Hz body bending frequency. Here, in terms of ride comfort, the desired limit of 0.051 g peak has been exceeded at the rearward locations of both leading and trailing cars. Since the vehicle suspension parameters have not been optimized, these acceleration levels can undoubtedly be reduced.

The comparable example of guideway structure mid-span vertical acceleration and beam bending moment response is given in Figure 6.2-3 Peak guideway mid-span vertical accelerations are less than the design limit of 0.3 g; and the peak bending moments are well below the design maximum of 5,732 kN-m. This vehicle and guideway are therefore (at this speed) a satisfactory combination. Note, however, that an essentially smooth (but flexible) guideway has been simulated: only 2 mm of positive (upward) camber has been added.

To provide an evaluation of vehicle/guideway combinations over a broad speed range, we relied on the summary maximum/minimum value tables. These tables reflect the peak transient response values. As seen in Figures 6.2-1 through -3, however, the car body transient peak is little different from repeated peak values over a number of spans. Guideway structure response is, on the other hand, a transient value by its very nature. A modest 5 mm positive camber was used for all of these runs, so that the response values reflect primarily the vehicle and structure dynamic interactions due to system flexibilities.

Car body acceleration peak values are shown in Figure 6.2-4 according to position in the car. For the EDS-type vehicle, the rear of the car is consistently rougher than the front over the whole speed range. The EMS-type vehicle may be rougher in the front position, depending on the speed range. The car center, in spite of the 8-Hz bending mode, is a consistently smoother ride except, with the EMS-type vehicle, at speeds above 500 km/h. On the lighter-weight

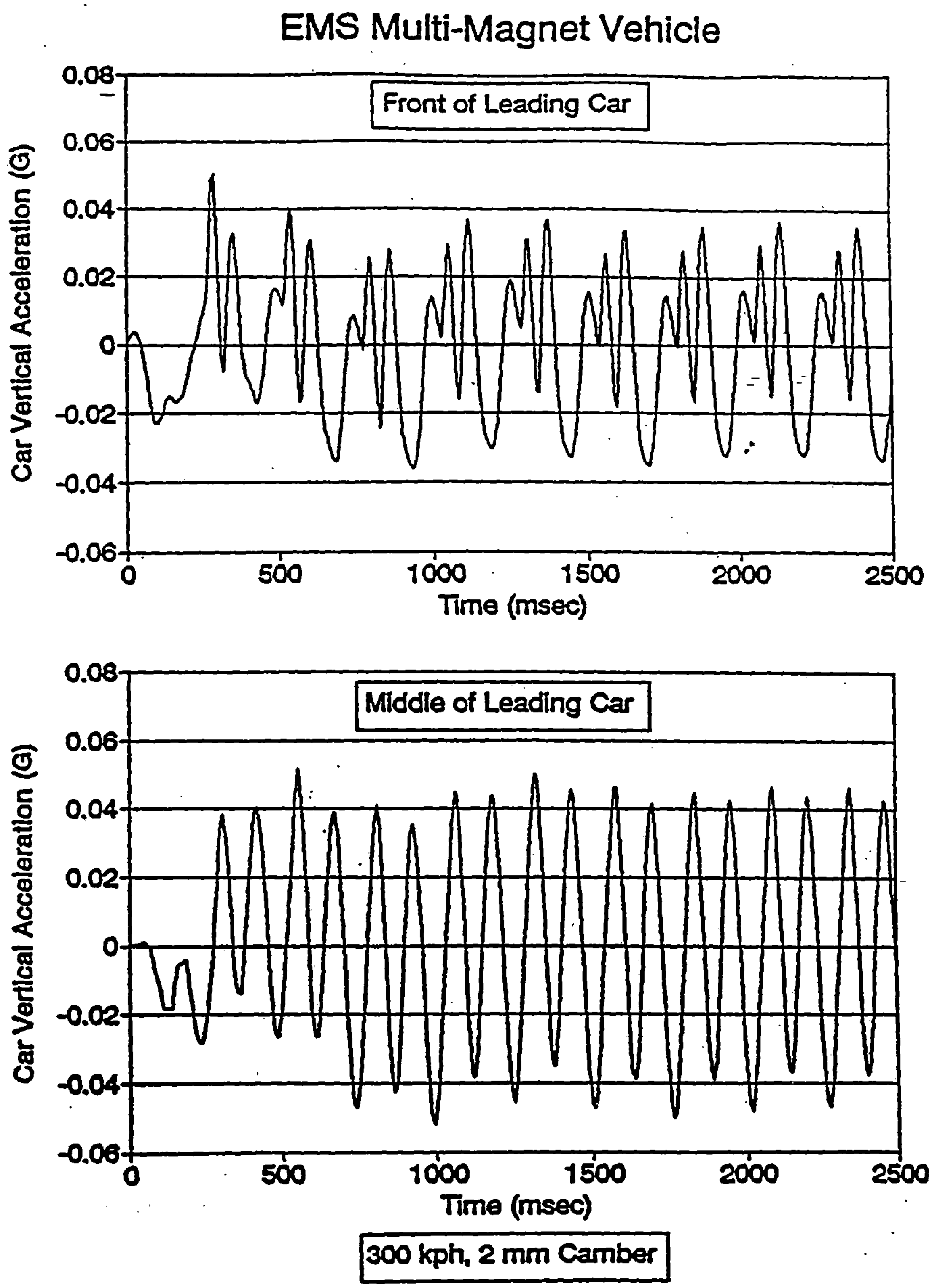

Figure 6.2-1 Typical Car Body Response, EMS-Type Vehicle.

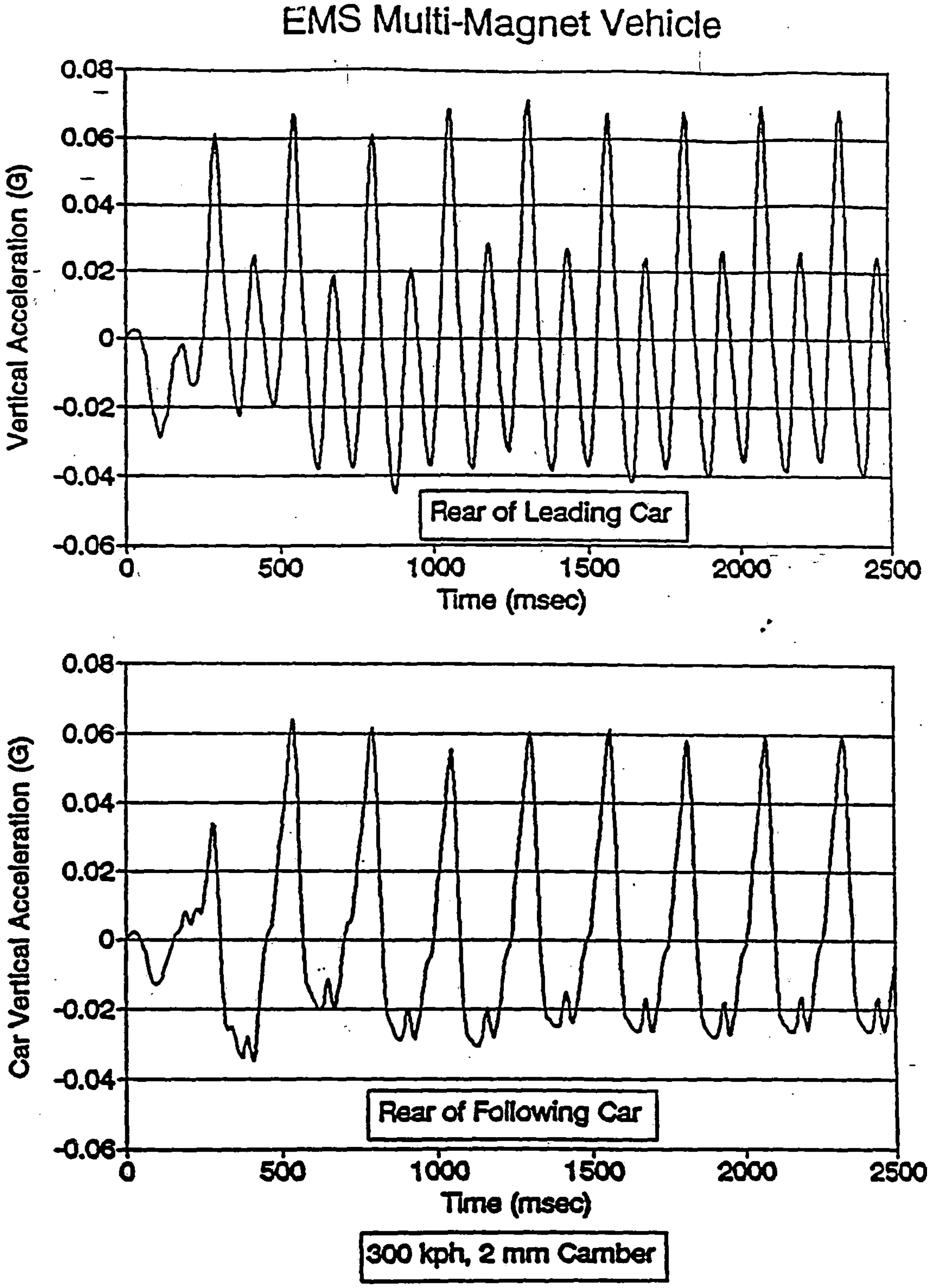

MAGLEV CAR VERTICAL ACCELERATIONS AT 300 km/h ON PBQ&D GUIDEWAY #1

Figure 6.2-2 Typical Car Body Response, EMS-Type Vehicle.

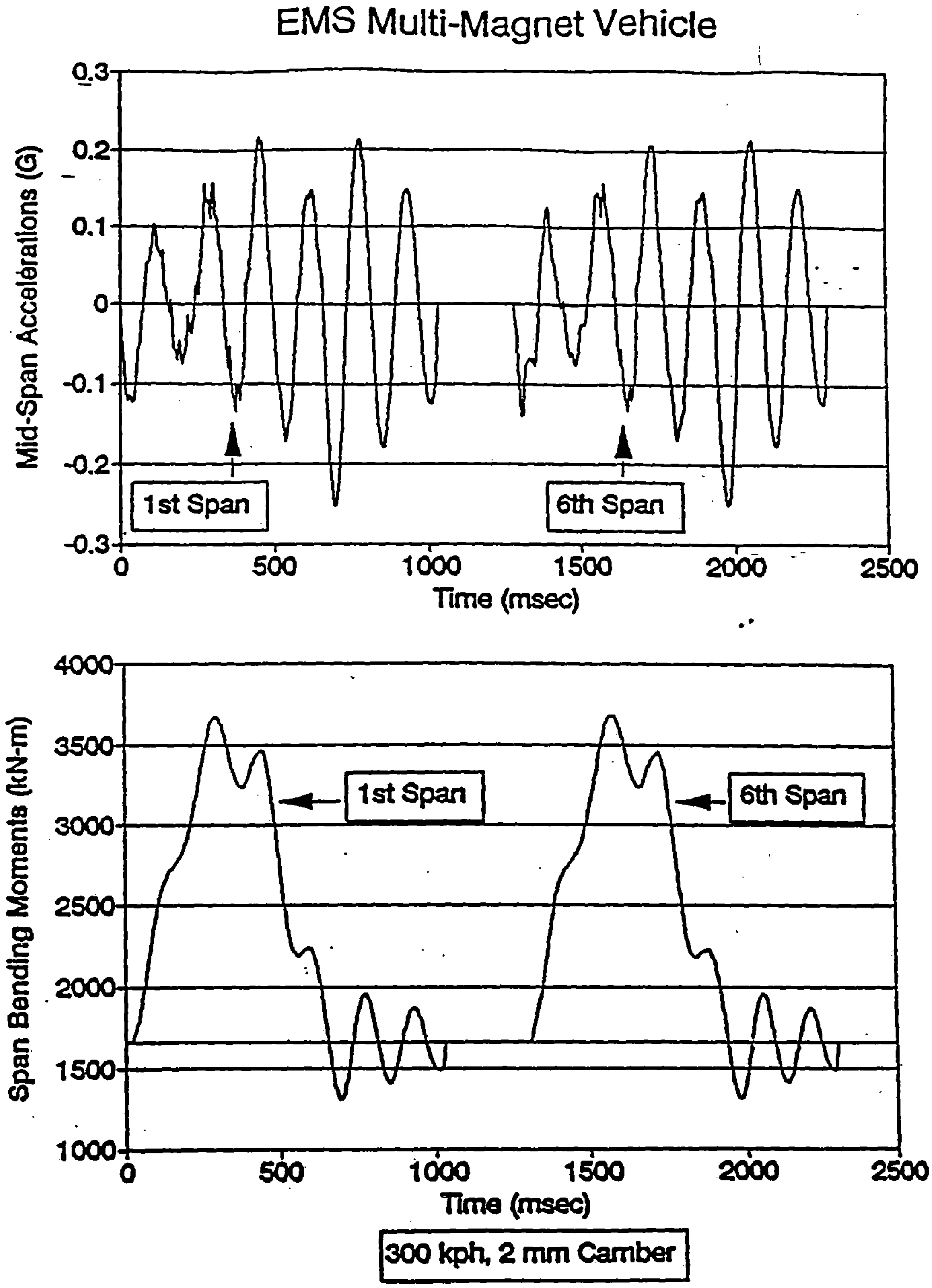

GUIDEWAY MIDSPAN BENDING MOMENTS
MAGLEV AT 300 km/h ON PBQ&D GUIDEWAY #1

Figure 6.2-3 Typical Guideway Response Under EMS-Type Vehicle.

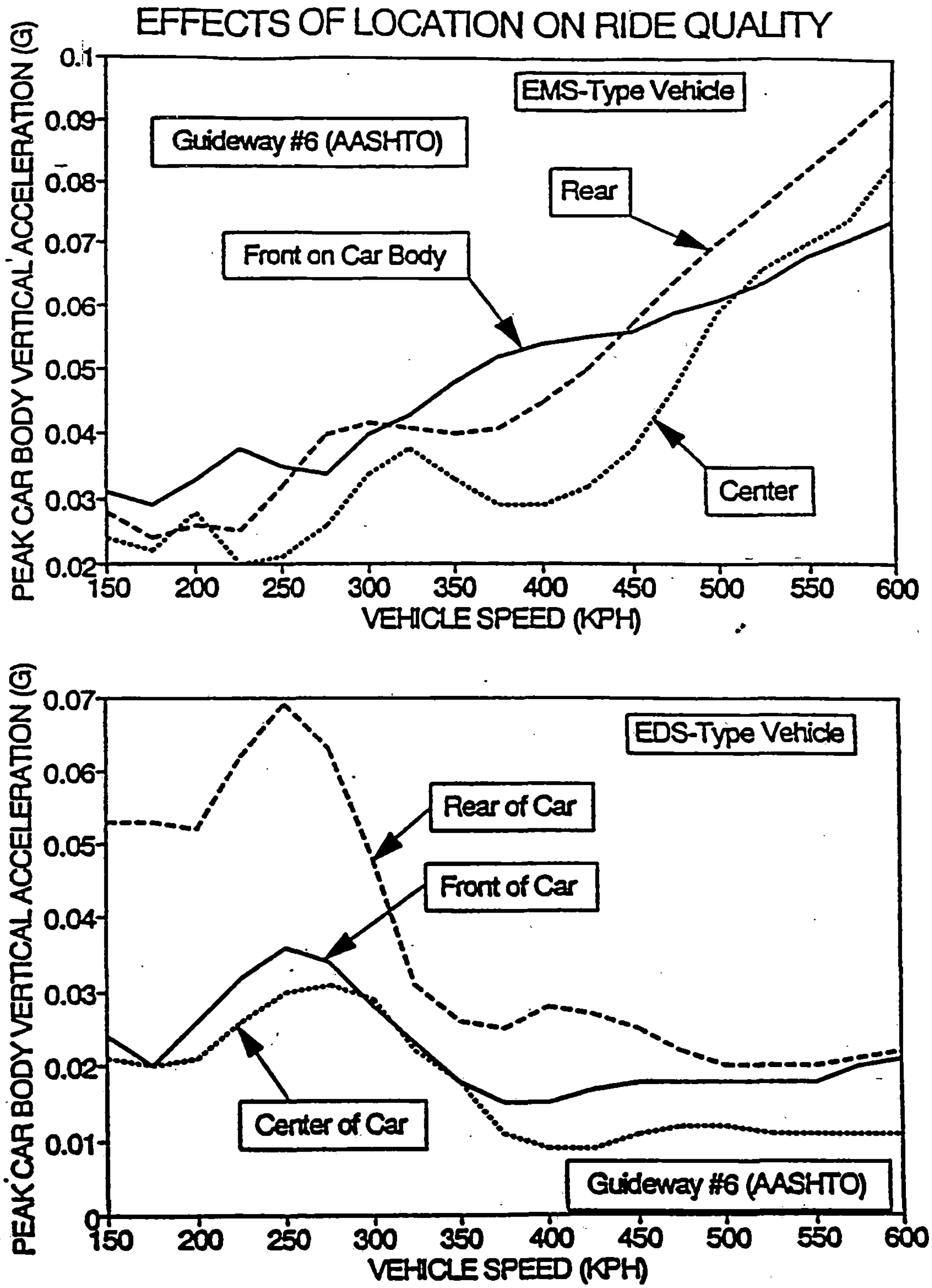

Figure 6.2-4 Car Body Vertical Accelerations by Position in Car.

Guideways 4 and 5, the car center position had the highest acceleration levels at speeds over 500 km/h (not illustrated).

For subsequent car body acceleration plots, we have used the highest peak value, regardless of position or polarity.

Car body and guideway vertical acceleration response levels for the six 21-meter guideway structures (see Figure 6.1-4) are shown in Figure 6.2-5 for the EMS-type vehicle. Guideways 1, 2, 3, and 6 provide almost identical ride quality, a monotonic increase in peak car body acceleration level with increasing speed. At speeds above about 500 km/h, the desired one-hour decreased comfort limit is exceeded. Much rougher ride is indicated for the lighter-weight Guideways 4 and 5. Guideways 4 and 5 also exceed the design mid-span acceleration limit of 0.3 g, particularly at higher speeds.

Similar response curves for the six 21-meter guideways under the EDS-type vehicle are shown in Figure 6.2-6 Here the salient resonant peak is seen produced by the "bogie vehicle" in the 250 to 350 km/h speed range. This phenomenon is reported in most technical publications on vehicle/guideway dynamic interactions. It is a product of beam bending and vehicle bounce/pitch dynamics. Car accelerations exceed the one-hour reduced comfort limit in this speed range; and mid-span beam accelerations exceed the design 0.3 g limit by substantial margins. The heavier-weight Guideways 2, 3 and 6 provide the best control of the resonance. These guideways range from 89 to 102 tonnes per span (compared with a 45-tonne vehicle), while Guideway 4 is 59 tonnes per span and Guideway 5 a mere 25 tonnes per span. These guideways (particularly Guideway 5) are dominated by the mass of the passing vehicle and respond accordingly. This is evident by mid-span accelerations of almost 2.5 g peak on Guideway 5. Although the structure is quite stiff, designed to a 1/4000 static deflection criterion, its light mass is overwhelmed by a vehicle/span mass ratio of almost two to one. (This structure was not, however, designed for an EDS-type vehicle.)

Longer (39-meter) span lengths are evaluated in Figures 6.2-7 and -8. Ride quality for the EMS-type vehicle, Figure 6.2-7, is seen to be unacceptable on representative Guideways 1 and 6, particularly at speeds above 250 km/h. For the EDS-type vehicle, ride quality is acceptable except for marginal ride at a resonant peak near 150 km/h. The other three guideways exhibit poor ride quality below about 200 km/h on the longer length spans. Mid-span acceleration plots in this figure show multiple peaks with speed as higher (second and third) beam bending modes come into resonance.

The effects of "continuous" two-span beams are explored in Figures 6.2-9 through 6.2-11. In Figure 6.2-9, the response of the one-span (21-meter) simply-supported Guideway 5 beam is compared with a two-span (43-meter) continuous beam with center column under an EMS-type vehicle. Substantial reductions in car body vertical accelerations are realized.

Mid-span (between columns) beam accelerations are also reduced except at a two-span beam resonance near 550 km/h.

The comparison of one-span and two-span guideway structures under an EDS-type vehicle, however, resulted in a "mixed bag" at best. Response of representative heavier structures, Guideways 1 and 6, are shown in Figure 6.2-10 While the two-span (center column) configuration resulted in reduced mid-span (between columns) acceleration levels, it also resulted in substantially reduced vehicle ride quality. Basically similar results were noted for the two lighter weight structures (Guideways 4 and 5) in Figure 6.2-11. It should be noted that the 5 mm camber for the two-span guideway extended over the full 43 meters with maximum amplitude over the center column.

Maximum guideway structure bending moments from the simulation runs and the speeds at which these occur are given in Table 6.2-A These values of dynamic maxima are listed for both the EMS and EDS-type vehicles. Static bending moments (no vehicle loading) and design maximum bending moments are also listed for reference. (No design maximum was given for Guideway 5, the triangular steel section.) The computer models show that the multiple-magnet EMS configuration generates higher maximum loads than the "two bogie" EDS arrangement. Maximum bending moments for most of the structures are comfortably within the design maxima. The exception is Guideway 4 (and probably 4P) under the EMS-type vehicle. We cannot judge Guideway 5, for which no design maximum is currently available. The two-span guideway structures (42.67 m in length with a center column) appear to be subjected to consistently lower bending moments than the comparable one-span (21.33 m length simply supported) structures.

Outline Sketches of Guideway Structures.

1 Steel Girders w/ concrete deck	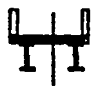
2 Concrete Box	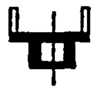
3 Trapezoidal Box	
4 Twin Box (HSST)	
5 Steel "V" (Transrapid)	
6 AASHTO Concrete Girders	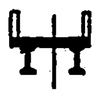

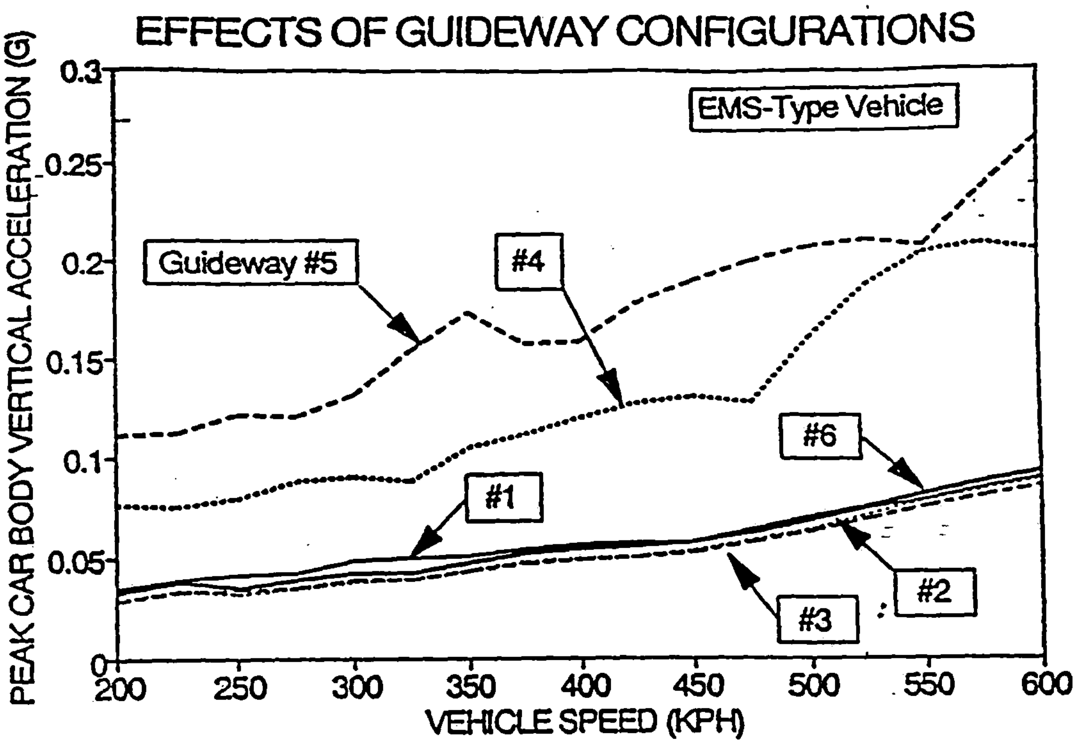

a. Maximum Car Body Vertical Accelerations.

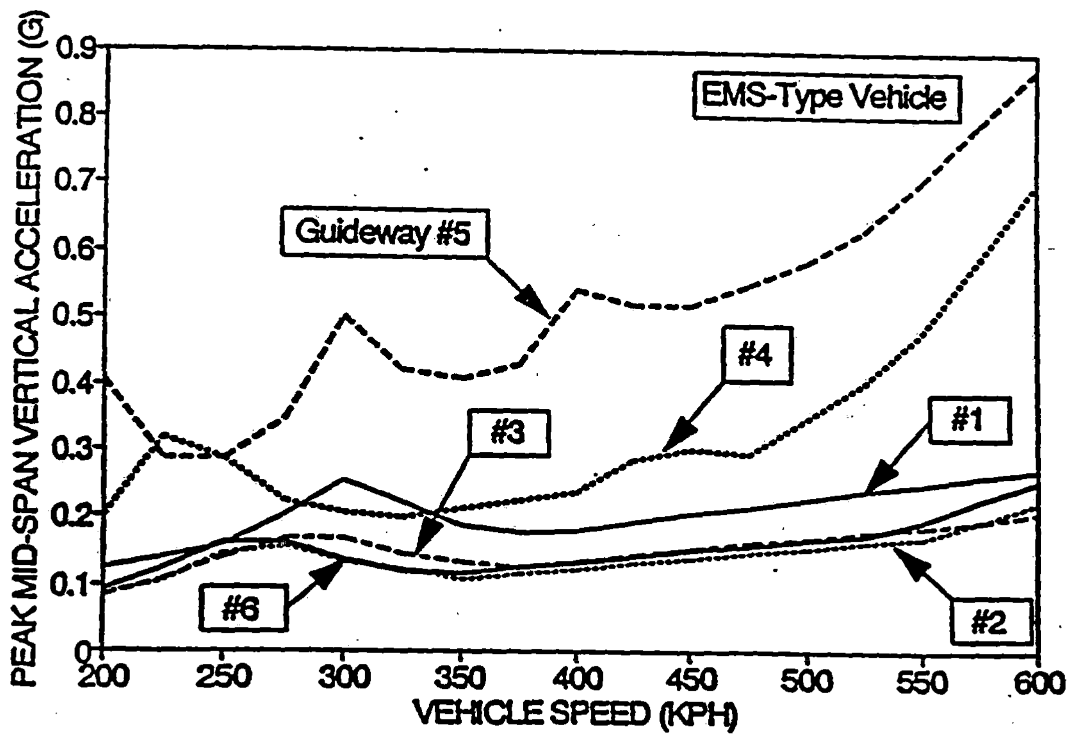

b. Maximum Guideway Mid-Span Vertical Accelerations.

Figure 6.2-5 Short Guideway Span Interactions EMS-Type Vehicle.

Outline Sketches of Guideway Structures.

1 Steel Girders w/ concrete deck	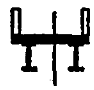
2 Concrete Box	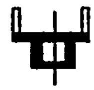
3 Trapezoidal Box	
4 Twin Box (HSST)	
5 Steel "V" (Transrapid)	
6 AASHTO Concrete Girders	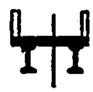

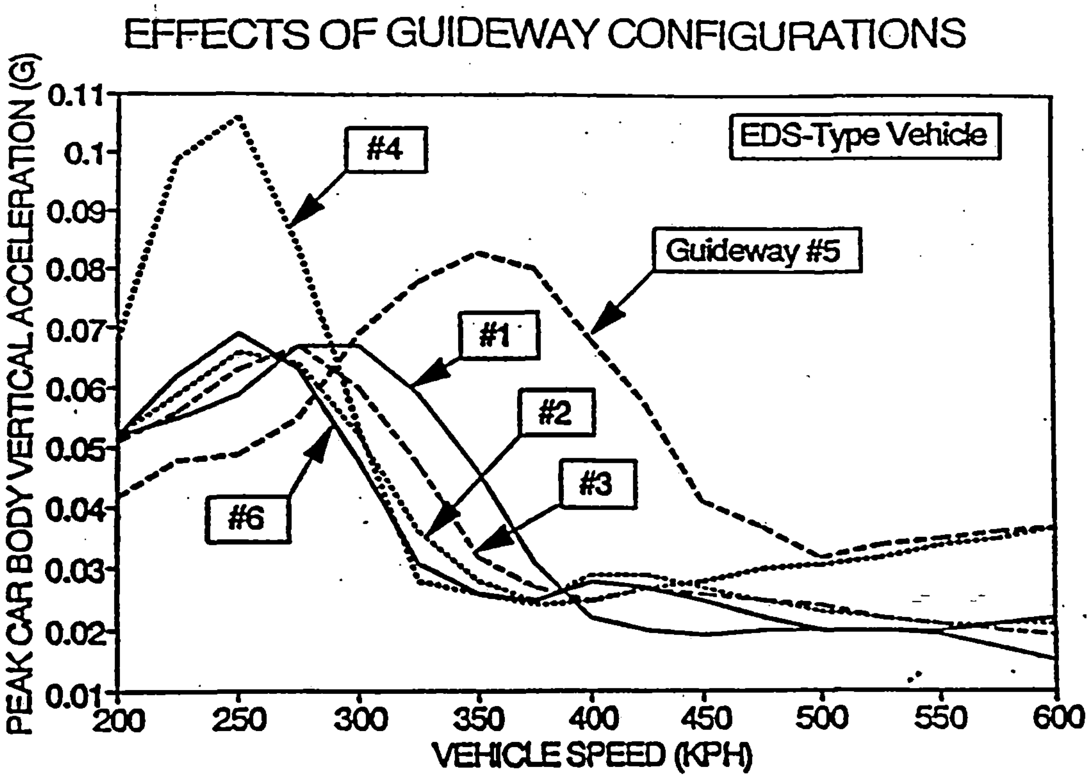

a. Maximum Car Body Vertical Accelerations.

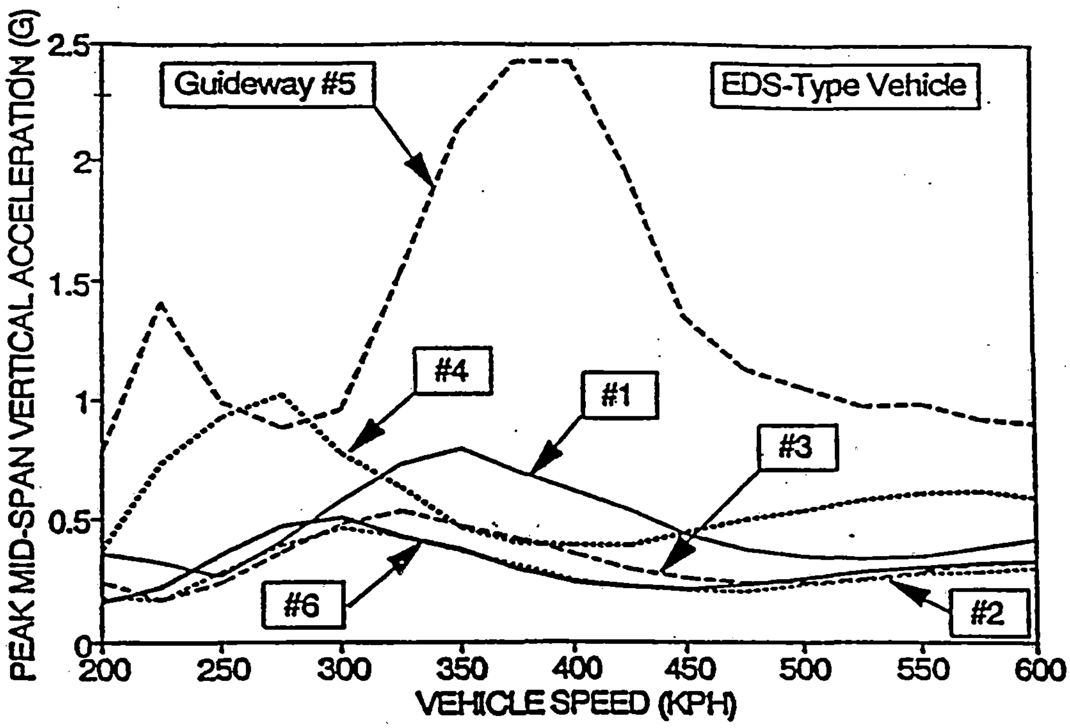

b. Maximum Guideway Mid-Span Vertical Accelerations.

Figure 6.2-6 Short Guideway Span Interactions with EDS-Type Vehicle.

Outline Sketches of Guideway Structures.

1 Steel Girders w/ concrete deck	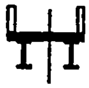
2 Concrete Box	
3 Trapezoidal Box	
4 Twin Box (HSST)	
5 Steel "V" (Transrapid)	
6 AASHTO Concrete Girders	

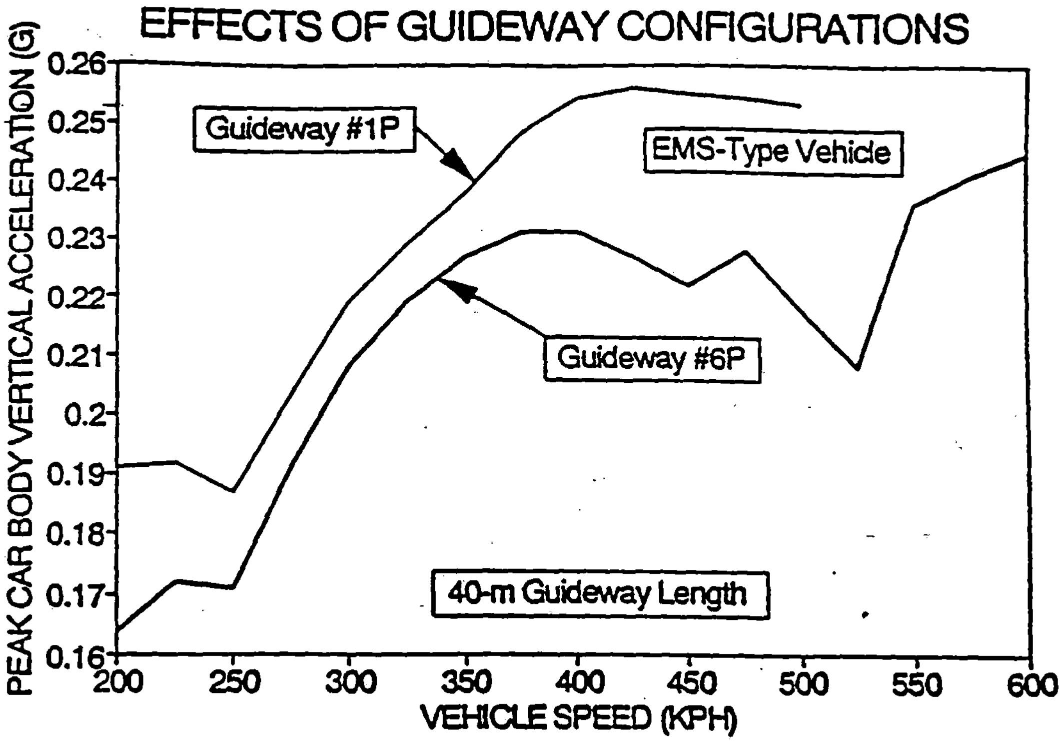

a. Maximum Car Body Vertical Accelerations.

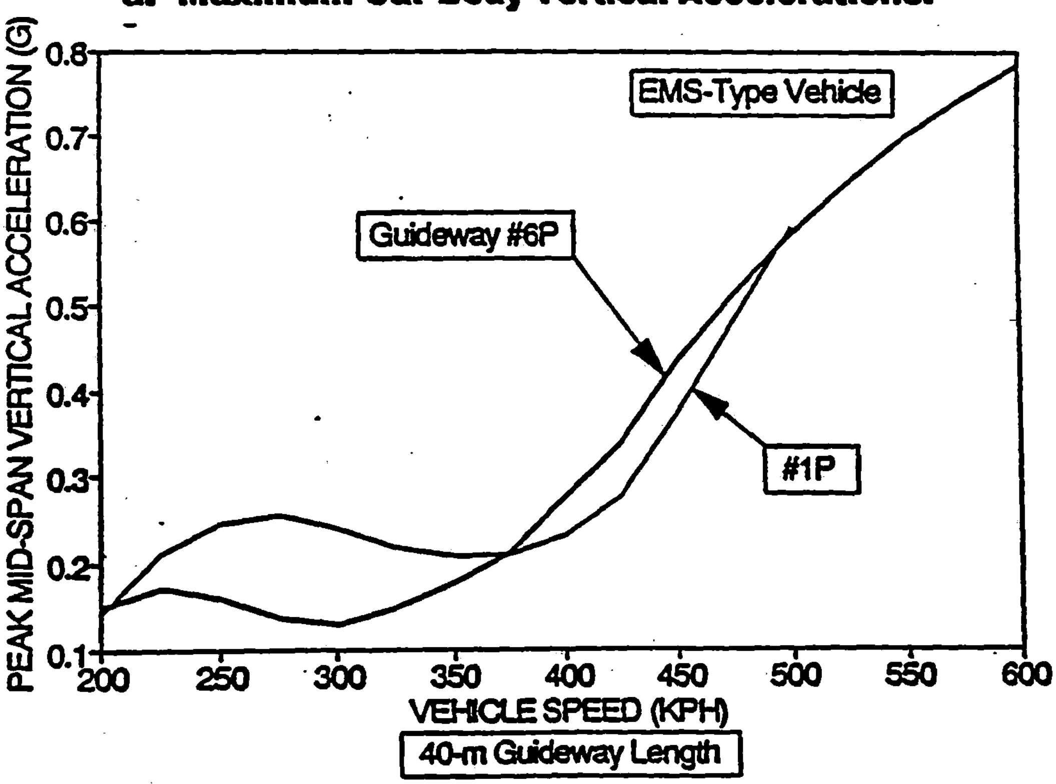

b. Maximum Guideway Mid-Span Vertical Accelerations.

Figure 6.2-7 Long Guideway Span Interactions with EMS-Type Vehicle.

Outline Sketches of Guideway Structures.

1 Steel Girders w/ concrete deck	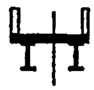
2 Concrete Box	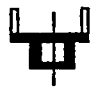
3 Trapezoidal Box	
4 Twin Box (HSST)	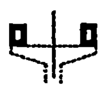
5 Steel "V" (Transrapid)	
6 AASHTO Concrete Girders	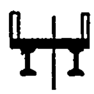

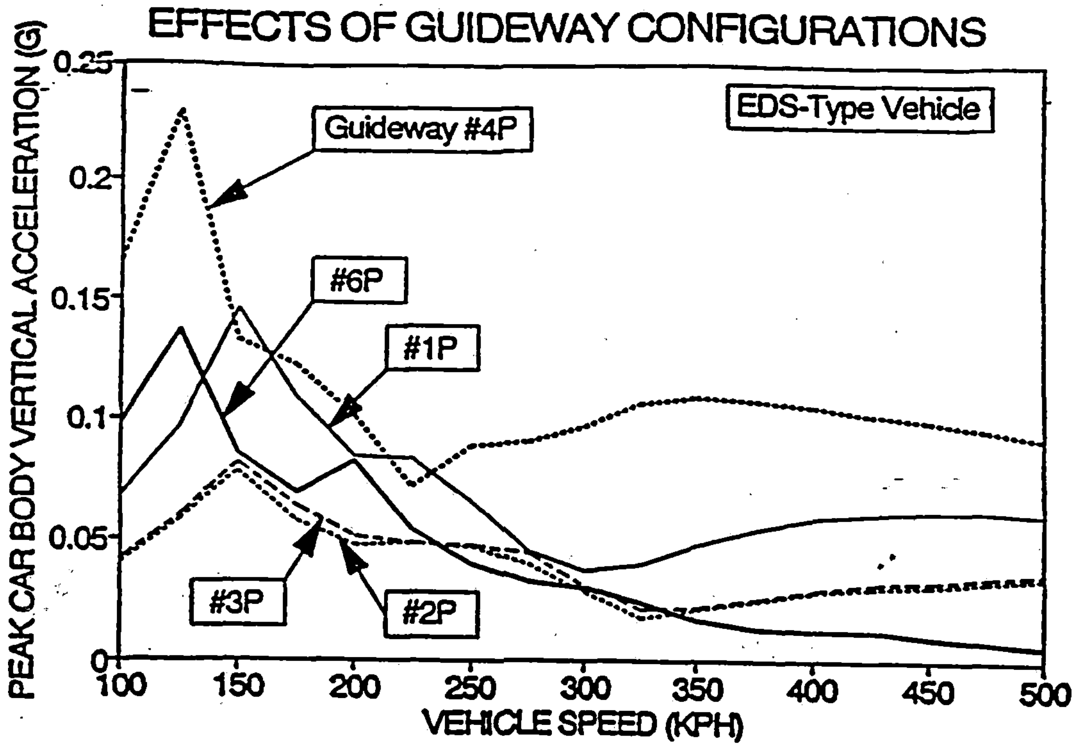

a. Maximum Car Body Vertical Accelerations.

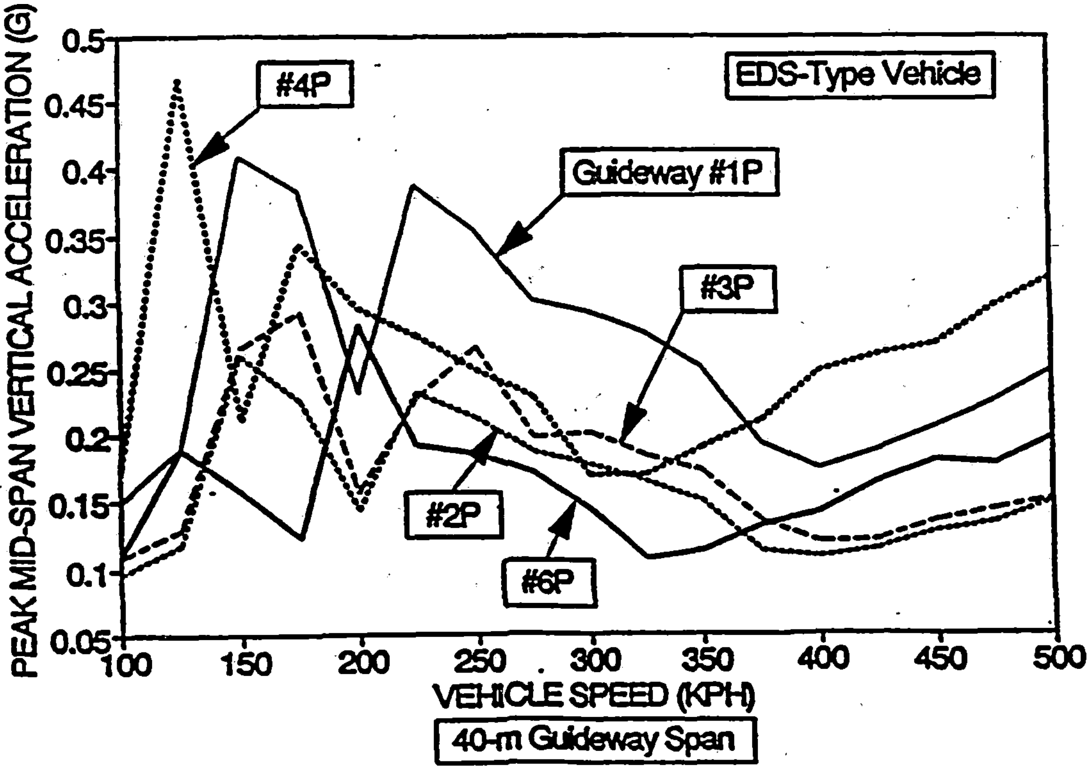

b. Maximum Guideway Mid-Span Vertical Accelerations.

Figure 6.2-8 Long Guideway Span Interactions with EDS-Type Vehicle.

Outline Sketches of Guideway Structures.

1 Steel Girders w/ concrete deck	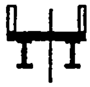
2 Concrete Box	
3 Trapezoidal Box	
4 Twin Box (HSST)	
5 Steel "V" (Transrapid)	
6 AASHTO Concrete Girders	

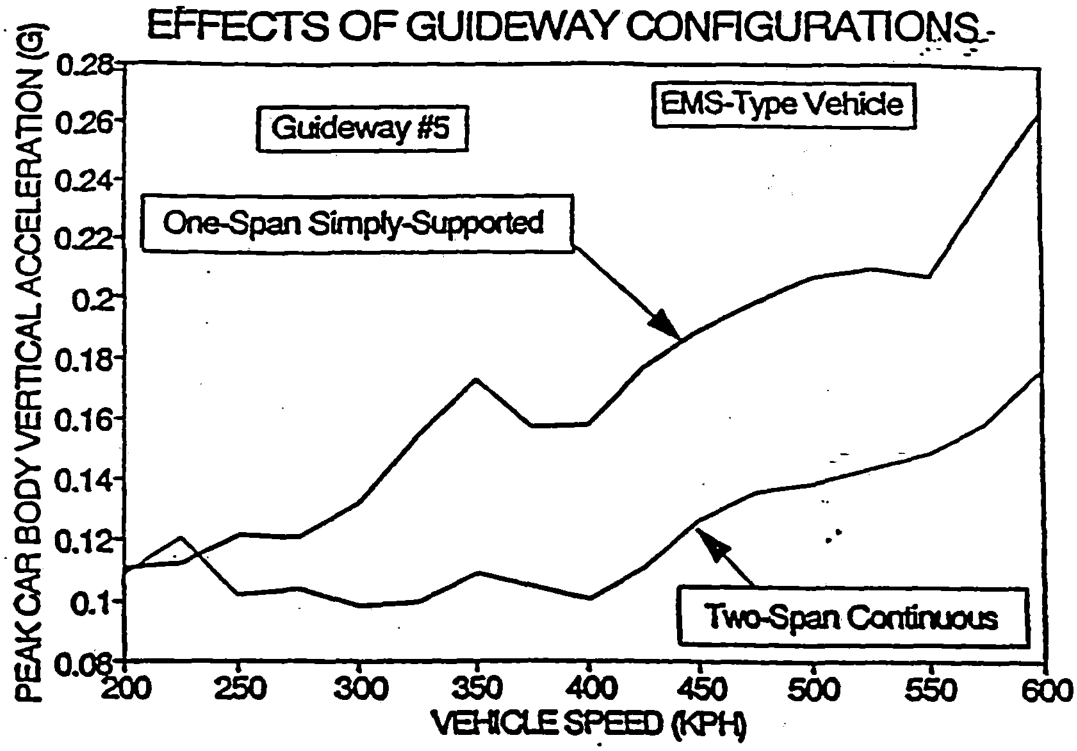

a. Maximum Car Body Vertical Accelerations

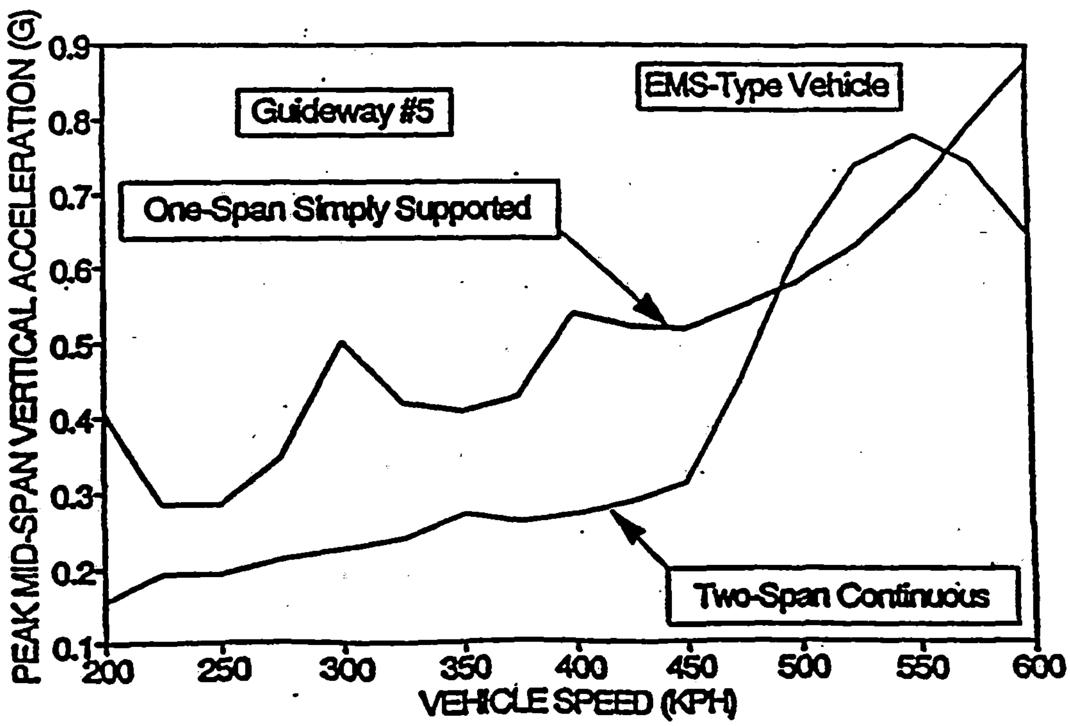

b. Maximum Guideway Mid-Span Vertical Accelerations.

Figure 6.2-9 One-Span vs. Two-Span Guideway Beams (EMS).

Outline Sketches of Guideway Structures.

1 Steel Girders w/ concrete deck	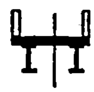
2 Concrete Box	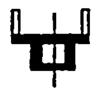
3 Trapezoidal Box	
4 Twin Box (HSST)	
5 Steel "V" (Transrapid)	
6 AASHTO Concrete Girders	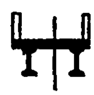

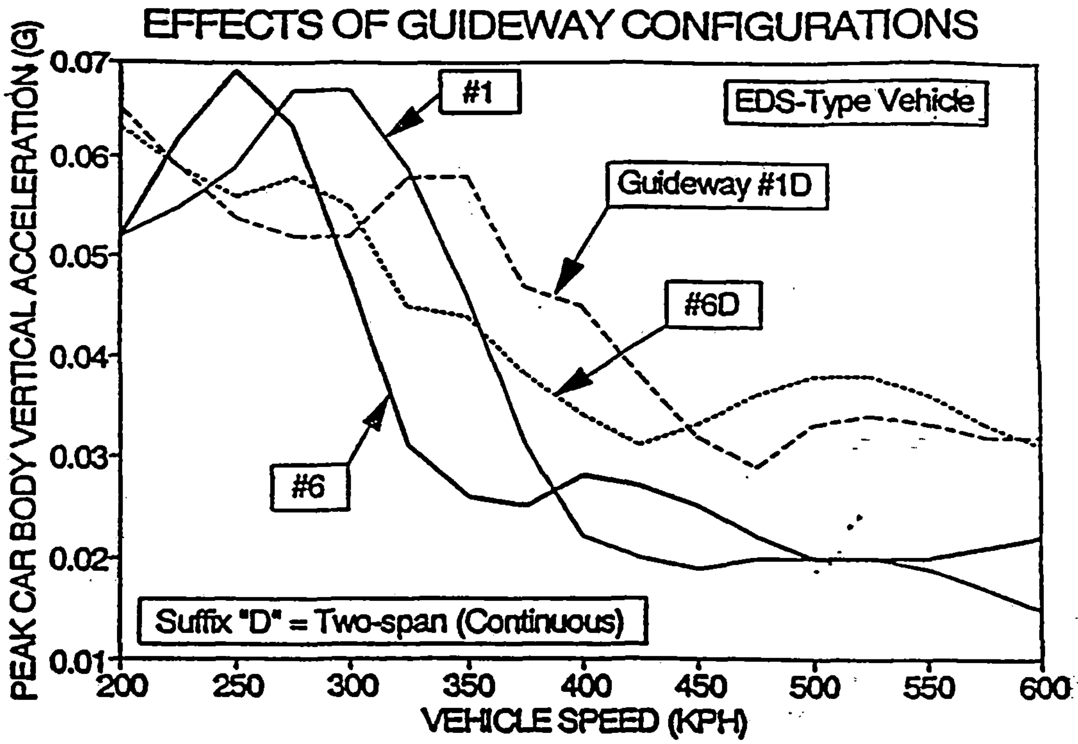

a. Maximum Car Body Vertical Accelerations

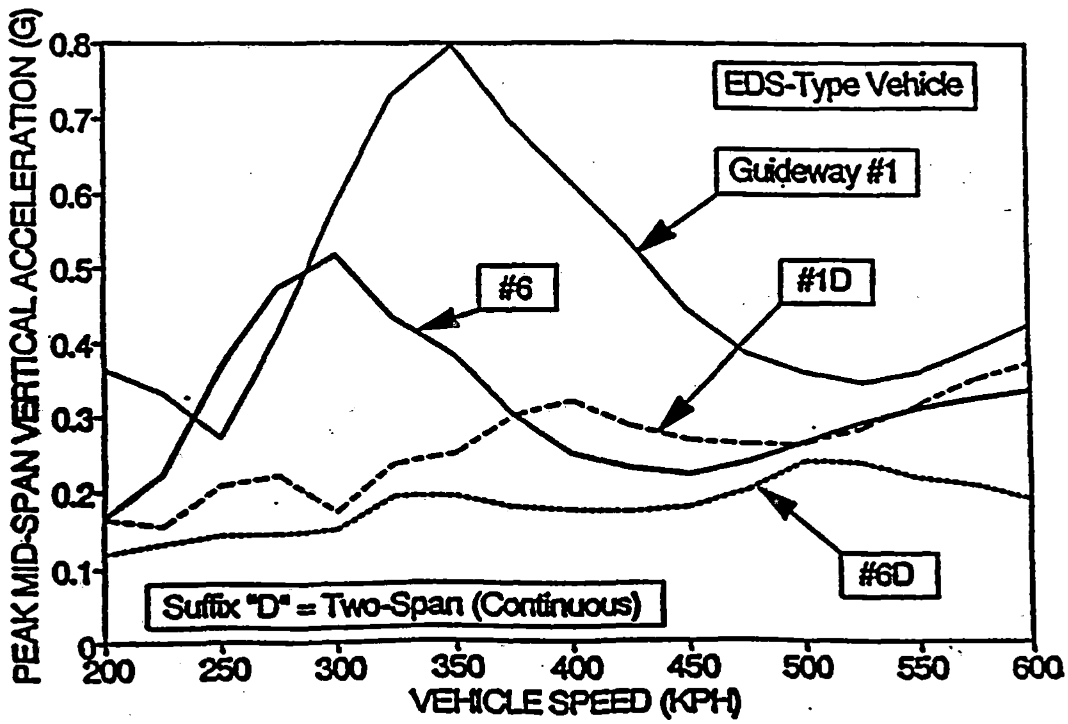

b. Maximum Guideway Mid-Span Vertical Accelerations

Figure 6.2-10 One-Span vs. Two-Span Guideway Beams (EDS).

Outline Sketches of Guideway Structures.

1 Steel Girders w/ concrete deck	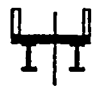
2 Concrete Box	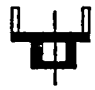
3 Trapezoidal Box	
4 Twin Box (HSST)	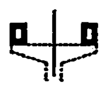
5 Steel "V" (Transrapid)	
6 AASHTO Concrete Girders	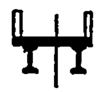

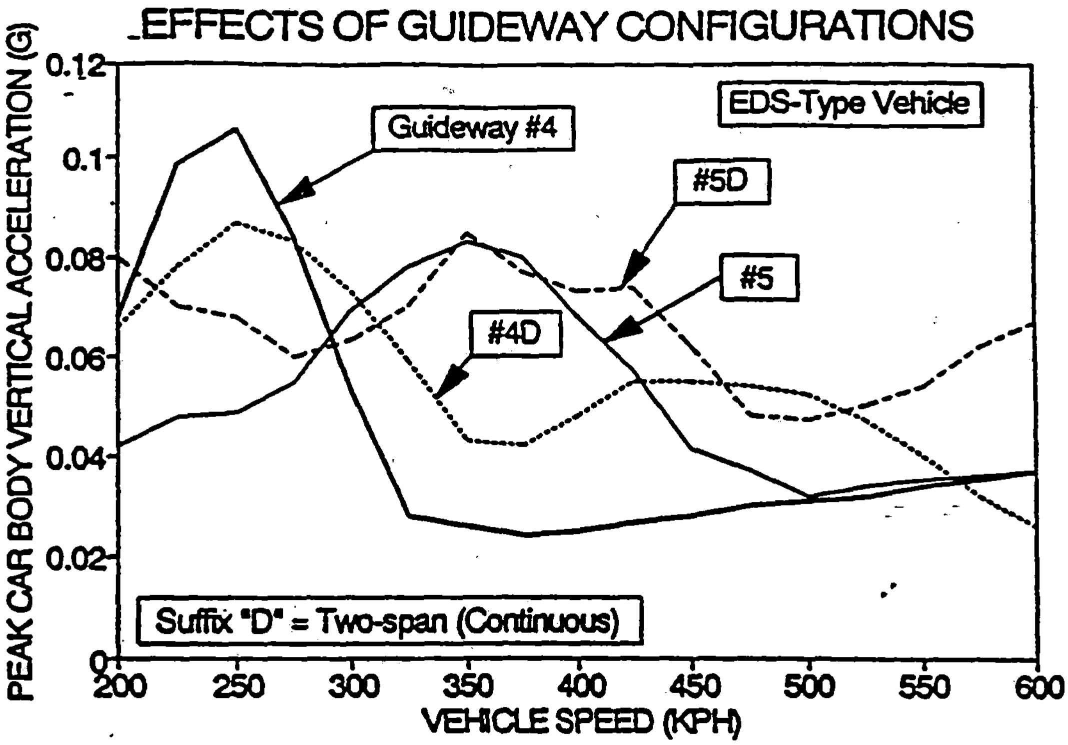

a. Maximum Car Body Vertical Accelerations

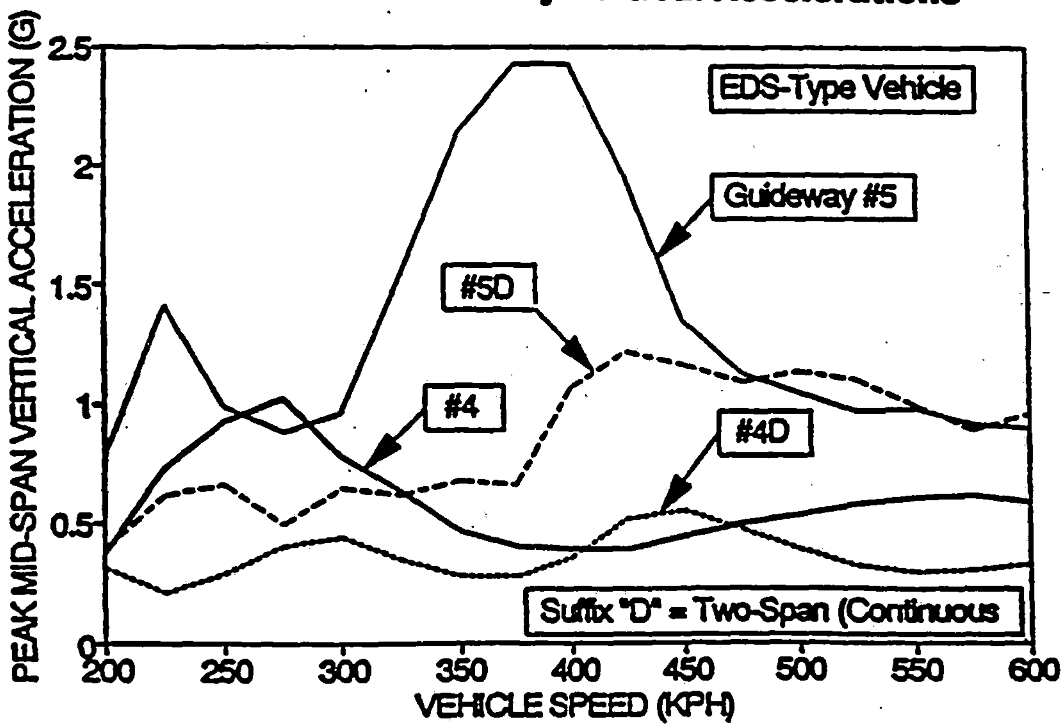

b. Maximum Guideway Mid-Span Vertical Accerlerations

Figure 6.2-11 One-Span vs. Two-Span Guideway Beams (EDS)

TABLE 6.2-A

Maximum Guideway Beam Dynamic Bending Moments.

			EMS-Type Vehicle		EDS-Type Vehicle	
Guideway	Design Maximum (kN-m)	Static[1] (kN-m)	Dynamic Maximum (kN-m)	Speed (km/h)	Dynamic Maximum (kN-m)	Speed (km/h)
1[a]	5,730	1,660	3,855	600[3]	3,068	325
2	6,600	2,664	4,983	600	4,046	300
3	6,180	2,315	4,550	600	3,684	300
4	4,300	1,544	4,264	600	3,132	275
5		736	3,700	600	2,525	375
6	6,370	2,564	4,952	600	3,993	275
1P[b]	17,900	6,616	14,180	500[3]	10,016	150
2P	21,900	10,624			14,114	150
3P	20,960	9,708			13,118	150
4P	14,670	7,445			11,286	125
6P	21,290	10,624	19,311	600	14,062	125
1D[c]		934[2]			1,830	375
2D		1,449			2,378	350
3D		1,303			2,174	375
4D		868	2,475		1,837	300
5D		414	2,192		1,570	425
6D		1,443	2,876		2,342	325

Notes:

a — One-span simply supported beam, 21.33 m length (Guideway 5 is 24 m length).

b — One-span simply supported beam, 39.62 m length.

c — Two-span "continuous" beam (center support), 42.67 m length.

1 — Static bending moment under guideway structure weight.

2 — Maximum assumed at 3/8th distance to center support.

3 — Highest speed run on computer.

6.3 Effects of Lateral and Torsional Dynamics Without Wind Gusts

Lateral and torsional dynamic vehicle/guideway loads are introduced by guideway geometry errors, by wind loads, and by curve negotiation. Curving behavior is beyond the scope of this current study, and only geometry or wind-induced loads have been considered.

A representative guideway geometry error was used to investigate vehicle and structural response. This geometry error consisted of a 5 mm versine alignment error and an 0.5 degree versine cross level (roll) error on a 20-meter wavelength. These errors were phased in a down-and-out relationship which was found to produce maximum response. Examples of car body lateral accelerations produced in the EMS and EDS-type vehicles by this disturbance are shown in Figure 6.3-1. Responses of the vehicle laterally and torsionally are much lower than the vertical responses. The following describes the results of the lateral and torsional analysis without a graph of the data.

Car body lateral acceleration response (at the body c.g. height) of the multi-magnet EMS-type maglev vehicle to this type of geometry error is nearly identical on the different guideways. It consists of a slight peak near 125 km/h, but in general a monotonic increase in peak acceleration with speed to 0.066 to 0.068 g at 600 km/h, the highest speed computed. Similarly, roll accelerations range from 0.446 to 0.492 rad/sec^2 peak. Peak lateral loads at the beam/column bearing pads range from 17 to 22 kN. The only significant differences in response appear to be the peak guideway lateral accelerations, which range from 0.041 g (Guideway 4) to 0.076 g (Guideway 6).

Response of the EDS-type vehicle is again the same for the different guideways, but markedly different from the EMS-type vehicle. A peak lateral acceleration of 0.036 g occurs at 75 km/h, dropping to 0.020 g at higher speeds. Roll accelerations range from 0.286 r/s^2 (Guideway 1, 325 km/h) to 0.296 r/s^2 (Guideway 6, 425 km/h). Peak lateral loads on the beam/column bearing pads range from 6.6 kN (Guideway 1, 600 km/h) to 12 kN (Guideway 6, 500 kN). Guideway beam lateral accelerations range from 0.020 to 0.030 g

In general, variations in lateral and torsional dynamics were more pronounced from one vehicle to the other than from one guideway configuration to another.

Maglev Vehicle/Guideway Interaction

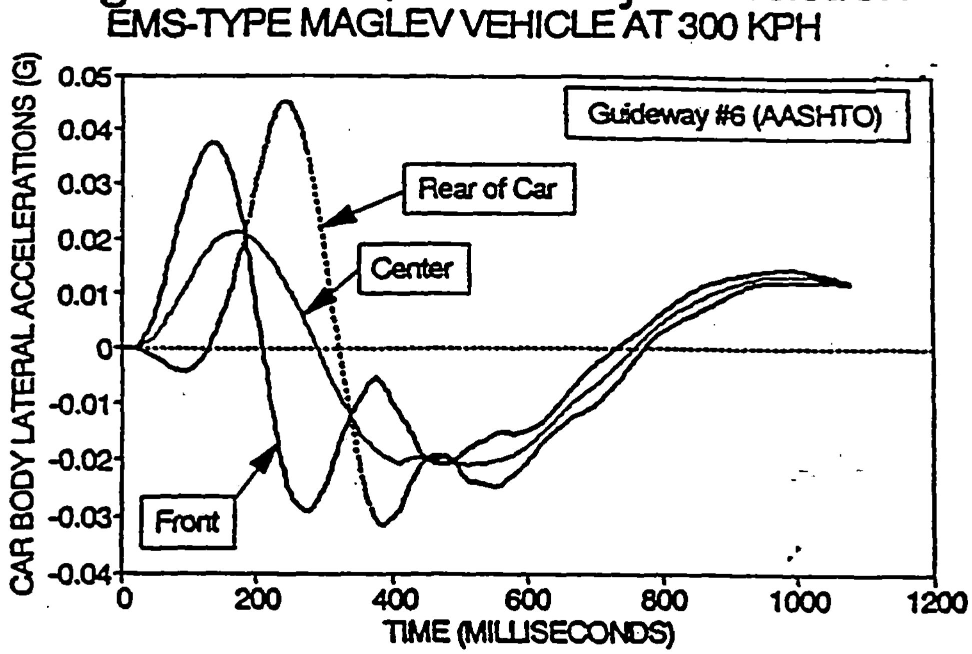

a. EMS-Type Maglev Vehicle.

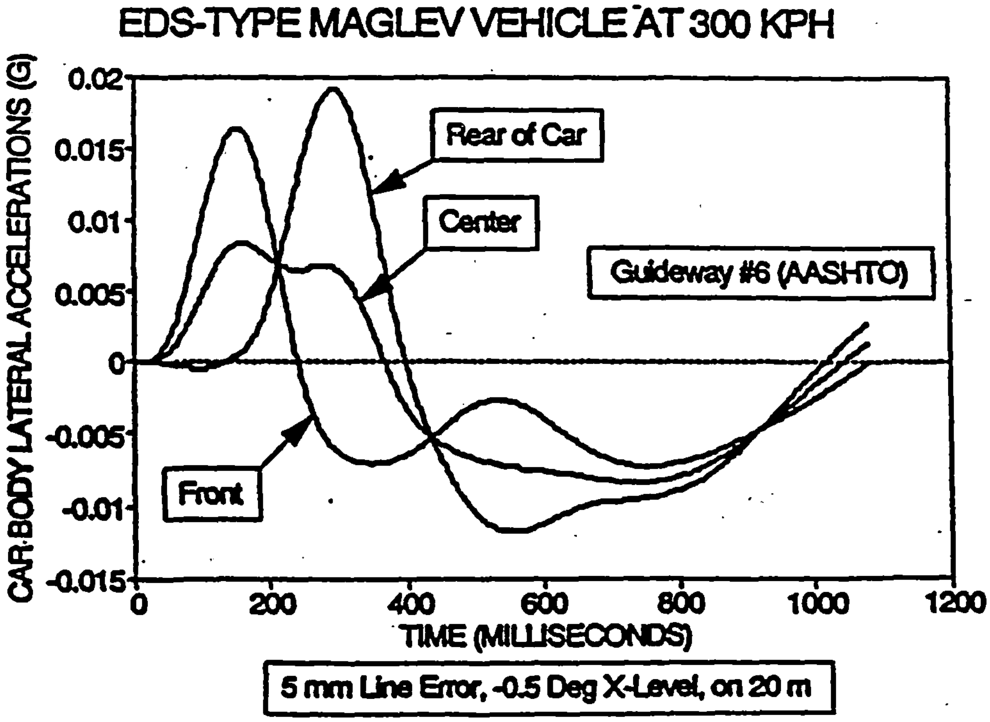

b. EDS-Type Maglev Vehicle.

Figure 6.3-1 Car Body Lateral Response to Geometry Errors.

6.4 Effects of Wind Gusts on Lateral and Torsional Dynamics

Steady-state wind loads and moments on the maglev vehicles were calculated by Gregorek and Boyd of Ohio State University. Information on the spatial change in wind gust velocity was not, however, readily available[1].

A worst-case condition was therefore assumed. Steady-state loads and moments on the two-car vehicle for a 115 km/h side wind gust for a 400 km/h vehicle speed were calculated. A sharply defined gust boundary was then assumed, and the vehicle simply allowed to enter the gust across this boundary. Loads and moments on leading and trailing cars were then modulated by exposed area and position of the assumed center of pressure. Lateral accelerations at different locations in the leading car and the resulting lateral loads on the beam/column bearing pads are plotted in Figure 6.4-1 showing the strong car yaw response to this disturbance. The ride is uncomfortable, but the vehicle is stable.

6.5 Effects of Guideway Structure Support Stiffness

A few computer runs were made to explored the effects of guideway beam bearing pad vertical stiffness with both the baseline EMS and EDS vehicle parameters. The results are, to say the least, interesting. Runs over a wide speed range were conducted with both types of simulated vehicles using Guideway 6, the standard AASHTO design, and stiffness ranging from one-third to three times the nominal bearing pad stiffness. With the EDS-type vehicle, Figure 6.5-1, substantial reductions in beam mid-span acceleration response are realized with safety bearing pads. This reduction, however, is not translated into a comparable reduction in car body vertical accelerations. The resonant peak can be reduced in speed from about 275 to 200 km/h by lowering the stiffness. However, the peak amplitude at this resonance is not reduced appreciably.

Predictions with the EMS-type vehicle are shown in Figure 6.5-2. Both beam response and ride quality are significantly worsened by reducing the bearing pad stiffness. Increasing the stiffness by a factor of three improves ride quality of the EMS vehicle, although beam response now exhibits a resonance at 300 km/h. These results show that

1 See, for example, Peter Sachs, Wind Forces in Engineering, 2nd Edition, Pergamon Press, 1978

Figure 6.4-1 Response to a Worst-Case 115 km/h Wind Gust.

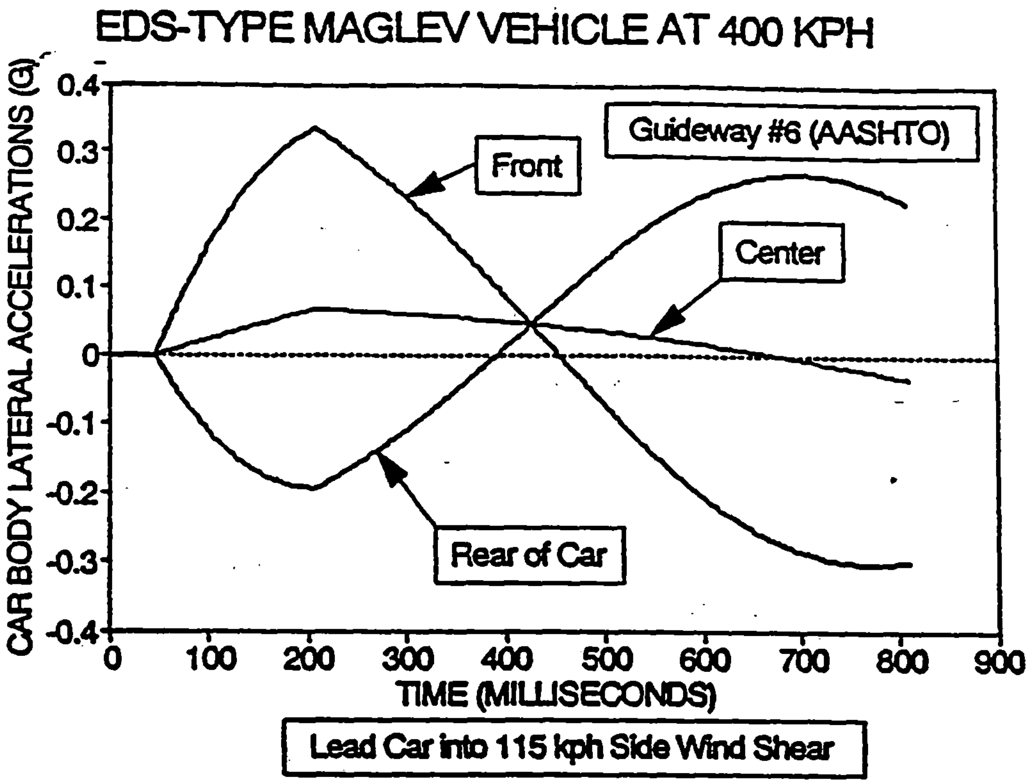

a. Car Body Accelerations

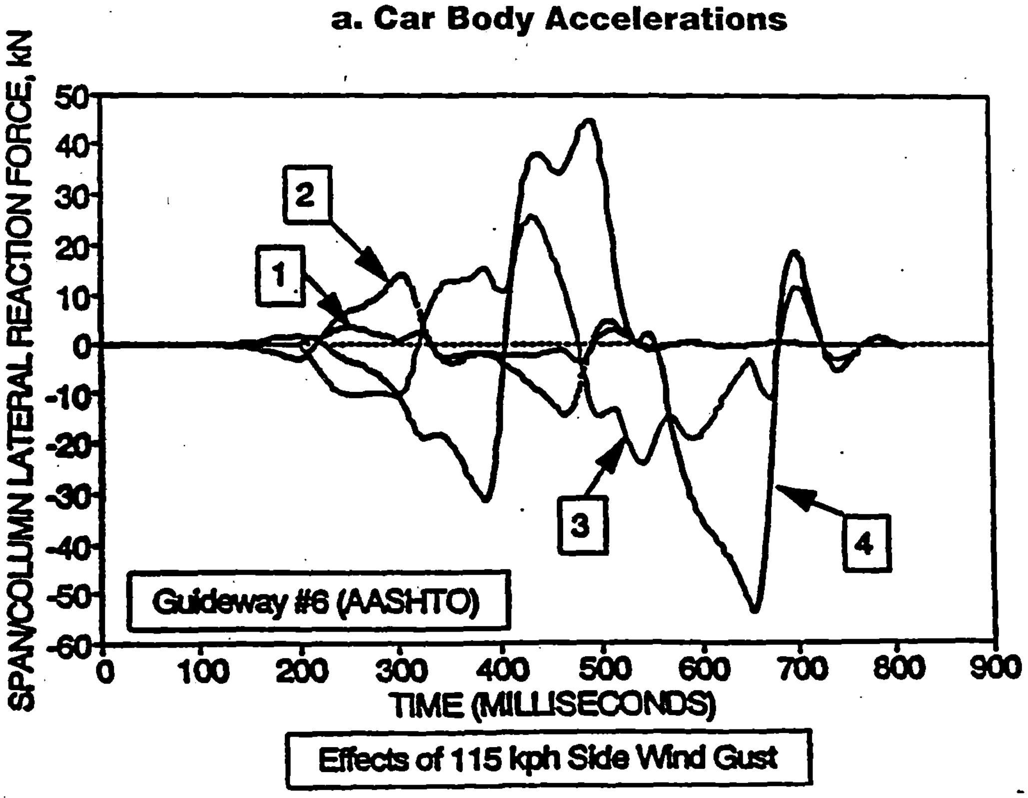

b. Span/Column Lateral Reaction

Figure 6.5-1 Variations of Bearing Pad Stiffness, EDS-Type Vehicle.

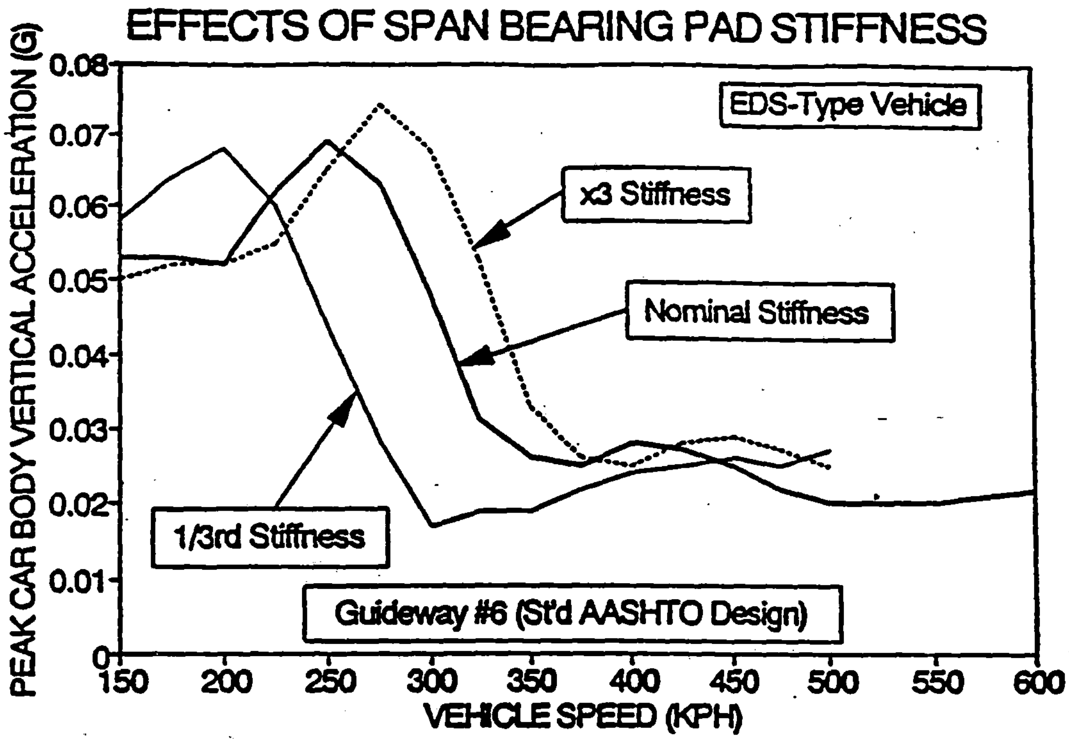

a. Car Body Accelerations

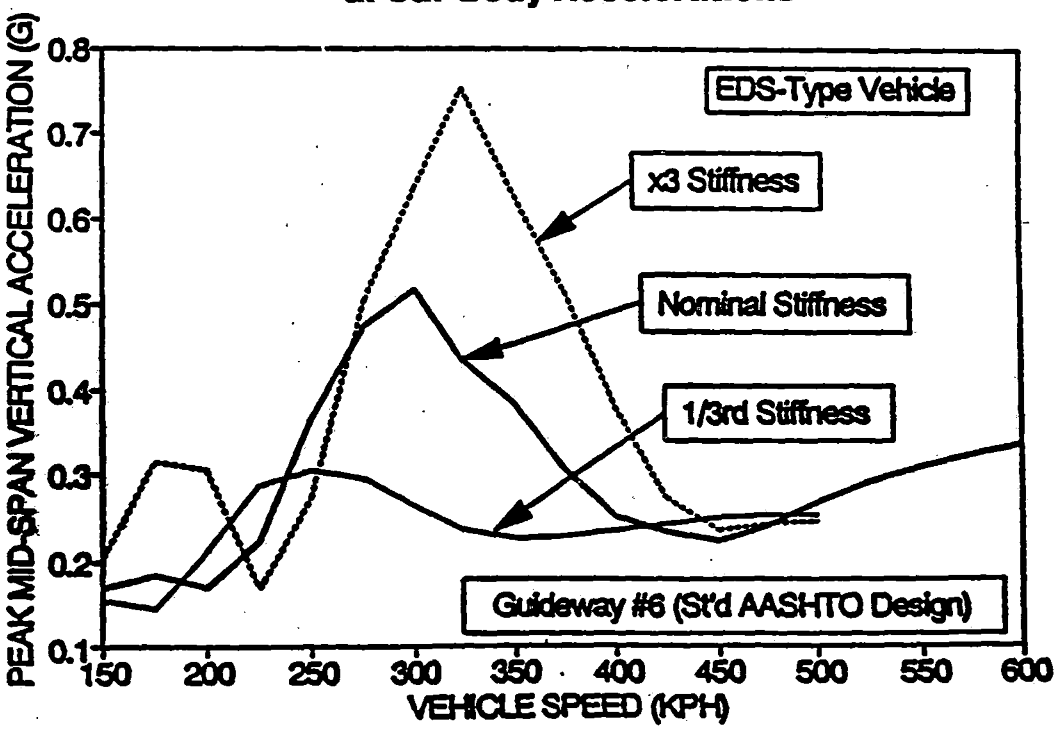

b. Beam Mid-span Accelerations

Figure 6.5-2 Variations of Bearing Pad Stiffness, EMS-Type Vehicle.

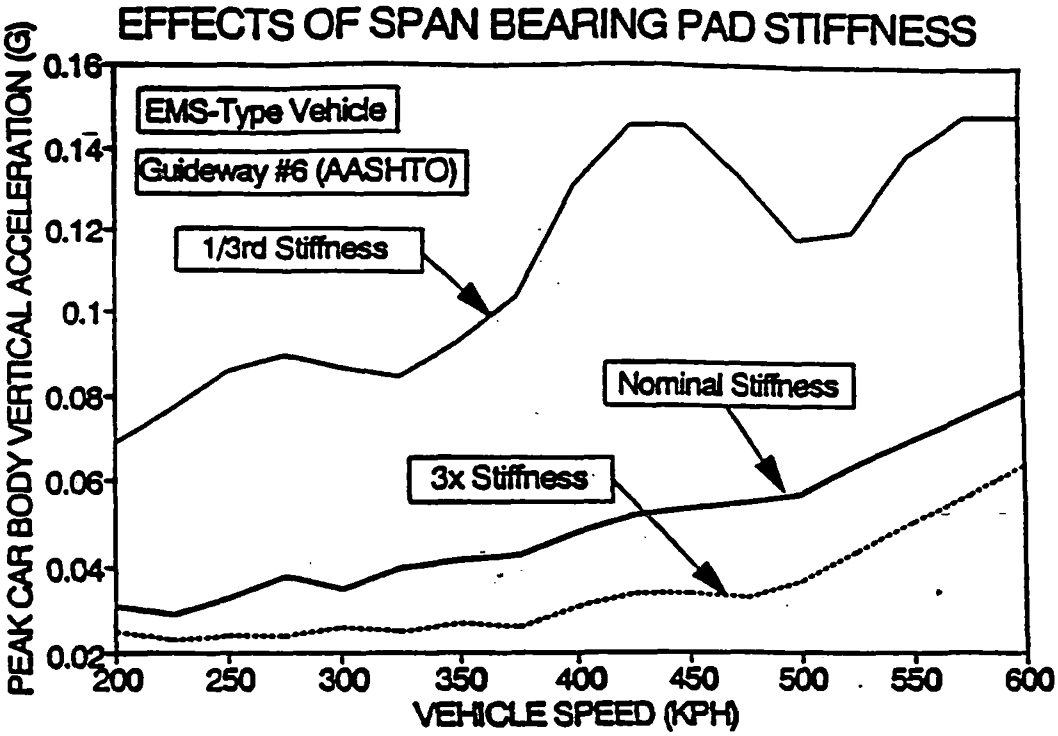

a. Car Body Accelerations

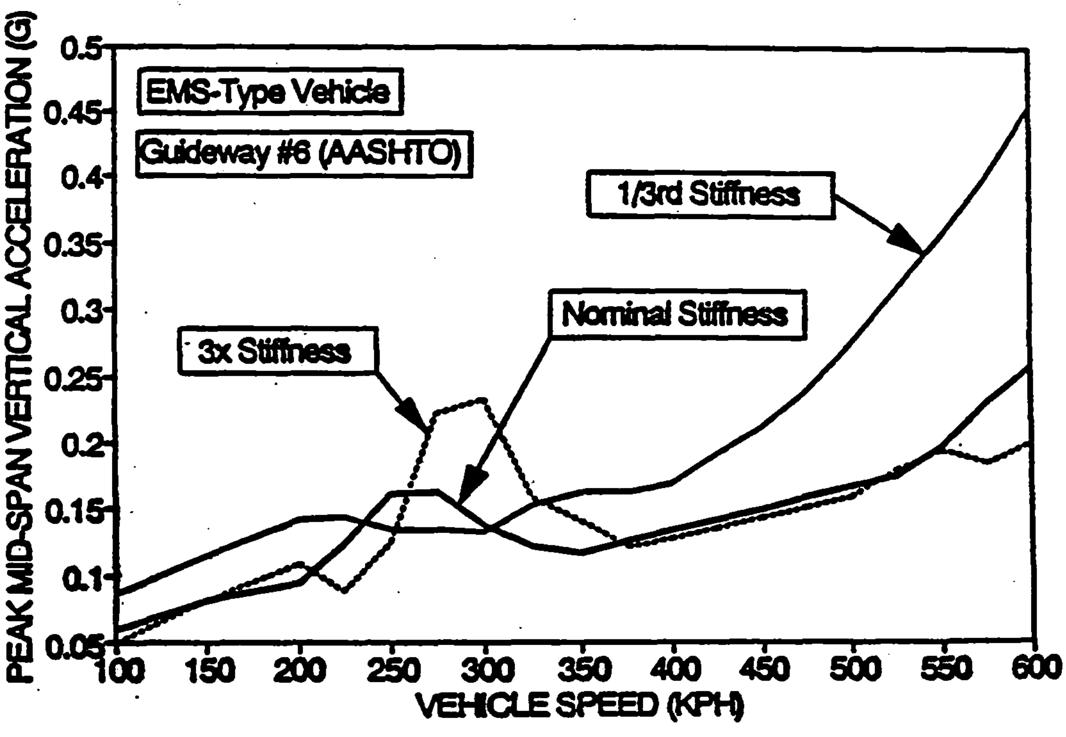

b. Beam Mid-span Accelerations

caution must be exercised in considering choice of bearing pads and, simultaneously, the characteristics of the guideway and the vehicle.

6.6 Effects of Vehicle Configuration

While an extensive variation of vehicle parameters was beyond the scope of this study, two additional runs were made to determine the influence of vehicle overall length on ride quality. The baseline runs were made with an EDS-type vehicle with an 18-meter car body. These additional runs were conducted with 21 and 24-meter overall car body lengths. Results are shown in Figure 6.6-1. These plots show that for the EDS-type vehicle (a "two-bogie" configuration), an overall length close to that of the most commonly-used span length is beneficial. This means that the pitch mode of car body oscillation is minimized, reducing the 250-km/h resonance.

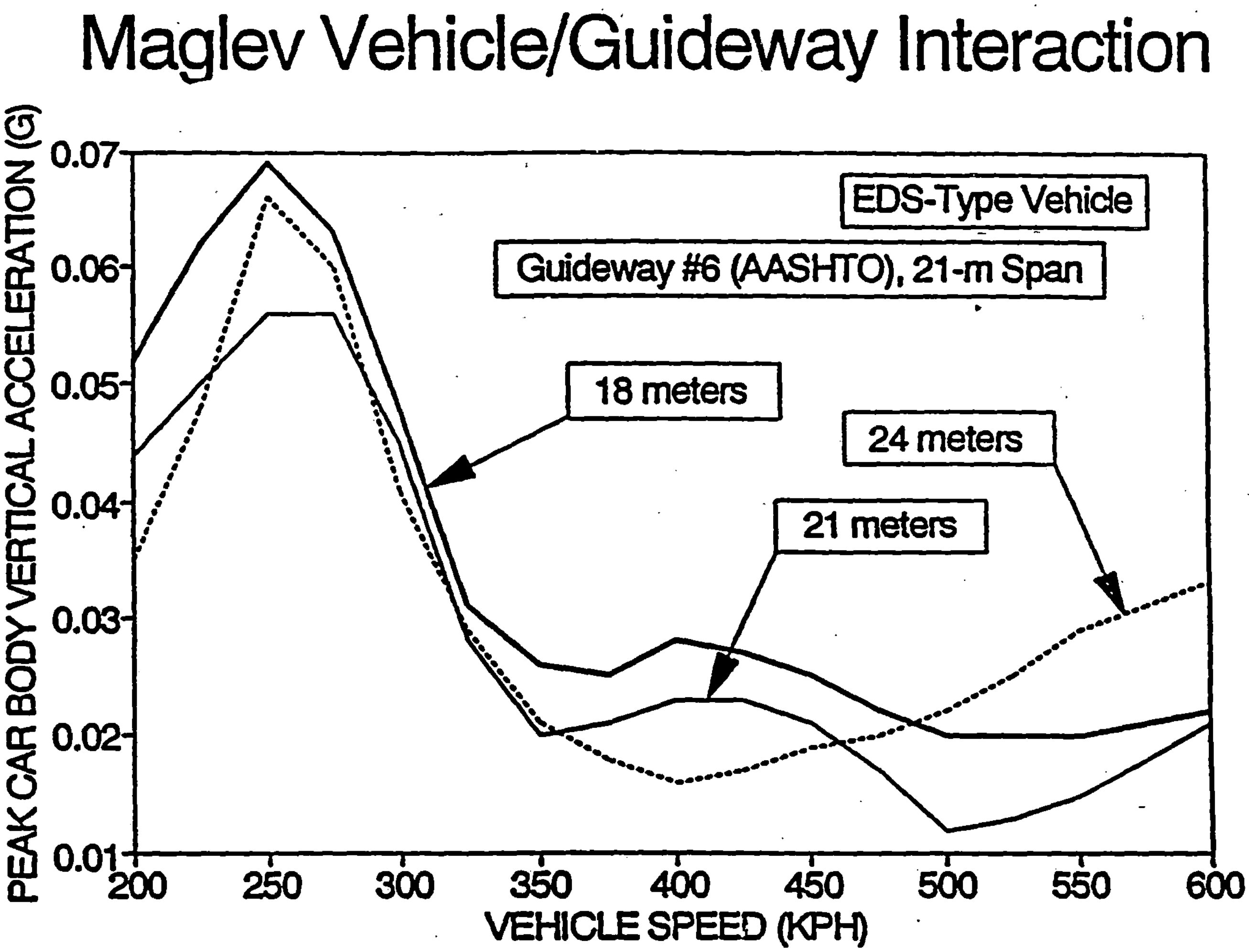

Figure 6.6-1 Effects of Vehicle Overall Length on Ride Quality, Car Body Vertical Accelerations

7.0 Structural Cost Analysis

7.1 Basis of the Estimates

This estimate develops a conceptual cost for the construction of maglev transit structures including beams/girders, piers with driven pile foundations, pile caps, column and cap beam. The beam/girder configurations are those illustrated in Section 4.2.

This estimate uses unit costs in-place derived from the 1992 R. S. Means Building Construction Costs Data. All piers are assumed to be 7.6 m (25 ft.) tall.

All quantities were derived either by direct measurement and calculation or from computer analysis. Those activities not detailed are from similar previous projects.

The estimates include 10% of the construction cost for mobilization and a 15% contingency. The level of contingency will decrease as the design level raises.

These estimates are considered to be accurate to within $\pm$20% for the conditions cited, which is typical of estimating errors at the preliminary engineering level of design development.

7.2 Estimate Exclusions and Assumptions

1. No engineering or construction management cost has been allowed.

2. No right of way cost has been allowed.

3. All costs are in 1992 Dollars; no escalation is included.

4. No magnets, propulsion hardware or systems related hardware has been included.

5. The Transrapid steel structure is not included in the estimates. Published data indicates that structure costs $15 million per kilometer($24 million per mile).

7.3 Comments on the Proposed Designs

- The twin box (i.e. HSST) configuration is too slender to handle as single boxes and difficult to handle if the boxes are cross connected. The costs of extraordinary handling are not included in the estimate.

- Delivery of any precast unit in excess of 21 meters to any site not directly over a navigable waterway will require special handling. Highway transportation of girders 39 meters long weighing in excess of 100 tons will require very special haul units as well as restrictive travel permits, all being major cost factors which are not included in the estimate.

7.4 Cost Summary

Table 7.4-A summarizes the results of the structural Cost Analysis. The costs of structures in this study is between $9 million and $10 million per route kilometer excluding the Tranrapid Steel V beam and the HSST Twin Box. This difference is less than the ±20% estimating error and therefore we conclude there is no significant difference between costs of these designs.

TABLE 7.4-A
STRUCTURE COSTS

Description		Beam Length (m)	Unit Cost ($/m)	Cost/km [One Gdwy] ($)	Cost/km [Dual Gdwy] ($)
1 Steel Girders w/ concrete deck		21.336	$5,090	$5,089,690	**$10,179,380**
		39.624	$4,809	$4,809,470	**$9,618,940**
2 Concrete Box		21.336	$4,401	$4,400,980	**$8,801,960**
		39.624	$4,943	$4,942,970	**$9,885,940**
3 Trapezoidal Box		21.336	$4,920	$4,920,220	**$9,840,440**
		39.624	$4,957	$4,957,430	**$9,914,860**
4 Twin Box (HSST)		21.336	$3,422	$3,422,230	**$6,844,460**
		39.624	$3,216	$3,216,330	**$6,432,660**
5 Steel "V" (Transrapid)		24		Costs not estimated	
6 AASHTO Concrete Girders	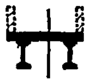	21.336	$4,622	$4,622,360	**$9,244,720**
		39.624	$4,372	$4,372,440	**$8,744,880**

Cost Estimates include:

1. **7.6m pier height**
2. **Complete substructure from piles upward**
3. **10% mobilization cost and 15% contingency**
4. **Costs in 1992 dollars, based on 1992 R.S. Means Building Construction Costs Data**

Cost Estimates do not include:

a. **Magnetic Reaction coils/plates in guideway**
b. **Engineering costs, Construction Management costs**
c. **Right of Way acquisition or preparation**
d. **Non-structural system components (power, signal facilities)**

8.0 Discussion

8.1 Direct Comparison of Maglev Vehicle Systems

Two fundamentally different types of Maglev vehicle systems have been developed by the German and Japanese research and development teams. The first of these is the attractive electromagnetic system (EMS) such as the German Transrapid TR-07 and the Japanese HSST designs. These vehicles employ a magnetic suspension that wraps around the active guideway elements, achieving levitation by attraction upward toward the guideway surface. The second, the electrodynamic system (EDS) such as the Japanese MLU-002 vehicle, achieves levitation through repulsive eddy currents generated in guideway-mounted coils. Some relatively high speed (150 km/h or more) is required for sufficient induction to levitate.

For the typical EMS-type vehicle, four to five magnet support frames (unsprung masses) are mounted over the length of the car, and a number of magnet pairs are mounted to or shared by these frames. Since each magnet must operate within a nominal 10 to 13 mm gap, the effective magnetic stiffness is high (in a closed-loop gap control system) and the dynamic coupling to the guideway structure is strong. The EDS-type vehicle, on the other hand, assumes the more typical "bogie" vehicle configuration with two magnet frames (unsprung masses) per car body, one at each end, and two (or more) magnet pairs per frame. Typically, the EDS magnetic suspension operates at a nominal gap of 100 to 130 mm with an effective vertical stiffness nearly an order of magnitude less than the EMS magnetic stiffness.

Because of these differences in configuration and in coupling stiffness, the two different Maglev systems produce quite different vehicle and guideway interactive responses. Ride quality of the two vehicle types on the 21-meter simply-supported guideway spans is compared in Figures 8.1-2 through 8.1-6 . (Guideways 2 and 3 are dynamically similar, therefore results for Guideway 3 have not been plotted.) On the more standard guideway designs (Guideways 1, 2, 3 and 6), the ride of the EDS-type vehicle is characterized by a resonance in vertical car body accelerations in the 200 to 300 km/h speed range with amplitudes somewhat higher than the desired one-hour reduced comfort limit of 0.051 g peak. Above 300 km/h, these acceleration levels drop well below this limit. Acceleration levels for the EMS-type vehicle, on the other hand, remain below the desired limit up to about 400 km/h. Above this speed, the EMS-type vehicle exhibits a monotonic increase in acceleration levels with increased speed.

Similar response is seen on the two light-weight Guideways 4 and 5. On Guideway 4, the EDS-type vehicle produces a vertical acceleration resonance at 250 km/h that is more than twice the desired ride comfort limit. On Guideway 5, the resonance is broader, peaking about 350 km/h at about 0.08 g. On both Guideways 4 and 5 (and particularly Guideway 5), the EMS-type vehicle generates vertical acceleration levels well above the desired limit over the whole speed range of 200 to 600 km/h.

Figure 8.1-1 Guideway Structures

1 **Steel Girders w/ concrete deck**	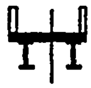
2 **Concrete Box**	
3 **Trapezoidal Box**	
4 **Twin Box (HSST)**	
5 **Steel "V" (Transrapid)**	
6 **AASHTO Concrete Girders**	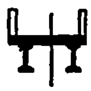

Figure 8.1-2 EMS vs EDS Car Body Vertical Accelerations
21m, Steel Girders with Concrete Deck

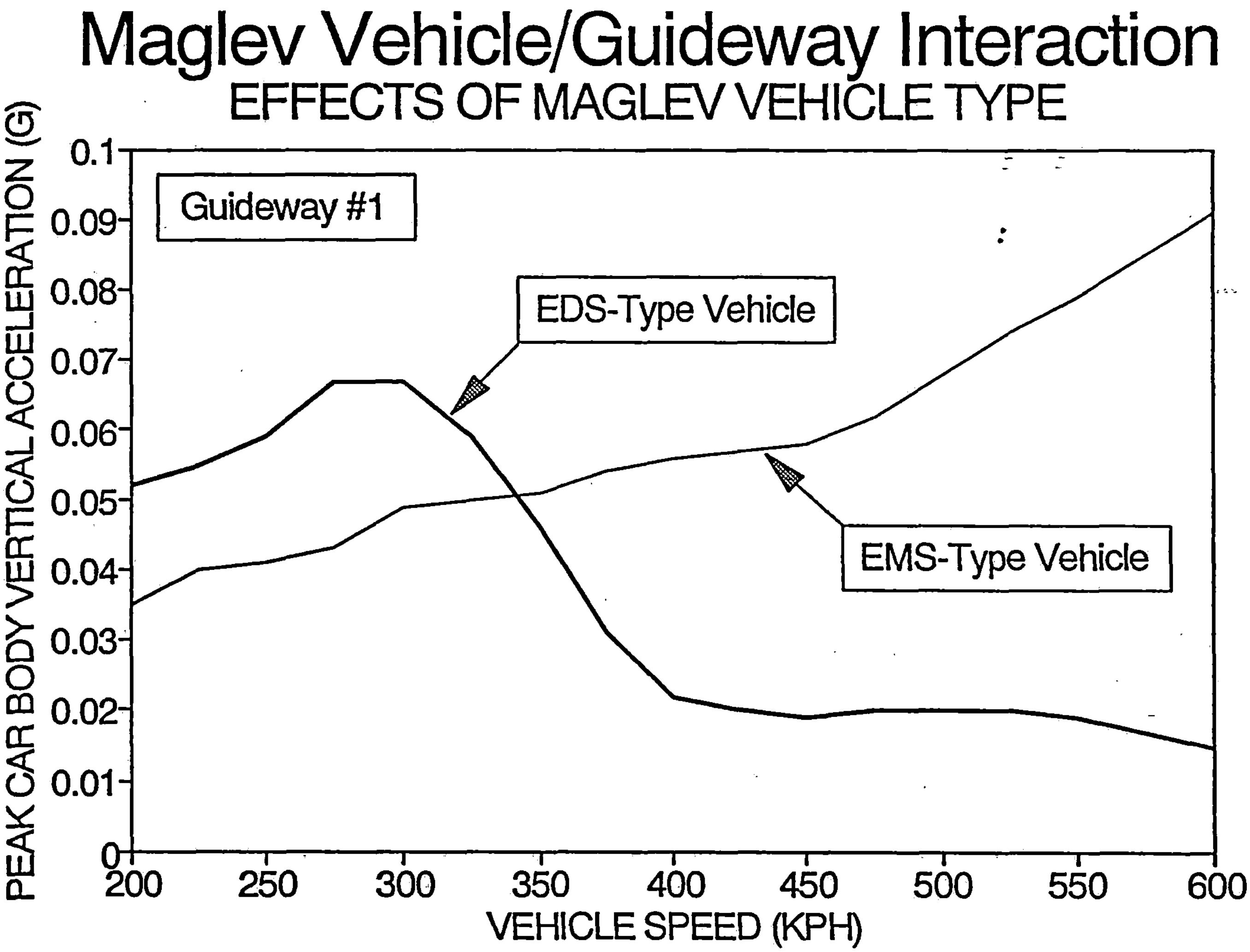

Figure 8.1-3 EMS vs EDS Car Body Vertical Accelerations
21m, Concrete Box Guideway

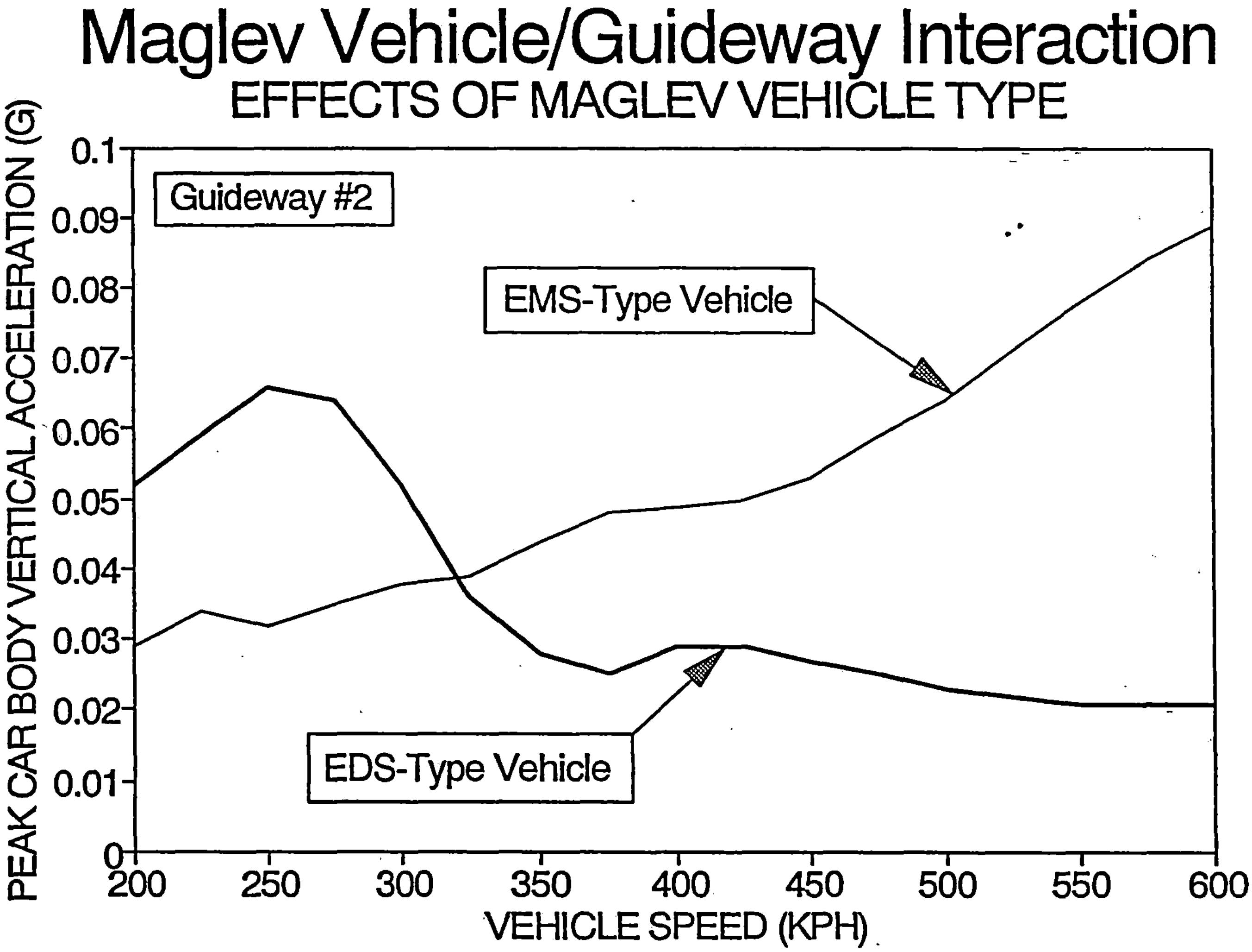

Figure 8.1-4 EMS vs EDS Car Body Vertical Accelerations
21m, Twin Concrete Box Beam Guideway (HSST)

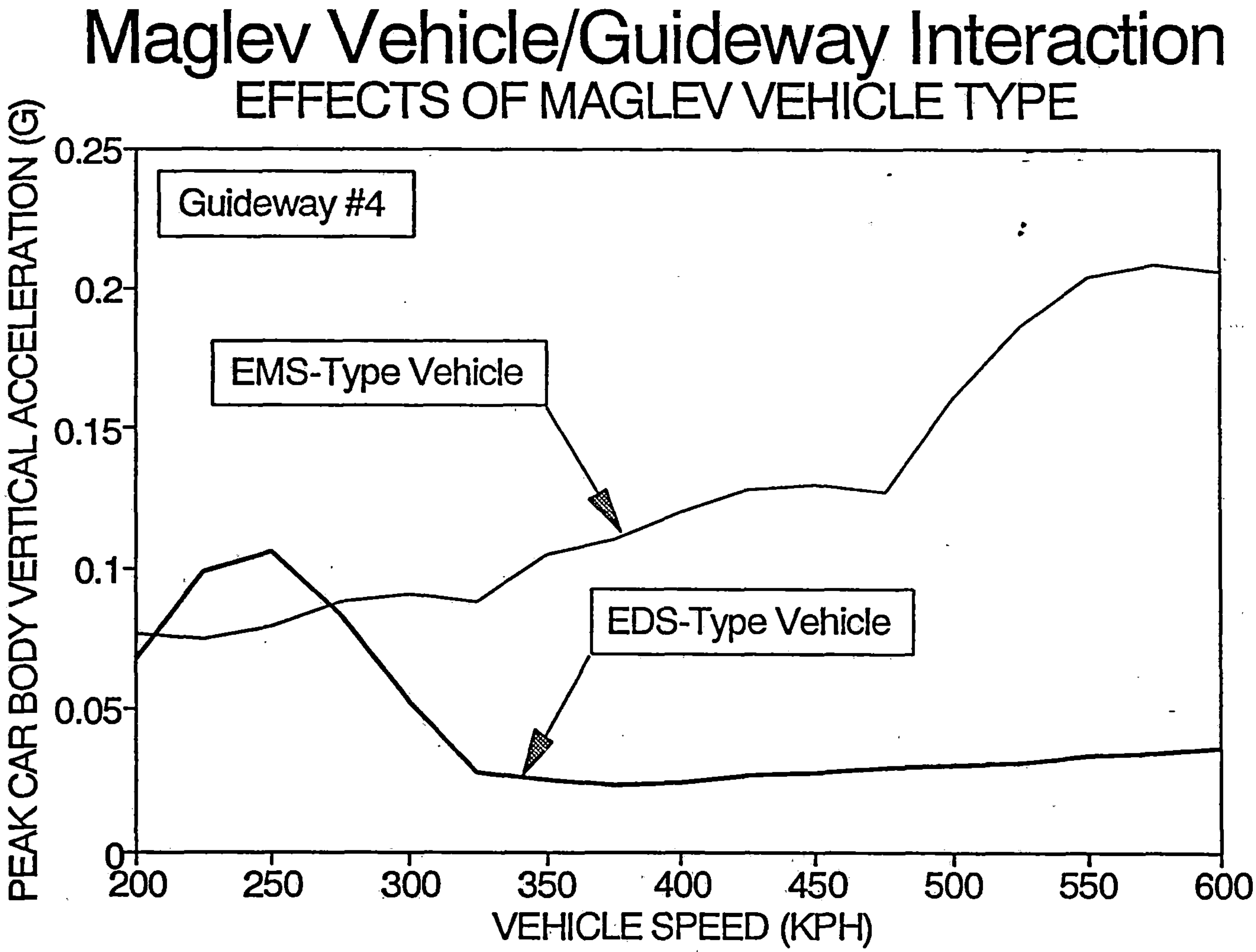

Figure 8.1-5 EMS vs EDS Car Body Vertical Accelerations
21m, Steel "V" Guideway (Transrapid)

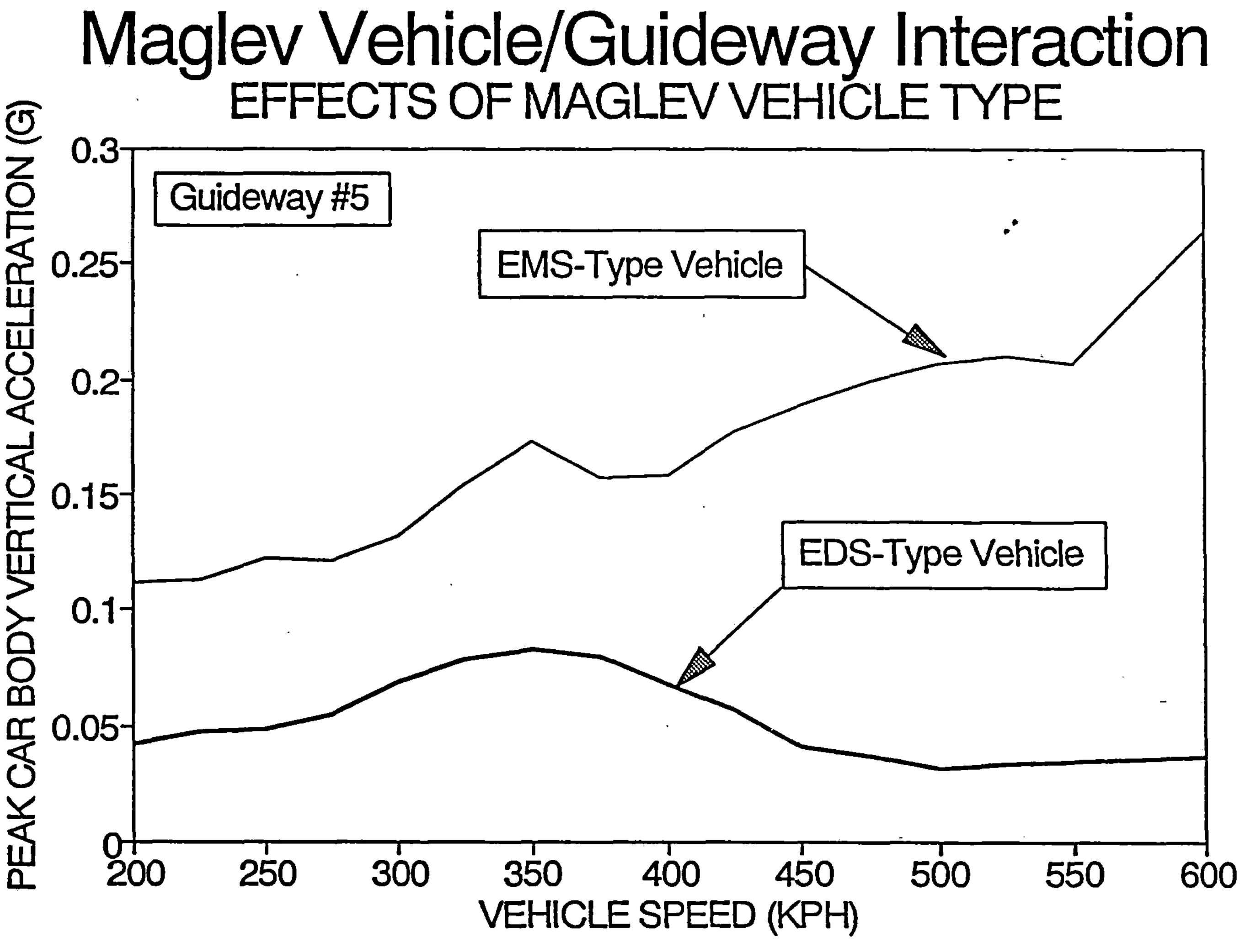

Figure 8.1-6 EMS vs EDS Car Body Vertical Accelerations
21m, AASHTO Concrete Girders

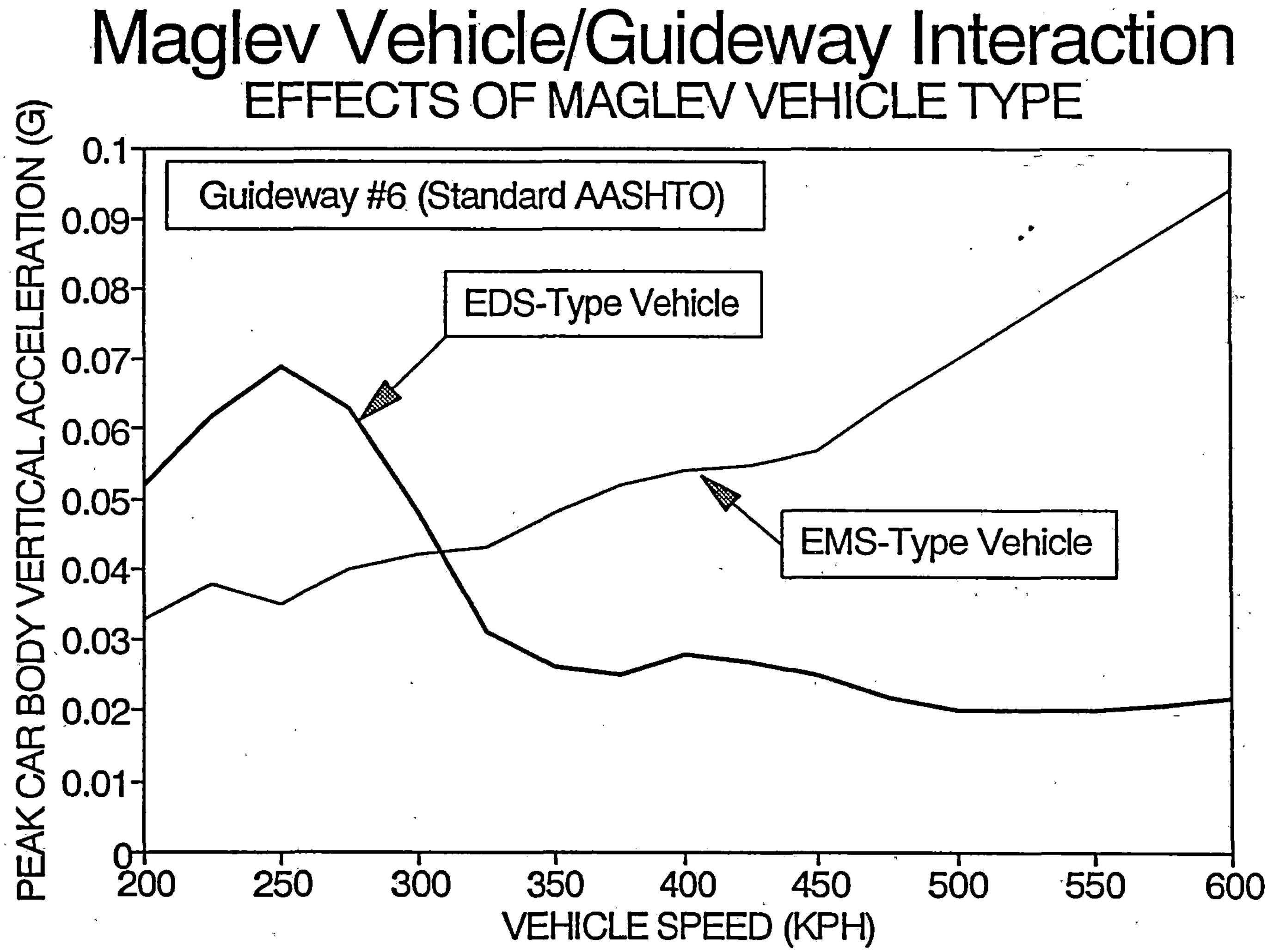

The effect of a longer (40-meter) simply-supported guideway span is illustrated in Figure 8.1-7 for Guideway 6P (the standard AASHTO design). The EDS-type vehicle generates a resonant peak in vertical car body acceleration at 125 km/h. At higher speeds, acceleration levels decrease. However, higher modal resonances (above the third bending mode) of the longer span not included in the model may be excited at these speeds, again decreasing ride comfort. The EMS-type vehicle generates high levels of vertical acceleration across the speed range well above the desired ride comfort limits.

The effects of two-span "continuous" beams on ride quality (a 43-meter beam with a center column support) are shown for Guideways 5D and 6D in Figures 8.1-8 and 8.1-9. In both cases, improvements are noted over the simply-supported 21-meter beam. The light-weight Guideway 5 still presents marginal ride quality, particularly with the EMS-type vehicle. On Guideway 6D the ride quality for both vehicles is marginally acceptable over much of the speed range.

Figure 8.1-7 EMS vs EDS Car Body Vertical Accelerations
40m, AASHTO Concrete Girders

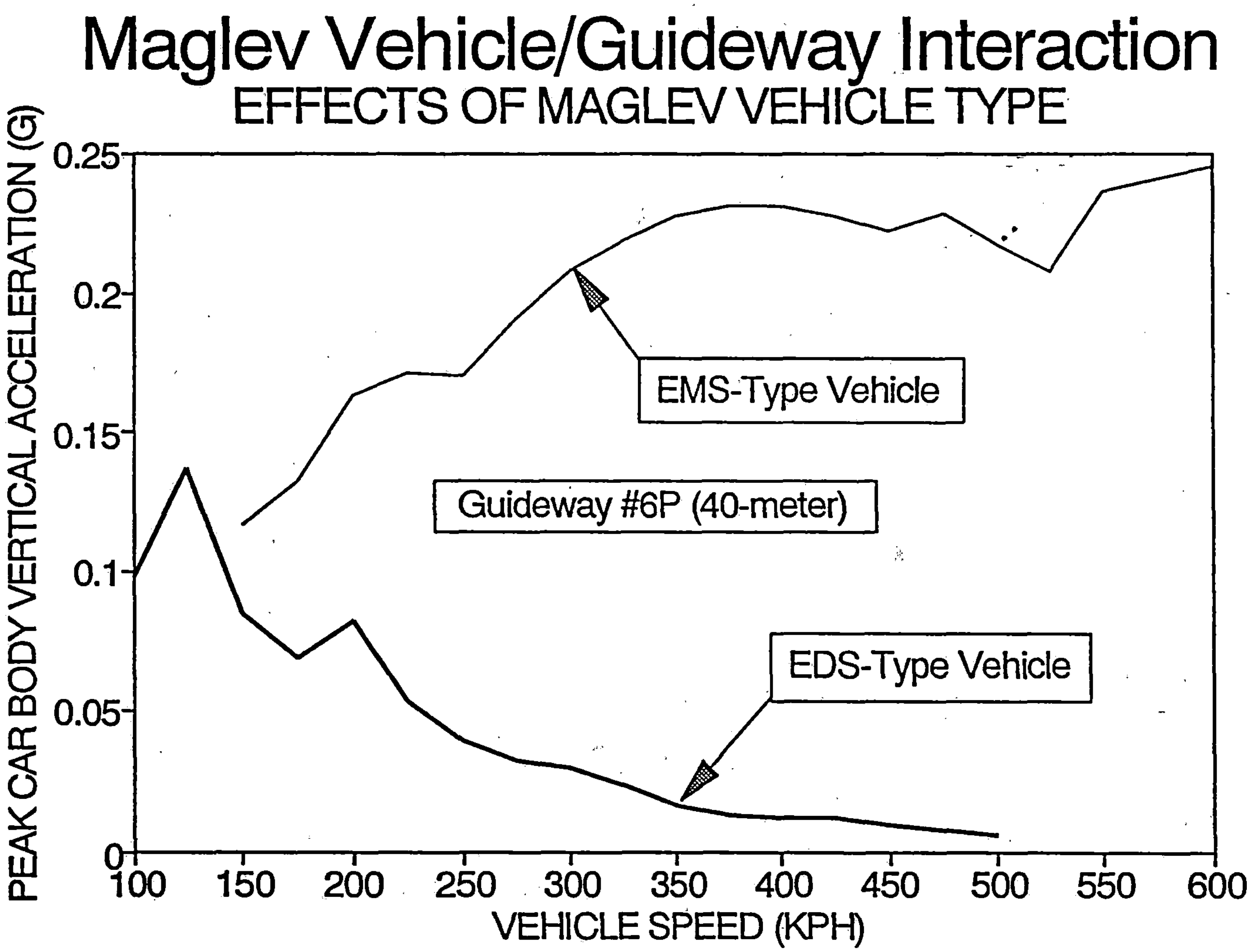

Figure 8.1-8 EMS vs EDS Car Body Vertical Accelerations
Two-span continuous, Steel "V" (Transrapid) Guideway

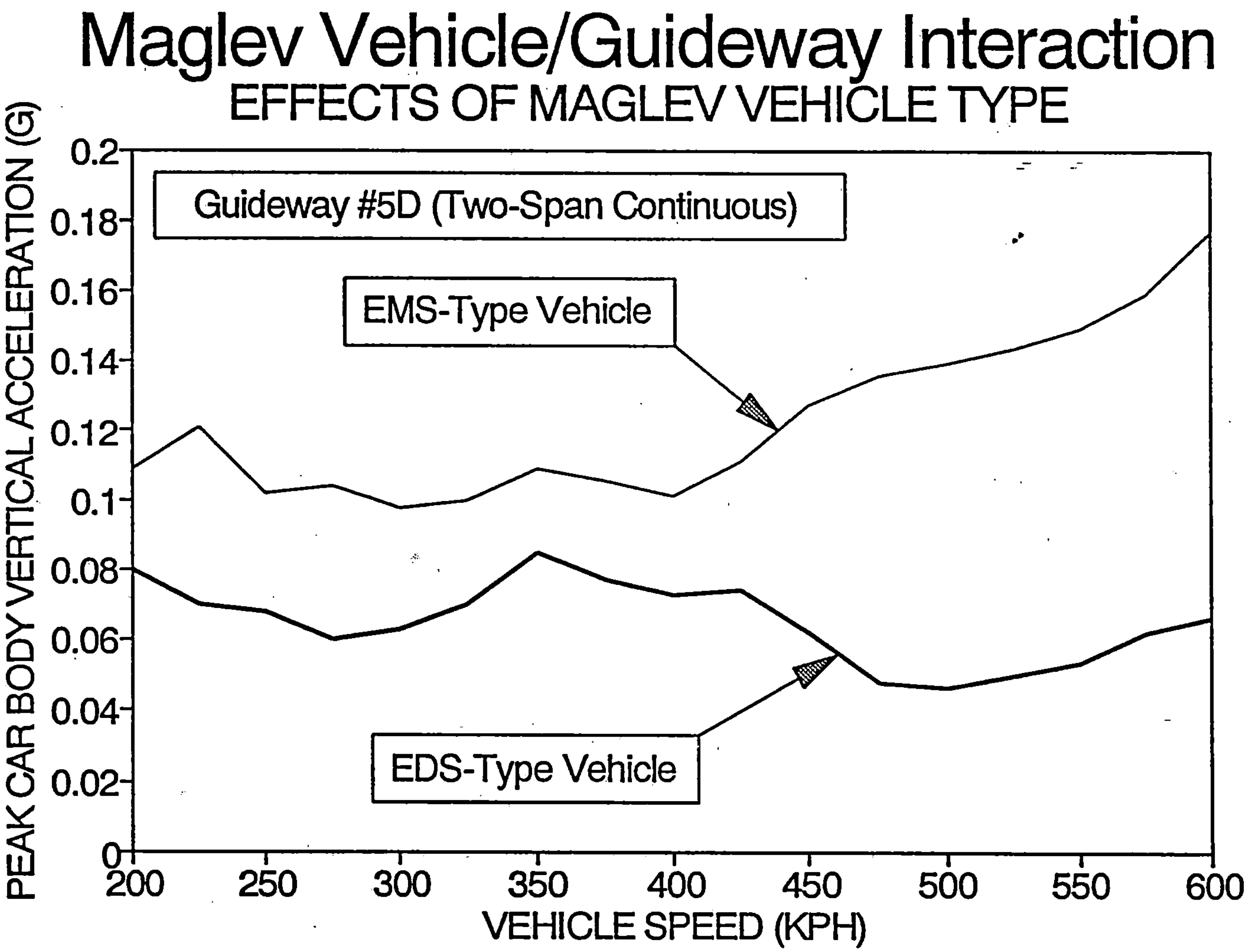

Figure 8.1-9 EMS vs EDS Car Body Vertical Accelerations
Two-span continuous, AASHTO Concrete Girders

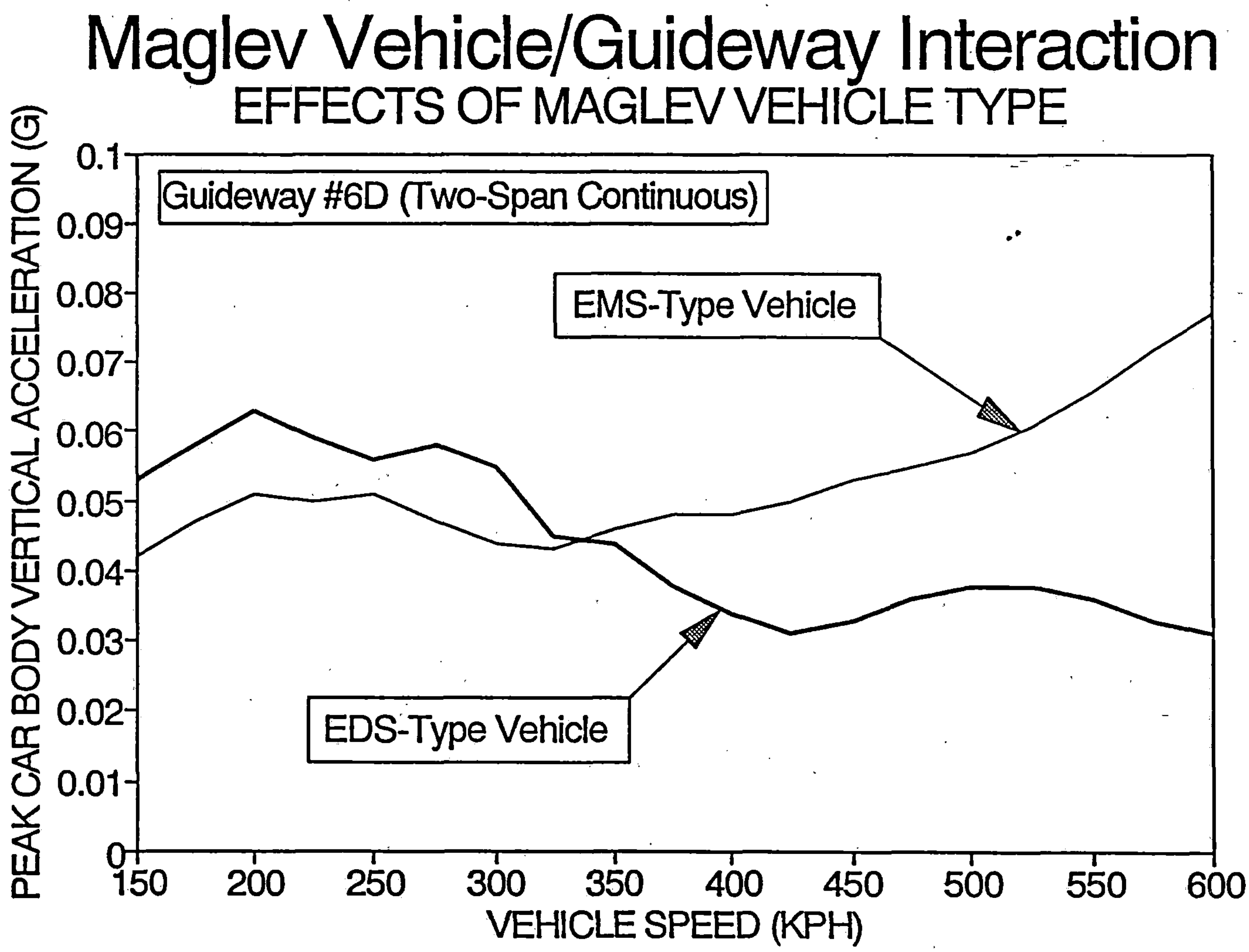

A companion set of plots of mid-span vertical beam accelerations is shown for these cases in Figures 8.1-10 through 8.1-17. For the 21-meter simply-supported guideway beams, response under the EDS-type vehicle is typified by a pronounced resonance in the 250 to 400 km/h speed range. For the standard guideway configurations (Guideways 1, 2, 3 and 6), peak accelerations of 0.5 to 0.8 g are developed at the resonant speed. The light-weight guideways (Guideway 4 and 5) are simply overwhelmed by the more massive vehicle, and peak midspan acceleration levels over 1g (Figure 8.1-12, Guideway 4) and over 2 g (Figure 8.1-13, Guideway 5) are predicted. The EMS-type vehicle, with its distributed load, produces much lower levels of guideway vertical acceleration. In general, the midspan response remains below the desired 0.3 g peak level.

The response of the longer (40-meter) simply-supported beam, Guideway 6P, is shown in Figure 8.1-15. Here the response for both vehicles remains within the desired limit of 0.3 g peak up to 400 km/h. Above this speed, the EMS-type vehicle generates progressively higher response levels. It must be noted, however, that higher modal resonances of the beam not included in the current model (4th bending mode and higher) may come into play at these higher speeds.

The effects of two-span "continuous" beams (a 43-meter beam with a center column support) on guideway beam response are shown in Figures 8.1-16 and 8.1-17 for Guideways 5D and 6D. In both cases, reductions in response level are achieved over the simply-supported spans. On light-weight Guideway 5D, the EDS-type vehicle develops midspan acceleration levels well above the desired 0.3 g limit. The EMS-type vehicle stays below this limit up to about 450 km/h. On Guideway 6D, both vehicles stay below the limit, although the EDS-type vehicle again produces generally higher response levels.

Figure 8.1-10 EMS vs EDS Mid-Span Vertical Beam Accelerations
21m, Steel Girders with Concrete Deck

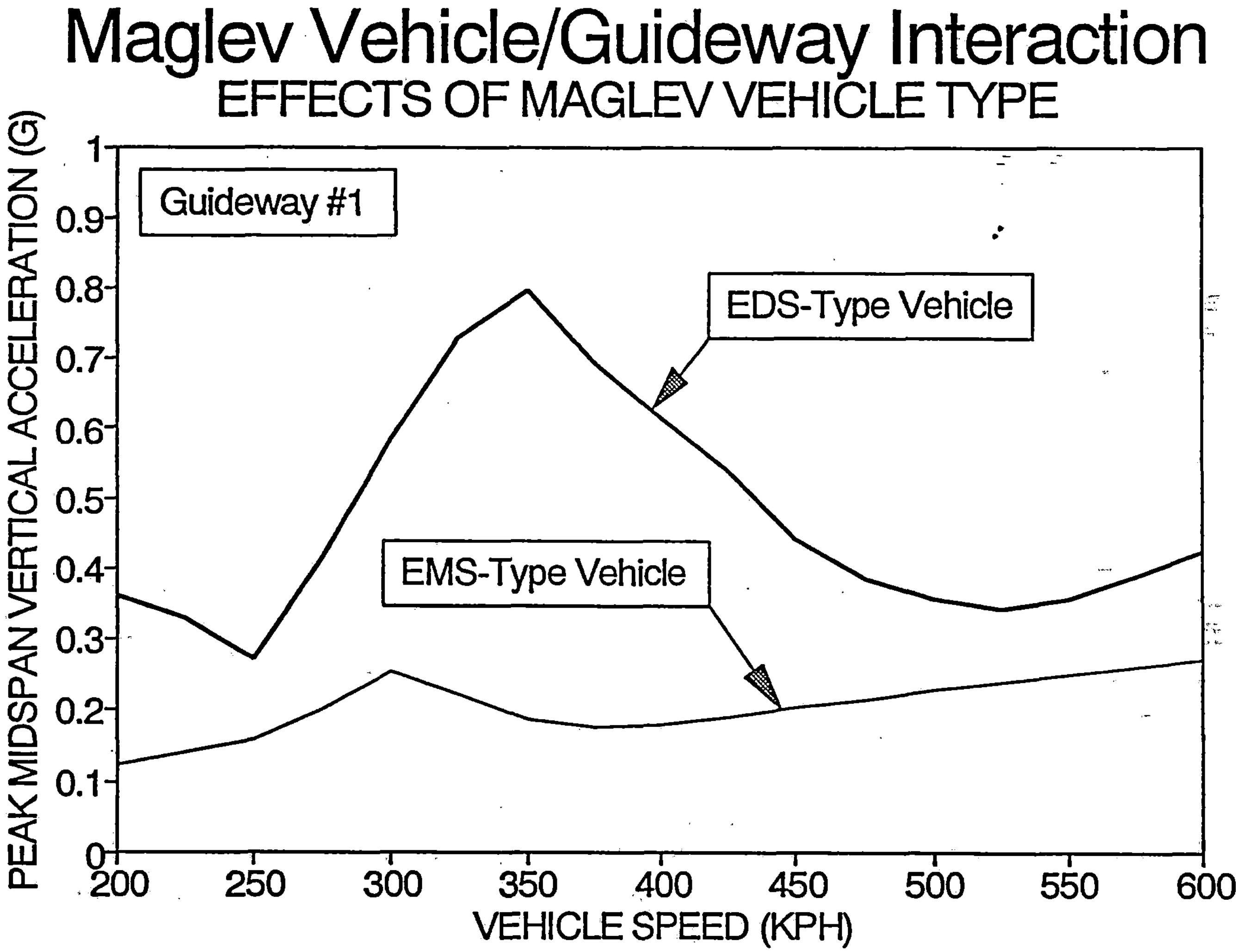

Figure 8.1-11 EMS vs EDS Mid-Span Vertical Beam Accelerations
21m, Concrete Box Guideway

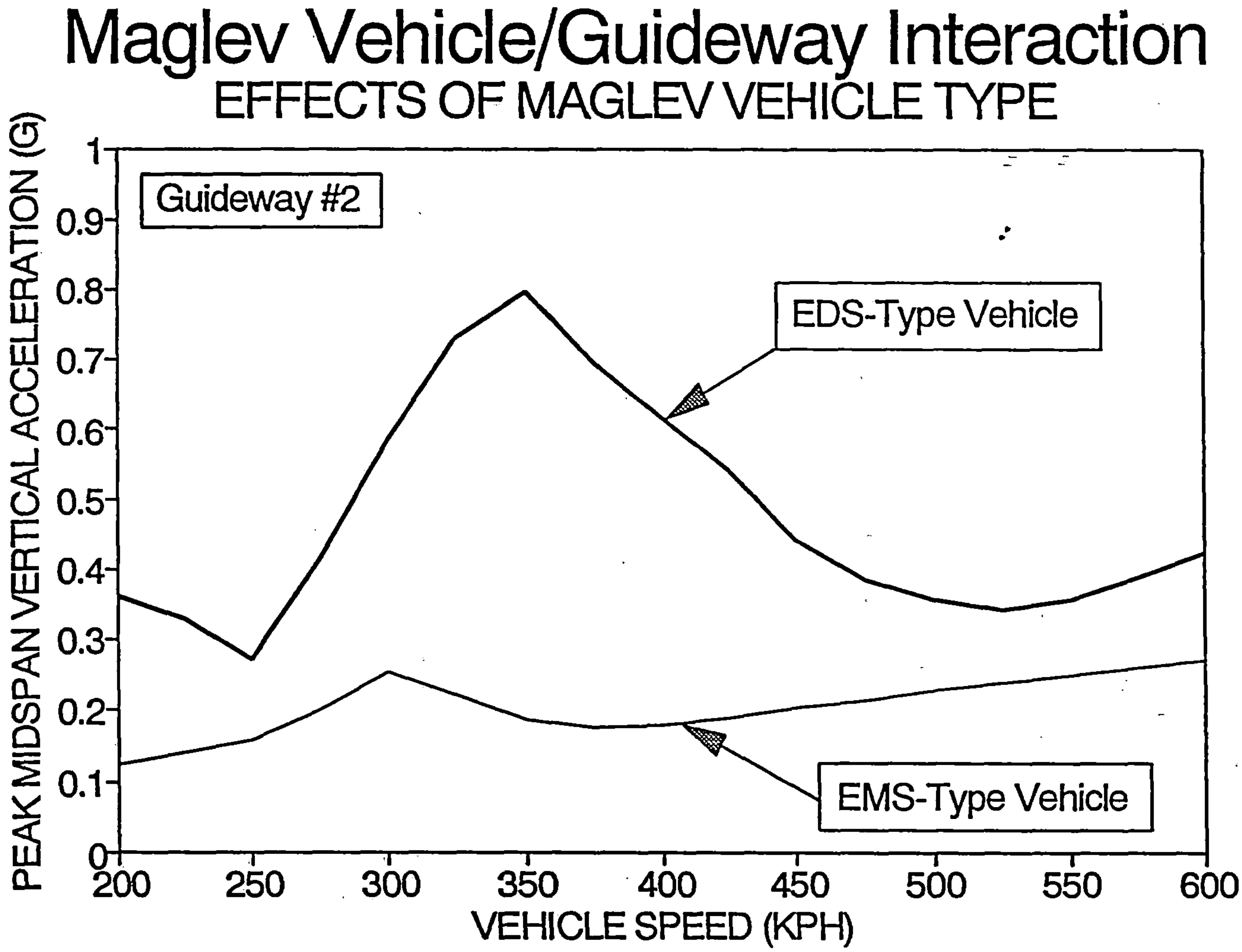

Figure 8.1-12 EMS vs EDS Mid-Span Vertical Beam Accelerations
21m, Twin Concrete Box Beam Guideway (HSST)

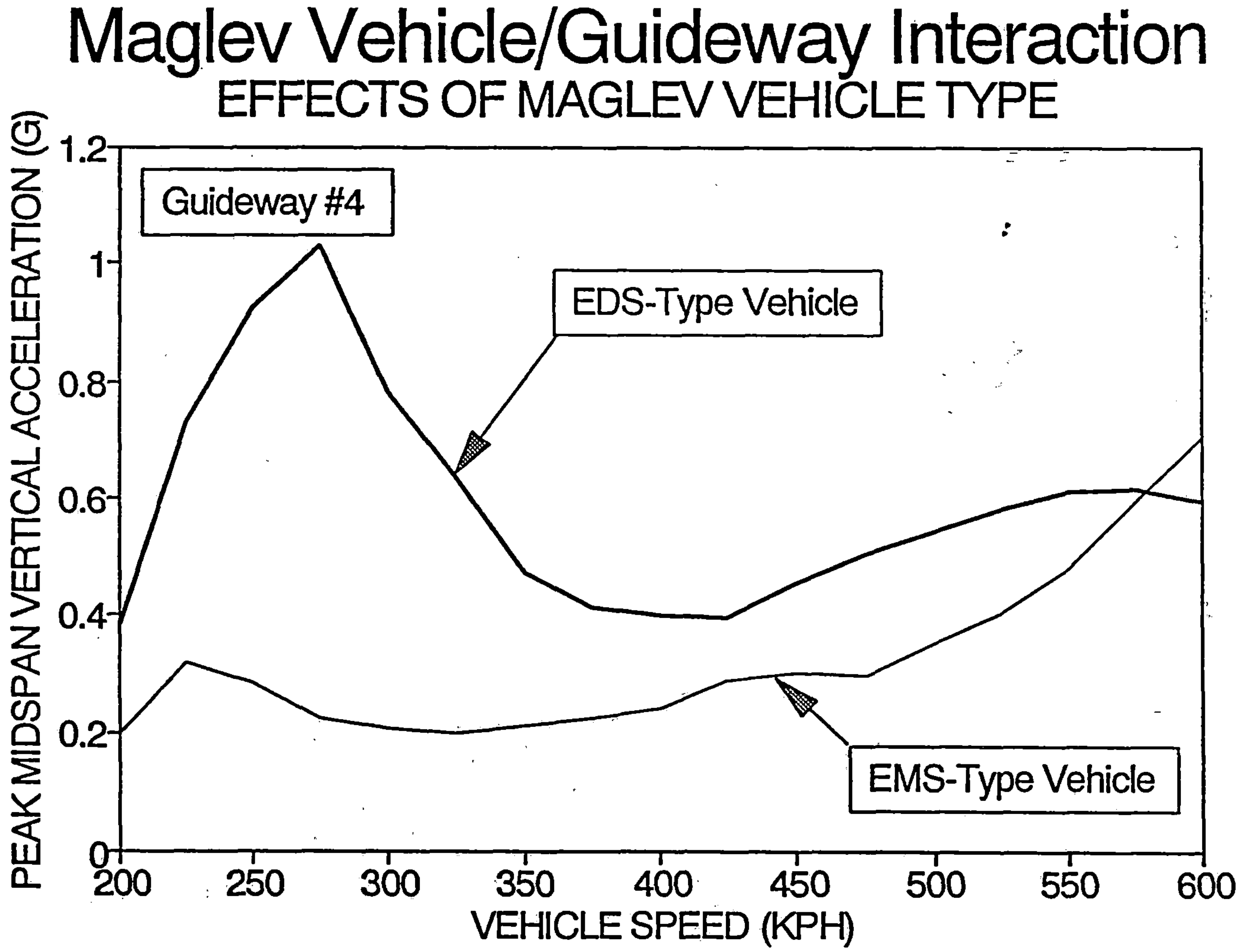

Figure 8.1-13 EMS vs EDS Mid-Span Vertical Beam Accelerations
21m, Steel "V" Guideway (Transrapid)

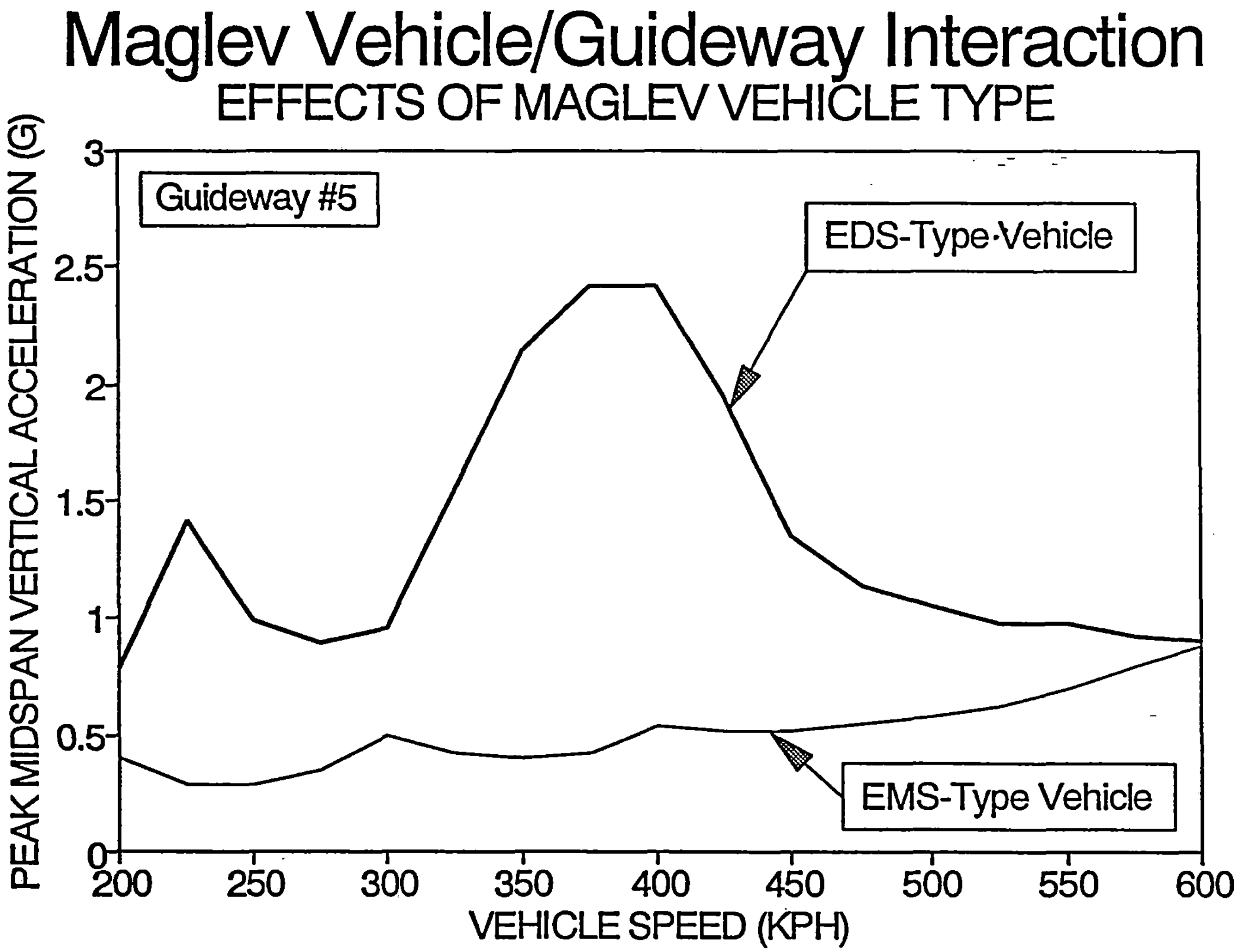

Figure 8.1-14 EMS vs EDS Mid-Span Vertical Beam Accelerations
21m, AASHTO Concrete Girders

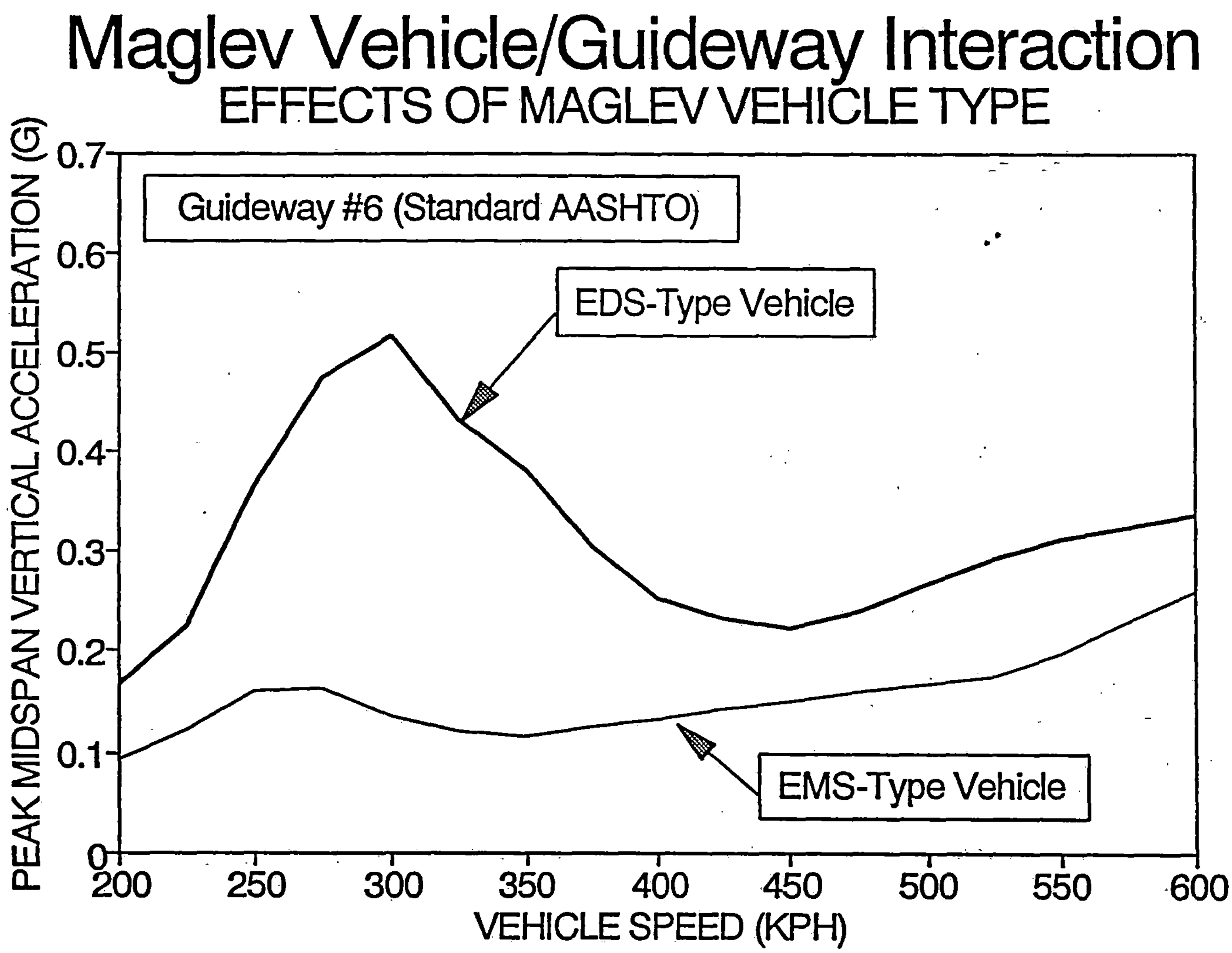

Figure 8.1-15 EMS vs EDS Mid-Span Vertical Beam Accelerations
40m, AASHTO Concrete Girders

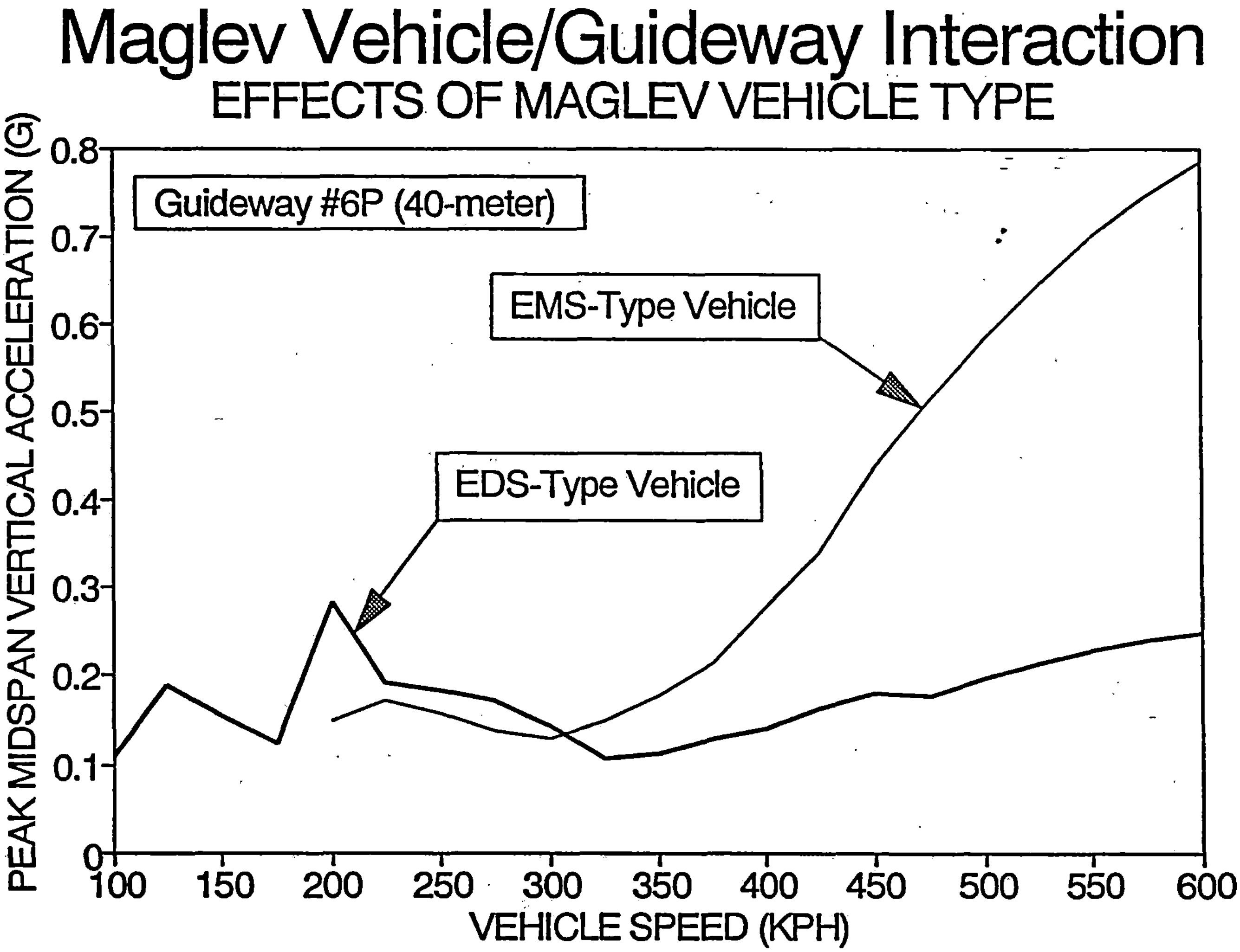

Figure 8.1-16 EMS vs EDS Mid-Span Vertical Beam Accelerations
Two-span continuous, Steel "V" (Transrapid) Guideway

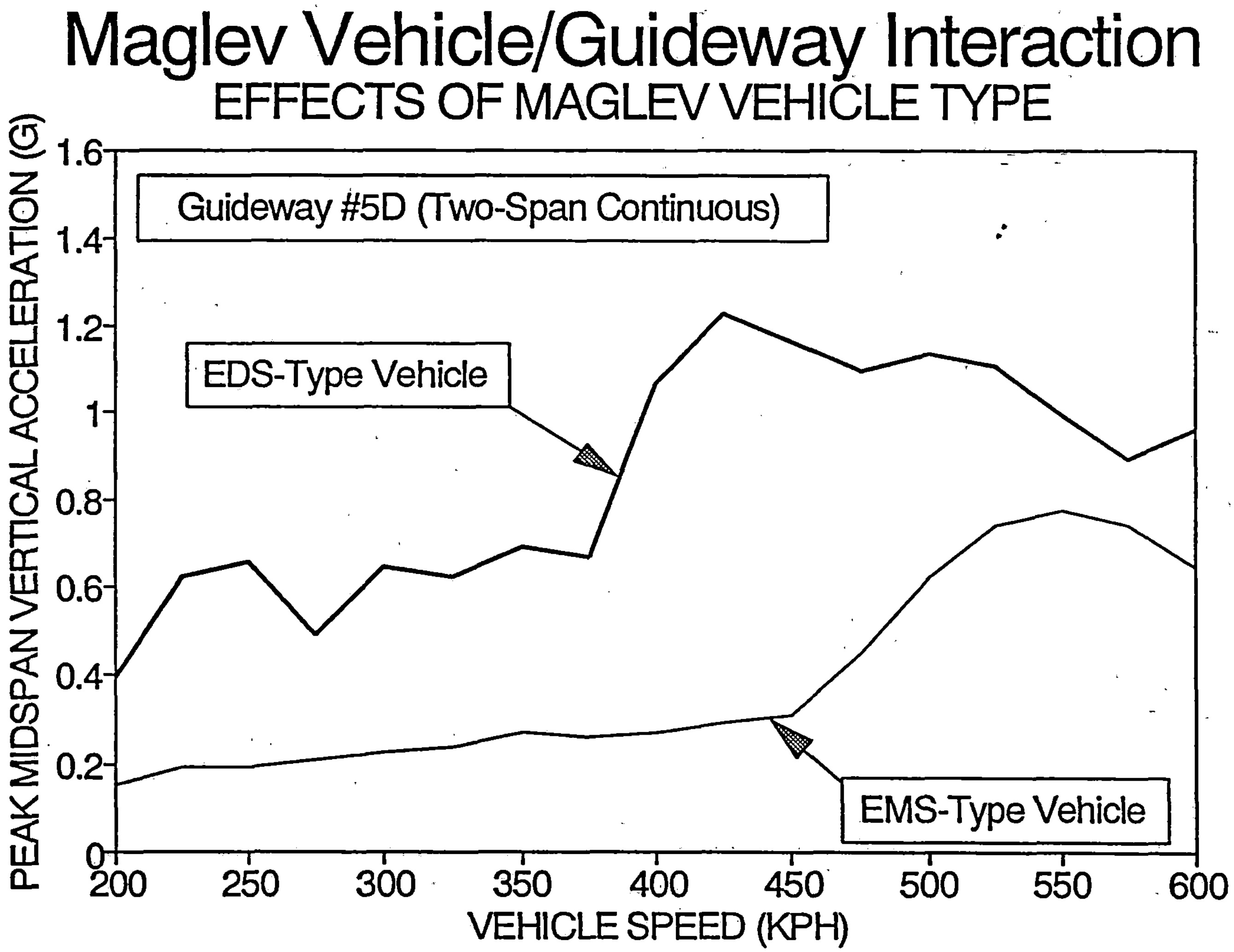

Figure 8.1-17 EMS vs EDS Mid-Span Vertical Beam Accelerations
Two-span continuous, AASHTO Concrete Girders

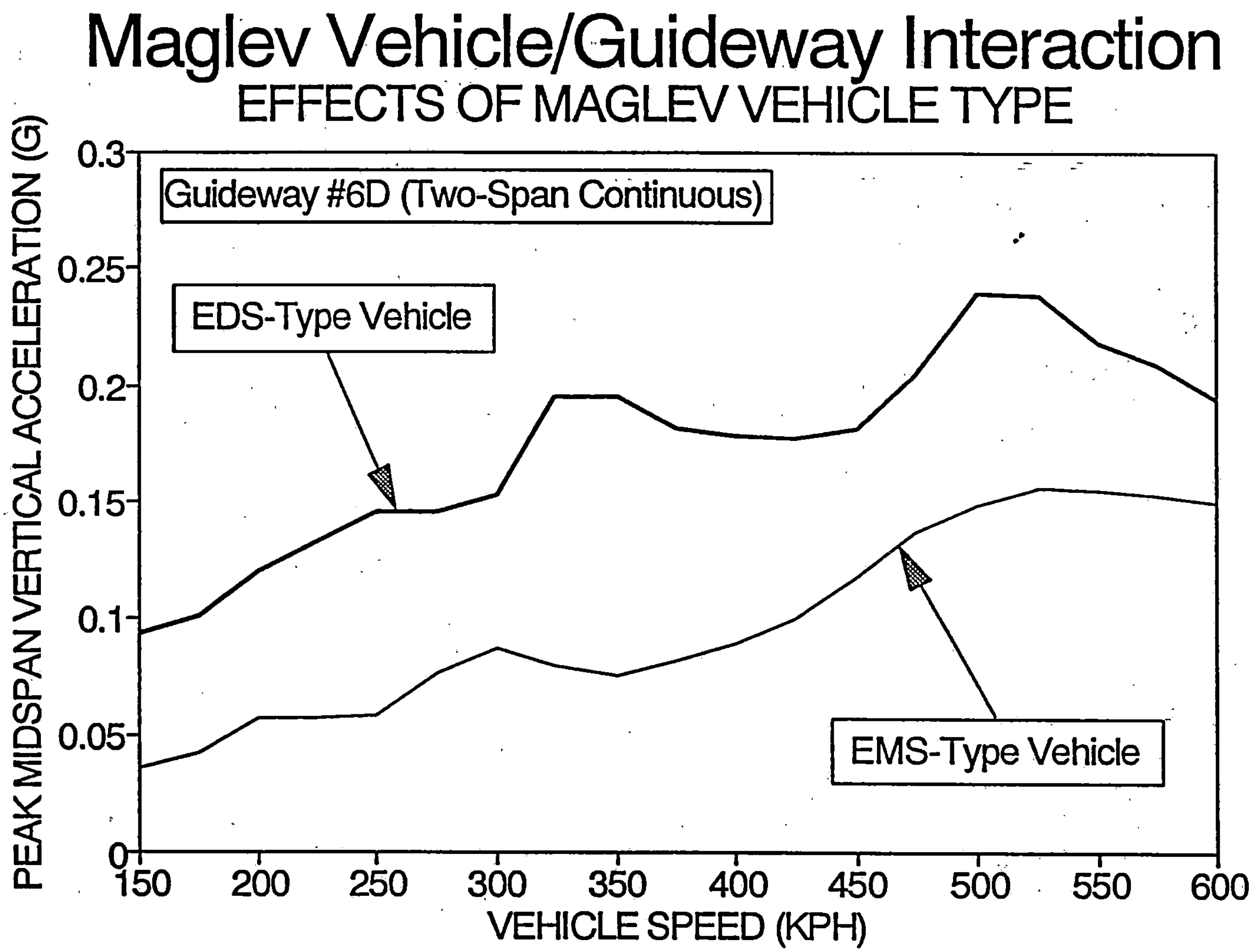

8.2 Implications for Design of Aerial Structures

This study develops four beams (beams numbered 1, 2, 3, and 6) designed to conventional U.S. guidelines and practice. It is only partial comfort that these beams provide generally better dynamic response than the comparison guideway (Transrapid) since the U.S. design guidelines offer no criteria for optimizing the dynamic response of structures for high speeds. The following subsections review the implication of these results for structural design of future systems.

8.2.1 Impact Factors

Impact factor design guidelines vary over a wide range for existing transit aerial structures as observed in Section 1.0 of this report. The variety of guidelines reflects divergent definitions of impact. For example, AASHTO provides impact factors that are qualified for types of service but leave the actual selection of a value to the judgement of the designer. Wormley, et al [68] and [69] suggest the impact factor is the ratio of the peak dynamic deflection to the static deflection. This report uses acceleration as the measure of impact, or dynamic load increase over static load. And ACI 358.1R uses the crossing frequency ratio to determine an impact factor.

From the results shown in this study, the dynamic accelerations exceed the 30% design impact factors in many cases but the maximum beam bending moments are not exceeded in any case (for beams where the maximum value is known), suggesting a higher actual impact factor is permissible for these designs.

From a structural design viewpoint, impact factors must be stated as % increase in live load for dynamic load amplification. The definition of dynamic load amplification for high speed systems requires a rational method for assessing and designing for dynamic interactions between vehicle and guideway. Methods such as proposed by Wormley [69] provide a technical basis which will remove the divergence of impact factor definition. Without such design methodology, the future designs may be at risk even though the designs in this study, developed to existing guidelines, provided acceptable dynamic performance in most cases.

8.2.2 Mass Ratios and Crossing Frequency Ratios

The results indicate that the highest accelerations for any vehicle and guideway configuration occurs in the Transrapid configuration [Beam number 5 in this report]. The difference is attributed in part to the lower beam mass of the Transrapid guideway compared to the other designs in this study.

Richardson and Wormley [63] state that the vehicle and guideway deflections or motions "becomes essentially independent of M [the ratio of the vehicle sprung mass to the guideway mass] when M is less than 0.25. Others [47 and 77] suggest beams with mass ratios of 0.30 using the total mass of all vehicles on the span will have negligible resonance if the crossing frequency ratio is less than 0.2. Note that the crossing frequency ratio, CFR, is

$$CFR = V / \ell_s f_1$$

V = vehicle speed
ℓ_s = span length
f_1 = span fundamental natural frequency

Mass ratios of each of the configuration is shown in Table 8.2.2-A. Comparing the Mass ratios to peak guideway accelerations in Figures 6.2-5, through 6.2-8, the ordering of the guideways by maximum acceleration (for all speeds) can be shown to be the same as the order of increasing mass ratio.

Table 8.2-A

Mass Ratios

[Vehicle Sprung Mass, m_v = 35,700 kg]

Guideway Description	Length (m)	Guideway [A_s] (kg)	Mass Ratio m_v / A_s	Nat'l Freq. (Hz)	Max beam Acceleration (g) EMS	EDS
1. Steel Girder	21	63,500	0.56	7.4	0.25	0.73
	39	136,208	0.26	2.9	*	0.40
2. Concrete Box	21	101,918	0.35	6.8	0.14	0.40
	39	218,760	0.16	3.0	NA	0.26
3. Trapezoidal Box	21	88,583	0.40	7.2	0.15	0.49
	39	199,891	0.18	3.1	NA	0.28
4. Twin Box (HSST)	21	59,056	0.60	5.3	0.31	1.00
	39	153,309	0.23	2.2	NA	0.47
5. Steel "V" Transrapid	24	25,001	1.43	7.0	0.50	NR
6. AASHTO Girders	21	98,107	0.36	6.4	0.15	0.48
	39	218,760	0.16	2.5	*	0.27

NA = Not Analyzed
NR = Not Relevant
* increased acceleration above 400-500 km/h.

In this study for EMS Systems, the desired 0.3g impact factor is not exceeded on 21m spans for mass ratios less than 0.6 until speeds above approximately 500 km/h where acceleration generally increased. The 39m span length with EMS is analyzed only for beams 1 and 6 with 0.26 and 0.16 mass ratios, respectively, neither producing accelerations above 0.3g until approximately 400 to 450 km/h where the maximum accelerations increased non-linearly with speed for both beams.

For the EDS System, the 0.3g limit was exceeded by all 21m length beams where the minimum mass ratio is 0.35 and increased with speed above 250 km/h. For 39m spans with the EDS system, the 0.3g limit is not exceeded by mass ratios less than 0.18 until speeds of approximately 500 km/h for some beams (other beams did not exceed the limit at any speed analyzed).

Nearly all systems exhibit increasing peak span accelerations at higher speeds. The crossing frequency ratio (CFR) is used by many researchers as an expression of this effect, which is the coincidence of passing speed over a span length with beam natural frequency, something of an indicator of resonance. Wormley, in several papers, suggests that deflection amplitudes increase as CFR approaches a value of 1.0 and the maximum resonance occurs above a value of 1.0 (between 1.2 and 1.4, generally, depending on parameter values) for simple spans and 2.0 for 2-span continuous structures.

With those ideas in mind, the CFR is calculated in Table 8.2-B for the speeds at which the 0.3g limit is crossed on the high speed end of the response (ignoring lower speed resonances). Table 8.2-B is developed from Figures 6.2-5 to 6.2-8. The results tend to confirm Wormley's concept, although results are scattered. Beam #5 is problematic because most of the response is above the 0.3g limit except at slower speeds.

In all cases, beams with CFR less than 1.0 appears to indicate conditions for dynamic accelerations less than the 0.3g, ignoring lower speed resonances which appear to be dominated by mass ratios.

Table 8.2-B

CFR at which 0.3g is exceeded for speeds over 400 km/h

Beam	Mass Ratio	Nat'l Freq.	Span Length	CFR & Speed at which 0.3g exceeded EMS Speed km/h	CFR	EDS Speed km/h	CFR
1	0.56	7.4	21	>>600	>>1.07	550	0.98
	0.26	2.9	39	440	1.08	>500 (600)	>1.22
2	0.35	6.8	21	>>600	>>1.17	550	1.07
	0.16	3.0	39	NA		>>>500	>>>1.19
3.	4.00	7.2	21	>>600	>>1.10	550	1.01
	0.18	3.1	39	NA		>>>500	>>>1.15
4.	0.60	5.3	21	475	1.18	550	1.37
	0.23	2.2	39	NA		500	1.62
5.	1.43	7.0	24	250	0.41?	NA	
6.	0.36	6.4	21	>600	1.24	550	1.14
	0.16	2.5	39	420	1.20	>>500	>>1.42

NA = response not analyzed
> = value is unknown but greater than that shown
>> = value is much greater than that shown
>>> = value is very much greater than that shown

The two parameters of mass ratio and crossing frequency ratio appear to provide reasonable indications of dynamic thresholds, based on this study's results.

Summarizing for the beams and conditions in this study, beam accelerations can be expected to be less than the 0.3g limit when the crossing frequency ratio is less than 1.0 and the mass ratio is less than that shown in Table 8.2-C

Table 8.2-C
Mass Ratio Limits

Span Length	MagLev System EMS	EDS
21	0.6	0.3 Note 2
39	0.3 Note 1	0.18

Notes:

1. The maximum mass ratio value available in the study is 0.26 and did not generate 0.3g accelerations below CFR=1.0.

2. The minimum mass ratio value available in the study is 0.35 with all beams including the one with a 0.35 value exceeded the 0.3g acceleration limit. Therefore some lower value is needed than 0.35.

Table 8.2-C shows that future design requirements consider maglev system type, span length as well as mass ratios and crossing frequency ratios.

8.2.3 Vehicle Length

This study chooses an 18m vehicle length because it allows some marginal benefit in accessing existing inner city transit tunnels and structures compared to proposed maglev vehicles which are on the order of 30m in length. The shorter 18 m. vehicle can have natural frequencies in the range of 14 to 20 Hz, reducing the potential guideway/vehicle resonance at the frequencies of highest ride comfort sensitivity.

Longer vehicles will have lower natural frequencies and larger mid-ordinate off sets that require either larger radius curves or wider clearances in curves.

The study results appear to indicate that lower accelerations occur when the vehicle length is near that of the span length. The limited sampling of parameters does not allow conclusions to be drawn however.

Design parameters for vehicle-structure dynamic interaction involving vehicle length have been suggested [68], [69] where the speed at which resonant conditions exist is estimated:

V_{cr} = Resonant Speed = $1/k \, \ell_c \cdot f_1$

k = integer [1,2,3,....]
ℓ_c = car length
f_1 = span first mode of natural frequency (Hz)

Unfortunately, the peak accelerations in this study for the various configurations (Figures 6.2-5, -6, -8, -9) did not appear to correlate with the speeds estimated by V_{cr} for either EMS or EDS system. Mass ratios, damping coefficients and suspension spring rates can shift resonant frequencies significantly.

8.2.4 Guideway Irregularities and Tolerances

Guideway construction tolerances for maglev are expected to be in accordance with current practices summarized in Table 8.2.4-A.

Table 8.2.4-A
Guideway Construction Tolerances

	Concrete Aerial Structures [44]	Steel Structures [79]
Deviation from design	+/- 25mm	+/- 9.5mm
Relative Deviation per span	+/- 12mm in 18m	---
Local irregularity	+/- 6mm in 3m	+/- 1:500
Cross level	+/- 6mm in 3m	+/- 1:500

Guideway irregularities can be expected to increase with time in response to service, and local conditions (pier shifting, settlement, change of camber), as well as daily changes in geometries from thermally induced forces. This study assumes guideway irregularities of +2mm span camber as a vertical deviation, and 5mm versine lateral alignment error combined with 0.5 degree versine cross level deviation for lateral deviations. These deviations' purpose is simply to "trigger" a response in the system, without which the idealization in the models would remain at the steady state level. These deviations, however, are much less than those expected in construction.

The primary questions are what irregularities can be allowed and how can the irregularities be controlled to tolerances required by maglev systems.

In the case of attractive maglev systems with levitation gaps on the order of the construction tolerances shown in Table 8.2.4-A, the guideway tolerance controls must be explicitly designed into the construction tolerances, and into future maintenance adjustment features For example, the Transrapid positioning of beam seats on tops of piers is to:

+/- 2mm in the x-direction
+/- 1mm in the y-direction
+/- 1mm in the z-direction

The beams are then set and grouted to the following tolerances:

+/- 0.5mm lateral position
+/- 0.3mm vertical position

[Transrapid tolerances are found in Ref 80]

It is not known if the Transrapid design includes the means to adjust guideway magnet coils and linear motor stator packs for lateral and vertical alignment after installation.

Variants on the attractive maglev scheme include Grumman's proposed 50mm gap EMS system, which largely mitigates the exceptionally close tolerances witnessed in the Transrapid application for guideway interference.

The EDS, or repulsive maglev system, permits a 100mm gap between vehicle and guideway, which relegates guideway interference to a lesser concern.

Irrespective of the gap distance, the tolerances to control of dynamic response is expected to be narrow for any operation above 200 km/h, as witnessed in this study where the small irregularities produced exceedances in both ride comfort and beam impact criteria for both EMS & EDS systems.

The study results for the long wave surface deviations used in the models show excessive accelerations in the Transrapid (Guideway 5) and HSST (Guideway 4) systems over the range of speeds analyzed. Also, all EDS configurations produce accelerations greater than the ride comfort criteria between 200 km/h and 400 km/h for 21 m spans and between 125 km/h and 250 km/h for 39 m spans. Long span EMS accelerations exceed the ride comfort criterion as well. Noting that the vehicle secondary suspension is not optimized, reduction in these accelerations can be anticipated for a properly designed secondary suspension. Hedrick et al [70] and Snyder [17] develop methods for analyzing and designing vehicle response to guideway roughness to meet ride comfort criteria.

These results suggest that magnet alignment tolerance must be on the order of the irregularities used in the model which is +/- 2mm. Attaining tolerance compliance of that order is expected to be costly and may not be possible without some adjustability between magnets and guideway.

If installation and long term maintenance of a precision alignment is not likely to be attained with conventional construction practice (Table 8.2.4-A), the magnet mounting designs should consider adjustment capabilities that permit future realignment of the magnets to design geometries. The range of magnet adjustment should be designed to accommodate the full range of guideway construction tolerances shown in Table 8.2.4-A.

8.2.5 Bearing Pads

The analysis results suggest that beam bearing pad stiffness has a significant influence on the vehicle and guideway response. The analysis treated bearing pad stiffness ranging from 525 kN/cm to 5250 kN/cm. Subsequent analysis was conducted to determine the minimum and maximum practical bearing pad stiffness that are compatible with design codes and other design guidelines.

Assuming a typical bearing pad material (neoprene) and a temperature variation of 44 degs C, the allowable bearing pad thickness and stiffness for guideways in this study are shown in Table 8.2.5-A.

Table 8.2.5-A
Bearing Pad Properties

Beam Length	Minimum Bearing Pad Thickness	Maximum Bearing Pad Stiffness
21m	38.1mm	2977 kN/cm
39m	63.5mm	2073 kN/cm

Beam Length	Maximum Bearing Pad Thickness	Minimum Bearing Pad Stiffness
21m	130mm	820 kN/cm
39m	130mm	820 kN/cm

The bearing pad thickness are the minimum permitted by AASHTO [81], paragraphs 14.2.3 and 14.2.6, to accommodate beam movement caused by thermal expansion; as a result, the pad stiffness values are the maximum that can be permitted.

The maximum bearing pad thickness for both beams in Table 8.2.5-A is on the order of 130mm thick if sandwiched pad construction method is used. The thickness is governed by pad proportions required to maintain shape factors.

For the conditions studied, the practical bearing pad stiffness range is about 800 kN/cm to 3000 kN/cm, a somewhat narrower range than assumed in the analysis (Section 6.0).

8.3 Implications of Magnetic Fields on Beam Design

8.3.1 Disruption of Magnetic Fields by Guideway Steel

Use of iron reinforcing bars in concrete in maglev systems may have an effect on the magnetic forces generated.

Two effects can result. Eddy currents are the major effect. The other effect is the fact that the rebars are ferromagnetic and may affect the local value of field.

Eddy currents can be induced in closed electrical circuits made up of the rebar and any conducting wire used to hold rebars in place. Any conducting medium will allow eddy currents to flow such as guideway surface water that contains salt.

Eddy currents can be minimized either by replacing rebars with nonconducting fibers (fiberglass is routinely used in MRI installations for this reason). Another approach is to space the individual rebars within the concrete with enough space between bars to prevent any current flow.

However, these mitigation measures may be unnecessary. For example, the ferromagnetic material increases the permeability of the concrete and is not necessarily a detrimental effect. It may enhance the coupling between vehicle and track coils, increasing lift and guidance force potential with no increase in power.

Most concern with this effect arises for repulsive systems. In attractive systems, the eddy currents are nearly all contained within the air gap. An estimate of the magnitude of the effect in repulsive systems was arrived at as follows: the magnetic force was computed assuming no eddy currents or magnetic permeability in the concrete. The magnetic force was then computed assuming no track currents for eddy currents flowing on the surface of the concrete.

The ratio of the eddy current force on the concrete to the track current force is presented as the force reduction ratio in Table 8.3.1-A. The table shows the reduction of magnetic force with distance of the concrete surface from the track coils.

The table overestimates the effect since in an actual case when both track currents and concrete eddy currents flow, the effect is reduced. The table is also a good estimate of the maximum effect due to the permeability of the iron.

The second column shows the distance from track coil to concrete divided by the separation between the superconducting conductors on the vehicle and the track coils. The third column shows the actual distance in meters for w - 0.5m. To achieve a reduction to .01 (1%) the concrete surface, if laden with salts and water, or a conductive structural member such as rebar or steel structural shapes must be at least .366m from the track coils. All distances are to the center of conductors, and the reacting surface or reacting guideway steel member. For example, a 5cm radius track coil should be about 0.315m from a guideway conductor that is 2.5cm in diameter.

Clearly the limitation specified in this table are for the case where eddy currents or highly permeable materials are present.

Table 8.3.1-A
DISTANCE OF TRACK COILS TO IRON REINFORCED CONCRETE

Force Reduction Ratio	Normalized Distance /coil gap (deflection/coil gap)	Distance between guideway coil and rebar (m)
1.0	0.000	0.000
0.5	0.1103	0.005
0.2	0.2561	0.128
0.1	0.3665	0.183
0.05	0.4768	0.238
0.02	0.6226	0.311
0.01	0.7329	0.366
0.005	0.8433	0.422
0.002	0.9891	0.495
0.001	1.0994	0.550
0.0005	1.2097	0.605
0.0002	1.3556	0.678
0.0001	1.4659	0.733

8.3.2 Magnetic Field Effects on Guideway Corrosion

Concerns have been raised by others regarding the possibility that magnetic fields may increase the rate of corrosion, or increase the potential for corrosion, in guideway components. The concern has obvious implications for designs of structures containing or made from steel or other conductors.

There are several aspects of this question which will be treated separately.

The first appears to be a perception that magnetic fields will inductively generate currents in rebar or other components, or leave a net charge on these components which will then activate corrosive mechanisms. Corrosion occurs when there is a net flow of current between objects. Current flows within rebar does not initiate corrosion unless the flow exits to ground at some point; corrosion will then occur at that exit point. Known methods of design and construction provide multiple methods, with layers of protection, to mitigate transfer of rebar currents to ground.

Accumulation of charge on metal surfaces from magnetic fields is unlikely in maglev systems because rebar (and other fixed guideway components) will receive cyclic fields as the train passes much like AC current in which half the cycle is positive and the other half negative, canceling any residual.

A second issue is direct current leakage from guideway coils or plates to ground. Consider a repulsive (EDS) system because it has the higher guideway coil currents. An individual guideway coil will have about 350 amps of induced current for a 5cm coil bundle that is 0.5m wide and 2m long during a 0.1g acceleration of the train. The coil to ground voltage under that condition is about 1 volt. It is assumed that the guideway coil is appropriately insulated and mounting hardware is suitably isolated from the coil. By comparison, existing transit systems generate 900 to 1360 amps of current in return rail at voltages of 600 to 1500 volts.

Because guideway levitating coils are not continuously active (except in the systems designed to provide levitation, guidance and propulsion with the same coils), current leakage from one coil will have only a short time opportunity to distribute the stray current. Further, the unintended leakage path is expected to be a poor conductor, disallowing full current drain from the coil. Current flow from a coil to ground is therefore expected to be highly localized, intermittent and a weakly transmitted occurrence, with a very low possibility of occurrence in the first place.

The third aspect of the corrosion question is the propulsion system which in any design has conductors running the length of the guideway to provide both positive power supply and negative return. These supply and return lines for maglev systems are expected to be fully insulated in compliance with power distribution norms for at-grade installations, aerial structures notwithstanding. Unlike discrete isolated coils, these cables are continuous, with variations of power switching that are system dependent.

Comparing these insulated power cables to the open air third rail supply and running rail return of many transit systems, the current leakage potential of maglev propulsion systems is far less than the open air transit system which are successfully mitigated. It is a reasonable assumption that technology exists to minimize corrosive stray currents in maglev propulsion systems that have lower voltages and more insulation than existing transit systems.

While analysis of any planned transit system for corrosion potential and stray current control is required for future maglev systems, the designs offered in this study are compatible with any stray current and mitigation control measures which may be implemented, under the expectation that corrosion influences from maglev physics are no worse than conditions experienced in existing D.C. transit systems.

8.4 Benefits of Covering the Guideway

Enclosed guideways are under consideration to reduce hazards to high speed trains from encroaching objects (birds, weather, most forms of vandalism, etc..).

Section 5.2 of the study discusses aerodynamic benefits and trade offs from an enclosed guideway, and is summarized here.

Enclosed Guideways:

- Reduce side wind effects on vehicles

- Control overall drag if the enclosure is properly vented and has suitable side clearances.

Full pneumatic (vacuum) tube systems are considered unlikely candidates because the complexity and power requirements of such a system may not have a positive cost/benefit ratio.

From a structural viewpoint, the addition of a lightweight enclosure will increase the permanent side wind exposure area, while eliminating lateral wind-induced train dynamics. The lateral guideway structural properties would probably not be affected since the vertical requirements governed the design. The structures developed in this study have excess lateral capacity.

The added dead load of lightweight enclosures is expected to have minimal effect on the designs used in this study.

8.5 Effects of Beam Design Assumptions on Results

8.5.1 Effects of Load Distribution Assumptions on Beam Design

The four beams designed in this study (configurations numbered 1,2,3 and 6) and the dimensions derived for the HSST beam (beam no. 5) assume point loading as in railroad wheel loading with two "axles" fore and two aft on the vehicle. In reality, Maglev loads are distributed over "pads" roughly the length and width of the on-board magnets. In the EMS system, magnets are placed at uniform spacing along the vehicle length to provide a close approximation to a uniform load distribution to the guideway. In the EDS system, magnet pairs are placed at the forward end and rear end of the car similar to railroad bogies but the magnet-pair length is 4 to 5 meters in length with a fairly uniform load distribution over that distance.

The difference in beam design loads between uniform live load and concentrated wheel loads is analyzed in Table 8.5.1-A.

TABLE 8.5.1-A
Comparison of Design Moments Between Concentrated and Distributed Load Assumptions

Structure Type	21 m Span			39m Span, Multiple Cars			39m Span, 2 car-consist		
	Moments (kN-m)		Change	Moments (kN-m)		Change	Moments (kN-m)		Change
	Concentrated	Uniform	(%)	Concentrated	Uniform	(%)	Concentrated	Uniform	(%)
1 Steel Girders w/ concrete deck 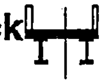	5,732	5,278	-7.9%	18,339	18,049	-1.6%	17,923	17,888	-0.2%
2 Concrete Box 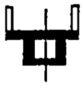	6,605	6,151	-6.9%	22,337	22,047	-1.3%	21,921	21,886	-0.2%
3 Trapezoidal Box 	6,179	5,725	-7.3%	21,382	21,091	-1.4%	20,965	20,930	-0.2%
4 Twin Box (HSST) 	4,311	3,857	-10.5%	15,091	14,801	-1.9%	14,675	14,639	-0.2%
5 Steel "V" (Transrapid) 		Designed by others							
6 AASHTO Concrete Girders 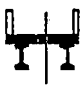	6,440	5,918	-8.1%	21,704	21,414	-1.3%	21,288	21,253	-0.2%

The results show:

- For the 21m span, the critical total dead load plus live load moment for the uniform load is 7% to 10% less than for the concentrated load assumption.

- For 39m span, the critical total dead load plus live load for the uniform load assumption is 2% less than the concentrated load assumption.

The beam designs in this study are therefore slightly conservative for EMS applications. The beams are closely representative of the design required for EMS maglev systems.

8.5.2 Assumption of Simple Span Properties for Continuous Span Analysis

To preserve project resource, the simple span beam properties are used in this study to represent continuous spans by allowing moments to be transmitted at the pier in the middle of the continuous span.

The continuous span is expected to have smaller sections than a simple span at the same pier spacing. The beam weight and natural frequency would be marginally reduced for continuous spans compared to single spans.

The results in the study for continuous spans is expected to be within the overall variance that exists in actual construction. The speeds at which peak accelerations occur will shift slightly from those shown in the analysis. Other differences are difficult to quantify without performing a full design, but are expected to be small.

8.6 Computer Model Validation Requirements

The computer models developed for this study use published values or derived values that are a reasonable reflection of what is known of each system.

Validating the models requires comparison with test data. Test data for mechanical dynamics must come from actual operation of a maglev vehicle at full speed. Aerodynamic aspects of the validation can be obtained from scale modeling and wind tunnel evaluations. Primary data for validation is listed.

Required Data:

Vehicle Parameters

- Detailed Geometry
  - length, width, cross section dimensions.
  - magnet frame sizes and mounting point location on vehicle.
  - centers of gravity for car body magnet frames.

- Vehicle Mechanical Characteristics
  - Secondary magnet damping and spring rate
  - Magnet operating, characteristics
    - force/deflection characteristic
    - drag/damping
  - Car body bending stiffness, mass.
  - Magnet frame mass.

- Guideway
  - Geometry - length, cross section dimensions
  - Weight per unit length
  - Vertical & lateral bending stiffness
  - Connecting details - bearing pad stiffness
  - Pier characteristics

- Test Data
  - Forces
    - guideway mid span and ends
    - vehicle at support points

  - Accelerations
    - guideway, mid span and end
    - vehicle, magnet frames, car body middle and ends and over supports

  - Deflections
    - guideway mid span
    - pier to guideway

- Operational Data
  - Train speed
  - braking
  - power consumption, current
  - ambient conditions of test - wind, temperature, humidity.

9.0 SUMMARY

This study investigates the dynamic interactions between magnetically levitated vehicles and elevated guideways.

General - Vertical Dynamics

- The dynamic load did not exceed the maximum allowable bending moment for any guideway designed to existing U.S. guidelines, although the dynamic acceleration exceeded the 30% design impact factor in many cases.

- Beams designed to existing U.S. guidelines experience lower dynamic accelerations than the comparison beam designs. The lower dynamics in the beams designed to U.S. guidelines are attributed to their significantly larger mass even though the span deflection to span length ratio used in the U.S. designs is 1/1000 whereas the comparison beams use a stiffer 1/4000 ratio. The beam used for comparison is all steel whereas the other designs are composite steel-concrete or all concrete designs.

- Mid-car accelerations are lower than the forward end of the car which, in turn, are generally lower than the rear end of the car for both EMS and EDS maglev systems.

- Mid-car peak accelerations exceed ride comfort criteria for the **EDS system** on all guideway configurations for speeds between 200 and 350 km/h on shorter spans, and between 100 and 250 km/h on longer spans.

- Mid-car peak accelerations exceed ride comfort criteria for the **EMS system** on all guideway configurations above approximately 500 km/h on short span lengths, and for all speeds on longer spans. The analysis of longer spans with EMS systems only included a steel girder design and a AASHTO concrete girder span design.

- **EMS systems** on short, light structures generate vertical car body accelerations well above the desired comfort limit over the entire speed range analyzed.

- Where ride comfort criteria is marginally exceeded, optimization of the vehicle's secondary suspension is expected to provide compliance.

Comparison of Continuous Span Structures to Simple Spans

- In **EMS systems**, continuous span structures generally offer significant reductions in vertical car body and beam accelerations compared to simple spans (exceptions are expected; a 500 to 550 km/h exception is documented in guideway accelerations for the single configuration analyzed).

- In **EDS systems**, continuous span structures reduced vertical beam accelerations while reducing ride quality (that is, adversely affecting ride comfort) in the beams analyzed.

Lateral and Torsional Dynamics

- All of the systems and configurations analyzed on tangent guideway produced acceptable lateral ride comfort and beam accelerations. In the worst case analyzed with vehicle speeds of 400 km/h and 115 km/h side wind gust, the vehicle was stable but the ride is rough. Curved geometries remain to be analyzed.

Guideway Support Stiffness - Bearing Pads

- At high speeds, the beam bearing pad stiffness is observed to be a larger influence on vehicle/guideway interaction than previously documented. For a 21 m AASHTO concrete girder and within the practical ranges of bearing pad stiffness,

    - **EMS system's** ride comfort becomes unacceptable when the softest bearing is used, while the **EDS system's** ride comfort is unaffected by bearing pad stiffness value;
    - **EMS system's** beam acceleration is unaffected by bearing stiffness, while **EDS system's** beam accelerations decrease as the bearing is made softer.

Design Criteria and Guidelines for High Speed Aerial Structures

- There are no U.S. design codes, guidelines or formalized methods for assessing dynamic loads and deflections on aerial structures for speeds over 200 km/h.

- The amplitude of peak guideway accelerations increases with the ratio of vehicle mass to guideway mass (mass ratio) for a given span length for both EMS and EDS maglev systems.

- The mass ratio and the crossing frequency ratio (the ratio of crossing frequency, V/l_s, to fundamental span frequency) appear to provide reasonable indications of dynamic thresholds.

- Under conditions studied, beam accelerations are expected to be less than the 30% impact factor when the crossing frequency ratio is less than 1.0 and, simultaneously, when the mass ratio is less than the following values:

	Maximum Allowable Mass Ratio for 21m spans	Maximum Allowable Mass Ratio for 39m spans
EMS Systems	0.6	0.3*
EDS Systems	0.3*	0.18

* approximate

Construction Issues Effecting Design

- Guideway steel such as rebar will interfere with magnetic fields only in EDS Systems and only when the steel is sufficiently close to track coils. Magnetic force loss of 1% is expected when guideway steel is within 0.37 m of the track coil center and a 5% loss for 0.24 m clearance, using conservative estimates. However, rebar may be placed at normal 25mm to 50mm concrete cover to track coils if the rebar is electrically discontinuous.

- Published structural construction tolerances are large compared to the expected alignment irregularity allowances for maglev. Consideration is urged for guideway magnet mounting designs that permit construction and maintenance adjustment.

- The design of the beams is effected by requirements for transportation of beams to construction sites and handling requirements of the beams during construction.

- Design analysis for corrosion effects from magnetic fields and stray current control is required for maglev systems as is the current practice for new transit systems. There is no concern at this time that magnetic flux fields will have any more corrosive effect on conductive structural elements than is currently experienced in existing DC powered transit systems with proper design using existing technology.

Other Issues

The report also discusses effects of vehicle length on dynamic performance, the benefits of covering or enclosing the guideway, the requirements for validating the computer models developed for this study, and the variances in the results associated with the study's assumptions. Additional topics for research are also offered.

Overall Summary

This study offers insights on the nature of increased dynamics that can be expected in high speed maglev systems. Future vehicle and guideway designs for these systems require detailed dynamic analysis to accomplish cost effective configurations with acceptable ride quality. The guidelines and methodology for executing these designs is unavailable in accepted U.S. standards and criteria. It is important that suitable design guidelines for high speed applications are validated early in the development of maglev technology.

10.0 Recommendations for Future Development

Recommended Additional Vehicle/Guideway Dynamics Computer Model Runs and/or Areas for Further Investigation

1. Effects of different amplitudes of beam camber: run -5, 0 +2, (+5 already used), +10 m and +15 mm camber; EMS and EDS vehicles; Guideways 1, 2, 6, 1D, 2D, 6D. (Suffix D = two-span beam).

2. Effects of other wavelengths, amplitudes, and shapes of guideway geometry errors: EMS and EDS vehicles, representative guideways.

3. Effects of longer vehicle (25 m overall length) with lower-frequency (6.5 Hz) body vertical bending mode; also effects of 18 m vehicle with 15 Hz body vertical bending frequency.

4. Effects of wind gusts: EMS vehicle at 400 km/h, 115 km/h wind gust at 0, 45, and 90 degrees; EDS vehicle at 400 km/h wind gust at 0 and 45 degrees.

5. Fill in more of the two-span run matrix: EMS vehicle on Guideway 1D, 2D, and 3D.

6. Effects of torsional disturbances (line and cross level geometry errors) on two-span guideways, both EMS and EDS vehicles.

7. Effects of torsional disturbances with different geometry wavelengths and amplitudes, both EMS and EDS vehicles, representative guideways.

8. Vary some of the vehicle parameters such as vehicle car body mass (empty, half-load, crush load), secondary suspension stiffness and damping, magnet frame position, magnet effective stiffness and damping. Representative guideways.

9. Introduce guideway spiral and curve, vehicle banking into the simulation.

10. Develop beam bearing pad, stiffness criteria to mitigate vehicle and beam accelerations for incorporation into design guidelines.

11. Identify structure design parameters for dynamics such as mass ratios and crossing frequency ratios and develop design limit criteria.

12. Investigate dynamic design methods for high speed aerial structures.

REFERENCES

1. Baltimore Light Rail System, 10/90 bid results for 1,521 foot aerial structure (extrapolated to $/mi. based on footage); structure design is an AASHTO Type 4 prestressed concrete girder, single track. Double track costs approximately 50% more than single track. (Personal communication with F.P. Balsamo, Structural Managing Engineer, PBQ&D)

2. "New York State Technical and Economic Maglev Evaluation", Grumman Space Systems et al, for New York State Energy Research and Development Authority, October 1990.

3. "Super Speed Ground Transportation System: Las Vegas/Southern California Corridor Phase II Final Report:, City of Las Vegas, June 1987. (Cited in reference 5)

4. "High Speed Rail in the Midwest: An Economic Analysis", Federal Reserve Bank of Chicago, 1984 (Cited in reference 14).

5. "Superconducting Machines and Devices", Ed. by S. Foner & B. Swartz, Plenum Press, NY, pp 347-399 (cited in reference 14)

6. "Conceptual Design and Analysis of the Tracked Magnetically Levitated Vehicle Technology Program (TMLV) - Repulsive Scheme", by Ford Motor Company, for Department of Transportation, February 1975 (cited in reference 14).

7. Whitelaw, Robert L., et al, "Cable-Stayed Guideway. An Analysis and Dynamic Model Tests", Virginia Polytechnic Institute and State University, April 2974, NTIS Report No. PB-238 915.

8. Personal communication, 12/11/90, F.P. Balsamo, PBQ&D Structural Managing Engineer.

9. Coffey, H.T., et al, "An Evaluation of the Dynamics of a Magnetically Levitated Vehicle", March, 1974, Stanford Research Institute under contract to the Federal Railroad Administration, NTIS Report No. PB-236 671.

10. Wallarapp, O., "Schingungs-und Stabilitatsprobleme von Magnet schwebe-Fahrzeugen bei Wechselwirkung mit elastichen Fahrwegen" (Vibration and Stabilizing Problems of Magnetic Levitation Vehicles by Interactions with Flexible Track), Vehicle Dynamics International-Berichte Nr., 1978.

11. Kortum, W., "Modelling and Simulations of Actively Controlled Mechanical Systems", Modelling and Simulation in Engineering, W. F. Ames et al (eds.), IMACS (NTH-HOLLAND) Publishing Company, 1983, pp. 91-101.

12. Kortum, W., Utzt, A., "Control Law Design and Dynamic Evaluations for a MAGLEV Vehicle with a Combined Lift and Guidance Suspension System", Journal of Dynamic Systems Measurement, and Control, Vol. 106, December 1984, pp 286-292.

13. Kortum, W. Utzt, A., "Simulation of Active Suspensions in Ground Transportation Systems", Proc. 11th IMACS World Congress Modelling and Simulation in Engineering, Oslo, 1985.

14. Johnson, L.R., et al, "An Evaluation of High Tc Superconductivity Applied to Magnetically Levitated Vehicles", May 1988 [Draft], Argonne National Laboratory, pp 70-76.

15. Wilson, James F., Experiments in Guideway-Levitation Vehicle Interaction Dynamics, January 1976, under contract to the Federal Railroad Administration, NTIS Report No. PB-257 941.

16. "Proposal Abstract for Influence of Guideway Flexibility on Maglev Vehicle/Guideway/Dynamic Forces", by Parsons Brinckerhoff Quade & Douglas, October, 1990, submitted to the FRA in response to BAA No. 90-1.

17. Snyder, J.E., Wormley, D.N., "Dynamic Interactions between Vehicles and Elevated, Flexible Randomly Irregular Guideways", Journal of Dynamic Systems, Measurement and Control, March 1977, ASME, pp 23-33.

18. Chung, Y.I., Genin, J., "Stability of a Vehicle on a Multispan Simply Supported Guideway", Journal of Dynamic Systems, Measurement and Control, Vol 100, ASME, December, 1978, pp 326-332.

19. Cherchas, D.B., "A Dynamics Simulation for a High Speed Magnetically Levitated Guided Ground Vehicle", Journal of Dynamic Systems, Measurement and Control, Vol. 101, ASME, September 1979, pp 223-229.

20. Wilson, J.F., Babas, S.T., "Responses of Continuous, Elastically Supported Beam Guideway to Transit Loads", Journal of Dynamic Systems, Measurement and Control, Vol. 102, ASME, December 1980, pp 247-254.

21. Kortum, W., Wormley, D.N., "Dynamic Interactions Between Traveling Vehicles and Guideway Systems", Vehicle System Dynamics, Vol. 10, 1981, pp 285-317.

22. National Maglev Initiative Government-Industry Workshop, Final Report, 11/1/90, Argonne National Laboratory by U.S. DOT, U.S. DOE, U.S. Army Corps of Engineers, "Revised Draft system Parameters", 8/90.

23. Doher, Robert M. and Hathaway, William T., "Safety of High Speed Magnetic Levitation Transportation Systems: Preliminary Safety Review of the Transrapid Maglev System", U.S. DOT, Federal Railroad Administration, Interim Report, Nov. 2990, Report No. DOT/FRA/Ord-90/9.

24. Conceptual Design and Analysis of the Tracked Magnetically Levitated Vehicle Technology Program (TMLV). Rep? Scheme. Vol. 1 Technical Studies, by Philco-Ford Corp., Feb. 2975, Final Report DOT-FR-4002M PB-247-931

25. High-Speed Ground Transportation Systems Engineering Study -- Elevated Guideway Structures, by TRW Systems Group for DOT, Dec. 1969, Report No. FRA-RT-70-35, PB 191-670

26. The Feasibility of Magnetically Levitating High-Speed Ground Vehicles, by the Stanford Research Institute for FRA, Report No. FRA-RT-72-39, PB 210-505, Feb. 1972.

27. Johnson, R.A., Aerodynamic Drag and Stability characteristics of a Magnetically Levitated Vehicle, AVSD-0391-72-CR, AVCO Systems Division, Wilmington, MA, Nov. 1, 1972.

28. Watson, T.C., Grahm, H. R., and Dietrich, W. H., Operational Potential of Suspended vehicle Systems (SVS), Final Report, TRW, Report FRA-04D&D-74-7B, July 1973

29. Grumman Corporation, Benefits of Magnetically Levitated High Speed Transportation for the United States, Vols. 1 and 2, for The Maglev Technology Advisory Committee, Grumman Corp., Bethpage, NY, 1989.

30. He, J.L., Rote, D.M. and Coffey, H.T., "Survey of Foreign Maglev Systems", Center for Transportation Research, Argonne National Laboratory, Argonne, IL, Nov. 1990.

31. Parsons Brinckerhoff International, Inc., et al, "West Taiwan High Speed Rail Feasibility Study, Evaluation of Alternative High Speed Rail Technologies", for Institute for Transportation, Republic of China, Dec. 1989.

32. Phelan, Randal S., Construction and Maintenance Concerns for High Speed Maglev Transportation Systems, Thesis Paper, Massachusetts Institute of Technology, Dept. of Civil Engineering, June 1990.

33. "Transrapid Safe to Operate on a Single Guideway", Railway Gazette International, July 1991, pp.479-480.

34. TRW Systems Group, Elevated Guideway Structures, U.S. Department of Transportation, Report No. FRA-RT-70-35, PB 191670, Dec. 1969.

35. Rote, Donald M., "Maglev Technology Overview", Maglev Government/Industry Forum, Center for Transportation Research, Argonne National Laboratory, Argonne, IL, May 2, 1990.

36. Klinger, et al, "Guideway-Vehicle Cost Reduction, Part I: Guideway Vehicle Performance and Costs", NTIS PB-265966, 7/9/76, and "Part 2: Active Suspension Feasibility", NTIS PB-265967, 7/9/76.

37. Wong, J.Y., Howell, J.P., Rhodes, R.G., Mulhall, B.E., "Performance and Stability Characteristics of an Electrodynamically Levitated Vehicle Over a Split Guideway", Journal of Dynamic Systems, Measurement and Control, Sept. 1976, pp. 277-282.

38. Ravera, R.J., "Analysis and Simulation of Vehicle/Guideway Interactions with Application to a Tracked Air Cushion Vehicle", Federal Railroad Administration, Report No. FRA-ORD&D-75-38, NTIS PB-242014, Feb. 1975.

39. Kortum, W, "Simulation of the Dynamics of High Speed Ground Transportation Vehicles with MEDYNA - Potentials and Case Studies", 1988.

40. "Magnetic Levitation Transportation System Technology Assessment", Broad Agency Announcement No. 90-1, Federal Railroad Administration, DOT/FRA/ORD-90-08, Sept. 1990.

41. He, J.L., Coffey, H.T. and Rote, D.M., Publications on Maglev Technologies, Argonne National Laboratory, Argonne, IL, Oct. 1990.

42. "Safety Factors Related to High Speed Rail Passenger Systems", Transportation Research Board, Transportation Research Circular No. 351, July 1989.

43. "Safety Relevant Observations on the TGV High Speed Train", USDOT, Federal Railroad Administration, July 1991.

44. American Concrete Institute, "Standard Tolerances for Concrete Construction and Materials (ACI 117-90) and Commentary (ACI 117R-90)", ACI, Detroit, Michigan, June 1990.

45. American Concrete Institute, "Analysis and Design of Reinforced Concrete Guideway Structures", ACI 358.1R-86, Detroit, Michigan, 1986.

46. Dorton, R.A. and Grouni, H.N., "Review of Guideway Design Criteria in Existing Transit System Codes", ACI Journal, April 1978, pp. 134-144.

47. Muotoh, D.U., "Investigation of Structural Design Criteria for Automated Transit Aerial Guideways", USDOT, UMTA Report UMTA-IT-06-0311-84-1, NTIS No. PBB 4196419, April 1984.

48. American Concrete Institute, "State-of-the-Art Report on Concrete Guideways", ACI 358R-80, Detroit, Michigan, July 1980.

49. Tabatake, Hideo, "Effect of Dead Loads on Natural Frequencies of Beams", ASCE Journal of Structural Engineering, Vol. 117, No. 4, April 1991, pp. 1039-1052.

50. Akin, John E. and Mofid, Massood, "Numerical Solution for Response of Beams with Moving Mass", ASCE Journal of Structural Engineering, Vol. 115, No. 1, January 1989, pp. 120-131. Discussion by Klasztorny and Sniady, Ibid., May 1989, pp 1568-1570.

51. Oral, Suha, "Anisoparametric Interpolation in Hybrid-Stress Timoshenko Beam Element", ASCE Journal of Structural Engineering, Vol. 117, No. 4, April 1991, pp. 1070-1078.

52. Stallings, James M. and Frank, Karl H., "Stay-Cable Fatigue Behavior", ASCE Journal of Structural Engineering, Vol. 117, No. 3, March 1991, pp. 936-950.

53. Arbabi, F. and Loh, C.U., "Reliability Analysis of Railroad Tracks", ASCE Journal of Structural Engineering, Vol. 117, No. 5, May 1991, pp. 1435-1447.

54. Stekly, Z.J.J., et al, "New York State Technical and Economic Maglev Evaluation - Electrodynamic Suspension - Superconducting Magnet Design", Draft Report, Oct. 3, 1990.

55. Hwang, E.S. and Nowak, S., "Simulation of Dynamic Load for Bridges", ASCE Journal of Structural Engineering, Vol. 117, No. 5, May 1991, pp. 1413-1434.

56. Farhan, I. H. and Mahmoud, S. M., "Maglev Train Design for Aerodynamics Using the Panel Method," Computer Applications in Railway Operations, Proc. of the Second International Conference on Computer Aided Design, Mfr. and Operation in the Railway and Other Advanced Mass Transit Systems, Computational Mechanics Publications, Boston, March 1990, pp. 107-118.

57. Behr, R.A., et al, "Cost Comparison of Timber, Steel and Prestressed Concrete Bridges", ASCE Journal of Structural Engineering, Vol. 116, NO. 12, December 1990, pp. 3448-3457.

58. American Concrete Institute, "Models of Concrete Structures: State of the Art", ACI 444R-79, Detroit, Michigan, 1979, Rev. 1984.

59. Stekly, Z.J.J., "Simplified High Speed Magnetic Suspension Analysis", Draft Copy, correspondence with L.E. Daniels dated 10/11/91 from Intermagnetics.

60. United States Steel Corporation, "Aerial Structures for Mass Transit Systems", from The Practical Answer for Modern Mass Transit Rights-of-Way, Book 3, U.S.S. Corp., Pittsburgh, Pennsylvania, Undated

61. American Iron and Steel Institute, "Steel Structures for Mass Transit", AISI, Washington, DC, Undated.

62. C.C. Smith, et al, "Multiple Continuous Span Elevated Guideway - Vehicle Dynamic Performance", ASME Journal of Dynamic Systems, Measurement, and Control, March 1975, pp 30-40

63. H.H. Richardson, D.N. Wormley, "Transportation Vehicle/Beam-Elevated Guideway Dynamics Interactions: A State-of-the-Art Review," ASME Journal of Dynamic Systems and Control, June 1974, pp. 169-179.

64. W.S Chiu, R.G. Smith, D.N. Wormley, "Influence of Vehicle and Distributed Guideway Paramenters on High Speed Vehicle - Guideway Dynamic Interactions," ASME Journal of Dynamic Systems, Measurement and Control, March 1971, pp. 25-34.

65. D.N. Wormley, J.K. Hedrick, et al, "Elevated Guideway Cost-Ride Quality Studies," Proceedings, ASCE Specialty Conference on Advances in Civil Engineering (Raleigh, 5/1977) ASCE NY 1977, pp. 150-154

66. H.H. Richardson, D.N. Wormley, "Coupled Dynamics of Transportation Vehicles and Beam-Type Elevated Guideways," AMD Vol 5, American Society of Mechanical Engineers, NY, 1973 pp. 1-30.

67. W.S. Chiu, D.N. Wormley, R.C. Smith, H.H. Richardson, "Coupled Dynamic Interactions Between High Speed Ground Transport Vehicles and Discretely Supported Guideways," U.S. DOT, PB 199 136, 7/70, 117 pgs.

68. D.N. Wormley, M.L. Naqurka, G. Isaacs, "Rail Transit Train/Elevated Structure Dynamic Interactions," December 1981, prepared for UMTA/DOT (no. Report #), 98 pgs.

69. D.N. Wormley, C.C. Smith, A.J. Gilchrist, "Multispan Elevated Guideway Design for Passenger Transport Vehicles" Volume I, Report # PB 253 008, Volume II, Report # PB 253 009, April 1975.

70. J.K. Hedrick, R.J. Ravera, J.R. Anderes, "The Effect of Elevated Guideway Construction Tolerances on Vehicle ride Quality", ASME Journal of Dynamic Systems, Measurements, and Control, Dec. 1975, pp. 408-416.

71. Grunwald, Kalman J., "Aerodynamic Characteristics of Vehicle Bodies at Crosswind Conditions in Ground Proximity", NASA TN-D-5935, NASA Langley Research Cener, Hampton, VA., 1970.

72. Hammitt, Andrew G., The Aerodynamics of High Speed Ground Transportation, Western Periodicals Co., North Hollywood, Ca., 1973.

73. Schlichting, Dr. Hermann, Boundary Layer Theory, McGraw-Hill, New York, 1987.

74. F.S. Tse, I.E. Morse and R.T. Hinkle, Mechanical Vibrations - Theory and Applications, Allyn and Bacon, Inc., 2nd Ed., 1978 Chapter 7.

75. Dr. P-J. G. Gaede and S. Kunz, "The Coach Body", Transrapid Maglev System, ISBN 3-7771-0209-1, 1989 p.80.

76. Reference to : ASCC ADV PUB 61/17A (18 August 1982).

77. Wilson, J.F., Optimum Design Methodology for Elevated Transit Structures, October 1981.

78. Roster of North American Rapid Transit Cars, July 1980, American Public Transit Association, for U.S. DOT, Urban Mass Transportation Administration, UMTA-DC-06-0121-801.

79. "AISC Code of Standard Practice", "Manual of Steel Construction, Allowable Stress Design", 9th ed., Part 5, pp. 5-223 to 5-261. American Institute of Steel Construction, copyright 1989.

80. Transrapid Maglev System, Exec. Ed. Dr-Ing. Klaus Heinrich, Dipl.-Ing. Rolf Kretzschmar, Copyright 1989, Hestra-Verlag, ISBN 3-7771-0209-1.

81. Standard Specifications for Highway Bridges, American Association of State Transportation Officials, 1991.

APPENDIX A

STRUCTURAL ESTIMATE COST DETAIL

BID SUMMARY
PROJECT NAME ________ MAGLEV SUPERSTRUCTURE STUDIES
JOB NO. ________ 4232F101
DATE ________ MARCH 25, 1992
ESTIMATOR ________ R.ROBERTS

ALTERNATIVE DESIGNS	QUANTITY	UNIT	SUPERSTRUCTURE AMOUNT	SUPERSTRUCTURE UNIT
DOUBLE TEE - AASHTO TYPE IV 21.336 M SPAN "A"	21.336	M	$61,809.82	$2,896.97
DOUBLE TEE - AASHTO TYPE VI 39.624 M SPAN "A'	39.624	M	$123,298.60	$3,111.72
STEEL GIRDER W/ CONCRETE DECK 21.336 SPAN "B"	21.336	M	$71,780.86	$3,364.31
STEEL GIRDER W/ CONCRETE DECK 39.624 FT SPAN "B"	39.624	M	$140,615.30	$3,548.74
SINGLE BOX -PRESTRESSED CONCRETE 21.336 SPAN "C"	21.336	M	$59,747.59	$2,800.32
SINGLE BOX -PRESTRESSED CONCRETE 39.624 M SPAN "C"	39.624	M	$147,169.23	$3,714.14
CIP POST TENSIONED SINGLE BOX 21.336 M SPAN "D"	21.336	M	$69,438.86	$3,254.54
CIP POST TENSIONED SINGLE BOX 39.624 MSPAN "D"	39.624	M	$147,742.34	$3,728.61
TWO PRESTRESSED BOX GIRDERS w/o DECK 21.336 M SPAN "E"	21.336	M	$36,126.33	$1,693.21
TWO PRESTRESSED BOX GIRDERS w/o DECK 39.624 M SPAN "E"	39.624	M	$77,080.81	$1,945.31

BID SUMMARY
PROJECT NAME MAGLEV SUPERSTRUCTURE STUDIES
JOB NO. 4232F101
DATE MARCH 25,1992
ESTIMATOR R.ROBERTS

ALTERNATIVE DESIGNS	QUANTITY	UNIT	SUPERSTRUCTURE		SUBSTRUCTURE		TOTAL FOR 1 SPAN	
			AMOUNT	UNIT	AMOUNT	UNIT	AMOUNT	UNIT
DOUBLE TEE - AASHTO TYPE IV 21.336 M SPAN "A"	21.336	M	$61,809.82	$2,896.97	$36,812.75	$1,725.38	$98,622.57	$4,622.36
DOUBLE TEE - AASHTO TYPE VI 39.624 M SPAN "A"	39.624	M	$123,298.60	$3,111.72	$49,954.99	$1,260.73	$173,253.59	$4,372.44
STEEL GIRDER W/ CONCRETE DECK 21.336 SPAN "B"	21.336	M	$71,780.86	$3,364.31	$36,812.75	$1,725.38	$108,593.61	$5,089.69
STEEL GIRDER W/ CONCRETE DECK 39.624 FT SPAN "B"	39.624	M	$140,615.30	$3,548.74	$49,954.99	$1,260.73	$190,570.29	$4,809.47
SINGLE BOX -PRESTRESSED CONCRETE 21.336 SPAN "C"	21.336	M	$59,747.59	$2,800.32	$34,151.74	$1,600.66	$93,899.33	$4,400.98
SINGLE BOX -PRESTRESSED CONCRETE 39.624 M SPAN "C"	39.624	M	$147,169.23	$3,714.14	$48,691.04	$1,228.83	$195,860.27	$4,942.97
CIP POST TENSIONED SINGLE BOX 21.336 M SPAN "D"	21.336	M	$69,438.86	$3,254.54	$35,539.03	$1,665.68	$104,977.89	$4,920.22
CIP POST TENSIONED SINGLE BOX 39.624 MSPAN "D"	39.624	M	$147,742.34	$3,728.61	$48,691.04	$1,228.83	$196,433.38	$4,957.43
TWO PRESTRESSED BOX GIRDERS w/o DECK 21.336 M SPAN "E"	21.336	M	$36,126.33	$1,693.21	$36,890.28	$1,729.02	$73,016.61	$3,422.23
TWO PRESTRESSED BOX GIRDERS w/o DECK 39.624 M SPAN "E"	39.624	M	$77,080.81	$1,945.31	$50,363.05	$1,271.02	$127,443.86	$3,216.33

BID SUMMARY
PROJECT NAME______ MAGLEV SUPERSTRUCTURE STUDIES
JOB NO.___________ 4232F101
DATE______________ MARCH 25,1992
ESTIMATOR_________ R.ROBERTS

DESCRIPTION	QUANTITY	UNIT	UNIT COST	TOTAL	COST/M OF SPAN
SUPERSTRUCTURE					
DOUBLE TEE - AASHTO TYPE IV 21.336 M SPAN "A"					
AASHTO TYPE IV 2 EA=	42.672	M	$265.00	$11,308.08	$265.00
DIAPHRAGM CONCRETE/FORMS	8.155	M3	$675.00	$5,504.79	$675.00
DECK					
DECK SLAB CONCRETE-PLACE	19.170	M3	$52.70	$1,010.29	$47.35
WALL CONCRETE-PLACE	16.849	M3	$59.24	$998.11	$46.78
DECK SLAB FORM	166.916	M2	$80.28	$13,400.00	$628.05
WALL FORMS	128.076	M2	$85.12	$10,901.81	$510.96
REINFORCING STEEL IN SLAB	3011.802	Kg	$2.10	$6,324.78	$296.44
SUPERSTRUCTURE TOTAL	21.336	M		$49,447.86	$2,317.58
SUB TOTAL COST/SPAN	21.336	M		$49,447.86	$2,317.58
MOBILIZATION	10.00%			$4,944.79	
CONTINGENCY	15.00%			$7,417.18	
TOTAL COST/SPAN	21.336	M		$61,809.82	$2,896.97
DESCRIPTION					
SUBSTRUCTURE					COST/M
DOUBLE TEE - AASHTO TYPE IV 21.336 M SPAN "A"					OF SPAN
DRIVEN PILES 100TON	160.000	M	$105.00	$16,800.00	
PILE CAP EXCAVATION	47.147	M3	$23.54	$1,109.83	
PILE CAP CONCRETE-PLACE	27.184	M3	$33.74	$917.19	
PIER COLUMN CONCRETE-PLACE	8.896	M3	$45.31	$403.08	
PIER CAP BEAM CONCRETE-PLACE	2.588	M3	$64.93	$168.06	
PILE CAP FORMS	23.783	M2	$62.30	$1,481.69	
PIER COLUMN FORMS	29.186	M2	$87.71	$2,559.93	
PIER CAP BEAM FORMS	5.145	M2	$92.12	$473.93	
REINFORCING	2636.419	Kg	$2.10	$5,536.48	
SUBSTRUCTURE TOTAL	1.000	EA		$29,450.20	$29,450.20
SUB TOTAL COST/PIER	1.000	EA		$29,450.20	$29,450.20
MOBILIZATION	10.00%			$2,945.02	
CONTINGENCY	15.00%			$4,417.53	
TOTAL COST/PIER	1.000	EA		$36,812.75	$36,812.75

DESCRIPTION					
SUPERSTRUCTURE					
DOUBLE TEE - AASHTO TYPE VI 39.624 M SPAN "A'					
TOTAL GIRDER 2 EA=	79.248 M	$395.00	$31,302.96	$395.00
DIAPHRAGMS	10.874 M3	$675.00	$7,339.73	$675.00
DECK				
DECK SLAB CONC RETE-PLACE	35.602 M3	$52.70	$1,876.24	$87.94
WALL CONCRETE-PLACE	31.290 M3	$59.24	$1,853.63	$86.88
DECK SLAB FORM	309.986 M2	$80.28	$24,885.71	$1,166.37
WALL FORMS	237.855 M2	$85.12	$20,246.21	$948.92
REINFORCING STEEL	5302.095 Kg	$2.10	$11,134.40	$521.86
SUPERSTRUCTURE TOTAL	39.624 M		$98,638.88	$2,489.37
SUB TOTAL COST/SPAN	39.624 M		$98,638.88	$2,489.37
MOBILIZATION	10.00%		$9,863.89	
CONTINGENCY	15.00%		$14,795.83	
TOTAL COST/SPAN	39.624 M		$123,298.60	$3,111.72
DESCRIPTION				
SUBSTRUCTURE				
DOUBLE TEE - AASHTO TYPE VI 39.624 M SPAN "A'				
DRIVEN PILES 100TON	240.000 M	$105.00	$25,200.00	
PILE CAP EXCAVATION	60.972 M3	$23.54	$1,435.28	
PILE CAP CONCRETE-PLACE	36.246 M3	$33.74	$1,222.93	
PIER COLUMN CONCRETE-PLACE	8.896 M3	$45.31	$403.08	
PIER CAP BEAM CONCRETE-PLACE	2.588 M3	$64.93	$168.06	
PILE CAP FORM	26.756 M2	$62.30	$1,666.90	
PIER COLUMN FORM	29.186 M,2	$87.71	$2,559.93	
PIER CAP BEAM FORM	5.145 M2	$92.12	$473.93	
REINFORCING	3254.225 Kg	$2.10	$6,833.87	
SUBSTRUCTURE TOTAL	1.000 EA		$39,963.99	$39,963.99
SUB TOTAL COST/PIER	1.000 EA		$39,963.99	$39,963.99
MOBILIZATION	10.00%		$3,996.40	
CONTINGENCY	15.00%		$5,994.60	
TOTAL COST/PIER	1.000 EA		$49,954.99	$49,954.99

DESCRIPTION				
SUPERSTRUCTURE				
STEEL GIRDER W/ CONCRETE DECK 21.336 SPAN "B"				
TOTAL GIRDER Kg	14748.498 Kg	$1.76	$25,957.36	$1,216.60
DECK				
DECK SLAB CONCRETE-PLACE	19.170 M3	$52.70	$1,010.29	$47.35
WALL CONCRETE-PLACE	16.849 M3	$59.24	$998.11	$46.78
DECK SLAB FORMS	166.916	$80.28	$13,400.00	$628.05
WALL FORMS	128.076	$85.12	$10,901.81	$510.96
REINFORCING STEEL	2455.777 Kg	$2.10	$5,157.13	$2.10
SUPERSTRUCTURE TOTAL	21.336 M		$57,424.69	$2,691.45
SUB TOTAL COST/SPAN	21.336 M		$57,424.69	$2,691.45
MOBILIZATION	10.00%		$5,742.47	
CONTINGENCY	15.00%		$8,613.70	
TOTAL COST/SPAN	21.336 M		$71,780.86	$3,364.31
DESCRIPTION				
SUBSTRUCTURE				
STEEL GIRDER W/ CONCRETE DECK 21.336 SPAN "B"				
DRIVEN PILES 100TON	160.000 M	$105.00	$16,800.00	
PILE CAP EXCAVATION	47.147 M3	$23.54	$1,109.83	
PILE CAP CONCRETE-PLACE	27.184 M3	$33.74	$917.19	
PIER COLUMN CONCRETE-PLACE	8.896 M3	$45.31	$403.08	
PIER CAP BEAM CONCRETE-PLACE	2.588 M3	$64.93	$168.06	
PILE CAP FORMS	23.783 M2	$62.30	$1,481.69	
PIER COLUMN FORMS	29.186 M2	$87.71	$2,559.93	
PIER CAP BEAM FORMS	5.145 M2	$92.12	$473.93	
REINFORCING	2636.419 Kg	$2.10	$5,536.48	
SUBSTRUCTURE TOTAL	1.000 EA		$29,450.20	$29,450.20
SUB TOTAL COST/PIER	1.000 EA		$29,450.20	$29,450.20
MOBILIZATION	10.00%		$2,945.02	
CONTINGENCY	15.00%		$4,417.53	
TOTAL COST/PIER	1.000 EA		$36,812.75	$36,812.75

DESCRIPTION					
SUPERSTRUCTURE					
STEEL GIRDER W/ CONCRETE DECK 39.624 FT SPAN "B"					
TOTAL Kg	30711.884 Kg		$1.76	$54,052.92	$2,533.41
DECK					
DECK SLAB CONCRETE-PLACE	35.602 M3		$52.70	$1,876.24	$87.94
WALL CONCRETE-PLACE	31.290 M3		$59.24	$1,853.63	$86.88
DECK SLAB FORMS	309.986 M2		$80.28	$24,885.71	$1,166.37
WALLFORMS	237.855 M2		$85.12	$20,246.21	$948.92
SUPERSTRUCTURE TOTAL	39.624 M			$112,492.24	$2,838.99
SUB TOTAL COST/SPAN	39.624 M			$112,492.24	$2,838.99
MOBILIZATION	10.00%			$11,249.22	
CONTINGENCY	15.00%			$16,873.84	
TOTAL COST/SPAN	39.624 M			$140,615.30	$3,548.74
DESCRIPTION					
SUBSTRUCTURE					
STEEL GIRDER W/ CONCRETE DECK 39.624 FT SPAN "B"					
DRIVEN PILES 100TON	240.000 M		$105.00	$25,200.00	
PILE CAP EXCAVATION	60.972 M3		$23.54	$1,435.28	
PILE CAP CONCRETE-PLACE	36.246 M3		$33.74	$1,222.93	
PIER COLUMN CONCRETE-PLACE	8.896 M3		$45.31	$403.08	
PIER CAP BEAM CONCRETE-PLACE	2.588 M3		$64.93	$168.06	
PILE CAP FORM	26.756 M2		$62.30	$1,666.90	
PIER COLUMN FORM	29.186 M2		$87.71	$2,559.93	
PIER CAP BEAM FORM	5.145 M2		$92.12	$473.93	
REINFORCING	3254.225 Kg		$2.10	$6,833.87	
SUBSTRUCTURE TOTAL	1.000 EA			$39,963.99	$39,963.99
SUB TOTAL COST/PIER	1.000 EA			$39,963.99	$39,963.99
MOBILIZATION	10.00%			$3,996.40	
CONTINGENCY	15.00%			$5,994.60	
TOTAL COST/PIER	1.000 EA			$49,954.99	$49,954.99

DESCRIPTION					
SUPERSTRUCTURE					
SINGLE BOX -PRESTRESSED CONCRETE 21.336 SPAN "C"					
BOX					
BOT DECK SLAB CONC-PLACE	9.296	M3	$52.70	$489.88	
BOX WALL CONCRETE-PLACE	10.624	M3	$59.24	$629.34	
TOP SLAB CONCRETE-PLACE	22.741	M3	$52.70	$1,198.43	
WALL CONCRETE-PLACE	18.502	M3	$59.24	$1,096.04	
BOT DECK SLAB FORM	45.522	M2	$80.28	$3,654.55	
BOX WALLFORMS	104.051	M2	$85.12	$8,856.86	
TOP SLAB (B) FORMS	94.297	M2	$80.28	$7,570.13	
WALL FORMS	121.402	M2	$85.12	$10,333.72	
REINFORCING STEEL LBS	2908.561	Kg	$2.10	$6,107.98	
PRE STRESSING LBS	1628.760	Kg	$4.75	$7,736.61	
GROUT M3	0.125	M3	$1,000.00	$124.53	
TOTAL SUPERSTRUCTURE	21.336	M		$47,798.07	$2,240.25
SUB TOTAL COST/SPAN	21.336	M		$47,798.07	$2,240.25
MOBILIZATION	10.00%			$4,779.81	
CONTINGENCY	15.00%			$7,169.71	
TOTAL COST/SPAN	21.336	M		$59,747.59	$2,800.32
DESCRIPTION					
SUBSTRUCTURE					
SINGLE BOX -PRESTRESSED CONCRETE 21.336 SPAN "C"					
DRIVEN PILES 100TON	160.000	M	$105.00	$16,800.00	
PILE CAP EXCAVATION	47.147	M3	$23.54		
PILE CAP CONCRETE-PLACE	27.184	M3	$33.74	$917.19	
PIER COLUMN CONCRETE-PLACE	11.259	M3	$45.31	$510.15	
PILE CAP FORM	23.783	M2	$64.93	$1,544.24	
PIER COLUMN FORM	32.835	M2	$62.30	$2,045.60	
REINFORCING	2621.055	Kg	$2.10	$5,504.22	
TOTAL SUBSTRUCTURE	1.000	EA		$27,321.40	$27,321.40
SUB TOTAL COST/PIER	1	EA		$27,321.40	$27,321.40
MOBILIZATION	10.00%			$2,732.14	
CONTINGENCY	15.00%			$4,098.21	
TOTAL COST/PIER	1	EA		$34,151.74	$34,151.74

DESCRIPTION					
SUPERSTRUCTURE					
SINGLE BOX -PRESTRESSED CONCRETE 39.624 M SPAN "C"					
BOX					
BOT DECK SLAB CONC-PLACE	17.263	M3	$52.70	$909.78	
BOX WALL CONCRETE-PLACE	43.466	M3	$59.24	$2,574.93	
TOP SLAB CONCRETE-PLACE	42.233	M3	$52.70	$2,225.66	
WALL CONCRETE-PLACE	34.360	M3	$59.24	$2,035.50	
BOT DECK SLAB FORM	84.542	M2	$80.28	$6,787.01	
BOX WALLFORMS	425.720	M2	$85.12	$36,237.31	
TOP SLAB (B) FORMS	175.122	M2	$80.28	$14,058.81	
WALL FORMS	225.461	M2	$85.12	$19,191.20	
REINFORCING STEEL LBS	7019.961	Kg	$2.10	$14,741.92	
PRE STRESSING LBS	3931.096	Kg	$4.75	$18,672.70	
GROUT M3	0.301	M3	$1,000.00	$300.56	
TOTAL SUPERSTRUCTURE	39.624	M		$117,735.39	$2,971.32
SUB TOTAL COST/SPAN	39.624	M		$117,735.39	$2,971.32
MOBILIZATION	10.00%			$11,773.54	
CONTINGENCY	15.00%			$17,660.31	
TOTAL COST/SPAN	39.624	M		$147,169.23	$3,714.14
DESCRIPTION					
SUBSTRUCTURE					
SINGLE BOX -PRESTRESSED CONCRETE 39.624 M SPAN "C"					
DRIVEN PILES 100TON	240.000	M	$105.00	$25,200.00	
PILE CAP EXCAVATION	60.972	M3	$23.54	$1,435.28	
PILE CAP	36.246	M3	$33.74	$1,222.93	
PIER COLUMN	11.259	M3	$45.31	$510.15	
PILE CAP FORM	26.756	M2	$64.93	$1,737.27	
PIER COLUMN FORM	32.835	M2	$62.30	$2,045.60	
REINFORCING	3238.861	Kg	$2.10	$6,801.61	
TOTAL SUBSTRUCTURE	1.000	EA		$38,952.83	$38,952.83
SUB TOTAL COST/PIER	1	EA		$38,952.83	$38,952.83
MOBILIZATION	10.00%			$3,895.28	
CONTINGENCY	15.00%			$5,842.92	
TOTAL COST/PIER	1	EA		$48,691.04	$48,691.04

DESCRIPTION					
SUPERSTRUCTURE					
CIP POST TENSIONED SINGLE BOX 21.336 M SPAN "D"					
BOX					
BOT DECK SLAB	13.380 M3	$52.70	$705.11		
BOX WALLS	13.221 M3	$59.24	$783.21		
TOP SLAB (A)	1.806 M3	$52.70	$95.15		
TOP SLAB (B)	19.170 M3	$52.70	$1,010.29		
WALLS	15.857 M3	$59.24	$939.39		
BOT DECK SLAB FORM	43.897 M2	$80.28	$3,524.03		
BOX WALL FORMS	130.064 M2	$85.12	$11,071.07		
TOP SLAB (A) FORMS	67.473 M2	$80.28	$5,416.73		
TOP SLAB (B) FORMS	94.297 M2	$80.28	$7,570.13		
WALL FORMS	104.051 M2	$85.12	$8,856.86		
REINFORCING STEEL Kg	3243.786 Kg	$2.10	$6,811.95		
POST TENSIONING LBS	1816.482 Kg	$4.75	$8,628.29		
GROUT CY	0.139 M3	$1,000.00	$138.88		
TOTAL SUPERSTRUCTURE	21.336 M		$55,551.09	$2,603.63	
SUB TOTAL COST/SPAN	21.336 M		$55,551.09	$2,603.63	
MOBILIZATION	10.00%		$5,555.11		
CONTINGENCY	15.00%		$8,332.66		
TOTAL COST/SPAN	21.336 M		$69,438.86	$3,254.54	
DESCRIPTION					
SUBSTRUCTURE					
CIP POST TENSIONED SINGLE BOX 21.336 M SPAN "D"					
DRIVEN PILES 100TON	160.000 M	$105.00	$16,800.00		
PILE CAP EXCAVATION	47.147 M3	$23.54	$1,109.83		
PILE CAP	27.184 M3	$33.74	$917.19		
PIER COLUMN	11.259 M3	$45.31	$510.15		
PILE CAP FORM	23.783 M2	$64.93	$1,544.24		
PIER COLUMN FORM	32.835 M2	$62.30	$2,045.60		
REINFORCING	2621.055 Kg	$2.10	$5,504.22		
TOTAL SUBSTRUCTURE	1.000 EA		$28,431.23	$28,431.23	
SUB TOTAL COST/PIER	1 EA		$28,431.23	$28,431.23	
MOBILIZATION	10.00%		$2,843.12		
CONTINGENCY	15.00%		$4,264.68		
TOTAL COST/PIER	1 EA		$35,539.03	$35,539.03	

DESCRIPTION				
SUPERSTRUCTURE				
CIP POST TENSIONED SINGLE BOX	39.624 MSPAN "D"			
BOX				
BOT DECK SLAB	24.848 M3	$52.70	$1,309.49	
BOX WALLS	36.830 M3	$59.24	$2,181.81	
TOP SLAB (A)	3.353 M3	$52.70	$176.71	
TOP SLAB (B)	35.602 M3	$52.70	$1,876.24	
WALLS	29.450 M3	$59.24	$1,744.59	
BOT DECK SLAB FORM	81.522 M2	$80.28	$6,544.62	
BOX WALL FORMS	362.322 M2	$85.12	$30,840.84	
TOP SLAB (A) FORMS	125.307 M2	$80.28	$10,059.64	
TOP SLAB (B) FORMS	175.122 M2	$80.28	$14,058.81	
WALL FORMS	193.238 M2	$85.12	$16,448.45	
REINFORCING STEEL Kg	6861.197 Kg	$2.10	$14,408.51	
POST TENSIONING LBS	3842.190 Kg	$4.75	$18,250.40	
GROUT CY	0.294 M3	$1,000.00	$293.76	
TOTAL SUPERSTRUCTURE	39.624 M		$118,193.88	$2,982.89
SUB TOTAL COST/SPAN	39.624 M		$118,193.88	$2,982.89
MOBILIZATION	10.00%		$11,819.39	
CONTINGENCY	15.00%		$17,729.08	
TOTAL COST/SPAN	39.624 M		$147,742.34	$3,728.61
DESCRIPTION				
SUBSTRUCTURE				
CIP POST TENSIONED SINGLE BOX	39.624 MSPAN "D"			
DRIVEN PILES 100TON	240.000 M	$105.00	$25,200.00	
PILE CAP EXCAVATION	60.972 M3	$23.54	$1,435.28	
PILE CAP	36.246 M3	$33.74	$1,222.93	
PIER COLUMN	11.259 M3	$45.31	$510.15	
PILE CAP FORM	26.756 M2	$64.93	$1,737.27	
PIER COLUMN FORM	32.835 M2	$62.30	$2,045.60	
REINFORCING	3238.861 Kg	$2.10	$6,801.61	
TOTAL SUBSTRUCTURE	1.000 EA		$38,952.83	$38,952.83
SUB TOTAL COST/PIER	1 EA		$38,952.83	$38,952.83
MOBILIZATION	10.00%		$3,895.28	
CONTINGENCY	15.00%		$5,842.92	
TOTAL COST/PIER	1 EA		$48,691.04	$48,691.04

DESCRIPTION				
SUPERSTRUCTURE				
TWO PRESTRESSED BOX GIRDERS w/o DECK 21.336 M SPAN "E"				
BOX				
BOT SLAB CONCRETE-PLACE	7.933 M3	$52.70	$418.05	
BOX WALL CONCRETE-PLACE	8.808 M3	$59.24	$521.76	
TOP SLAB CONCRETE-PLACE	7.933 M3	$52.70	$418.05	
BOT SLAB FORM	39.019 M2	$80.28	$3,132.47	
BOX WALL FORMS	138.701 M2	$85.12	$11,806.23	
TOP SLAB FORM	56.370 M2	$80.28	$4,525.36	
REINFORCING STEEL Kg	1682.188 Kg	$2.10	$3,532.60	
PRE STRESSING STEEL Kg	942.006 Kg	$4.75	$4,474.53	
GROUT M3	0.072 M3	$1,000.00	$72.02	
TOTAL SUPERSTRUCTURE	21.336 M		$28,901.06	$1,354.57
SUB TOTAL COST/SPAN	21.336 M		$28,901.06	$1,354.57
MOBILIZATION	10.00%		$2,890.11	
CONTINGENCY	15.00%		$4,335.16	
TOTAL COST/SPAN	21.336 M		$36,126.33	$1,693.21
DESCRIPTION				
SUBSTRUCTURE				
TWO PRESTRESSED BOX GIRDERS w/o DECK 21.336 M SPAN "E"				
DRIVEN PILES 100TON	160.000 M	$105.00	$16,800.00	
PILE CAP EXCAVATION	36.246 M3	$23.54	$853.22	
PILE CAP CONCRETE-PLACE	27.184 M3	$33.74	$917.19	
PIER COLUMN CONCRETE-PLACE	11.259 M3	$45.31	$510.15	
PIER CAP BEAM CONC-PLACE	3.417 M3	$64.93	$221.84	
PILE CAP FORMS	23.783 M2	$64.93	$1,544.24	
PIER COLUMN FORMS	32.835 M2	$62.30	$2,045.60	
PIER CAP BEAM FORMS	6.802 M2	$92.12	$626.58	
REINFORCING	2854.000 Kg	$2.10	$5,993.40	
TOTAL SUBSTRUCTURE	21.336 M		$29,512.22	$1,383.21
SUB TOTAL COST/PIER	1 EA		$29,512.22	$29,512.22
MOBILIZATION	10.00%		$2,951.22	
CONTINGENCY	15.00%		$4,426.83	
TOTAL COST/PIER	1 EA		$36,890.28	$36,890.28

DESCRIPTION				
SUPERSTRUCTURE				
TWO PRESTRESSED BOX GIRDERS w/o DECK 39.624 M SPAN "E"				
BOX				
BOT SLAB CONCRETE-PLACE	14.732 M3	$52.70	$776.38	
BOX WALL CONCRETE-PLACE	34.353 M3	$59.24	$2,035.07	
TOP SLAB CONCRETE-PLACE	14.732 M3	$52.70	$776.38	
BOT SLAB FORM	72.464 M2	$80.28	$5,817.44	
BOX WALL FORMS	450.826 M2	$85.12	$38,374.31	
TOP SLAB FORM	104.687 M2	$80.28	$8,404.24	
REINFORCING STEEL Kg	4351.040 Kg	$2.10	$9,137.18	
PRE STRESSING Kg	2436.531 Kg	$4.75	$11,573.52	
GROUT M3	0.186 M3	$1,000.00	$186.29	
	39.624 M		$77,080.81	$1,945.31
DESCRIPTION				
SUBSTRUCTURE				
TWO PRESTRESSED BOX GIRDERS w/o DECK 39.624 M SPAN "E"				
DRIVEN PILES 100TON	240.000 M	$105.00	$25,200.00	
PILE CAP EXCAVATION	60.972 M3	$23.54	$1,435.28	
PILE CAP	36.246 M3	$33.74	$1,222.93	
PIER COLUMN	11.259 M3	$45.31	$510.15	
PIER CAP BEAM	3.417 M3	$64.93	$221.84	
PILE CAP FORMS	26.756 M2	$64.93	$1,737.27	
PIER COLUMN FORMS	32.835 M2	$62.30	$2,045.60	
PIER CAP BEAM FORMS	6.802 M2	$92.12	$626.58	
REINFORCING	3471.805 Kg	$2.10	$7,290.79	
TOTAL SUBSTRUCTURE	39.624 M		$40,290.44	
SUB TOTAL COST/PIER	1 EA		$40,290.44	$40,290.44
MOBILIZATION	10.00%		$4,029.04	
CONTINGENCY	15.00%		$6,043.57	
TOTAL COST/PIER	1 EA		$50,363.05	$50,363.05

BID SUMMARY
PROJECT NAME______ MAGLEV SUPERSTRUCTURE STUDIES
JOB NO.____________ 4232F101
DATE______________ MARCH 25,1992
ESTIMATOR________ R.ROBERTS
QUANTITY TAKEOFF

DESCRIPTION	NO.	W	T	AREA	SPAN	VOL	M3/M	AREA	FORMWORK
SUPERSTRUCTURE				M2	M	M3		M2	M2/M
DOUBLE TEE - AASHTO TYPE IV 21.336 M SPAN "A"									
WEB	2	0.2033	1.3716	0.56	21.336	11.90	0.56	0.56	58.53
TOP BULB	4	0.2795	0.1524	0.17	21.336	3.64	0.17	0.17	31.22
LOWER BULB	4	0.3176	0.2286	0.29	21.336	6.20	0.29	0.29	5.28
TOTAL GIRDER						21.73	1.02	1.018489	95.03
DIAPHRAGMS	3	0.3048	1.2192		2.4384	2.72			
END DIAPHRAGMS	2	0.9144	1.2192		2.4384	5.44			
						8.16			
DECK									
DECK SLAB	1	4.42	0.20	0.90	21.336	19.17	0.90	0.90	166.92
WALLS	2	0.30	1.22	0.74	21.336	15.86	0.74	0.74	112.73
FILLETS	2	0.15	0.15	0.05	21.336	0.99	0.05	0.05	15.35
TOTAL DECK				1.69		36.02	1.69	243.10	294.99
								Kg	
REINFORCING STEEL IN SLAB								2456	
REINFORCING STEEL IN DIAPHRAGMS								556	
TOTAL REINFORCING Kg								3012	

DESCRIPTION	NO.	W	L	AREA	DEPTH	VOL		AREA	FORMWORK
SUBSTRUCTURE		M	M	M2	M	M3		M2	M2/M
DOUBLE TEE - AASHTO TYPE IV 21.336 M SPAN "A"									
DRIVEN PILES 100TON	8		20		160				
PILE CAP EXCAVATION	1	4.1576	6.596	27.42353	1.7192	47.146532			
PILE CAP	1	3.6576	6.096	22.29673	1.2192	27.184173			23.78318
PIER COLUMN	1	1.2192		1.167454	7.62	8.8959997			29.18635
PIER CAP BEAM	1	0.6858	3.81	2.612898	0.9906	2.5883368			5.144725
TOTAL CONCRETE						38.668509			58.11425
REINFORCING								2636.419 Kg	

DESCRIPTION	NO.	W	T	AREA	SPAN	VOL	M3/M	AREA	FORMWORK
SUPERSTRUCTURE				M2	M	M3		M2	M2/M
DOUBLE TEE - AASHTO TYPE VI 39.624 M SPAN "A"									
WEB	2	0.2033	1.3716	0.56	39.624	22.10	0.56	0.56	108.70
TOP BULB	4	0.4317	0.2159	0.37	39.624	14.77	0.37	0.37	57.98
LOWER BULB	4	0.3303	0.254	0.34	39.624	13.30	0.34	0.34	209.37
TOTAL GIRDER						50.17	1.27	1.266093	376.05
DIAPHRAGMS	6	0.3048	1.2192		2.4384	5.44			17.84
END DIAPHRAGMS	2	0.9144	1.2192		2.4384	5.44			5.95
						10.87			24
DECK									
DECK SLAB	1	4.42	0.20	0.90	39.624	35.60	0.90	0.90	309.99
WALLS	2	0.30	1.22	0.74	39.624	29.45	0.74	0.74	209.35
FILLETS	2	0.15	0.15	0.05	39.624	1.84	0.05	0.05	28.51
TOTAL DECK				1.69		66.89	1.69	243.10	547.84
								Kg	
REINFORCING STEEL IN SLAB								4561	
REINFORCING STEEL IN DIAPHRAGMS								741	
TOTAL Kg								5302	Kg

DESCRIPTION	NO.	W	L	AREA	DEPTH	VOL		AREA	FORMWORK
SUBSTRUCTURE		M	M	M2	M	M3		M2	M2/M
DOUBLE TEE - AASHTO TYPE VI 39.624 M SPAN "A"									
DRIVEN PILES 100TON	12		20		240				
PILE CAP EXCAVATION	1	5.3768	6.596	35.46537	1.7192	60.972069			
PILE CAP	1	4.8768	6.096	29.72897	1.2192	36.245564			26.75608
PIER COLUMN	1	1.2192		1.167454	7.62	8.8959997			29.18635
PIER CAP BEAM	1	0.6858	3.81	2.612898	0.9906	2.5883368			5.144725
TOTAL CONCRETE						47.7299			61.08715
REINFORCING								3254.225	Kg

DESCRIPTION	NO.	T	H	WT/SF	WT/LF	SPAN FT	TOTAL WT	WT/LF	AREA
SUPERSTRUCTURE		INCHES	FT	LBS	LBS		LBS		SQ IN
STEEL GIRDER W/ CONCRETE DECK 21.336 SPAN "8"									
WEB	4	0.375	4	17.85	71.40	21.336	6093.56	285.60	72.00
TOP FLANGE	4	2	1.333	102.00	135.97	21.336	11603.88	543.86	127.97
STIFFNERS @ 10 C-C	60	0.375	4	17.85	71.40	0.75	3213.00	150.59	0.00
LOWER FLANGE	4	2	1.333	102.00	135.97	21.336	11603.88	543.86	127.97
TOTAL GIRDER LBS							32514.33	1523.92	327.94
TOTAL GIRDER Kg							14748.50	Kg	

	NO.	W	T	AREA	SPAN	VOL	M3/M	AREA	FORMWORK
DECK		M	M	M2	M	M3		M2	M2/M
DECK SLAB	1	4.42	0.20	0.90	21.336	19.17	0.90	0.90	166.92
WALLS	2	0.30	1.22	0.74	21.336	15.86	0.74	0.74	112.73
FILLETS	2	0.15	0.15	0.05	21.336	0.99	0.05	0.05	15.35
TOTAL DECK				1.69		36.02	1.69	243.10	294.99

	Kg
REINFORCING STEEL IN SLAB	2456
TOTAL Kg	2456 Kg

DESCRIPTION	NO.	W	L	AREA	DEPTH	VOL	AREA	FORMWORK
SUBSTRUCTURE		M	M	M2	M	M3	M2	M2/M
STEEL GIRDER W/ CONCRETE DECK 21.336 SPAN "8"								
DRIVEN PILES 100TON	8		20		160			
PILE CAP EXCAVATION	1	4.1576	6.596	27.42353	1.7192	47.146532		
PILE CAP	1	3.6576	6.096	22.29673	1.2192	27.184173		23.78318
PIER COLUMN	1	1.2192		1.167454	7.62	8.8959997		29.18635
PIER CAP BEAM	1	0.6858	3.81	2.612898	0.9906	2.5883368		5.144725
TOTAL CONCRETE						38.668509		58.11425
REINFORCING							2636.419 Kg	

DESCRIPTION	NO.	T	H	WT/SF	WT/LF	SPAN FT	TOTAL WT	WT/LF	AREA
SUPERSTRUCTURE		INCHES	FT	LBS	LBS		LBS		SQ IN
STEEL GIRDER W/ CONCRETE DECK 39.624 FT SPAN "B"									
WEB	4	0.4375	3.9167	17.85	69.91	39.624	11080.95	279.65	82.25
TOP FLANGE	4	2.50	1.667	102.00	170.03	39.624	26949.71	680.14	200.04
STIFFNERS @ 10 C-C	52	0.4375	3.9167	17.85	69.91	0.75	2726.61	68.81	0.00
LOWER FLANGE	4	2.50	1.667	102.00	170.03	39.624	26949.71	680.14	200.04
TOTAL GIRDER							67706.97	1708.74	482.33
TOTAL Kg							30711.88 Kg		

	NO.	W	T	AREA	SPAN	VOL	M3/M	AREA	FORMWORK
DECK SLAB	1	4.42	0.20	0.90	39.624	35.60	0.90	0.90	309.99
WALLS	2	0.30	1.22	0.74	39.624	29.45	0.74	0.74	209.35
FILLETS	2	0.15	0.15	0.05	39.624	1.84	0.05	0.05	28.51
TOTAL DECK				1.69		66.89	1.69	1.69	547.84
REINFORCING STEEL IN SLAB							115.10	4561	
TOTAL Kg								4561	Kg

DESCRIPTION	NO.	W	L	AREA	DEPTH	VOL		AREA	FORMWORK
SUBSTRUCTURE		M	M	M2	M	M3		M2	M2/M
STEEL GIRDER W/ CONCRETE DECK 39.624 FT SPAN "B"									
DRIVEN PILES 100TON	12		20		240				
PILE CAP EXCAVATION	1	5.3768	6.596	35.46537	1.7192	60.972069			
PILE CAP	1	4.8768	6.096	29.72897	1.2192	36.245564			26.75608
PIER COLUMN	1	1.2192		1.167454	7.62	8.8959997			29.18635
PIER CAP BEAM	1	0.6858	3.81	2.612898	0.9906	2.5883368			5.144725
TOTAL CONCRETE						47.7299			61.08715
REINFORCING								3254.225	Kg

DESCRIPTION	NO.	W	T	AREA	SPAN	VOL	M3/M	AREA	FORMWORK
SUPERSTRUCTURE		M	M	M2	M	M3		M2	M2/M
SINGLE BOX -PRESTRESSED CONCRETE 21.336 SPAN "C"									
BOX									
BOT DECK SLAB	1	2.13	0.20	0.44	21.336	9.30	0.44	0.44	45.52
BOX WALLS	2	0.20	1.22	0.50	21.336	10.62	0.50	0.50	104.05
TOP SLAB (A)	2	0.10	0.80	0.16	21.336	3.49	0.16	0.16	
TOP SLAB (B)	1	4.42	0.20	0.90	21.336	19.26	0.90	0.90	94.30
WALLS	2	0.30	1.42	0.87	21.336	18.50	0.87	0.87	121.40
TOTAL DECK				2.00		42.66	2.00	2.00	365.27
REINFORCING STEEL LBS							136.32	2909 Kg	
PRE STRESSING LBS							76.34	1629 Kg	
GROUT M3								0.12 M3	

DESCRIPTION	NO.	W	L	AREA	DEPTH	VOL	AREA	FORMWORK
SUBSTRUCTURE		M	M	M2	M	M3	M2	M2/M
SINGLE BOX -PRESTRESSED CONCRETE 21.336 SPAN "C"								
DRIVEN PILES 100TON	8		20		160			
PILE CAP EXCAVATION	1	4.1576	6.596	27.42353	1.7192	47.146532		
PILE CAP	1	3.6576	6.096	22.29673	1.2192	27.184173		23.78318
PIER COLUMN	1	1.3716		1.477559	7.62	11.259		32.83464
TOTAL CONCRETE						38.443172		
REINFORCING							2621.055 Kg	

DESCRIPTION	NO.	W	T	AREA	SPAN	VOL	M3/M	AREA	FORMWORK
SUPERSTRUCTURE		M	M	M2	M	M3		M2	M2/M
SINGLE BOX -PRESTRESSED CONCRETE 39.624 M SPAN "C"									
BOX									
BOT DECK SLAB	1	2.13	0.20	0.44	39.624	17.26	0.44	0.44	84.54
BOX WALLS	2	0.20	2.69	1.10	39.624	43.47	1.10	1.10	425.72
TOP SLAB (A)	2	0.10	0.80	0.16	39.624	6.47	0.16	0.16	
TOP SLAB (B)	1	4.42	0.20	0.90	39.624	35.76	0.90	0.90	175.12
WALLS	2	0.30	1.42	0.87	39.624	34.36	0.87	0.87	225.46
TOTAL DECK				2.60		102.96	2.60	2.60	910.84
REINFORCING STEEL LBS								7020	Kg
PRE STRESSING LBS								3931	Kg
GROUT CY								0.30	M3

DESCRIPTION	NO.	W	L	AREA	DEPTH	VOL		AREA	FORMWORK
SUBSTRUCTURE		M	M	M2	M	M3		M2	M2/M
SINGLE BOX -PRESTRESSED CONCRETE 39.624 M SPAN "C"									
DRIVEN PILES 100TON	12		20		240				
PILE CAP EXCAVATION	1	5.3768	6.596	35.46537	1.7192	60.972069			
PILE CAP	1	4.8768	6.096	29.72897	1.2192	36.245564			26.75608
PIER COLUMN	1	1.3716		1.477559	7.62	11.259			32.83464
TOTAL CONCRETE						47.504563			59.59072
REINFORCING								3238.861	Kg

DESCRIPTION	NO.	W	T	AREA	SPAN	VOL	M3/M	AREA	FORMWORK
SUPERSTRUCTURE		M	M	M2	M	M3		M2	M2/M
CIP POST TENSIONED SINGLE BOX 21.336 M SPAN "D"									
BOX									
BOT DECK SLAB	1	2.06	0.30	0.63	21.336	13.38	0.63	0.63	43.89669
BOX WALLS	2	1.52	0.20	0.62	21.336	13.22	0.62	0.62	130
TOP SLAB (A)	2	0.42	0.10	0.08	21.336	1.81	0.08	0.08	67
TOP SLAB (B)	1	4.42	0.20	0.90	21.336	19.17	0.90	0.90	94
WALLS	2	0.30	1.22	0.74	21.336	15.86	0.74	0.74	104
TOTAL DECK				2.23		47.58	2.23	2.23	439.7819
REINFORCING STEEL Kg								3244 Kg	
POST TENSIONING Kg								1816 Kg	
GROUT CY								0.14 M3	

DESCRIPTION	NO.	W	L	AREA	DEPTH	VOL	AREA	FORMWORK
SUBSTRUCTURE		M	M	M2	M	M3	M2	M2/M
CIP POST TENSIONED SINGLE BOX 21.336 M SPAN "D"								
DRIVEN PILES 100TON	8		20		160			
PILE CAP EXCAVATION	1	4.1576	6.596	27.42353	1.7192	47.146532		
PILE CAP	1	3.6576	6.096	22.29673	1.2192	27.184173		23.78318
PIER COLUMN	1	1.3716		1.477559	7.62	11.259		32.83464
TOTAL CONCRETE						38.443172		
REINFORCING							2621.055 Kg	

DESCRIPTION	NO.	W	T	AREA	SPAN	VOL	M3/M	AREA	FORMWORK
SUPERSTRUCTURE		M	M	M2	M	M3		M2	M2/M
CIP POST TENSIONED SINGLE BOX 39.624 MSPAN "D"									
BOX									
BOT DECK SLAB	1	2.06	0.30	0.63	39.624	24.85	0.63	0.63	81.52242
BOX WALLS	2	2.29	0.20	0.93	39.624	36.83	0.93	0.93	362
TOP SLAB (A)	2	0.42	0.10	0.08	39.624	3.35	0.08	0.08	125
TOP SLAB (B)	1	4.42	0.20	0.90	39.624	35.60	0.90	0.90	175
WALLS	2	0.30	1.22	0.74	39.624	29.45	0.74	0.74	193
TOTAL DECK				2.54		100.63	2.54	2.54	937.5118
REINFORCING STEEL LBS							173.16	6861 Kg	
POST TENSIONING LBS							96.97	3842 Kg	
GROUT CY								0.29 M3	
PRE STRESSING LBS							0.00	0	
GROUT CY								0.00	

DESCRIPTION	NO.	W	L	AREA	DEPTH	VOL		AREA	FORMWORK
SUBSTRUCTURE		M	M	M2	M	M3		M2	M2/M
SINGLE BOX -PRESTRESSED CONCRETE 39.624 M SPAN "D"									
DRIVEN PILES 100TON	12		20		240				
PILE CAP EXCAVATION	1	5.3768	6.596	35.46537	1.7192	60.972069			
PILE CAP	1	4.8768	6.096	29.72897	1.2192	36.245564			26.75608
PIER COLUMN	1	1.3716		1.477559	7.62	11.259			32.83464
TOTAL CONCRETE						47.504563			
REINFORCING								3238.861 Kg	
GROUT CY								0.25 M3	
REINFORCING STEEL LBS								0	
PRE STRESSING LBS								0	
GROUT CY								0.00	

DESCRIPTION	NO.	W	T	AREA	SPAN	VOL	M3/M	AREA	FORMWORK
SUPERSTRUCTURE		M	M	M2	M	M3		M2	M2/M
TWO PRESTRESSED BOX GIRDERS w/o DECK 21.336 M SPAN "E"									
BOX									
BOT SLAB	2	0.91	0.20	0.37	21.336	7.93	0.37	0.37	39
BOX WALLS	4	0.81	0.13	0.41	21.336	8.81	0.41	0.41	139
TOP SLAB	2	0.91	0.20	0.37	21.336	7.93	0.37	0.37	56
TOTAL DECK				1.16		24.67	1.16	1.16	234.0901
REINFORCING STEEL Kg								1682 Kg	
PRE STRESSING Kg								942 Kg	
GROUT M3								0.07 M3	

DESCRIPTION	NO.	W	L	AREA	DEPTH	VOL		AREA	FORMWORK
SUBSTRUCTURE		M	M	M2	M	M3		M2	M2/M
TWO PRESTRESSED BOX GIRDERS w/o DECK 21.336 M SPAN "E"									
DRIVEN PILES 100TON	8		20		160				
PILE CAP EXCAVATION	1	4.1576	6.596	27.42353	1.7192	47.146532			
PILE CAP	1	3.6576	6.096	22.29673	1.2192	27.184173			23.78318
PIER COLUMN	1	1.3716		1.477559	7.62	11.259			32.83464
PIER CAP BEAM	1	0.6858	5.0292	3.449025	0.9906	3.4166045			6.801825
TOTAL CONCRETE						41.859777			
REINFORCING								2854 Kg	

DESCRIPTION	NO.	W	T	AREA	SPAN	VOL	M3/M	AREA	FORMWORK
SUPERSTRUCTURE		INCHES	FT	M2	M	M3		M2	M2/M
TWO PRESTRESSED BOX GIRDERS w/o DECK 39.624 M SPAN "E"									
BOX									
BOT SLAB	2	0.91	0.20	0.37	39.624	14.73	0.37	0.37	72
BOX WALLS	4	1.42	0.15	0.87	39.624	34.35	0.87	0.87	451
TOP SLAB	2	0.91	0.20	0.37	39.624	14.73	0.37	0.37	105
TOTAL DECK				1.61		63.82	1.61	1.61	627.977
REINFORCING STEEL LBS								4351 Kg	
PRE STRESSING LBS								2437 Kg	
GROUT CY								0.19 M3	

DESCRIPTION	NO.	W	L	AREA	DEPTH	VOL		AREA	FORMWORK
SUBSTRUCTURE		M	M	M2	M	M3		M2	M2/M
TWO PRESTRESSED BOX GIRDERS w/o DECK 39.624 M SPAN "E"									
DRIVEN PILES 100TON	12		20		240				
PILE CAP EXCAVATION	1	5.3768	6.596	35.46537	1.7192	60.972069			
PILE CAP	1	4.8768	6.096	29.72897	1.2192	36.245564			26.75608
PIER COLUMN	1	1.3716		1.477559	7.62	11.259			32.83464
PIER CAP BEAM	1	0.6858	5.0292	3.449025	0.9906	3.4166045			6.801825
TOTAL CONCRETE						50.921168			66.39255
REINFORCING								3471.805 Kg	

Final Report -Influence of Guideway Flexibility on MAGLEV Vehicle/Guideway Dynamic Forces, Parsons, Brinckerhoff, Quade & Douglas, Inc , Battelle, Intermagnetics General, G Gregorek, 1992 -11-Advanced Systems